HYDROGEOLOGIC PARAMETERS OF AN EPHEMERAL STREAM:

THE RIO SALADO OF CENTRAL NEW MEXICO

by

JEFF HAVLENA

Submitted in partial fulfillment of requirements for the degree of
Master of Science in Hydrology

New Mexico Institute of Mining and Technology

Spring 1988

HYDROGEOLOGIC PARAMETERS OF AN EPHEMERAL STREAM:

THE RIO SALADO OF CENTRAL NEW MEXICO

by

JEFF HAVLENA

Submitted in partial fulfillment of requirements for the degree of
Master of Science
in Hydrology

New Mexico Institute of Mining and Technology

Spring 1988

Volume I: Report

RIO SALADO DRAINAGE BASIN

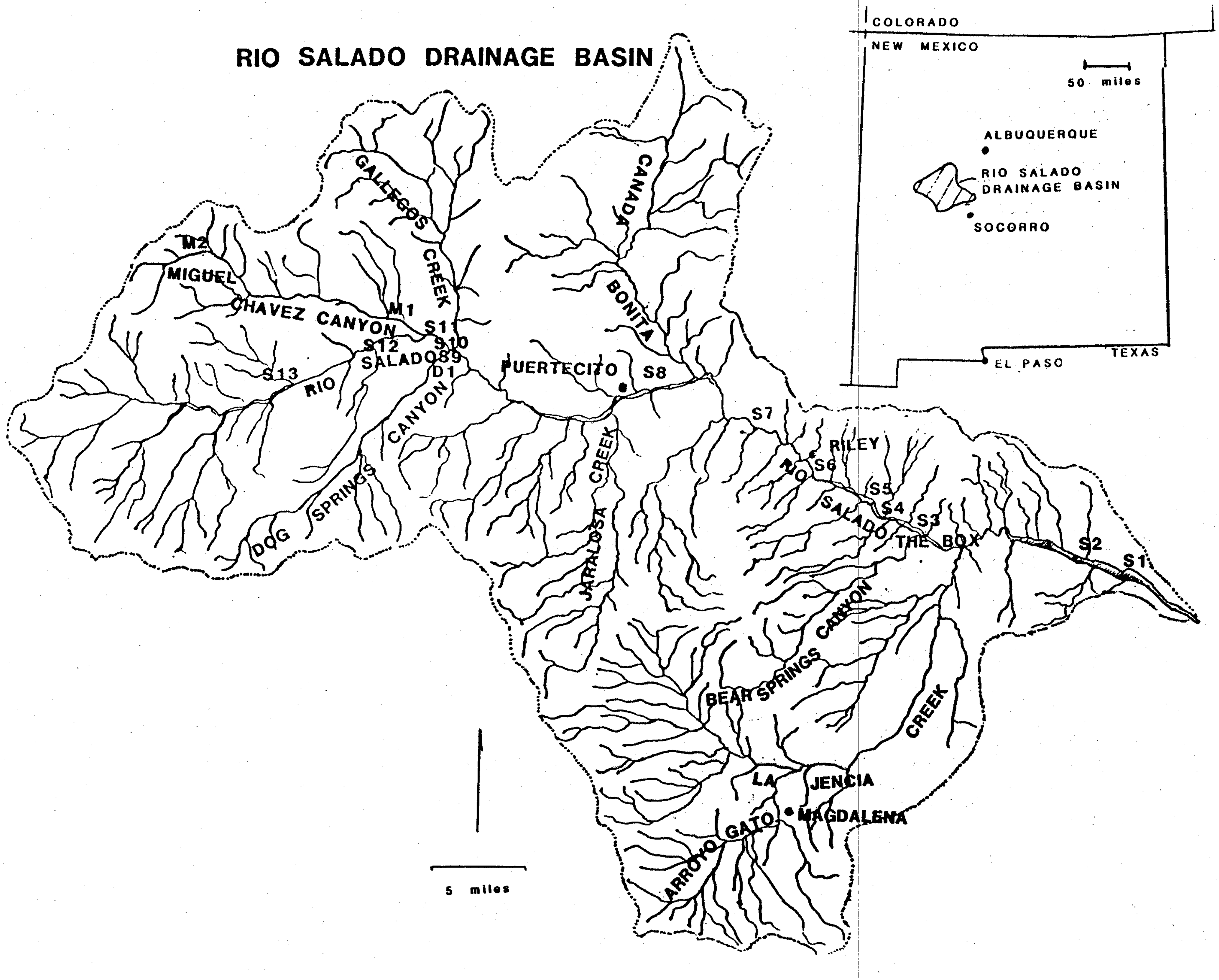

ABSTRACT

The Rio Salado of central New Mexico is an ephemeral stream that rises along the continental divide, flows approximately 90 miles eastward, and empties into the Rio Grande near San Acacia, New Mexico. The Rio Salado drains approximately 3635 km2. Streamflow in the Rio Salado occurs only in the late summer in response to intense thunderstorms. The Rio Salado flows in an alluvial, sand-bedded channel throughout most of its reach. The Rio Salado drainage basin consists predominantly of relatively flat-lying Mesozoic and Cenozoic clastic and volcanoclastic rocks, with occasional exposures of Tertiary intrusives and Paleozoic rocks. Ongoing uplift centered over the Socorro Magma Body includes approximately the lower half of the Rio Salado drainage basin.

Quantitative analysis of the Rio Salado drainage basin and channel network indicates that the Rio Salado behaves predictably according to Horton's laws. Analysis of channel geometry, however, indicates that the Rio Salado does not behave according to models for ephemeral streams proposed by other investigators. The channel geometry of the Rio Salado appears to be controlled by the tectonic uplift over the Socorro Magma Body.

ACKNOWLEDGEMENTS

This study grew out of a series of class discussions and assignments for the Quantitative Geomorphology class taught by Dr. G. W. Gross, during the Fall semester, 1984. Many individuals provided support and assistance during the various phases of this study. Most notable are: The New Mexico Geological Society who provided financial support through a grant-in-aid; Dr. G. W. Gross, Dr. Dave Love, and Dr. John Hawley who provided the author with new ideas, moral support, and encouragement; the ranchers and landowners who allowed access to the Rio Salado accross their property, and opened up their ranches to myself and my field assistant, especially, Mr. and Mrs. Tom Kelly, Mr. and Mrs. Mike Kelly - the managers of the Criswell Ranch, the managers of Red Lake Ranch, the manager of Spears Ranch, the manager of Ligon Ranch, and Mr. Ted Stans, the manager of the Sevilletta National Wildlife Refuge; and lastly, my highly skilled and ever patient field assistant, Janice.

TABLE OF CONTENTS

LIST OF FIGURES

LIST OF PLATES
(in pocket)

LIST OF TABLES

LIST OF APPENDICES

(Contained in Volume II)

1.0 INTRODUCTION

1.1 Intent of Study

This study was undertaken in an attempt to quantitatively and qualitatively describe the Rio Salado of Central New Mexico. Another important intent of this study is to provide a foundation for future investigations, and to develop a better understanding of the conditions and processes which have contributed to the development of the Rio Salado and its drainage basin.

In order to accomplish the above goals, the present study was undertaken to provide base-line information about the drainage basin and channel network of the Rio Salado from morphometric and topologic analysis, and to investigate how such information relates to the adjustment of the Rio Salado to its environment. Historical and present-day adjustment of the Rio Salado incorporates channel incision, migration, and sediment transport; stream-aquifer interactions; drainage basin and channel network evolution; and response to climatic influences. It is hoped that an investigation into the relationship of the physical nature of the drainage basin and channel network to certain of the above dynamic variables will help to provide an understanding of how the system functions, and aid in the development of predictive methods.

1.2 Related Work

Quantitative geomorphologists have long been involved in the attempt to better understand the nature and behavior of fluvial systems. Considerable work has been done to identify and quantify the parameters which best describe fluvial systems and their adjustment to their environment. The implicit purpose of such undertakings has been to provide a means for predicting the response of rivers to a given set of inputs, as well as to derive information about past and present climatic, geologic, tectonic, and geomorphological conditions.

Many investigators have contributed to the science of quantitative basin and channel analysis, as well as to the application of theory based upon such analyses. Among the most notable are:

i) Horton (1945), who pioneered the discipline of quantitative drainage basin analysis. Horton was the first to develop methods for the quantitative classification and analysis of drainage basins and channel networks. In order to accomplish these goals, Horton developed a series of morphometric parameters, often known as Horton's Laws, which describe certain hydrophysical aspects of the drainage basin. He also proposed a method of channel ordering. With these tools Horton was able to quantitatively describe any drainage basin, with the ultimate intent of developing a better understanding of the interelationships and physical nature of the various features contained in the drainage basin.

ii) Leopold and Maddock (1953) proposed the concept of hydraulic geometry to relate channel dimensions of a stream to the dynamic variables of streamflow. They developed a set of empirical power functions to describe the relationships. With these allometric relationships, Leopold and Maddock were able to investigate channel response to various inputs, and the orderly downstream changes in channel geometry and streamflow variables.

iii) Wolman (1955) utilized the allometric relationships proposed by Leopold and Maddock in a study of a perennial creek in Pennsylvania. He expanded on some of Leopold and Maddock's original work by using the allometric relationships for a detailed investigation of channel equilibrium and grade.

iv) Strahler (1952 and 1964) refined the Hortonian method of stream ordering, thereby greatly expanding its utility. He also proposed the use of hypsometric curves and integrals for the quantitative study of the erosional stage of drainage basins.

v) Schumm (1960, 1961) looked at the relationship of silt and clay sized material along the channel perimeter and width:depth ratios to channel stability. To accomplish this goal, he proposed the use of the parameter "M", which is a weighted silt-clay content of the channel perimeter. Channel stability is identified by the position of a particular channel cross section on a plot of width:depth ratio versus "M".

vi) Shreve (1966) used combinatorial and statistical theory to describe the mathematical structure of channel networks. In order to allow such a detailed analysis of the network, Shreve found it necessary to develop an alternative method of channel ordering. He proposed the use of link and basin magnitude as a mathematically more meaningful system of ordering. Shreve's work also initiated the formulation of a theoretical basis to Hortons Laws, which allowed the development of predictive methods for the generation of synthetic streamflow.

vii) Rodriguez-Iturbe and Valdez (1979), Valdez et al (1979), and Rodriguez-Iturbe et al (1982), used the geomorphological structure of a drainage basin as a basis in the development of methods to generate synthetic instantaneous hydrographs for the outlet of a basin. They were able to express the instantaneous unit hydrograph (IUH) as a function of certain of the Horton numbers. Their model heavily draws on the statistical work pioneered by Shreve (1966).

Although it is apparent that considerable work has been accomplished in the area of drainage network analysis, most of the studies have been directed towards perennial streams in humid climates. Very little work to date has been aimed specifically at the description and functioning of ephemeral systems. Leopold and Miller (1956) were able to successfully apply the relationships developed by Leopold and Maddock (1953) during their study of small ephemeral streams in northern New Mexico. Cherkauer (1972) investigated the interrelationship of certain morphometric parameters of several small ephemeral streams in southeast Arizona. Cherkauer developed empirical regression relationships to describe channel gradient as a function of basin and dry-channel geometry. More recently, Begin and Inbar (1984) were able to use channel geometry and particle size as a basis for the estimation of discharge-frequency relationships for a 1410 km^2 ephemeral drainage basin in Israel.

1.3 Description of Study

Work undertaken for the study has involved the generation of information by means of field observation, along with map and aerial photographic interpretation. Existing sources were consulted for additional information.

Channel characteristics were determined from field surveys and data collection reconnaisance conducted during the summers of 1985 and 1986. Office-based analyses were initiated during the spring of 1985. Whenever possible, field visits were designed to complement information obtained during office-based investigation.

Field work involved the derivation of quantitative information about channel geometry, pattern, and gradient; channel bottom characteristics, including low-flow channel and overall channel sediment particle size distributions; bank and floodplain geometry and material characteristics; along with more qualitative investigations into the geologic and geomorphic nature of each station visited. A total of fourteen field stations were investigated. These stations were selected on the basis of their geographical distribution along the mainstem of the Rio Salado, and their relationship to major tributaries. During the selection of field station locations, every attempt was made to obtain representative information from each of several initially identified segments of the main channel. Station sites were also selected according to their geographical placement within the drainage basin.

Map analysis work required the initial identification of channel segments, and the classification of each channel segment according to two different schemes. The majority of the map work was completed using United States Geological Survey 7.5 minute series topographic maps. An entire set of 39 topographic maps was required for complete coverage of the basin. Several smaller scale maps were also consulted.

Once the channel pattern was clearly defined on the topographic maps, quantitative information was extracted. Among the most important are: channel length, channel elevation, channel gradient, channel sinuosity, mainstem valley side slope and cross section, tributary location and class, as well as basin elevation at discrete points.

1.4. Report Organization

This report is organized into two volumes and seven major chapters. Volume I contains the text portion of the report; Volume II contains the appendices under separate cover. The first chapter of Volume I contains the introduction. Chapter 2 contains brief descriptions of the geography and geology of the Rio Salado drainage basin. Chapter 3 contains a brief discussion of the Rio Salado channel network. Chapters 2 and 3 also contain discussion of the methods used during the present study to describe the channel network and drainage basin parameters of the Rio Salado. Chapters 4 through 7 contain discussion, conclusions, recommendations, and a list of references, respectively. All pertinent data and maps are included within the appendices in Volume II.

2.0 THE RIO SALADO DRAINAGE BASIN

2.1 Basin Geography

2.1.1. LOCATION

The Rio Salado drains approximately 1404 square miles in Socorro, Catron, Cibola, and Valencia counties in central New Mexico. The drainage basin of the Rio Salado lies between 106 51'12" and 108 02'07" west longitude, and 34 00'54" and 34 43'45" north latitude. The major axis is 70 miles long, and is oriented approximately east-west. The drainage basin is just under 50 miles wide in the north-south direction. Plate 1 shows the important features of the drainage basin. (See map on p. ii for quick reference).

The basin is bounded to the north and northwest by the Rio San Jose arm of the Rio Puerco drainage basin, to the south and southwest by the closed drainage of the San Augustin Plains, and to the east by the Rio Grande and associated minor tributaries. Several small, closed basins lie along isolated portions of the borders, however the size and impact of these areas on the drainage of the Rio Salado is considered to be negligible.

2.1.2. CULTURE

Land use within the drainage basin is almost entirely devoted to range-land cattle ranching. Several large scale ranching operations are headquartered within the basin, including the Criswell, Drag-Ace, Field, Red Lake, Martin, La Jencia, Majors, and Ligon Ranches. Approximately 86 square miles near the center of the basin is included within the Alamo Band Navajo Indian Reservation. Most of the land within the reservation is devoted to sheep and cattle ranching. The Sevilleta National Wildlife Refuge comprises the portion of the basin lying roughly east of 107 05', and includes a total of approximately 80 square miles. Since the late 1960's the Sevilleta National Wildlife Refuge has been administered by the U.S. Fish and Wildlife Service. Land use within the refuge has been restricted to small scale, non-destructive scientific research. The village of Magdalena, population 1,200, encompasses approximately two square miles along U.S. Highway 60. A total of 55 miles of two-lane blacktop roads lie within the southern portion of the basin. However, many improved and unimproved gravel and dirt roads provide access to the interior of the basin.

2.1.3. CLIMATE

The Rio Salado drainage basin lies near the northeast corner of the Sonoran Border Meterologic Zone. The climate within the basin is predominantly semi-arid. Magdalena (elev. 6556 msl) is the site of the only Class A, long term National Weather Service weather station within the basin. Approximately one half of the total annual precipitation falls during late summer thunderstorms. Climatic parameters are included in Table 1.

Table 1: Climatic Parameters (after Gabin and Lesperance, 1977; Maker et al; USDA, 1985)

Station	Elevation (msl)	Mean Annual Air Temp (F)	Mean Daily Minimum Temp (F)	Mean Daily Maximum Temp (F)	Mean Annual Precipitation (in)	2-yr/24hr Maximum Rainfall (in)	100-yr/24hr Maximum Rainfall (in)	Potential E.T. (in)	Number of Frostfree days
Grants Airport	6520	49.0	-	-	10.1	1.2	2.8	33.6	-
Magdalena	6556	52.0	37.0	67.0	11.9	1.6	3.8	36.8	167
Socorro	4585	58.0	41.0	74.0	9.6 (4.5 during July-Sept)	1.4	3.2	46.2	197

Two Class A, long term weather stations lie just outside the periphery of the basin: Socorro, 38 miles to the southeast of the center of the basin, and Grants Airport, 40 miles to the north of the center of the basin. Climatic parameters for these stations are also included in Table 1.

Mean annual precipitation within the basin, as interpolated from climatic data provided in part by the Magdalena, Socorro, and Grants weather stations (USDA, 1985), ranges from approximately 10 inches at lower elevations, to over 18 inches along mountain crests. Isohyetal contours provided by the USDA (1985), along with maximum rainfall intensity isohyets indicate that considerable orographically induced precipitation occurs along the mountain ranges within the basin. Mean annual air temperatures throughout the basin vary predominantly according to land surface elevation. Comparison of the mean annual air temperatures at the three stations listed above suggests that the mean annual lapse rate ranges between 3 and 4 F per 1000 feet elevation. However, the instantaneous lapse rate may be considerably greater during the daylight hours of the summer months. This may provide a mechanism for the generation of orographically induced, localized thunderstorms in response to the convergent lifting of warm air along mountain slopes.

As indicated earlier, most of the annual precipitation within the basin occurs during the late summer months as intense thunderstorms. The moisture which contributes to these storms is predominantly from the Gulf of Mexico (Thomas, 1962), in response to a seasonal shift in the position of the Bermuda High. Precipitation events during the remainder of the year are typically less intense, and occur in response to eastward tracking storm cells which move inland from off the Pacific Ocean. These storms are mostly depleted of moisture by the time they reach New Mexico, due to orographically induced precipitation upon the mountain ranges of California and Arizona (Thomas, 1962).

The weather station at Magdalena has been in near-continuous service since 1889. Total July through September precipitation during the period of record ranges from a low of 1.55 inches in 1922, to a maximum of 14.72 inches in 1914. Although isolated instances of wet-following-dry years do exist, there does appear to be a general tendency for clustering of wet years and dry years. The time-series of precipitation at Magdalena for the period of record indicates that precipitation was greatest during the first 15 years of the 20th century. Records of other long-term weather stations throughout the region also indicate a similar distribution of precipitation during the past century. For example, the time-series of precipitation at Magdalena is remarkably similar to that of Lordsburg, New Mexico, as shown by Thomas (1962, figure 7), even though the geographic situation of the two stations is dissimilar.

The entire region has undergone considerable climatic fluctuations during the past 12,000 years, as is evidenced from archeological, palynological, paleobotanical, paleontological, and sedimentological studies. Several investigators cited by Gile et al (1981) have concluded that the period following the last full glacial was warm and dry, excepting for several brief pluvial periods which occurred around 11,500 to 11,000 years before present (YBP), 10,500 to 10,000 YBP, and 8,500 to 8,000 YBP. It is generally agreed that the period from 7,500 to 5,000 YBP was warm, with intense warm-weather precipitation events, and may represent a period of considerable landscape instability and erosion-sedimentation (Gile et al, 1981). Love (1979) lists several arroyo cut-and-fill sequences in Chaco Canyon during the past 10,000 years which may be attributable to climatic fluctuations.

Thomas (1962) quotes Schulman in reference to more recent climatic changes in the southwest, who states that the period since 1870 has been more climatically variable than the previous several centuries, largely in response to a major disturbance in the upper-atmospheric circulation over western North America.

2.1.4. VEGETATION

The density and type of vegetation varies widely within the basin according to elevation, soil type, drainage, and depth to water. Predominant upland species include grasses, such as grama, dropseed, and galleta; shrubs - chamisa, rabbitbrush, sagebrush, snakeweed, cholla, mahogany; pinyon and juniper trees, as well as ponderosa pine, tree oaks, cedar, and mountain mahogany at higher elevations (Maker, et al, 1985). Locally thick stands of tamarisk interspersed with cottonwoods, willows, and oak occur along creek bottoms and where the water table is near to the surface.

2.1.5. PHYSIOGRAPHY

The Rio Salado drainage basin encompasses a wide variety of landforms within portions of the Datil-Mogollon Section and the Rio Grande Subsection of the Basin and Range Physiographic Province, and the Acoma-Zuni Section of the southern Colorado Plateau. Most of the basin lies within the Datil-Mogollon Section, which represents a transition zone between the Basin and Range Province and the Colorado Plateau, and exhibits characteristics of each, including volcanic upland with basins; high tablelands, with fault-block ranges, basins, and canyons (Gile et al, 1981). Other features included within the basin are: hogbacks and cuestas, basalt-capped mesas, pediment remnants, broad alluvial plains, and piedmonts. The geographic distribution of these elements within the basin reflects local geology and tectonic activity. Elevations within the drainage basin range from just under 4700' msl at the Rio Grande, to over 9000' msl along the mountain divides.

2.2. Basin Geology

Information included within this report regarding the geology and tectonic history of the Rio Salado drainage basin has been assembled from several sources. Principal investigators who have studied the geology of portions of the basin include: Winchester, 1920; Spiegel, 1955; Dane, Wanek, and Reedside, 1957; Givens, 1957; Tonking, 1957; Jicha, 1958; Bruning, 1973; Chapin and Seager, 1975; Callender and Zilinski, 1976; Condie, 1976; Machette, 1978; Massingill, 1979; Meyerson, 1979; Harrison, 1980; LaRoche, 1980; Reilinger et al, 1980; Coffin, 1981; Robinson, 1981; Cather, 1982; Osburn, 1982, 1983, 1984, 1985; Barker, 1983; Chamberlin, 1983; Johansen, 1983; Ouchi, 1983; Sanford et al, 1983; Cather and Johnson, 1984. These, and other, sources have been used to develop the following discussion.

2.2.1. GEOLOGIC UNITS

Most of the drainage basin of the Rio Salado is underlain by nearly flat-lying Triassic through Tertiary clastic and volcanoclastic rocks. Locally thick sequences of Quaternary alluvial fill covers the older consolidated units across several wide interior basins and along the course of the present drainage net. However, considerable exposures of bedrock occurs along the flanks of mesas and hillslopes, and along the erosional scarps of the drainage network. Plate 2 is a generalized depiction of the more prominent geologic features of the Rio Salado drainage basin.

2.2.1.1. Precambrian Rocks

Exposures of Precambrian rocks within the drainage basin is limited to the upper elevations of the Ladron and Magdalena Mountains. Within the Ladron Mountains several rock types occur, including metasedimentary and metavolcanic rocks, and granite, quartz-monzonite, and pegmatite plutons (Condie, 1976). Exposures of these units is limited to the high mountain slopes. The combined effects of land surface slope, orographic precipitation, and the low permeability of the outcrops may serve to make the Ladron Mountains an important source area for runoff within the lower reach of the Rio Salado. The Precambrian rocks within the Magdalena Mountains are similar to those of the Ladron Mountains in lithology and occurrence, but their limited exposure and distance from the Rio Salado reduces their importance as a source area for runoff into the Rio Salado.

2.2.1.2. Upper-Paleozoic Rocks

Rocks of Mississippian through Permian age underlie the northeast margin of the drainage basin. Representative units include the limestones, sandstones, and siltstones of the Pennsylvanian Magdalena Group and the Permian Abo, Yeso, and San Andres Formations. The Yeso and San Andres Formations contain intercalated beds of gypsum. Differential weathering of the Paleozoic rocks has led to the formation of irregular topography north of the Rio Salado between The Box and Puertecito (see Plate 2 for locations). Depending upon exposure, structural attitude, and degree of dissolution of the limestone, these rocks may serve as important sources of ground-water recharge, as well as sites of localized discharge. The near-perennial streamflow of the Rio Salado in the area of The Box is primarily a result of springs within the Pennsylvanian limestone walls (Spiegel, 1955). The source of this water is to the north along the southwest flank of the Ladron Mountains where several hogbacks are crossed by low-order ephemeral streams which carry runoff from the Precambrian rocks of the Ladron Mountains. A similar situation occurs at Riley Spring which surfaces along the contact between the Permian San Andres formation and the overlying mudstones and shales of the Triassic Chinle within the channel of the Rio Salado. This spring is the source of considerable input of water into the channel of the Rio Salado, and contributes greatly to the perennial flow of the Rio Salado along the reach downstream through Riley. The area surrounding The Box and portions of the reach between Riley and Puertecito are the only places within the basin where the mainstem of the Rio Salado or any of its major tributaries cross limestone or any other rocks of Paleozoic age.

2.2.1.3. Mesozoic Rocks

Much of the drainage basin of the Rio Salado is underlain by rocks of Mesozoic age. The most important are the mudstones, siltstones, and sandstones of the Triassic Chinle Formation; and the near-shore marine to continental clastic rocks of the Cretaceous System.

Exposures of the Chinle Formation are limited to the Riley-Puertecito area. Along the mainstem between Riley and the junction with Canada Bonita the Rio Salado has cut a narrow canyon into the Chinle Formation. The thickness of channel alluvium along this reach is presumed to be thin, and there are several exposures of the mudstone and siltstone facies of the Chinle Formation along the bottom and sides of the channel. The lower contact of the middle, resistant sandstone unit of the Chinle Formation roughly parallels the Rio Salado. This suggests that the Rio Salado between Puertecito and Riley preferentially follows the imcompetent mudstone and siltstone facies of the Chinle Formation, bordered to the south by the overlying, resistant sandstone facies of the Chinle Formation. Several springs occur at the facies contact along this reach. The Chinle Formation floors a large north-south trending basin just west of Sierra Lucero. However, Quaternary alluvial fill has all but covered the Chinle Formation within this basin, and exposures are limited to scattered outcrops. A narrow, fault emplaced wedge of the Chinle Formation crosses the channel of the Rio Salado adjacent to the west edge of the Red Lake Fault just east of D Cross Mountain.

The Cretaceous System includes the Dakota Sandstone, the Mancos Shale, the Tres Hermanos Formation, and the Mesa Verde Group, which includes the Gallup Sandstone, and the Crevasse

Canyon Formation. Of these units, the Crevasse Canyon Formation is the most ubiquitous, and is exposed throughout much of the basin interior from the Riley-Puertecito area westward. Differential erosive and weathering characteristics of rocks of the Cretaceous System contribute to the major landscape elements of the basin. Resistant sandstones typically form the crests of mesas and cuestas and less competent shales and siltstones form the adjacent valleys (Tonking, 1957). Landslide deposits commonly occur where large blocks of resistant Dakota Sandstone have slid downslope across the incompetent Chinle Shales, and where Cretaceous Sandstones have similarily slid off of mudstones of the Mancos Shale (Tonking, 1957; Osburn, 1982). The sandstones, mudstones, and shales of the Crevasse Canyon Formation contain thin intercalated beds of coal, dolomite, and limestone (Osburn, 1982). Large ironstone concretions have been documented within the Crevasse Canyon Formation (Tonking, 1957; Osburn, 1985), and have been observed along the channel of Miguel Chavez Canyon just north of Red Lake Ranch.

2.2.1.4. Cenozoic Rocks

2.2.1.4.1. TERTIARY SYSTEM. Rocks of Tertiary age crop out throughout the basin, and comprise the majority of bedrock exposures within the basin. The Tertiary System contains a wide variety of rock types and represents a considerable range of geologic processes. Included within the Tertiary System are the Eocene Baca Formation of continental intermontane basin fill (Cather and Johnson, 1984); the prograding alluvial fan volcanoclastics and associated flows of the Oligocene Spears Formation (Osburn, 1982; Massingill, 1979); the late Oligocene Hells Mesa and A-L Peak Tuffs; the Neogene LaJara Peak Basaltic-Andesite and associated mafic intrusives; and the Late Miocene-Pleistocene Santa Fe Group (Massingill, 1979).

The Baca Formation comprises a wide range of fan, lacustrine, meanderbelt, and arroyo-fill facies which represent deposition into the extensive Baca basin during Eocene time (Cather and Johnson, 1984). Principal exposures of the Baca Formation within the Rio Salado drainage basin occur as broad outcrops of redbed sandstone, siltstone, shale, and conglomerate along the north slopes of the Datil, Gallinas, and Bear Mountains.

The Oligocene Spears Formation consists of several distinct, mappable, lenticular units of moderately to poorly welded ash-flow quartz-latite tuffs, tuff breccias, laharic breccias, tuffaceous sandstones, pebble-cobble conglomerates, agglomerates, and basaltic-andesite flows, with occasional intercalated thin beds of siltstone and claystone (Givens, 1957; Tonking, 1957; Massingill, 1979; Harrison, 1980; Osburn, 1982). Principal exposures of the Spears Formation are confined to the higher elevations of the Datil, Gallinas, and Bear Mountains. The Spears Formation weathers easily to form rounded hills and ridges (Givens, 1957). The conglomeratic units within the Spears Formation are considered to be good aquifers (Tonking, 1957).

Several springs occur within the Bear Mountains along the upper contact of the Spears Formation with the overlying Hells Mesa rhyolitic tuff (Tonking, 1957). In the Datil and Bear Mountains, many springs occur within the Spears Formation itself, presumably in response to intraformational facies changes as well as to lithological differences between units.

The Spears Formation forms a basal volcanoclastic apron upon which the remainder of the Tertiary units were deposited (Massingill, 1979). The rhyolitic ash-flow tuffs of the Hells Mesa and A-L Peak Tuffs were deposited disconformably upon the Spears Formation along a north-sloping surface in response to the eruption of volcanic centers in the Magdalena and San Mateo Mountains (Massingill, 1979). Exposures of the Hells Mesa and A-L Peak Tuffs occur in the Datil, Gallinas, and Bear Mountains. The Hells Mesa Tuff is typically moderately to poorly welded, crystal rich, and contains interbeds of water-laid volcanic conglomerate (Givens, 1957; Willard and Givens, 1958; Harrison, 1980). The A-L Peak Tuff is crystal poor, moderately to densely welded, and contains interbedded basaltic-andesite flows (Harrison, 1980). Exposures of the Hells Mesa and A-L Peak Tuffs are limited to the higher elevations along or just below the crests of the Datil and Bear Mountains.

The remainder of the Neogene volcanic units includes a number of isolated, although possibly correlated basalt and basaltic-andesite flows throughout the center and northern portions of the basin. Several different episodes of volcanism have been identified, with distinct pulses occurring from the Late Oligocene through the Pliocene and into the Pleistocene. Many volcanic vents and necks have been identified as source areas for the individual flows. Correlation of basalt flows, source area distribution, and elevation suggests deposition onto widespread geomorphic surfaces which may have existed during Pliocene and Pleistocene times (Jicha, 1958; Massingill, 1979) (eg.the Ortiz surface of Wright <1946>). However, exact reconstruction of the surfaces is complicated by post-emplacement normal faulting and vertical tectonism.

The most important Pliocene-Pleistocene flows include: the La Jara Peak basaltic-andesite (Tonking, 1957; Massingill, 1979; Meyerson, 1979), which crops out along the crest of the Bear Mountains; the Sierra Lucero basalts (Jicha, 1958) which cap Chicken Mountain along the western slope of Sierra Lucero and appear to have been extruded onto portions of the Miocene-Pliocene Sierra Lucero Surface (Jicha, 1958); the basalt and basaltic-andesite of the Gallinas and Datil Mountains which is in part equivalent to the La Jara Peak basaltic-andesite (Willard and Givens, 1958; Osburn, 1982); the Blue Mesa olivine-tholeiite basalts of the northeastern Datil Mountains (Harrison, 1980); the vesicular porphyritic Santa Fe Basalts of Table Mountain, D Cross and Tres Hermanos, Techado, and Victorino Mesas (Givens, 1957; Osburn, 1984, 1985); and the basalt of Twin Peaks (Coffin, 1981); Some of the older flows contain interbedded units of the Lower Santa Fe Group (Massingill,1979), whereas the younger flows overlie and are interbedded with channel-fill of the Santa Fe Formation on Table Mountain and Tres Hermanos Mesa (Givens, 1957). Depending on the thickness of individual flows, vesicularity, the amount of fracturing, and the degree of weathering and soil formation, the basalt-capped mesas may serve as important source areas for ground-water recharge.

Concomitant with the onset of widespread volcanism during the Late Oligocene, numerous mafic to intermediate dikes, stocks, and sills were emplaced (Tonking, 1957; Massingill, 1979; Osburn, 1982). The majority of these intrusions occur north of the Bear Mountains between Riley and Puertecito and northward. The dikes trend predominantly north-northwest, and are typically less than 30 feet thick (Tonking, 1957), and average just over 9 feet thick (Massingill, 1979). The majority of the dikes appear to have been emplaced along the traces of the many north-trending normal faults which were developed during the time. A considerable number of the dikes cross the present channel of the Rio Salado between Riley and Puertecito, and are locally exposed along the channel bottom and banks.

The Santa Fe Group is made up of the Miocene Popotosa Formation, and the Pliocene-Pleistocene Sierra Ladrones Formation. The Popotosa Formation consists of bolson-fill, fanglomerates, and piedmont slope deposits which were deposited into the Rio Grande Rift and the Popotosa Basin during Middle Miocene (Machette, 1978; Massingill, 1979). The Popotosa Formation consists of locally derived subangular pebbles,cobbles, and boulders that have been well cemented with calcite. The Sierra Ladrones Formation is made up of typically weakly cemented alluvial fan, piedmont slope, alluvial flat, flood plain, and stream deposits. The La Jencia Basin and the Mulligan Gulch Graben between the Bear and Gallinas Mountains which were included within the Popotosa Basin were filled with rocks of the Santa Fe Group prior to segmentation of the basin during the late Pliocene (Massingill, 1979). Members of the Santa Fe Group are exposed along erosional scarps within the La Jencia Basin, and along the west flank of the Bear Mountains. Other less extensive outcrops of the Santa Fe Group occur within a belt which runs approximately along the central axis of the Rio Salado drainage basin (Osburn, 1984).

Isolated remnants of late Pliocene to Pleistocene piedmont and pediment gravels occur throughout the western half of the basin, along the north slopes of the Datil, Gallinas, and Bear Mountains, and along the western slope of Sierra Lucero. The oldest piedmont gravels generally indicate transport to the north, and deposition on a deeply eroded, northward sloping surface (Mayerson, 1979; Harrison, 1980; Coffin, 1981; Osburn, 1982), which may be approximately correlative to the ancestral Ortiz Surface. The youngest piedmont and pediment gravels grade towards the ancestral Rio Salado (Osburn, 1982; Mayerson, 1979). Development of the pediments and piedmonts appears to have continued into the Pleistocene, and may be contemporaneous with the later stage deposition of the Upper Santa Fe Group.

Consequently, Tertiary pediment and piedmont gravels have frequently been mapped as members of the Santa Fe Group (Givens, 1957; Harrison, 1980).

2.2.1.4.2. QUATERNARY SYSTEM. The Quaternary System within the drainage basin represents a variety of surficial processes, including alluvial fan, stream channel and terrace, piedmont slope, eolian, spring, and colluvial deposition, as well as several episodes of volcanic activity. At least three separate Pleistocene basalt flows cap Mesa del Oro in the northern portion of the basin (Jicha, 1958). Jicha (1958) suggests that these flows were extruded onto the Pleistocene Ortiz Surface.

Spring deposits of banded travertine occur within the Upper Santa Fe Formation 600+ feet above the Rio Salado from The Box westward nearly to Puertecito (Massingill, 1979). These deposits may be Late Pliocene to Early Pleistocene in age. Massingill (1979) postulates that the travertine was deposited in a warm, spring-fed lake which may have existed on the Plio-Pleistocene Ortiz Surface. Similar, possibly related travertine deposits occur on a surface which is correlated to the Ortiz Surface along the north end of Mesa del Oro (Jicha, 1958).

The travertine deposits described by Massingill (1979) have also been studied by other workers. Most recently, Barker (1983) has investigated the origin of the travertine deposits (generally referred to as the Riley Travertine). Barker concludes that the Riley Travertine is nonpedogenic, and is primarily the result of proximal and distal secondary carbonate deposition related to lateral groundwater flow. Barker (1983) further postulates that during the time of deposition of the Riley Travertine (Plio-Pleistocene), the drainage was from the north to the southeast throughout much of the area occupied by the Riley Travertine. Near the southernmost portion of the travertine area, the flow merged with an east-flowing drainage which flowed towards the Rio Grande just north of San Lorenzo Canyon. The Riley Travertine generally slopes several degrees to the south and southeast. However, near the southern limit of its occurrence just south of the Rio Salado approximately between La Jencia and Silver Creeks, the Riley Travertine slopes less than one degree to the south, and one to two degrees to the west (Barker, 1983).

Quaternary alluvial fan and piedmont gravels and sands overlie the Santa Fe Formation within the La Jencia Basin and the smaller basins of Canada Bonita, Gallegos Creek, and along the slopes of the Datil, Gallinas, and Bear Mountains (Massingill, 1979; Meyerson, 1979; Harrison, 1980; Laroche, 1980; Osburn, 1983, 1984). The many fans along the mountain fronts are typically coalesced into broad bajadas which slope towards the present day drainage. However, Massingill (1979) concludes that the incision of the present channel of the Rio Salado along the north end of the La Jencia Basin post-dates the onset of Quaternary piedmont development in the immediate area, since the Rio Salado dissects the piedmont gravels as well as the underlying Santa Fe Formation.

Older Quaternary alluvium has been mapped adjacent to the course of the present drainage network. These deposits represent old channel and valley fill, and tributary mouth alluvial fans which are dissected by the present drainage (Massingill, 1979; Laroche, 1980). Younger Quaternary valley alluvium occurs along the course of the present drainage network. This alluvium consists of Rio Salado and tributary channel sands and gravels, and flood plain deposits. Several flights of terraces have been mapped adjacent to the channels of the Rio Salado and several major tributaries (Jicha, 1958; Mayerson, 1979; Machette, 1978). At least four terraces have been identified along a reach of the Rio Salado near Riley (Love, 1987, personal communication). Because of the difficulty in distinguishing between young and old alluvium, both have often been mapped together as undifferentiated Quaternary Alluvium (Coffin, 1981).

The investigation and correlation of terraces along the Rio Salado and major tributaries is difficult, due to the lack of preserved exposures. Channel entrenchment and subsequent valley-wall erosion and badland development have apparently destroyed most of the older terraces.

Tonking (1958) and Meyerson (1979) have mapped Quaternary pediment gravels in the western Bear Mountains. Near the mountains the pediment surface on which the gravels rest slopes approximately 2 degrees northward, becoming discontinuous as it approaches the Rio Salado near Puertecito. The surface is graded to approximately 100 feet above the elevation of the present-day channel of the Rio Salado.

Talus, avalanche, landslide, and colluvial deposits form extensive aprons around the basalt and resistant sandstone-capped mesas and ridges. Although these deposits are isolated features, the total area that they encompass is quite large. Because of this, and the generally coarse nature of the materials and irregular topography, it is likely that these deposits, along with the mesa-capping fractured and vesicular basalts, contribute greatly to the overall ground-water recharge of the basin. This may be evidenced by the occurrence of springs along the base of Mesa del Oro and Techado Mesa.

Considerable eolian material is present adjacent to and within the mainstem of the Rio Salado throughout much of its reach. A major dune field exists north of the main channel, near the mouth of the Rio Salado (Machette, 1978). Blow sands occur on the top of Techado Mesa as discontinuous, topographically distributed patches (Osburn, 1985), and along tributaries to the Rio Salado (Laroche, 1980).

2.2.2. GEOLOGIC AND TECTONIC HISTORY

Although the region has undergone a complex series of geologic and tectonic events throughout geologic time, only those events which have an obvious direct bearing on the development of the morphology and drainage network of the Rio Salado drainage basin need be considered here. The tectonic events which have most influenced the present-day drainage network are: Laramide compressional folding and uplift; Neogene extensional faulting, drag folding, and associated volcanic activity; Neogene onset of epeirogenic uplift of the Colorado Plateau; and the Plio-Pleistocene onset of uplift associated with the Socorro Magma Body.

The Laramide orogeny occurred during the period 80 to 40 m.y. B.P. as a result of east-west compressive forces (Jicha, 1958; Cather and Johnson, 1984). Several uplifts and sags, along with low, broad folds occurred in the area of the Rio Salado drainage basin. The most prominent of these features are the Lucero Uplift, which marks the eastern boundary of the Colorado Plateau; the Zuni uplift to the northwest of the drainage basin; the Mogollon highlands to the south and far-west; the Baca basin within and to the west of the Rio Salado drainage basin; and the Acoma sag between the Lucero and Zuni uplifts (Cather and Johnson, 1984). Most of these features had been leveled by erosion and deposition to an extensive surface of low relief prior to the onset of Neogene tectonic activity (Massingill, 1979; Mayerson, 1979; Harrison, 1980). However, their presence has greatly influenced the distribution of lithologic units throughout the basin.

Late Oligocene-Neogene extensional faulting, horst and graben related mountain building, and volcanic activity corresponds to the relaxation of Laramide compressional forces and the development of tensional forces contemporaneous with the opening of the Rio Grande Rift (Jicha, 1958; Mayerson, 1979; Harrison, 1980; Laroche, 1980). Numerous north-trending normal faults and associated north-trending mafic to intermediate dikes were developed near the center of the basin during this period. The distribution of faults and dikes along the center-axis of the basin increases in number from west to east, and is suggestive of the effect of activity along the Rio Grande Rift (Laroche, 1980). Most of the faults have displacements in the range of tens of feet, however, several major faults and fault zones have experienced considerable movement. The important north-trending fault zones which cross the channel of the Rio Salado are: the D Cross, Red Lake, and Puertecito fault zones. Faulting has resulted in some disruption in the attitude of the previously near-horizontal dip of older strata. These effects are relatively minor throughout most of the area except where drag and reverse drag folding has accompanied faulting (Mayerson, 1979). Several faults have been active up to recent times (Massingill, 1979; Laroche, 1980). Fault-induced springs and seeps occur where less permeable rocks have been juxtaposed against more permeable, water-bearing units (Givens, 1957; Mayerson, 1979).

Starting around 24 m.y. B.P. the Southern Colorado Plateau began to undergo epeirogenic uplift. Uplift has continued through the Neogene and Quaternary, on through to Recent time. Based upon the correlation of Plio-Pleistocene geomorphic surfaces with the present day elevation of the outward-flaring volcanic necks of La Jara and La Cruz Peaks, Massingill (1979) has estimated that the southern Colorado Plateau has risen 700 feet during the past 3.5 million years. The most evident result of the uplift has been the southward tilting of previously near flat-lying strata and structural features along the southern margin of the Colorado Plateau (Massingill, 1979). A further consequence of the uplift has been the reversal of the predominantly northward flowing drainage in the area which presently encompasses the northern portion of the Rio Salado drainage basin. It appears that this reversal occurred during the late Pliocene, and may indicate the onset of development of the ancestral Rio Salado (Osburn, 1984).

Beginning in the late Pliocene to early Pleistocene, rapid uplift of the land surface has occurred in response to inflation of the Socorro Magma Body (Reilinger et al, 1980; Larsen and Reilinger, 1983; Ouchi, 1983; Sanford, 1983; Sanford et al, 1983; Larsen et al, 1986). The area of uplift is approximately coincident with the extent of the Socorro Magma Body, and includes most of the lower portion of the Rio Salado drainage basin. The zone of maximum uplift occurs approximately at the confluence of the Rio Salado with the Rio Grande. The rate of uplift during about the last 20,000 years is thought to be on the order of 1 to 5 mm per year. This rate of movement is about two orders of magnitude greater than the rate of uplift of the Colorado Plateau (Massingill, 1979), or Late-Pliocene-through-Quaternary vertical movement along some of the faults associated with the Rio Grande Rift (Chamberlin, 1983).

2.3. Quantitative Basin Parameters

Quantitative information about the Rio Salado drainage basin was developed during the course of the present study. Reference material included U.S.G.S. topographic maps, various aerial photographs, and first-hand aerial and land-based observations. At the outset of the study it was hoped that a detailed, quantitative investigation of the Rio Salado drainage basin would provide information to be used in conjunction with basin geology, streamflow, and channel network information in order to explore the functioning of the entire system. Primary data derived include main and tributary basin areas, and hypsometric information.

Drainage area and hypsometric information (Table 2) was computer generated from a large data base, using a series of terrain analysis routines developed specifically for the present study (see volume II). The data base used for the analysis was compiled from U.S.G.S. 7.5 minute series topographic maps, and consisted of 3635 sets of point location and elevation data. Point locations were selected at the intersections, or nodes, of one-kilometer coordinate lines of the Universal Transverse Mercator (UTM) grid system, which is indicated on the U.S.G.S topographic maps. The coordinates of the UTM grid system are based on the distance east (easting) and north (northing) of the reference origin of the grid. Each grid cell defined by the UTM

Table 2: Basin Parameters

Basin	Order	Area (km 2)	Hypsometric Integral(%)
Rio Salado	7	3635	40.67
Canada Popotosa	4	26	33.27
Silver Creek	4	25	49.90
Mule Canyon	4	13	34.04
La Jencia Creek	6	781	33.56
Ligon Creek	4	108	41.44
Arroyo Gato	5	204	24.33
Hop Canyon	4	33	47.20
Arroyo Gato	4	154	16.69
La Jencia Creek	5	265	48.67
Arroyo Montosa	4	65	42.04
La Jencia Creek	4	163	44.50
Rio Salado	6	2627	37.00
Bear Springs Canyon	5	87	43.00
Cedar Springs Canyon	4	13	37.88
Bear Springs Canyon	4	55	36.68
Unnamed I	4	14	37.50
Canon de las Cabras	4	24	30.00
Unnamed II	4	41	31.65
LaJara Canyon	4	101	41.16
Canada Bonita	5	433	33.14
Juan de Dios Creek	4	20	41.25
Field Ranch Creek	4	45	22.72
Waterbury Draw	4	108	38.29
Chicken Mountain Draw	4	46	37.61
Canada Bonita	4	107	38.44
Cottonwood Draw	4	44	23.64
Jaralosa Creek	5	156	41.06
Chavez Canyon	4	54	35.28
Jaralosa Creek	4	88	49.55
Alamo Creek	4	46	32.28
Navajo Creek	4	56	33.93
Jaramillo Canyon	4	60	39.83
Gallegos Creek	5	234	36.75
Canon de la Mosca	4	39	48.27
Gallegos Creek	4	34	51.76
Dog Springs Canyon	5	121	48.90
Chavez/Old Canyon	4	38	60.79
Dog Springs Canyon	4	55	43.77
Miguel Chavez Canyon	5	222	45.08
Unnamed III	4	22	31.36
Pine Springs Canyon	4	37	45.61
Wild Horse Canyon	4	13	53.27
Miguel Chavez Canyon	4	29	50.76
Rio Salado	5	554	35.03
Rock Tank Canyon	4	37	41.01
Pasture Canyon	4	40	40.50
Rock House Canyon	4	12	43.75
Red Canyon	4	92	34.46
Ox Springs Canyon	4	67	29.74
Harrington Canyon	4	30	42.17
Third Canyon	4	21	47.50
WH Canyon	4	18	33.33
Rio Salado	4	88	38.64

grid is 1 square kilometer, and has four associated nodes - one at each corner. For each node, UTM easting and northing were read directly from the UTM grid superimposed on each U.S.G.S. topographic map, and were entered into the data base as X,Y respectively. Nodal point elevations were interpolated from adjacent contours on the USGS topographic maps.

2.3.1. BASIN AREA

Drainage areas were computer-generated for the Rio Salado drainage basin, and for selected nested tributary sub-basins. The selection of tributary basins to be included in the analysis was based upon basin order, as defined by the highest order channel included within the tributary basin (channel ordering is discussed in section 3.1.2.). All tributary sub-basins of order four and higher were included in the analysis.

The routine for generating sub-basin areas used several data bases for performing the calculations. The nodal point location and elevation data base was used to supply raw data to an algorithm which computed sub-basin areas based upon the number of nodal points enclosed within the boundaries of each sub-basin. The algorihm utilized a second data base which contained the UTM coordinates of the drainage divides between the sub-basins. Once sub-basin boundaries were established, the computer routine summed up the number of nodal points included within the boundaries. This method used the assumption that the number of nodal points within a sub-basin approximates the area enclosed within the boundaries, since each nodal point represents one grid cell of 1 km2. Each grid cell was uniquely referenced by one node located in the southwest corner of the cell. The assumption that the number of inclusive nodes approximates sub-basin area is most valid for larger sub-basins. However, for several randomly selected fourth order sub-basins, a comparison between areas calculated by the above method with areas derived from planimetering suggests that the computer method is correct to approximately +/- 5%.

The sub-basin boundary data base was developed directly from basin boundaries drawn onto U.S.G.S. topographic maps. Boundaries were outlined on the topographic maps according to obvious topographic highs and surface-water divides. Nodal points were selected for inclusion according to the proportion of the grid cell they represent that lies within the boundaries of the sub-basin. A particular node was included if over 50% of the corresponding cell lay within the sub-basin of interest.

2.3.2. TERRAIN ANALYSIS

Computer-generated hypsometric information was obtained for all sub-basins of fourth and higher order. The computer routine used for the analysis referenced the X,Y,Z and basin-boundary data bases. Algorithms used for the generation of hypsometric curves and hypsometric integrals were based on the definitions proposed by Strahler (1952). Nodal point elevations were first normalized:

$$Z' = (Zi - Zmin)/(Zmax-Zmin)$$

Where Z' is the normalized elevation of a particular node; Zi is the absolute elevation (FMSL) of the node; Zmin and Z max are the elevations of the lowest and highest nodes, respectively, within the sub-basin of interest. Normalized elevations were then placed into one of 20 equally spaced groupings between 0 and 1. The number of nodes within each of the groups (normalized to the total number of nodes within the sub-basin) was then used to obtain a histogram approximation of the frequency distribution of normalized elevations. The normalized cummulative distribution of the histogram gives the hypsometric curve. Values for the hyposmetric integral were obtained by numerically integrating the area under the hypsometric curves.

Table 2 lists all fourth and higher order sub-basins, basin order, area, and hypsometric integral. The Rio Salado and sub-basins are nested in Table 2 in order to reflect basin hierarchy. Hypsometric curves are included in Appendix A.

3.0 THE RIO SALADO CHANNEL NETWORK

The Rio Salado rises along the northwest flank of the Datil Mountains in eastern Catron county, and empties into the Rio Grande approximately 66 miles (92 river miles) to the east. The channel is fairly steep, sand bedded, and braided throughout most of its reach. Several large tributaries empty into the Rio Salado, including: La Jencia Creek, which drains portions of the Mulligan Valley, the Bear and Magdalena Mountains, and the La Jencia Basin; Canada Bonita, which drains the west slope of Sierra Lucero and the southeast portion of Mesa del Oro; Jaralosa Creek and Dog Springs Canyon, which drain the east and north slopes of the Gallinas Mountains; Gallegos Creek, which drains Broom Mountain, Victorino Mesa, and portions of Mesa del Oro; and Miguel Chavez Canyon, which drains Techado (Bodenheimer) Mesa. The channel network formed by the Rio Salado and its tributaries is essentially dendritic, except near the Bear Mountains where it has developed a radial pattern. Further characterization of the channel and drainage network requires the development of quantitative parameters.

An investigation of certain quantitative parameters of the channel and drainage network of the Rio Salado was undertaken during the course of this study. Among the parameters investigated are: mainstem and tributary length and longitudinal profiles, channel geometry, channel sinuosity, valley side slope, bed and bank material particle size analysis, and channel gradient.

3.1. Map Analysis

3.1.1. CHANNEL DELINEATION

The initial task in the study of the drainage network was the definition and delineation of channels. There has been considerable debate among workers as to which method for channel delineation is the most representative of actual field conditions. Most workers rely on existing topographic maps for information about channel networks. However, the main topic for debate is whether or not to use the map compiler's definition of channels verbatim. Morisawa (1957, 1961), Schneider (1961), and Werritty (1972), among others, have addressed the issue, and have arrived at sometimes conflicting conclusions.

Since an effort has been made throughout the present study to eliminate operator bias and subjectivity, the channel network used was that defined by dashed and solid blue lines on U.S.G.S. 7.5 minute series topographic maps. This approach seems reasonable for the ephemeral channels of the Rio Salado net for several reasons:

i) The delineation of channels on the 7.5 minute series maps is based upon the visual identification of both wet and dry channels according to established criteria. The only opportunity for subjectivity is on the part of the presumably well trained map compiler. No additional bias is introduced. This provides a consistent method for channel delineation.

ii) Ephemeral arroyos and rills in semi-arid regions are easily distinguished on the aerial photographs used for map compilation.

iii) The extreme number of contour crenulations which occur as a result of the mountainous and highly irregular topography of the Rio Salado drainage basin precludes the use of contour crenulations as a basis for channel definition and extension.

iv) Leopold and Miller (1956) have demonstrated that only direct field observation can identify all of the smallest fingertip rills in an ephemeral system. They found that first order channels as identified on a 1:32000 map were in actuality fifth order channels as identified in the field. The scope of the present study prohibited such extensive fieldwork.

v) Gregory, as cited by Werritty (1972), postulated that contour crenulations might occasionally identify fossil drainages which are not integrated into the modern day network.

vi) On all of the topographic maps which encompass the Rio Salado drainage basin, the first order channels which cross over the borders of the maps are continuous across the map boundaries in all but a very small number of cases. This seems to verify the correct and consistent application of U.S.G.S channel identification criteria by the various map compilers.

vii) Most importantly, the definition of first order channels need not be absolute for the present analysis (first order channels are defined for this present study to be those channel segments which are delineated by blue lines on U.S.G.S. 7.5 minute series topographic maps whose upstream ends terminate without connection to other blue-line channel segments). Even if first order channels as defined on 7.5 minute series maps are in reality made up of several lower order channels, it may be safe to assume that at very least they represent channel segments of similar but undetermined order. Leopold and Miller (1956) used this assumption to correct channels of map-defined order to field observed order by simple order addition.

3.1.2. CHANNEL ORDERING

The channel network was classified according to two schemes: stream ordering as proposed by Strahler (1952), and the link magnitude scheme of Shreve (1966). It was felt that more flexibility for future analyses would arise from the use of both approaches. In addition, each of the methods includes different information about the drainage network. For example, the link-magnitude method carries direct information about the number of sources upstream from any point along the network, which may be useful in estimating the effective upstream drainage area influencing streamflow and channel geometry at that particular point. The Strahler stream ordering method carries information about the fit and inter-relationship of channels within the network.

The Strahler method of stream ordering is based upon the following principles: stream order increases by one wherever two confluent streams of equal order join; affluent streams of lower order do not affect the order of the dominant stream; source streams (or exterior links; In Shreves methods these are equivalent to first order channel segments) are assigned order one. The link magnitude scheme proposed by Shreve (1966) simply states that the magnitude of a stream at any point along its length is equal to the number of exterior (source) links upstream of that point.

First order streams - equivalent to magnitude one, exterior links in the Shreve system - were highlighted in blue on the U.S.G.S. topographic maps. First order streams were identified on the topographic maps as the generally-dashed blue lines, drawn by the cartographer, whose upstream ends terminate without connection to other stream segments, and are usually greater than 0.5 km long. The point where two first order streams join was taken to be the head of a second order channel, which was highlighted in orange on the U.S.G.S. topographic maps. The process was continued until the entire drainage network was delineated. Each order was assigned a different color. Link magnitude was penciled in alongside the terminus of each link. Appendix B contains the working topographic maps.

3.1.3. PARAMETER MEASUREMENT

Quantitative information about the channel network was extracted once the drainage network had been clearly defined on the working maps. Upstream distances from the mouth along the mainstem of each order 4 and higher system were recorded, as well as channel elevation and link magnitude. This information was entered into a computer data base.

All channel distances were measured on the maps using dividers set at 0.19 inch (400 feet map scale). The dividers were stepped upstream from the mouth, and the distance in feet from mouth, channel elevation, tributary magnitude, and the UTM coordinates of the tributary-mainstem junction were recorded into the data base. Mainstem order, and tributary orientation (i.e.: right - left handed tributary entry) were also recorded.

Every effort was made to accurately measure even the most sinuous channels. Some approximation is inherent in taking the measurements because of the relatively coarse setting of the dividers. Distances measured along extremely sinuous channels are therefore probably shorter than the channels are in reality, but a compromise had to be achieved between underestimation and the ability to manipulate the dividers. It was found that an increase in measurement error resulted from divider settings of less than 0.17 inches because of difficulty in lifting the divider points off the paper, and flex of the divider legs. When divider settings were less than 0.17 inches, measurements were repeatable to within 10%. With the divider points set 0.19 inches apart, measurements were repeatable to within 4%. Channel sinuosity was obtained from the ratio of the distance between adjacent contour crossings, as measured along the channel, to the straight-line distance between the contour crossings.

Valley cross sections were measured in order to allow future investigation of the fit of the present-day Rio Salado into its valley. This was accomplished by using dividers to step off the perpendicular distance to points 20, 40, 60, 80, and 100 feet in elevation above the bottom of the present-day channel. Measurements were taken at each contour line crossing of the channel, and entered into a computer data base. Valley cross sections were used to generate valley side slope information, which is listed in Table 3.

Channel gradient was measured by stepping the dividers along the dashed blue line within the main channel represented on the topographic maps. Channel gradient was measured on the maps for each of the field station locations (discussed below). The channel reach used for gradient measurement was typically 2000 feet in length, centered on the field station location.

Table 3 lists of the parameters derived from map analysis. Fourth and higher order networks are included in the table.

3.2 Field Investigation

Since an initial intent of the present study was to identify any interrelationships which may exist between the various hydrologic and morphometric parameters of the Rio Salado, a field data collection program to quantify channel characteristics was considered essential. Data obtained during the field portion of the study supplements information developed through map and aerial photographic interpretation.

Field sites were located along the mainstem of the Rio Salado, and at selected points along major tributaries. The locations of field stations are identified on Plate 1. A total of 16 field sites were investigated. The geographical distribution of the field sites was based upon the need for information about the entire course of the Rio Salado. Several of the sites were included specifically to investigate the effect of major tributaries on the main channel.

Wherever possible, notes of the particular features of each station were taken, and reconnaissance maps were drawn. Information typically included a plan view of the channel reach showing the location of the main channel, inner channels, the thalweg, bars, banks, vegetation, terraces, cobble and boulder accumulations, location of the cross section surveyed, and channel and bank geology. Any obvious signs of recent highwater marks were noted.

Table 3: Channel Network Parameters

Stream	Order	Magnitude	Distance From Mouth to Rio Grande (feet)	Length of Mainstem (feet)	Elevation of Head of Main-Stem (FMSL)	Elevation of Mouth of Main-Stem (FMSL)	Mainstem Channel Relief (FT)	Overall Channel Slope (%)
Rio Salado	7	2482	0	489230	8760	4678	4082	0.83
Canada Popotosa	4	28	44920	57145	7518	4939	2579	4.50
Silver Creek	4	24	60550	35940	5748	5036	712	2.00
Mule Canyon	4	22	74300	29910	6630	5110	1520	5.10
La Jencia Creek	6	371	84500	185625	7390	5168	2222	1.20
Ligon Creek	4	38	98800	70380	6581	5287	1294	1.80
Arroyo Gato	5	131	187570	80500	7179	6270	909	1.10
Hop Canyon	4	32	206130	35135	8318	6486	1832	5.20
Arroyo Gato	4	91	206130	61940	7179	6486	693	1.10
La Jencia Creek	5	160	187570	82555	7390	6270	1120	1.40
Arroyo Montosa	4	39	210360	55840	7440	6526	914	1.60
La Jencia Creek	4	113	210360	59765	7390	6526	864	1.40
Rio Salado	6	2020	84500	404730	8760	5168	3592	0.89
Bear Springs Canyon	5	89	98400	109130	7620	5280	2340	2.10
Cedar Springs Canyon	4	17	136970	33600	7550	5868	1682	5.00
Bear Springs Canyon	4	53	136970	70560	7620	5868	1752	2.50
Unnamed I	4	14	103510	32460	7040	5308	1732	5.30
Canon de las Cabras	4	30	109790	49570	7040	5340	1700	3.40
Unnamed II	4	24	111020	49560	7760	5347	2413	4.90
LaJara Canyon	4	97	181300	83840	7358	5691	1667	2.00
Canada Bonita	5	267	201720	133840	7420	5771	1649	1.20
Juan de Dios Creek	4	17	207320	41260	6733	5787	946	2.30
Field Ranch Creek	4	27	249040	44975	6662	5924	.738	1.60
Waterbury Draw	4	49	252560	57630	7365	5934	1431	2.50
Chicken Mountain Draw	4	36	272120	56240	7506	6037	1469	2.60
Canada Bonita	4	57	272120	63440	7420	6037	1383	2.20
Cottonwood Draw	4	30	228900	49612	6678	5901	777	1.60
Jaralosa Creek	5	138	232550	109160	7760	5921	1839	1.70
Chavez Canyon	4	46	251050	85740	8330	6100	2230	2.60
Jaralosa Creek	4	70	251050	90660	7760	6100	1660	1.80
Alamo Creek	4	31	246880	48180	6830	5998	832	1.70
Navajo Creek	4	38	254480	69280	7673	6032	1641	2.40
Jaramillo Canyon	4	38	265650	50025	7170	6089	1081	2.20
Gallegos Creek	5	133	287600	110645	7372	6235	1137	1.00
Canon de la Mosca	4	23	359735	43830	7580	6666	914	2.10
Gallegos Creek	4	25	359735	38510	7372	6666	706	1.80
Dog Springs Canyon	5	97	293300	104086	8510	6262	2248	2.20
Chavez/old Canyon	4	30	335600	32150	7830	6861	969	3.00
Dog Springs Canyon	4	46	335600	61786	8510	6861	1649	2.70
Miguel Chavez Canyon	5	176	301100	132440	8040	6294	1746	1.30
Unnamed III	4	17	315805	32600	7635	6377	1258	3.90
Pine Springs Canyon	4	35	373750	36320	7680	6894	786	2.20
Wild Horse Canyon	4	16	394550	19640	7780	7125	655	3.30
Miguel Chavez Canyon	4	26	394550	38990	8040	7125	915	2.40
Rio Salado	5	447	301100	188130	8760	6294	2466	1.30
Rock Tank Canyon	4	32	321800	65755	7758	6421	1337	2.00
Pasture Canyon	4	38	349670	44040	7490	6633	857	2.00
Rock House Canyon	4	16	363740	29600	7395	6755	640	2.20
Red Canyon	4	81	372298	55720	8341	6831	1510	2.70
Ox Springs Canyon	4	55	387313	64835	8717	6946	1771	2.70
Harrington Canyon	4	27	397453	44120	7940	7012	928	2.10
Third Canyon	4	21	403300	29260	7680	7066	614	2.10
WH Canyon	4	17	416960	33610	8230	7198	1032	3.10
Rio Salado	4	76	416960	72270	8760	7198	1562	2.20
Rio Salado	3	14	450500	38730	8760	7554	1206	3.10
Rio Salado	2	6	470270	18960	8760	7838	922	4.90
Rio Salado	1	1	478950	10280	8760	8105	655	6.30

3.2.1. HYDRAULIC GEOMETRY

At each station, channel cross-sections and channel gradients were measured; sediment samples were collected, and site reconnaissance maps were drawn. Notes were taken of any information which might serve to augment the basic data set.

All channel cross sections were measured with a level and stadia rod. Leveling traverses were run perpendicular to the main channel. The leveling instrument was generally set at a control point mid-channel, and shots were taken as the stadia rod was stepped incrementally across the channel, generally in five foot increments. However, some cross sections were so irregular that smaller increments were necessary. Wherever channel bed topography changed abruptly, or where the transverse slope was steep, for example, near bars, banks, and inner, entrenched channels, increments as small as several inches were used to better define these features. The elevation of the base and top of all steep bar and bank faces was measured. The leveling equipment was recalibrated between each pair of readings.

For some stations it was necessary to establish several control points, due to excessive channel depth and/or width. This was accomplished by adjusting the level to a reference point before and after moving to a new control point. Subsequent data manipulation was necessary to reduce the assemblage of readings to referenced channel depth.

Most horizontal distances were measured with a taut steel tape stretched across the channel bottom. A horizontal measuring staff was used wherever channel bottom irregularities warranted, and near the banks where channel side slope was steep.

At most stations only one, presumably representative, cross section was measured. The location for the cross section was selected based upon apparent upstream and downstream regularity of channel dimensions, straightness of the reach, definition of banks and/or high water demarcation, and representative channel and channel bottom pattern and topography. At certain stations more than one cross section was measured. Appendix C shows the cross-sectional channel profiles for each field station.

3.2.2. CHANNEL GRADIENT

Channel gradient was measured at each station with a level and stadia rod. The standard method used was to level to a point 300 feet upstream and a point 300 feet downstream. Distances were measured along the course of the main inner channel, so that the gradient of the channel that was representative of a typical, less than bank-to-bank flow could be measured. At several stations the channel gradient was measured in 5 to 50 foot increments in an attempt to identify bed forms.

Table 4 summarizes the features of each field station.

Table 4: Channel Geometry at Field Stations

Station	Distance from Rio Grande (ft x 1000)	Strahler Order	Shreve Magnitude	Bankfull Width (ft)	Bankfull Depth (ft)	Width/Depth Ratio	Surveyed Channel Gradient (%)	Map Derived Channel Gradient (%)	Valley Side Slope (%)
S1	16.0	7	2482	678	4.59	148.0	0.60	0.63	1.9
S2	33.5	7	2481	768	4.24	181.0	–	0.61	2.9
S3	99.9	6	1884	692	6.40	108.0	0.59	0.56	6.1
S4	115.4	6	1806	510	4.40	116.0	0.49	0.50	3.6
S5a	118.0	6	1802	213	2.09	102.0	0.53	0.60	3.0
S5b	118.3	6	1802	168	2.81	59.8	0.53	0.60	3.0
S5c	117.7	6	1802	306	3.44	89.0	0.53	0.60	3.0
S6a	140.3	6	1728	454	4.94	91.9	0.38	0.42	5.6
S6b	140.0	6	1728	458	4.84	94.6	0.38	0.42	5.6
S6c	140.6	6	1728	445	4.53	98.2	0.38	0.42	5.6
S7a	168.0	6	1663	267	6.30	42.4	0.87	0.50	3.8
S7b	168.2	6	1663	250	5.91	42.3	0.87	0.50	3.8
S8	217.5	6	1222	791	3.76	210.0	0.53	0.75	1.6
S9	293.3	6	728	–	–	–	–	0.69	6.7
S10	294.3	6	631	464	4.53	102.0	0.47	0.69	6.7
S11a	299.1	6	629	301	4.57	65.9	0.44	0.33	4.4
S11b	298.9	6	629	199	4.53	43.9	0.44	0.33	4.4
S12	323.4	5	405	790	5.49	144.0	0.53	0.70	5.6
S13	349.7	5	375	493	6.62	74.5	1.80	0.74	11.2
M1	305.2	5	173	186	10.81	17.2	0.49	0.50	2.6
M2a	426.0	3	18	62	5.60	11.1	1.16	1.25	17.3
M2b	425.8	3	18	53	6.70	7.9	1.16	1.25	17.3
M2c	425.7	3	18	64	5.60	11.4	1.16	1.25	17.3
D1	294.5	5	97	188	6.30	29.9	1.16	1.02	9.7

3.2.3. PARTICLE SIZE

Sediment samples were collected at most of the field stations. Several different sets of samples were obtained at each site, primarily: random channel, low-flow channel, and overbank samples. At some locations, low-flow channel or overbank deposits were so ill defined and/or disturbed that only a random channel sample could reasonably be collected.

3.2.3.1. Sample Collection

In order to insure a thorough understanding of each site prior to sampling, the actual collection of the samples did not occur until all other field work had been completed for the day. For example, low-flow channel samples were collected from that portion of the channel which exhibited the most obvious signs of flow; a cursory identification of the deepest portion of a channel segment was not considered sufficient to guarantee consistency of low-flow channel samples from one station to another. Every attempt was made to follow a consistent sampling regimen throughout.

3.2.3.1.1. RANDOM CHANNEL SAMPLES. Random channel samples were collected from within the main channel. Each random channel sample is a composite of generally ten 100cc samples taken from approximately equally-spaced points located across the width of the channel. Before each of the ten partial samples was collected, the top inch of surface material was removed in order to avoid the inclusion of any deflation lag or aeolian material within the sample. Since the primary intention of grain size analysis within the present study is to investigate downstream changes in channel bed size characteristics, a range of particle sizes encompassing material found throughout the entire length of the main channel was chosen. Only material smaller than 2 inches was collected for analysis. The presence of larger cobbles and boulders was noted wherever possible. A further rationale for using this approach is that the inclusion of larger sized particles in an analysis based upon weight fractions would introduce considerable bias into the analysis of the small amount of material that could be collected. An unbiased, representative sample for material larger than 2 inches would require a total volume of material far in excess of that which could be readily carried from the site. Point pebble counts were not made, because it was felt that sand-sized and smaller particles would not be accounted for (Leopold, Wolman, and Miller, 1964).

3.2.3.1.2. LOW-FLOW CHANNEL SAMPLES. Low-flow channel samples were collected from locations within the main channel which exhibited signs of frequent flow, as mentioned previously. Such signs include: a well-defined, linearly continuous inner channel; distinctly different bed material; flow debris, especially aligned along a high water mark; and obvious signs of moisture. Because most of the field work was done during the late spring to mid-summer - just prior to the annual flow season - it was difficult to satisfy certain of these criteria at several locations. The intervening months since the last flow had seen considerable alteration of the character of these channels. Aeolian deflation and deposition had occasionally obscured the flow channels, making their identification somewhat tentative. This was especially true for the station on Alamocita Creek (Rio Salado) at the mouth of Pasture Canyon, and for the station on the Rio Salado just east of Puertecito.

Low-flow channel samples were collected as combined, 100cc to 200cc spot samples taken from approximately 5 discrete locations along a 100 foot reach of the inner channel. Samples were collected from a depth of one inch in order to ensure representative sampling of undisturbed bed material.

3.2.3.1.3. OVERBANK SAMPLES. Overbank samples were collected from the nearest point on the bank closest to the current thalweg. These samples were generally collected from a depth of one foot. Wherever the height of the banks was greater than several feet, samples were collected directly from the face of the banks.

Overbank samples were included in this study because at the outset it was felt that the inclusion of bank erodibility estimates, as approximated by bank material character, may help to explain any anomalous width:depth values that might occur. Schumm (1960) defines a weighted mean percentage of silt and clay which characterizes the material composition of the banks and of the channel. This approach has utility in the estimation of the erodibility and degree of equilibrium of a given reach of channel (Gregory and Walling, 1983).

3.2.3.2. Particle Size Analysis

After collection and transport to the lab, the samples were analyzed for particle size. Oven-dried samples were sieved for 15 minutes in a mechanical sieve. U.S. Standard sieve numbers 4, 6, 10, 16, 40, 70, 140, and 200 were used for most analyses. All pebble gravel retained on the number 4 screen that had an intermediate axis diameter less than 1/2 inch, as well as all material accumulated in the bottom pan of the stack, was included in the analysis. Each sample was split into several 150 to 250 cc sub-samples, which were run individually through the sieve. Weight retained on each screen was recorded for each sub-sample. This procedure was used in order to eliminate the risk of bias which might be introduced by the use of a standard sample splitter, and the inherent difficulty in using a sample splitter on coarse material.

Table 5 summarizes the results of particle size analysis. Values for Schumm's "M" are included in the table. Schumm's "M" was calculated according to the formula (Schumm, 1960):

$$M = ((Sc \times w) + (Sb \times 2d))/(w + 2d)$$

Where Sc and Sb are the silt-clay content of the channel and the banks, respectively; w is the channel width; and d is the channel depth.

Appendix D contains particle size distribution plots.

Table 5: Particle Size Analyses

	Random Channel		Low-Flow Channel		Overbank		Schumm's
Station	D50 (mm)	%silt/clay	D50 (mm)	%silt/clay	D50 (mm)	%silt/clay	"M"
S1	0.34	2.4	0.30	1.0	-	-	-
S2	-	-	-	-	-	-	-
S3	0.38	4.2	0.50	0.35	-	-	-
S4	0.63	0.97	0.65	0.44	-	-	-
S5	0.35	1.7	0.35	0.39	0.42	2.8	1.7
S6	0.33	3.5	0.37	0.66	0.23	7.5	3.6
S7	0.48	2.0	0.69	0.55	0.26	6.2	2.2
S8	0.42	1.6	0.39	0.47	0.19	11.2	1.7
S9	0.39	0.63	-	-	-	-	-
S10	0.60	1.7	0.70	0.53	-	-	-
S11	0.39	1.4	0.54	0.10	0.23	5.8	1.6
S12	0.45	0.36	0.76	0.51	-	-	-
S13	0.31	2.4	0.28	4.9	-	-	-
M1	0.81	0.74	0.86	1.5	0.25	9.9	1.7
M2	-	-	1.8	1.2	-	-	-
D1	-	-	0.49	0.99	0.27	10.0	-

3.2.4. MISCELLANEOUS FIELD OBSERVATIONS

In addition to ground-based field investigation, several low altitude flights were made over points of interest within the Rio Salado drainage basin. Although no quantitative information was obtained from these flights, several aerial photographs were taken, and the general understanding of the overall fit of the channel network within the basin was greatly enhanced.

One of the more interesting features observed during a flight on May 30, 1986, was the presence of a steep drop-off, approximately one foot high at the mouth of La Jencia Creek, as well as at the mouths of several smaller tributaries to the Rio Salado upstream towards Riley. These hydraulic discontinuities indicate that a recent flow within the channel of the Rio Salado along that reach had originated somewhere up-basin, and was not complemented by an influx of water from tributaries between Riley and The Box. Since the low-flow channel was located along the north bank, opposite to the entrance of La Jencia Creek, and the knickpoint at the mouth of La Jencia Creek indicated that there was considerable flow along the south bank, it appeared that flow in the Rio Salado had been bank-to-bank along that reach. This further suggests that during that particular event the reach of the Rio Salado between Riley and The Box had carried a considerable flow of water from upstream in response to localized up-basin precipitation, and that the input from La Jencia Creek and nearby tributaries was negligible.

Another interesting feature observed during one of the flights was the excellent definition of braiding and inner anabranches within the main channel near I-25. These features were clearly visible from the air beacuse of the recent deposition of reddish brown mud and silt within the inner channels.

During the course of the field work, note was taken of indications of the historical adjustment of the Rio Salado. Morphological and sedimentary evidence of past episodes of channel erosion and fill indicated that the Rio Salado has experienced epicyclic cut and fill. The presence of terraces along the flanks of the channel at most locations indicates that aggradation within a previously cut valley had taken place. The widespread occurrence, and inset relationships of the terraces to the present-day channel indicates that the cut and fill episodes had occurred along major reaches of the Rio Salado.

The field station at Riley proved to be of particular interest. The station was situated just above the mouth of Arroyo Hondo, a tributary third order stream which drains the north end of the Bear Mountains. The arroyo exhibits signs of recent channel cutting. Within the lower reach, several short arroyos enter Arroyo Hondo discordantly at approximately 2 feet above the channel of Arroyo Hondo. A large longitudinal bar separates the present day channel of Arroyo Hondo from an old abandoned channel. The elevation of the surface of the bar is approximately the same as the channels of the discordant arroyos. The surface of the bar is strewn with recently deposited cobbles and large boulders. Boulders were found piled up against the upstream sides of young trees and vegetation, indicating deposition by a recent flow of exceptional intensity.

Subsequent discussion with a nearby landowner revealed that three separate earthen dam failures upstream appear to have been responsible for the boulder accumulations. The landowner stated that the most recent failure was coincident with the 1985 earthquake that struck Mexico City. The downstream dam had been constructed on an andesite dike which had been a natural knickpoint prior to construction of the dam. The dike had acted as a natural dam, as was evidenced by approximately 10 feet of elevation difference between the channel above and below the dike, and the accumulation of fine sand and silt behind the dam.

Approximately one mile upstream, evidence of past cut and fill episodes was observed along a cut bank. The exposure showed the erosional truncation of an upward fining pebble gravel to fine sand sequence. The erosional surface dips roughly 40 degrees towards the central axis of the present day arroyo. A weak to moderately developed paleosol was evident along the erosional surface. This indicates that the fluvial sequence had been truncated by a laterally shifting, downcutting stream, and the erosional surface had remained exposed for some time. Subsequent aggradation covered the paleosol with an upward fining sequence of pebble gravel to silt. The present day topographic surface above these units is covered with coarse material, including cobbles and boulders. It appears that after the hiatus during which the paleosol developed, the channel gradually aggraded, and the area became a flood plain. The presence of boulders on the surface tends to indicate the return of a high energy environment, possibly at the onset of a renewed episode of erosion.

Many opportunities to witness fluvial processes were made available during the course of field visits. Among the most interesting observations were: the passage of several flood waves, the lateral migration of the main channel, as well as the meandering of the inner channels, the deposition of alternating layers of grey and red clays during the waning stages of several flows, bank sloughing, channel cut and fill, and, most notably, the initiation of a moderate flow event along the lower reach of the Rio Salado in response to a localized summer thunderstorm along the southeast flank of the Sierra Ladrones.

4.0 ANALYSIS AND DISCUSSION

4.1 Hydraulic Geometry

At the outset of the present study it was anticipated that functional relationships between the various basin and channel parameters could be developed. An orderly downstream increase in channel width:depth ratios with a concomitant decrease in mean bed particle size and channel gradient are primary to the development of the desired relationships. Such empirical functions have been investigated by many workers, most notably Leopold and Miller (1956). More recently, Cherkauer (1972) investigated these relationships in the study of several small ephemeral streams in southern Arizona.

Cherkauer developed regression equations to express channel gradient as a function of upstream drainage area and relief, mean bed particle size, and channel width:depth ratio. He successfully used these variables as ephemeral stream surrogates for discharge, sediment load, and channel roughness. He developed two sets of equations, one for sedimentary channels, and the other for granitic channels. Each of the lithologically based sets of equations contained separate equations for the two segments of the longitudinal profiles of the ephemeral streams that he studied: high-concavity upstream, and low-concavity-to-straight downstream.

Cherkauer speculated that the apparent segmentation of the longitudinal profiles of ephemeral streams was primarily a function of the discharge the channel carried. The high-concavity upstream segments are adjusted to the higher drainage density and to the rapid increase in discharge with distance downstream that exists in the mountainous upstream reaches of smaller ephemeral streams. Conversely, the low-concavity-to-straight downstream segments are adjusted to a different set of conditions which exist in the intermontane basins below the mountain front, specifically, limited tributary input, little direct precipitation, and an overall decrease in discharge downstream due to channel and evaporative losses.

The success of Cherkauer's analysis hinged on the orderly downstream decrease in channel gradient and mean bed particle size with a corresponding increase in channel width:depth ratio for the streams that he studied. A similar analysis for the Rio Salado is not presently possible due to the lack of such relationships. Figures 1 through 3 show channel gradient, mean bed and low-flow channel particle size, and channel width:depth ratios plotted against distance along the Rio Salado. Based on the results illustrated in Figures 1 through 3, there do not appear to be significant correlations between any of the variables and location along the channel. Further analysis based upon any assumed relationships would be meaningless.

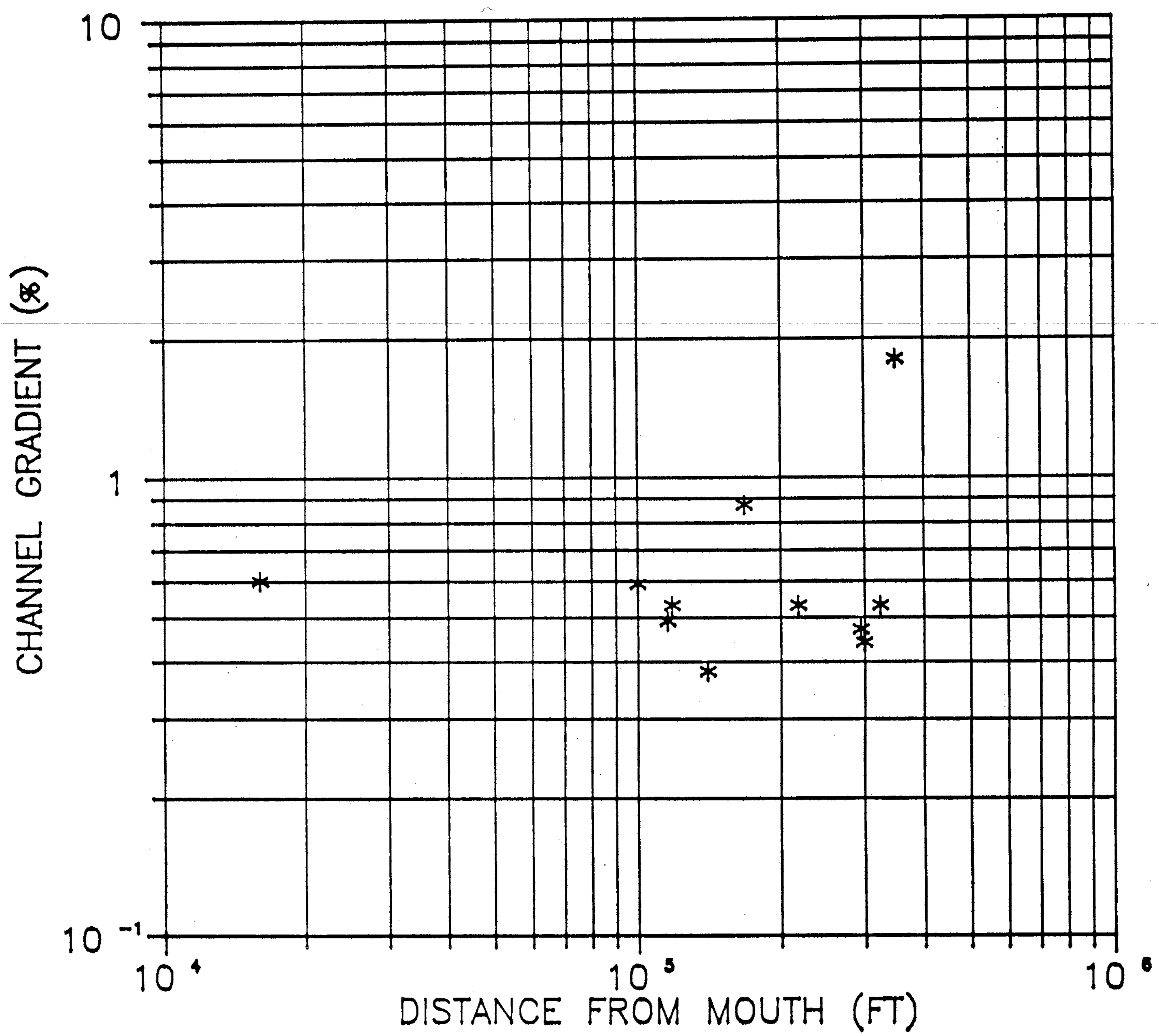

Figure 1. Channel Gradient vs Distance Along Mainstem of Rio Salado

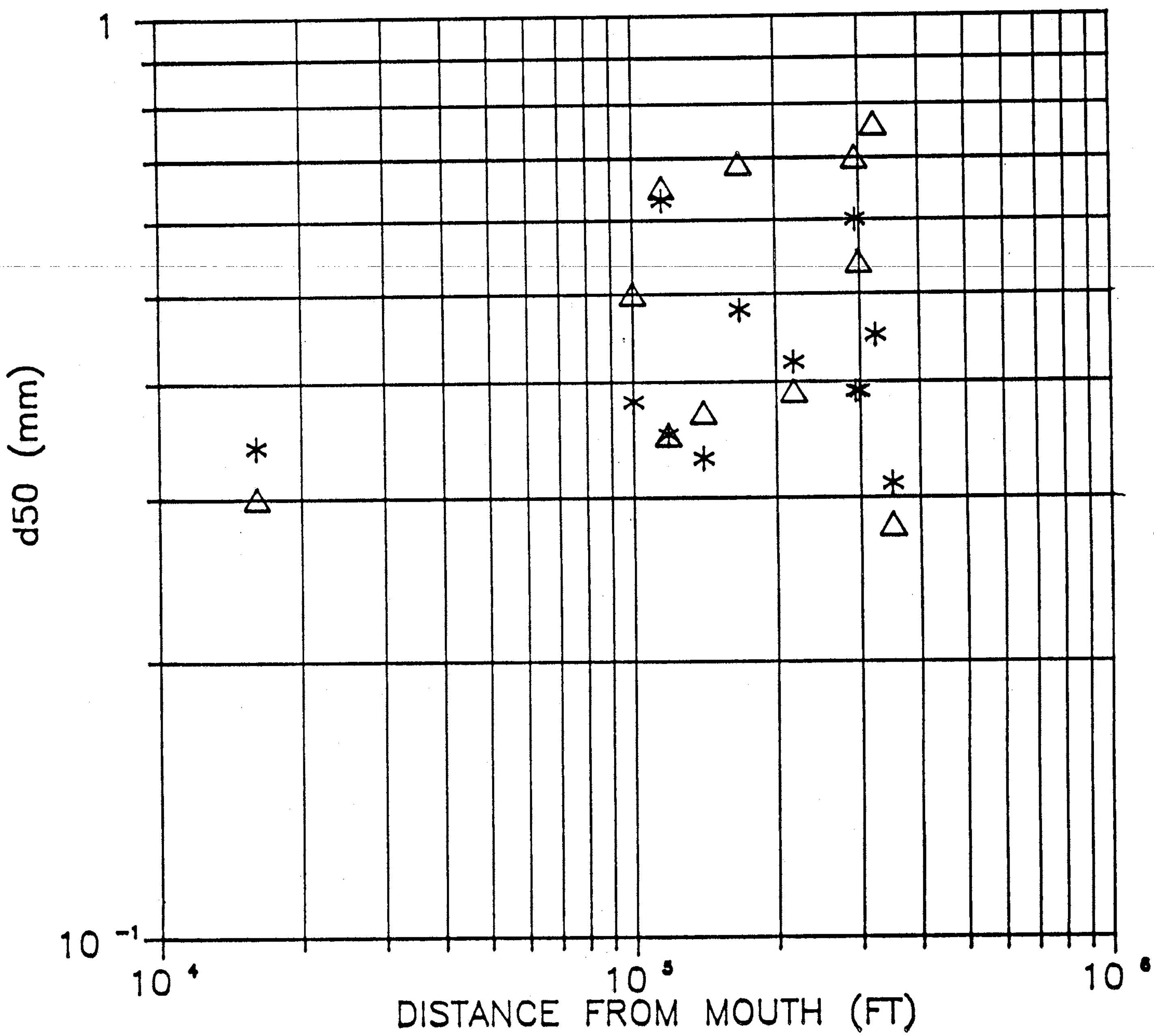

✳ Random Channel
△ Low-Flow Channel

Figure 2. Mean Particle Diameter vs Distance Along Mainstem of Rio Salado

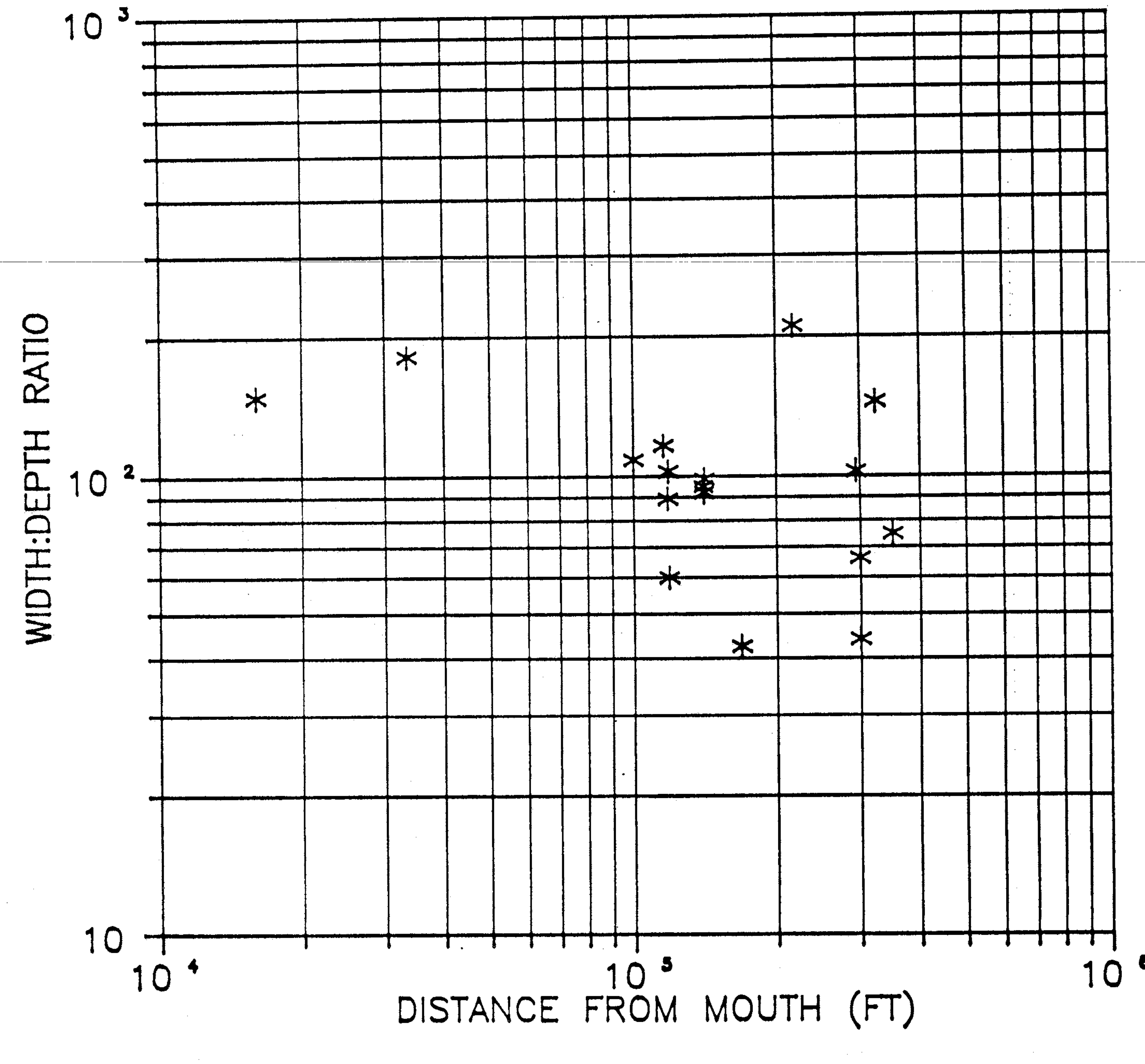

Figure 3. Width:Depth Ratio vs Distance Along Mainstem of Rio Salado

Further, the above variables do not appear to be correlated among themselves. Figures 4, 5, and 6 show mean bed particle size and channel gradient plotted against channel width:depth ratio (after Cherkauer, 1972), and channel gradient versus mean bed particle size (after Wolman, 1955), respectively. The extreme scatter of points suggests that there is no consistent relationship between any of the variables.

The lack of correlation between the parameters is somewhat anomalous. It is expected that certain correlations do indeed exist, at least for certain segments of the Rio Salado, but could not be revealed within the scope of the present study. For example, an overall downstream decrease in channel gradient is indicated by the overall upward concavity of the longitudinal profile (Appendix A), at least in the upper-half of the profile. However, this is not evident on Figure 1, due to the scope of the study and the selection of field site locations. Similarly, it is reasonable to assume that the bed material in the far upstream reaches is predominantly gravel, and that an overall decrease in particle size exists but is not evident on Figure 2.

Several additional observations can be made:

i) It appears that the Rio Salado behaves as a moderately well integrated series of three or more distinct systems. The systems are roughly defined as the uppermost system, which includes that portion of the Rio Salado from its head to the confluence with Miguel Chavez Canyon; the middle system, extending from the confluence of Miguel Chavez Canyon to Canada Bonita; and the lower system, from Canada Bonita to the Rio Grande. Definition of these three systems is based primarily upon the observation that channel width:depth ratios appear to define three separate segments on Figure 3, and upon map and aerial observations of changes in channel width.

These divisions correspond to points where major tributaries join the Rio Salado. Channel characteristics immediately downstream of the major tributaries appear to have adjusted themselves according to an increase in stream power and different flow characteristics supplied by the tributaries. The far downstream portions of the three systems also correspond to reaches on the Rio Salado with relatively little tributary inflow and at a considerable distance from mountainous source areas. Since the Rio Salado flows only in response to intense precipitation events and is influent throughout most of its course, it seems reasonable to expect that discharge decreases with distance from mountainous areas as the water infiltrates into the permeable alluvium. This may lead to aggradation along the downstream reaches of each segment.

Further indication that the major tributaries influence the channel characteristics of the Rio Salado is given by Figure 7, which shows channel sinuosity along the Rio Salado. Channel sinuosity is seen to increase immediately upstream of the points

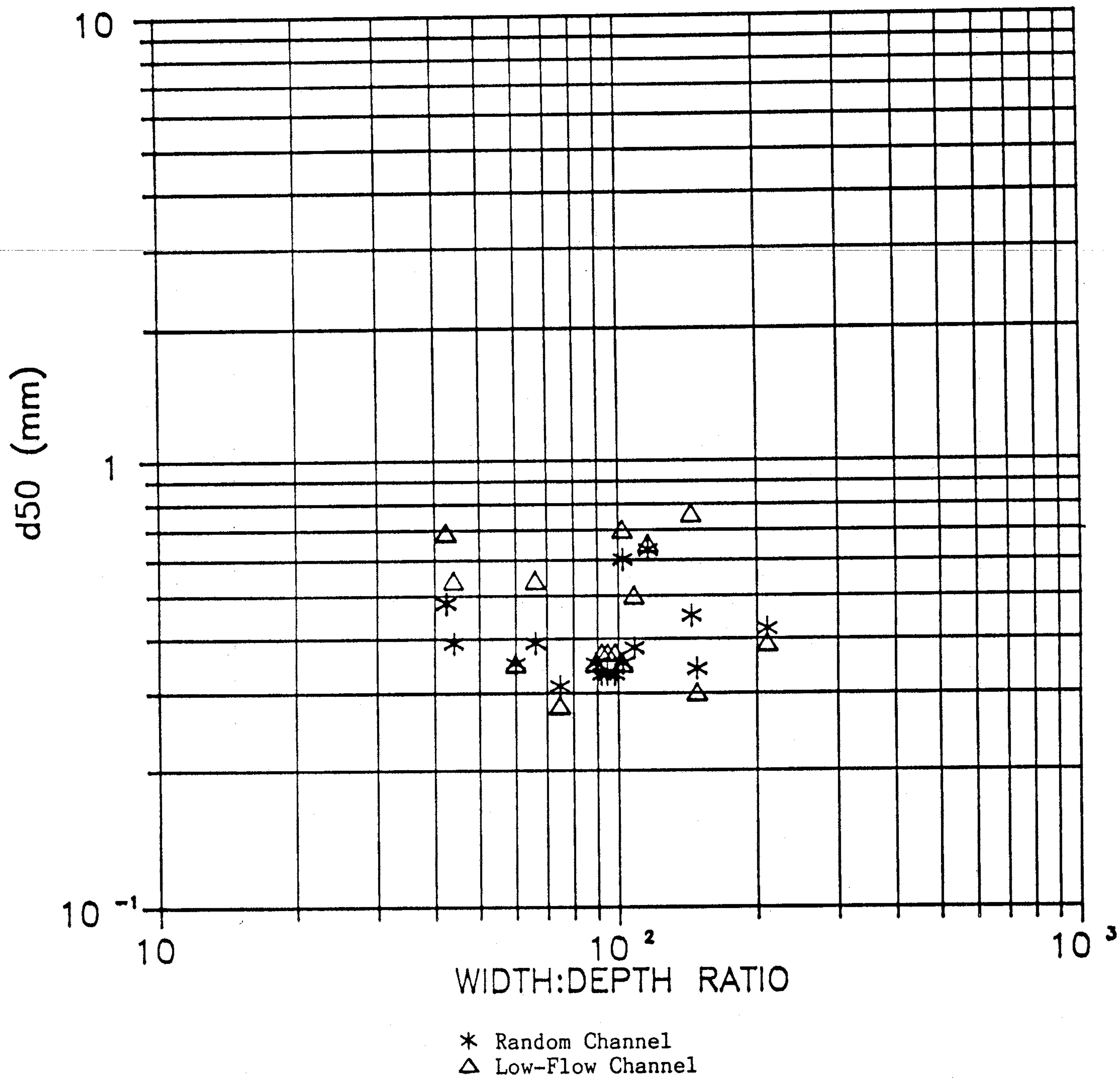

Figure 4. Mean Particle Diameter vs Width:Depth Ratio

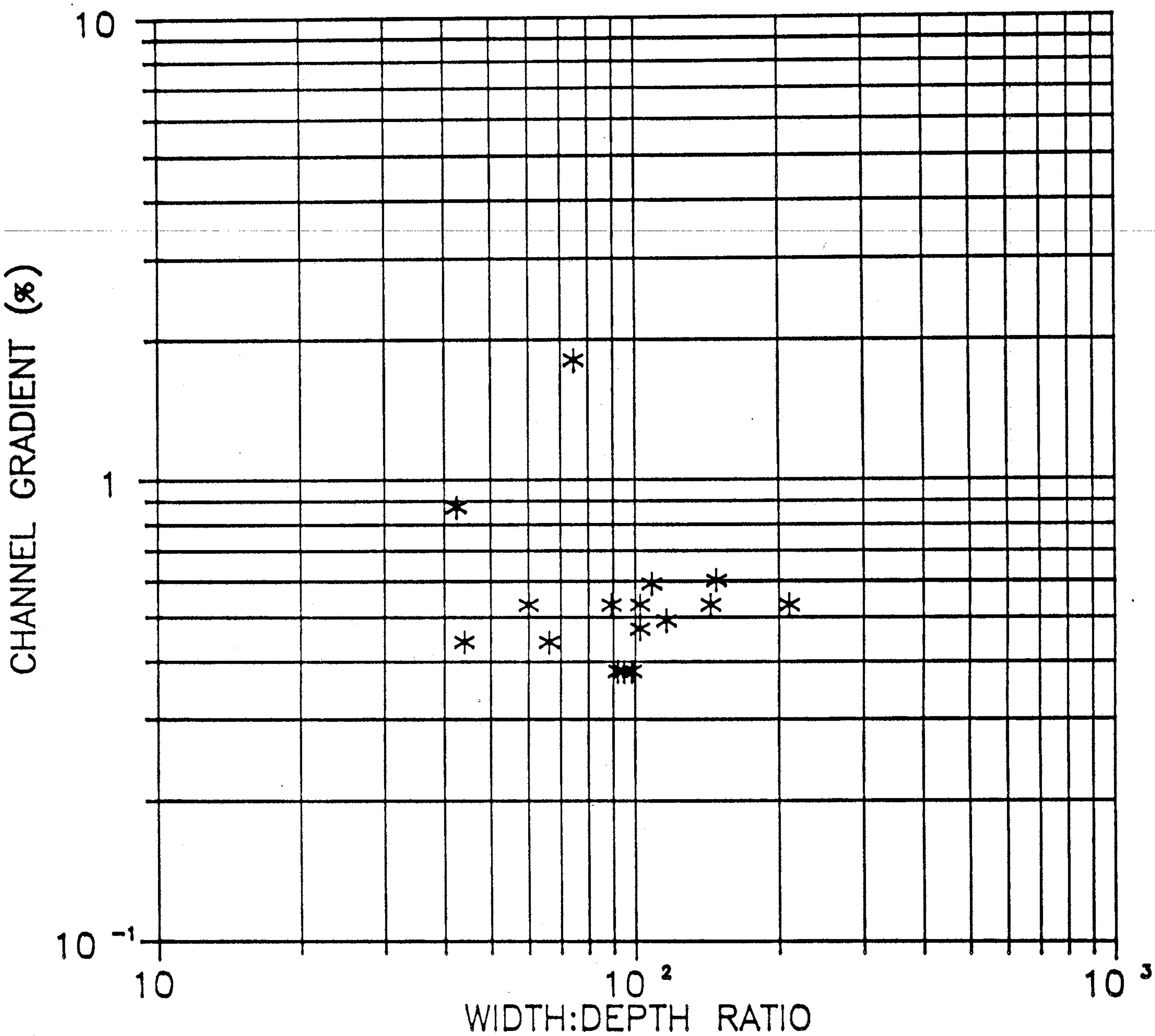

Figure 5. Channel Gradient vs
Width:Depth Ratio

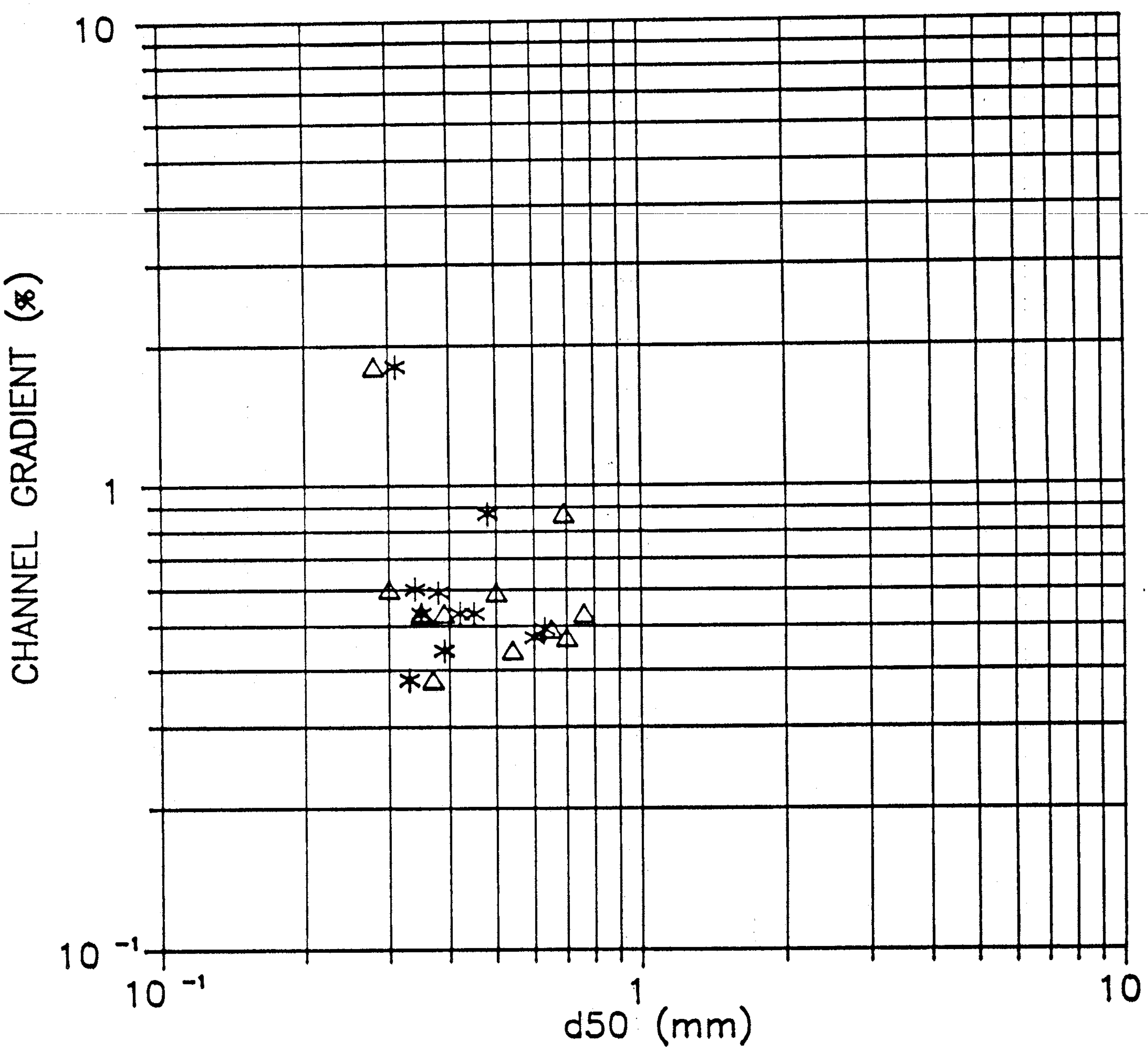

✱ Random Channel
△ Low-Flow Channel

Figure 6. Channel Gradient vs Mean Particle Diameter

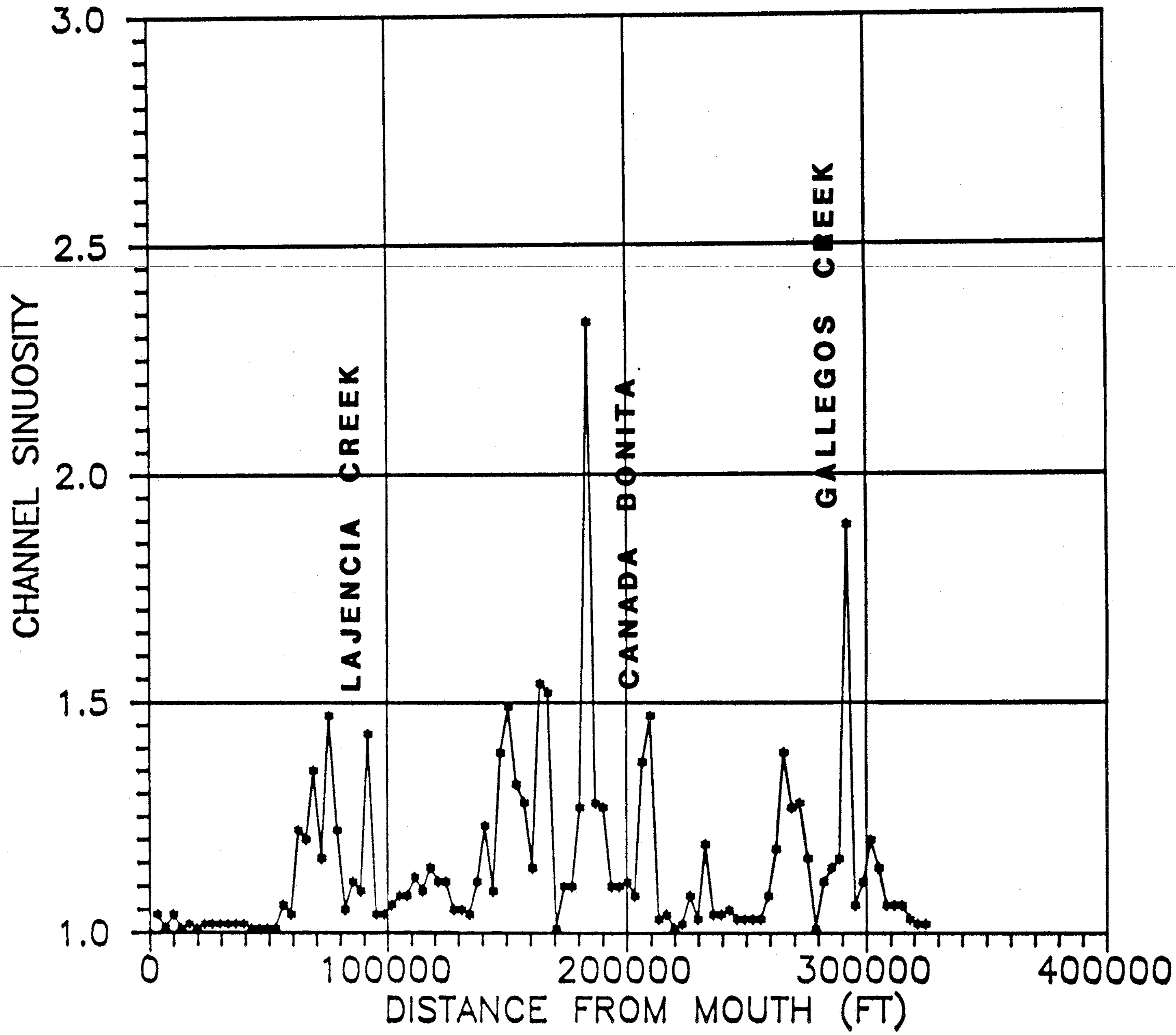

Figure 7. Channel Sinuosity vs Distance Along Mainstem of Rio Salado

of confluence of the Rio Salado with several of the major tributaries - most notably: Gallegos Creek, Canada Bonita, and La Jencia Creek. The increase in sinuosity is presumably due to the adjustment of the Rio Salado to alluviation at the mouths of the tributaries. Based on field observation, it appears that aggradation is presently occurring along the reach which includes the confluence of the Rio Salado and Canada Bonita.

ii) Because the basin is geologically diverse, it is possible that the apparent lack of correlation between some of the quantitative parameters may be the result of localized lithologic control. Supporting evidence for this is given by the low width:depth ratio of the Rio Salado between Canada Bonita and Riley where the channel crosses the Chinle Shale and numerous mafic to intermediate dikes, and at The Box where the channel crosses Pennsylvanian limestone. Although the geology along the remainder of the channel of the Rio Salado is fairly uniform throughout, it is possible that channel geometry and bed particle size could reflect the character and quantity of sediment delivered by tributaries which drain nearby areas of diverse geology and topography.

iii) Channel geometry may, in part, be controlled by the occurrence of ground water. Along reaches of the channel where ground water is shallow, the depth of scour of the unconsolidated alluvium may be limited (see Love, 1979). Since few wells have been completed along the Rio Salado and depth to ground water is largely unknown throughout most of the reach of the Rio Salado, it is difficult to speculate as to the extent of ground-water controls.

iv) The lack of orderly downstream decrease in channel gradient appears to be the result of geologic and tectonic controls (see section 4.2.).

v) The lack of orderly downstream decrease in particle size may be the result of several factors: a) The distribution of grain sizes of channel material may be an artifact arising from the composition and geographical distribution of the sedimentary source material. The particle size distribution of the sedimentary source material may greatly influence resulting particle size distribution of the channel material. b) The temporary storage of material within the channel and sporadic nature of streamflow may lead to the accumulation of 'pulses'of material from widely scattered source areas.

Although little correlation exists between channel geometry and particle size, application of Schumm's "M" to determine channel stability appears to have some merit. Figure 8 shows channel width:depth ratio plotted against "M" for several field stations. From the figure it appears that all of the stations included in the plot are relatively stable, except for the lower station on Miguel Chavez Canyon (M1). This is in agreement with observation. The lowest station on Miguel Chavez Canyon appeared to be actively degrading, as was evidenced by a channel deeply

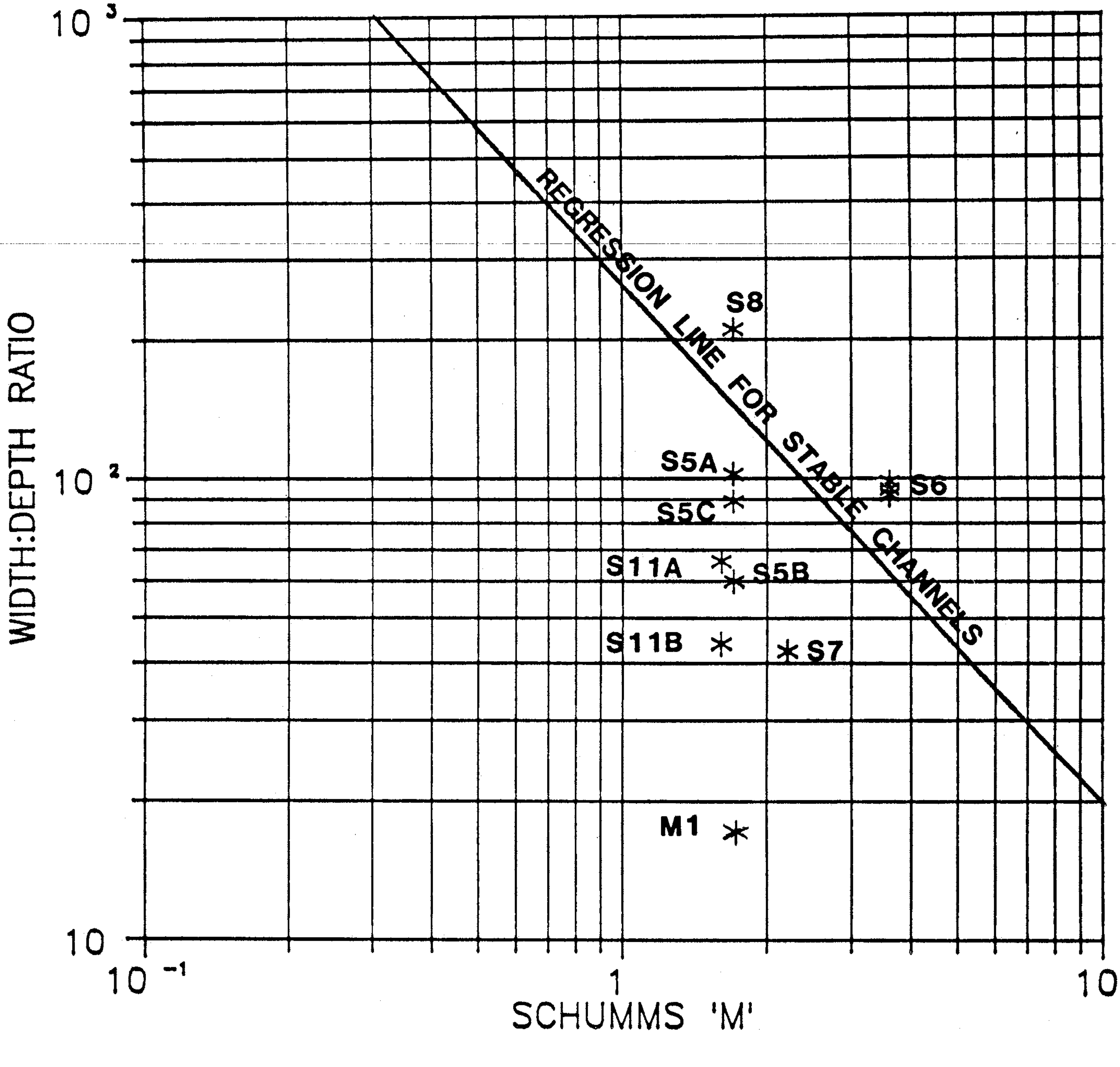

Figure 8. Width:Depth Ratio vs Schumm's 'M'

entrenched in the alluvium, and obvious fresh cut banks just downstream of the station. A knickpoint occurs approximately 1/4 mile downstream of the station, where the channel drops nearly 15 feet over a ledge of Crevasse Canyon Sandstone. The main channel of Miguel Chavez Canyon is cut approximately 8 feet into the sandstone ledge. Just upstream of the knickpoint a flight of several cut terraces descends from the elevation of the top of the ledge and considerable sandstone debris has collected downstream from the ledge below the knickpoint, suggesting that recent breaches in the knickpoint have led to episodes of channel degradation.

4.2 Response of the Longitudinal Profile to Active Tectonics

The longitudinal profile of the Rio Salado does not appear to conform to the idealized concave-upward throughout profile so commonly proposed by geomorphologists, nor does it conform to the two-segment model for ephemeral streams discussed by Cherkauer (1972). In contrast to these idealized models, the longitudinal profile of the Rio Salado is convex-upward throughout much of its lower half, from approximately Puertecito to the Rio Grande (Appendix A). One immediate result of the convex-upward profile is that the shallowest gradient does not occur near the mouth, but rather along an upstream reach within the convex region. This is in keeping with field observations (Figure 1).

It appears that the longitudinal profile of the Rio Salado is the result of a complex set of geologic and tectonic conditions. The key elements in developing the convex-upward profile appear to be:

1) Rapid uplift associated with the Socorro Magma Body. The approximate extent and magnitude of uplift in relation to the lower Rio Salado are shown in Figure 9. The reach of the Rio Salado that is convex-upwards approximately coincides with the western extent of uplift over the Socorro Magma Body.

2) The wedge of resistant Pennsylvanian limestone at The Box. The limestone acts as a barrier, preventing upstream adjustment of the Rio Salado to base-level changes.

3) The numerous intermediate to mafic dikes and associated down-to-the-east normal faults which cross the channel of the Rio Salado between Puertecito and Riley. The dikes act as barriers to upstream channel adjustment, and the most active faults provide limited offset of the longitudinal profile.

4) The Rio Grande. The Rio Grande is responsible for establishing the base level to which the Rio Salado must adjust. The Rio Grande has entrenched at least 120 feet into the alluvium in response to uplift over the Socorro Magma Body(Ouchi,1983a,b). Because of its great stream power, near-perennial nature, and the easily eroded nature of the sediments across which the Rio Grande flows, the Rio Grande has nearly kept pace with the rate of uplift. The magnitude of entrenchment (120+ feet) nearly equals

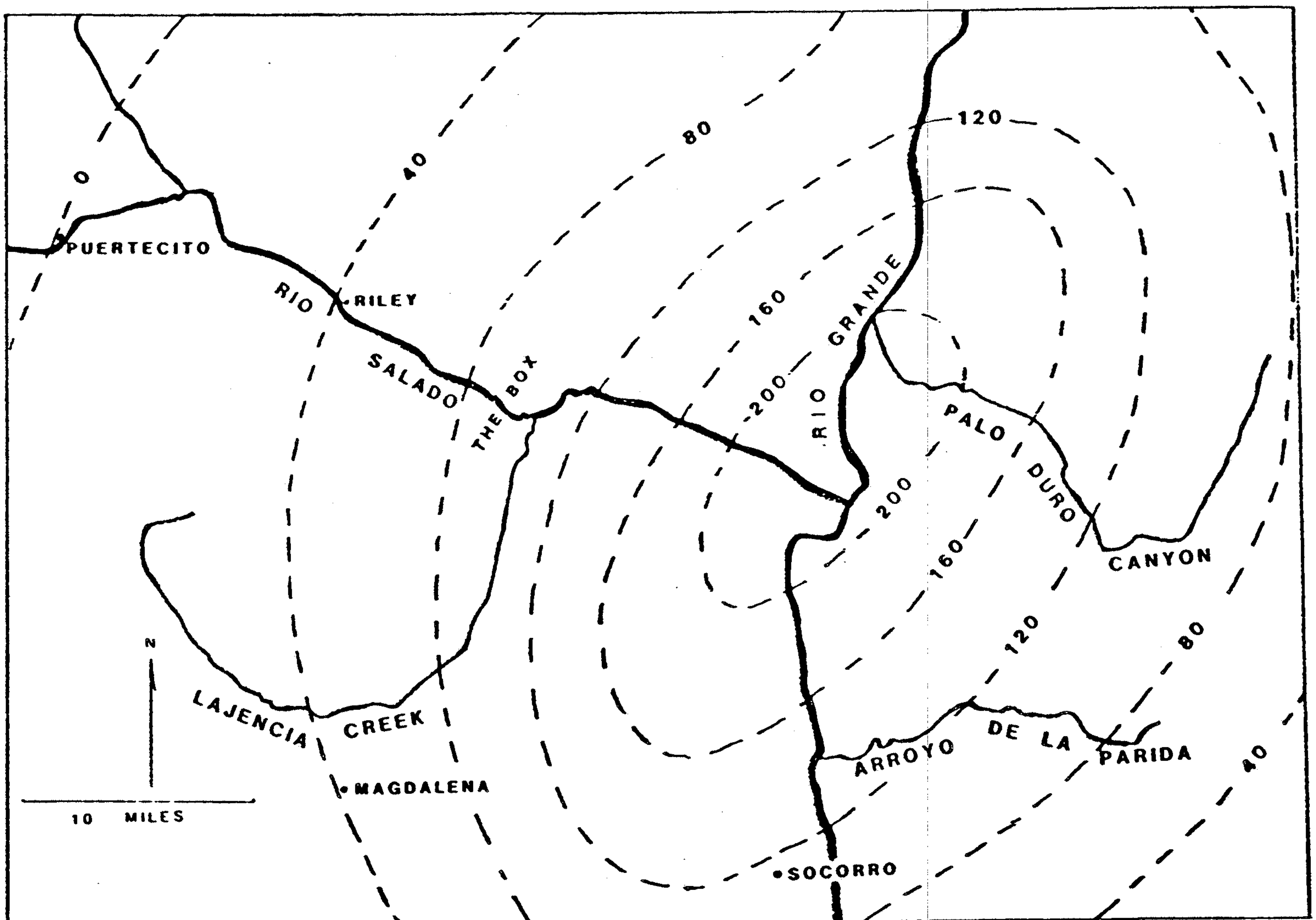

Figure 9. Approximate Uplift Over the Socorro Magma Body 1934 to 1978. Contour Interval is 40mm. (After Reilinger, ėt al, 1980)

the cumulative extent of uplift (180+ feet) (Ouchi, 1983). However, the longitudinal profile of the Rio Grande still does exhibit a slightly convex-upward section along the reach which includes the uplift, due at least in part to the influx of sediment provided by the Rio Salado (Ouchi, 1983).

The convex-upward profile of the lower Rio Salado appears to be the result of the interplay of the above four factors. Specifically, uplift centered over the Socorro Magma Body provides the initial mechanism for disruption of the longitudinal profile. The Rio Grande provides the base level to which the Rio Salado must adjust. Adjustment of the Rio Salado to the base level set by the Rio Grande is hampered by the occurrence of resistant limestone at The Box and the many dikes between Riley and Puertecito (Figure 10). The resulting longitudinal profile is convex-upward, with an oversteepened reach downstream of The Box, and an understeepened reach from about Puertecito to Riley.

4.3 Basin and Channel Network Relationships

Analysis of certain of the quantitative parameters derived during the course of the study indicate that in spite of active uplift over the Socorro Magma Body, the Rio Salado drainage basin and channel network behave predictably according to Horton's laws (Horton, 1945). That is, there exist interrelationships among the quantitative descriptors that are in accordance with the postulates of Horton, specifically, the law of stream numbers, the law of stream lengths, the law of drainage area, and the law of stream slope. Relationships among other variables tend to support the generally good adjustment of the Rio Salado.

Horton numbers have historically been used by quantitative geomorphologists in the analysis of drainage basins. Recently, their utility has been greatly enhanced by their incorporation into deterministic and stochastic streamflow models. Several workers have successfully used the Horton numbers as input parameters for predictive numerical models. Most notable among these are the Instantaneous Unit Hydrograph (IUH) based models of Rodriguez-Iturbe and Valdez (1979), Valdez et al, (1979), and Rodriguez-Iturbe et al (1982). The IUH models use Horton numbers as deterministic input parameters. Their work has subsequently been expanded to include climatic data as well. The development of such quasi-deterministic numerical models has fostered a new interest in quantitative basin description. The discipline of drainage basin analysis has been greatly rejuvenated by the advent of such new applications.

Figure 11 is a plot of the number of streams of a given order versus stream order. The close fit of the regression line indicates that there exists an inverse geometric relationship between the number of streams of different orders. This suggests that the basin behaves according to Hortons law of stream numbers. The concave-upward tail at higher orders is in keeping with Shreve's (1966) analysis of computer-generated, topologically distinct channel networks, where he found that for

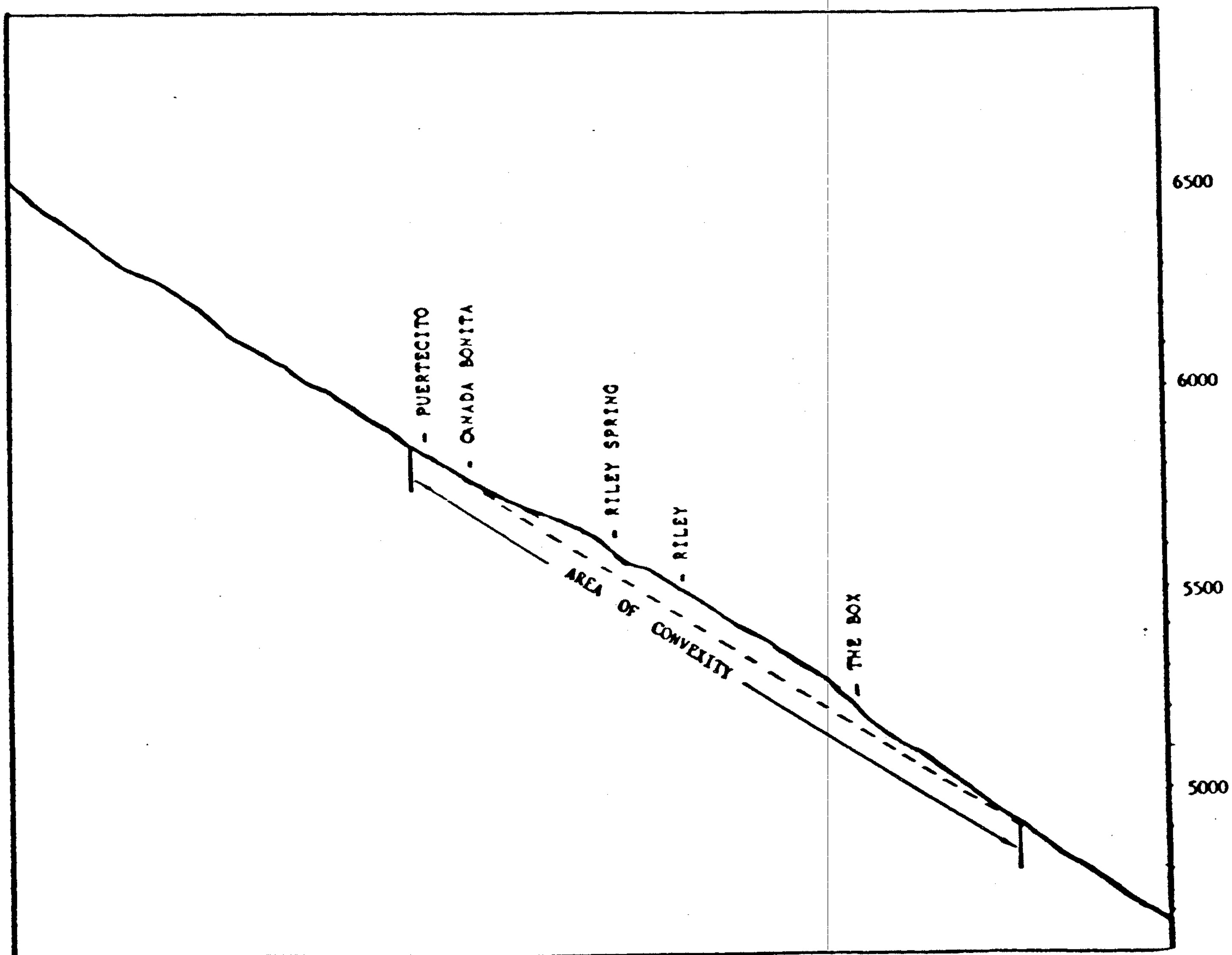

Figure 10. **Longitudinal Profile of Rio Salado Showing Area of Convexity**

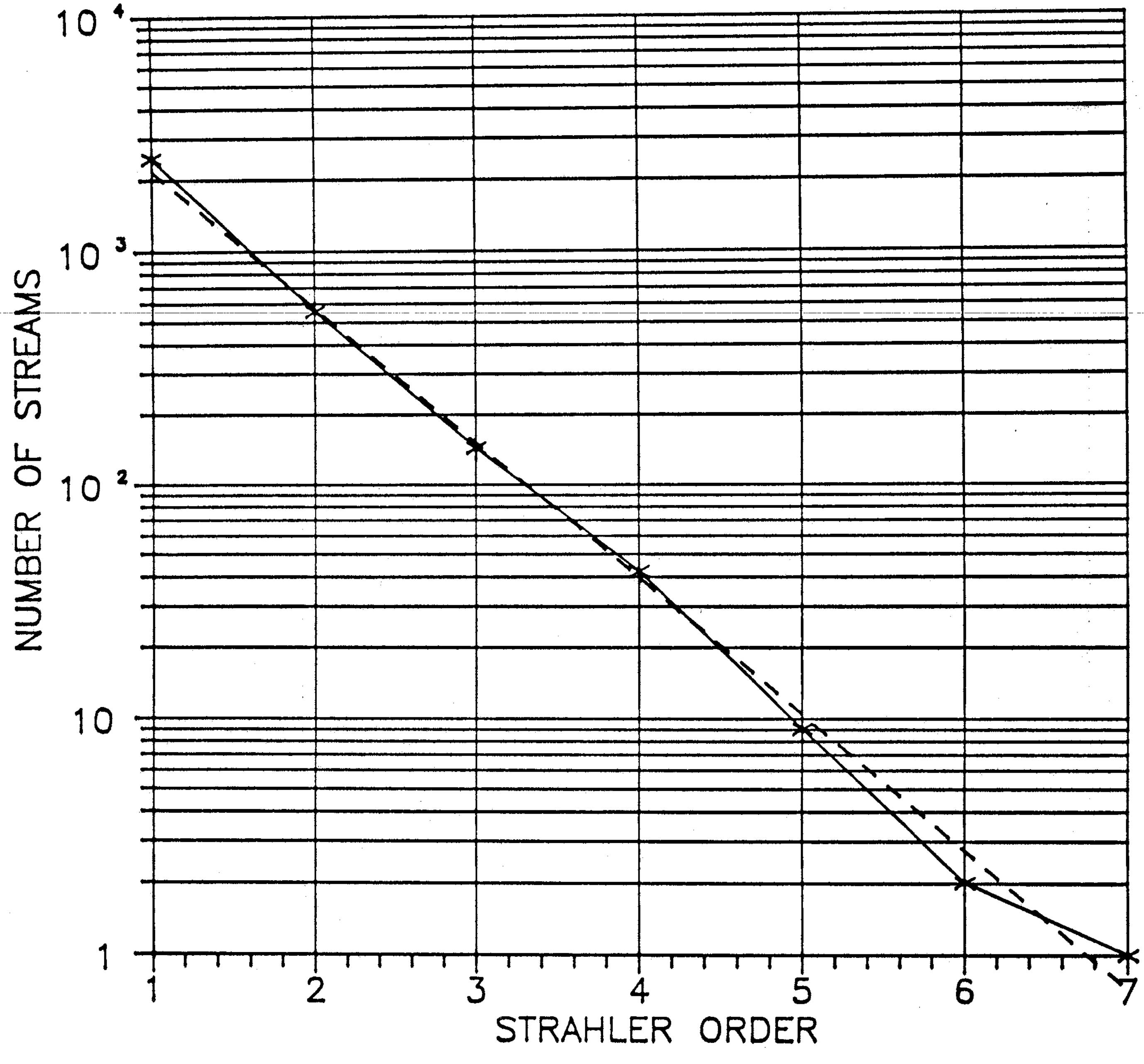

Figure 11. Stream Number vs Strahler Order

both randomly generated and real networks, stream number plots display a characteristic concave-upward tail.

The slope of the regression line in Figure 11 is 3.5. According to Horton's law of stream numbers, the slope of the line is equal to the bifurcation ratio, which is a measure of drainage composition. The bifurcation ratio is somewhat sensitive to geological control, and highly sensitive to structural control. Bifurcation ratio therefore gives an indication of the relative influence of geologic and structural controls on the structure of the channel network.

The value of 3.5 for the bifurcation ratio falls within the typical range of values for basins developed in areas of homogeneous lithology in the absence of structural controls. Bifurcation ratio may exceed 10 for basins influenced by extreme structural controls (Chorley, Schumm, and Sugden, 1984). A bifurcation ratio of 3.5 for the Rio Salado network therefore tends to indicate that even though the basin is geologically diverse, the channel network has developed in the absence of significant geologic and structural controls.

Figures 12, 13, and 14 show stream length, drainage area, and overall stream slope plotted against stream order. Figures 12 and 14 were developed using data for mainstem streams of all channel networks of order 4 and higher. The use of all channel networks of all orders within the Rio Salado drainage basin would be prohibitively time intensive, since there are 3240 distinct channel segments of all orders within the basin. The data set used for Figure 13 included areas for order 4 and higher basins only. The inclusion of lower order basins is not appropriate for the present analysis due to the increase in basin area approximation error with decreasing basin size when using a unit cell length of 1 km in the numerical determination of basin area.

The generally good fit of the regression lines on Figures 12, 13, and 14 suggests that the Rio Salado tends to obey Horton's laws of stream length, drainage area, and channel slope. Implicit within these plots is an inverse geometric relationship between stream lengths and stream slopes of different orders, and a direct geometric relationship between drainage areas of different orders.

These geometric relationships have their greatest utility in allowing the estimation of input parameters for numerical surface water modeling. The actual measurement of certain of these parameters often requires a prohibitive amount of work, which may be beyond the scope of the modeling effort. For example, a rainfall-runoff model used for determining streamflow at many points within the basin requires the measurement of drainage area upbasin from each point investigated. This could be extremely time consuming for all but the smallest basins.

One product of Figure 12 is the ability to estimate the average length of the streams of a given order. Reference to

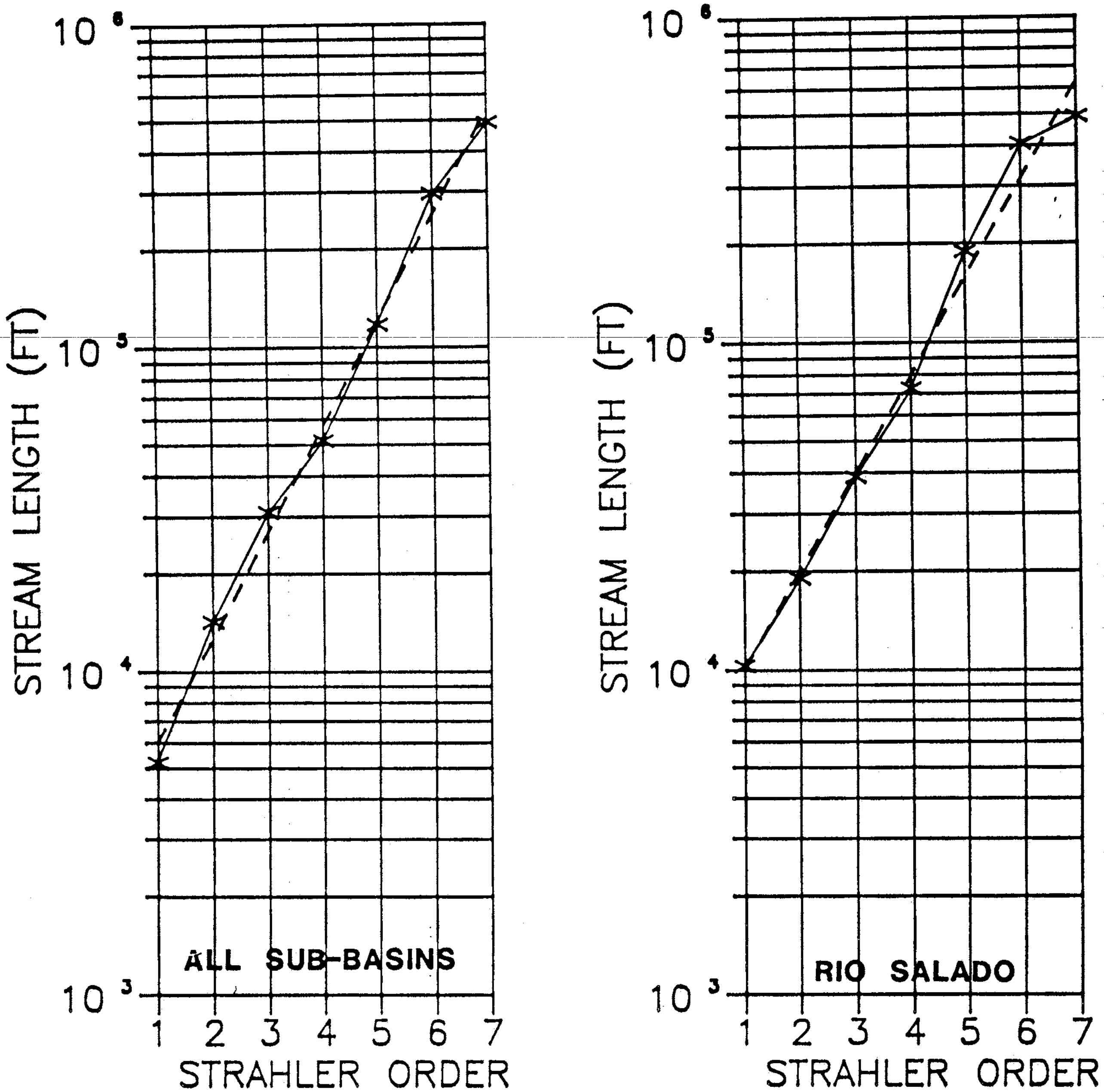

Figure 12. Stream Length vs Strahler Order

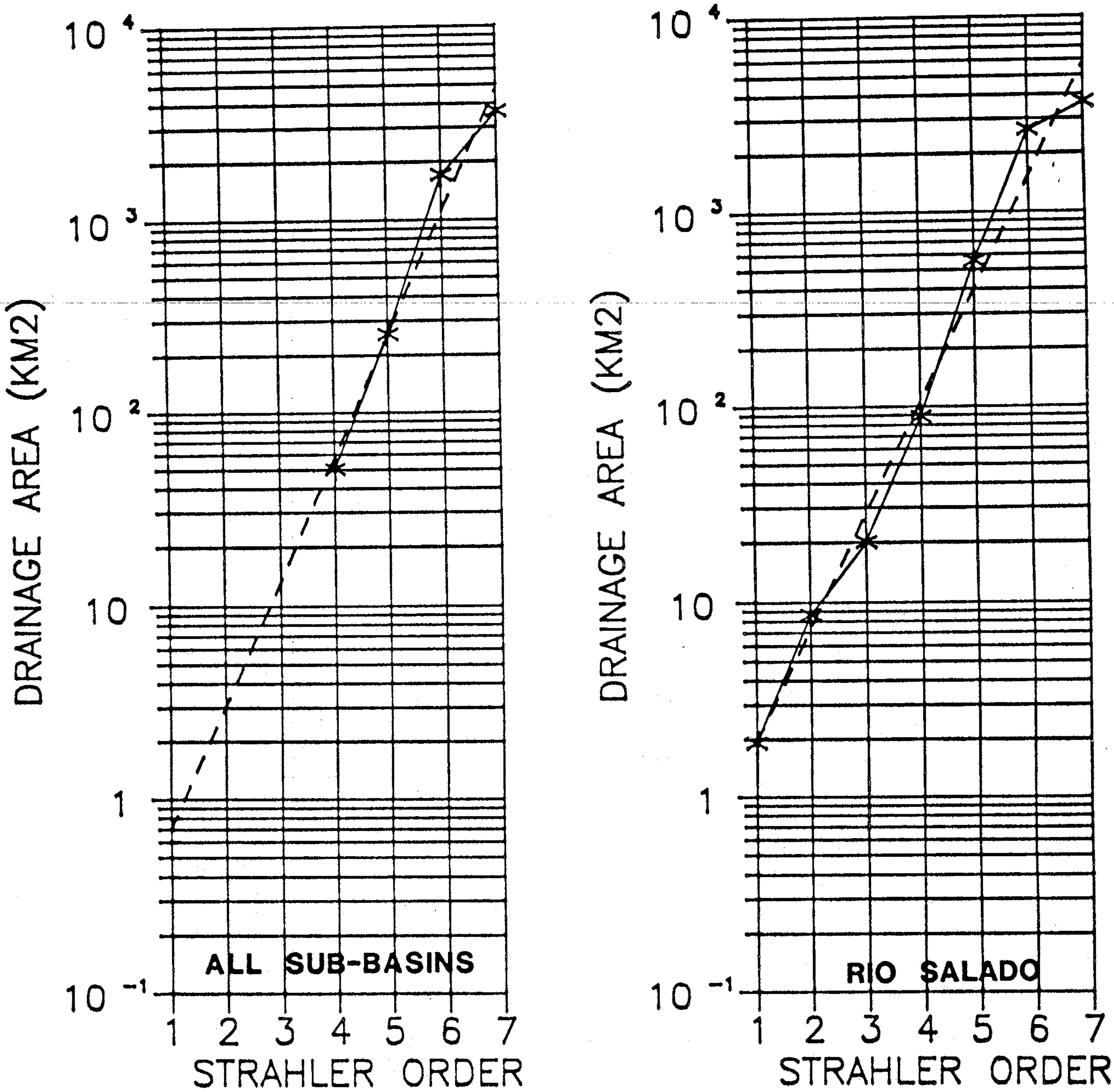

Figure 13. Drainage Area vs Strahler Order

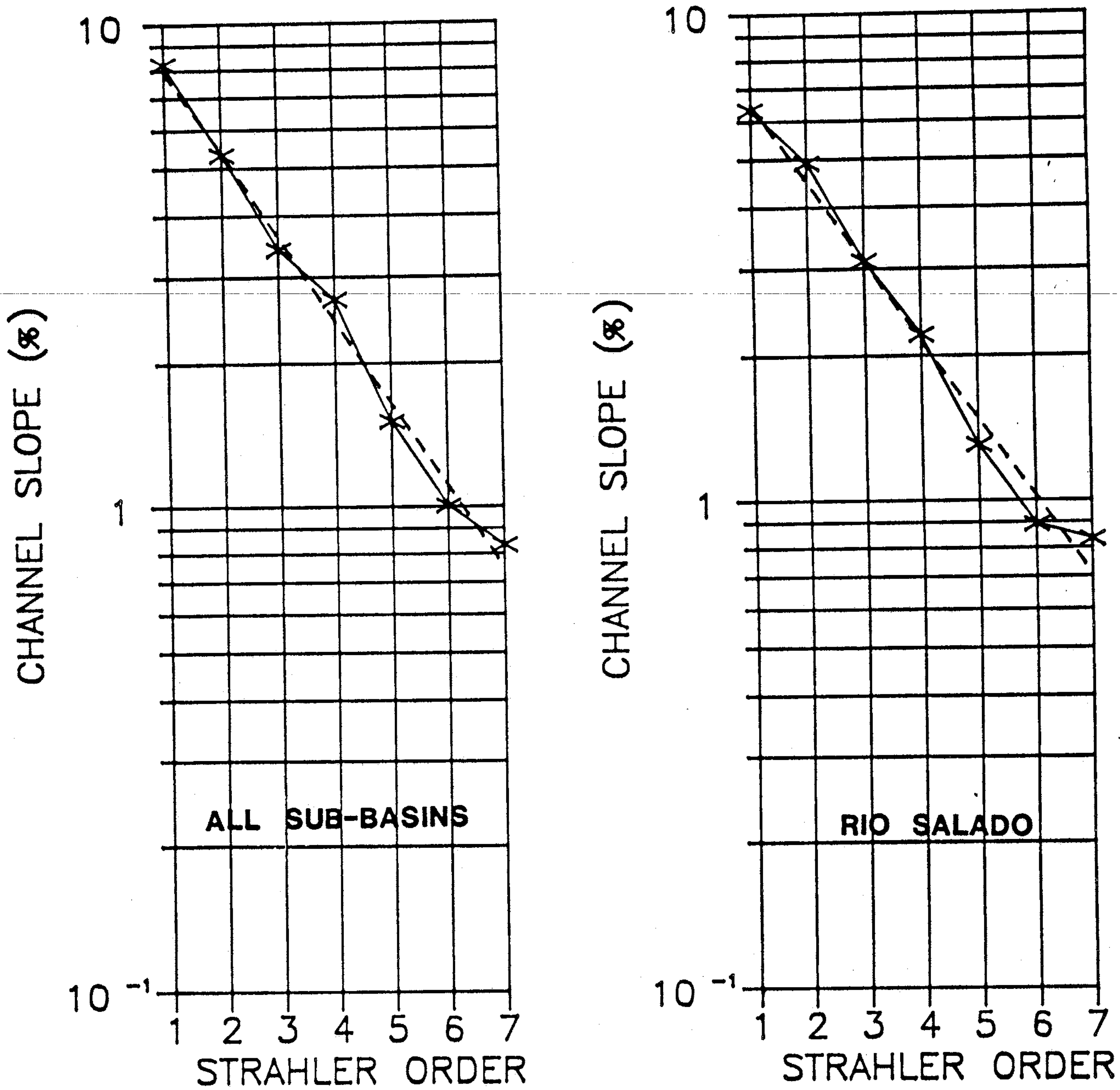

Figure 14. Channel Slope vs Strahler Order

Figure 12 gives the length of the average first order stream to be 5800 feet. This is in good agreement with photogrammetric criteria for definition of first order streams on 1:24000 topographic maps. Further use of Figure 12 allows the estimation of the total length of channel within the Rio Salado drainage network. Considering that there are $\sum_{i}^{6}(N_i - N_{i+1}) = 3240$ distinct channel segments within the network, where N is the number of streams of order i, Figure 12 shows a total of 4166 miles of channel within the Rio Salado network. Consequently, the overall drainage density and stream frequency for the basin are 3.0 mi/mi2, and 2.3 /mi2, respectively. Where drainage density is given by:

Dd = (the total length of channel) / (basin area)

and stream frequency:

F = (number of stream segments of all orders) / (basin area).

The value of 3.0 mi/mi2 for drainage density is quite low, suggesting that much of the Rio Salado drainage basin is poorly drained. This may be true for some of the broad intermontane plains within the basin. However, the low value may be an artifact of the delineation of first order streams from blue lines on 1:24000 series topographic maps. In spite of this, drainage density may have utility in comparing sub-basin drainage characteristics, provided a consistent method of delineating first order streams, and maps of the same scale and quality are used. Stream frequency is similarly sensitive to map scale and first order channel delineation. The value of 2.3 may likewise be artificially low.

The average length of overland flow is another parameter with application to rainfall-runoff modeling. Like drainage density and stream frequency, average length of overland flow is a measure of drainage composition which is sensitive to map scale and the delineation of first order channels. Average length of overland flow may be approximated from drainage density via:

L = 1/2Dd

For the Rio Salado drainage basin, the average length of overland flow is 0.167 mile. This suggests an average spacing between channels of 1760 feet.

One consequence of Figure 13 is that it allows estimation of the average drainage area for streams of any order. The primary use of such information is the estimation of the size of the area drained by a particular stream, which allows an approximation of the minimum area needed for channel initiation (in the case of first order streams) and maintenance.

Figure 13 can be used in conjunction with a functional relationship between distance from source and stream order (implicit in Figure 12) to estimate the total contributing drainage area upbasin from any point on the Rio Salado. The regression line for the basin-wide points on Figure 12 shows that the average first order channel drains approximately 0.74 km2. Information about upbasin drainage area is often useful for rainfall-runoff modeling. For example, the U S Soil Conservation Service uses a model which requires upbasin drainage area as an input parameter in a deterministic runoff model.

Figure 14 shows stream slope versus stream order. One important feature of this figure is the concave-upward tail. This implies that the slope of the 7th order segment of the Rio Salado is oversteepened. Inspection of the longitudinal profile of the Rio Salado (Appendix A and Figure 10) shows this to be the case. Oversteepening is a consequence of geologic and tectonic control along the reach between Puertecito and the Rio Grande valley, as discussed in section 4.2.

Figure 15 shows Shreve magnitude vs Strahler order. Figure 15 was developed in order to investigate the relationship between Shreve magnitude of the mainstem, and Strahler stream order. All networks of order 5 or higher are plotted individually to allow for comparison. The figure shows an apparent direct geometric relationship between stream magnitudes of different orders.

The bold dashed curves on the figures in Appendix A show the downstream growth of Shreve magnitude. The point of steepest slope indicates where tributary input is greatest. For networks within the Rio Salado system this typically occurs at approximately 60% to 70% of the distance from the head to the mouth. The region of greatest tributary input, therefore, tends to be near the middle of the individual basins. This appears to be a function of a small number of high-magnitude tributaries joining the mainstem, rather than a large number of low-magnitude tributaries. Typically, little tributary input occurs below this point.

The figures included in Appendix A also show longitudinal profiles and hypsometric curves for all basins of order 4 and higher. Detailed analysis of all of these curves is not included in the scope of the present study. However, several observations may be made:

i) The longitudinal profiles of all but a few of the streams are concave upward throughout, and generally indicate good adjustment. An important exception is the concave-downward profile of the Rio Salado below Puertecito. This is presumably due to geologic and tectonic control, as discussed in section 4.2. The longitudinal profile of La Jencia Creek is anomalously straight, and may also be the result of uplift over the Socorro Magma Body.

ii) The shapes of most of the hypsometric curves are in keeping with the ideal shapes proposed by Strahler (1952), suggesting relatively small proportion of the extreme highland

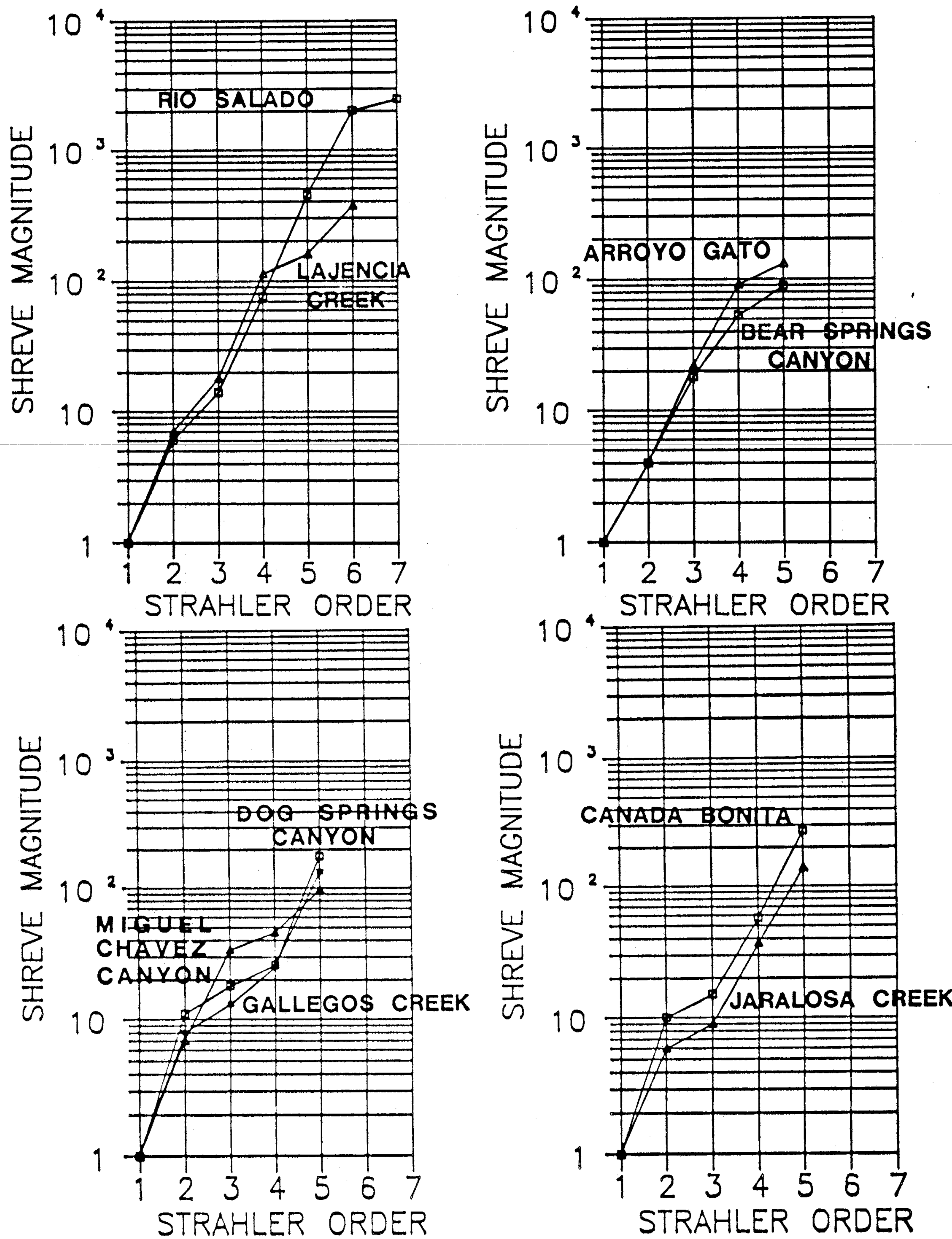

Figure 15. Shreve Magnitude vs Strahler Order

and lowland areas. Many of the 4th order curves display fairly steep slopes at their ends, reflecting irregular mountainous topography. There are no signs of obvious remnants of old geomorphic surfaces within any of the curves. If isolated portions of the Ortiz surface remain, they are not obvious, and they were not made evident from the scale of the present hypsometric analysis. Hypsometric integrals are generally within the range proposed by Strahler (1952) as being representative of uniformly erodible material.

5.0 CONCLUSIONS

* Hydraulic geometry and bed material size relationships of the Rio Salado do not conform to the results other investigators found for smaller ephemeral streams in the semi-arid southwest U.S. There are no predictable downstream trends in any of these parameters.

* The downstream distribution of channel geometry indicates that the Rio Salado may behave as an integrated system of three segments. The differentiation of these segments is due to the effect of major tributaries on the channel downstream from their respective confluences with the main channel.

* Morphometric drainage basin analysis shows that the Rio Salado drainage basin and channel network behave predictably and in accordance with other river systems.

* The longitudinal profile of the Rio Salado is convex-upward from Puertecito to the Rio Grande. This is presumably the result of the complex interplay of several geologic and tectonic factors. The major factors in producing the convex profile are rapid uplift over the Socorro Magma Body, the ability of the Rio Grande to maintain regional base level, and the resistance of different geologic materials at The Box and along the reach between Riley and Puertecito.

* The impact of geology, tectonics, and geologic structure appears to have played a minor role in the development of the remainder of the Rio Salado drainage network.

* The Rio Salado has undergone several epicycles of erosion and channel filling in the past. The present day episode of downcutting is just the most recent in a series of cut and fill episodes.

*Further work is required to fully understand the Rio Salado.

6.0 RECOMMENDATIONS FOR FURTHER WORK

6.1 Expansion of the Current Study

The most evident need for further work involves a detailed investigation of the anomalous results of the present study regarding hydraulic geometry and particle size relationships. The inconclusive results may reflect reality (i.e., the results of Cherkauer are valid for certain sizes or types of systems only); Cherkauer's findings may not be applicable to systems which are presently undergoing tectonic activity; or the present results may be an artifact of sampling methodology or site selection, among other causes. Although it is important that the results of the present study do not agree with Cherkauer's findings, it is equally important to investigate why they do not.

It is apparent that the orderly downstream decrease in channel gradient is not to be expected for the Rio Salado because of the convex-upward nature of the longitudinal profile due to active tectonics within the lower reaches. However, it is not readily obvious why channel particle size, and width:depth ratios do not show typical correlations.

One proposal for additional work requires an expansion of the current study, focusing on channel geometry and bed material size investigation only. Additional field sites should be selected along reaches not included within the present study, including several further upstream and in the headwater reach. During the course of the investigation, the use of different sampling and analysis methods should be considered. Point pebble counts, although tedious and possibly biased, may prove to be more appropriate. Channel width and depth should be carefully referenced to readily identifiable high-water marks. Consideration should also be given to scheduling the field activities shortly after the flow season.

This study could be expanded to include an investigation into the apparent segmentation of the Rio Salado into 3 sub-systems. Such a study would require detailed investigation upstream and downstream, as well as within the approximate boundaries of each of the segments. All available geologic and hydrologic information should be included. Hand or power-driven coreholes may be necessary to determine the depth of alluvial fill beneath the channel, and the depth to groundwater. Additional work could include an investigation of channel bottom permeability using an air-entry permeameter.

It is hoped that such an investigation may help to identify whether the system behaves as 3 integrated segments, and if so, what are the causes.

6.2 Investigation of the Response of The Rio Salado to Tectonic Uplift

The present study presented tentative evidence of the response of the Rio Salado to tectonic uplift over the Socorro Magma Body. While there are certain indications that such an adjustment is indeed taking place, the extent of the adjustment as well as the extent of the uplift itself are poorly defined. The present set of circumstances provides an excellent, and rare, opportunity to investigate the response of an alluvial, ephemeral river to active tectonics, and to allow a direct comparison with the response of a near-perennial river (e.g., Ouchi, 1983).

The expanded study of the response of the Rio Salado to active tectonics could include an attempt to map and correlate the oldest preserved terraces of the Rio Salado. If a set of terraces at least 10,000 to 20,000 years old is found, then the present elevation of the terraces could be plotted in a fashion similar to that used by Ouchi (1983) and Bull (1984). This would allow better definition of the geometry and extent of uplift, and the entrenchment and response of the Rio Salado. If sufficiently old enough terraces could not be found, then an old geomorphic surface (e.g., the Ortiz Surface), or a marker geologic horizon (e.g., the Riley Travertine) could be used.

The investigation of the response of the Rio Salado should also include a detailed study of the channel of the Rio Salado. This could include an in-depth survey of channel gradient at many locations, a determination of the depth of alluvium beneath the channel at various points along the profile, and an identification of aggradational and degradational reaches. The main focus of the study could center on the area along the convex portion of the profile, preferably near The Box or along the reach between Riley and Puertecito.

6.3 Paleohydrologic Reconstruction

The present study found evidence for past degradation and aggradation at several locations along the Rio Salado. The existence of features such as longitudinally extensive terraces, flood plains above the present erosional level, interfingering tributary and mainstem deposits all suggest that several epicycles of erosion and sedimentation have occurred in the past, possibly in response to climatic variations. An investigation into the paleohydrology of the Rio Salado may help to better define the chronology and circumstances under which these cycles occurred. The study would require extensive and detailed geologic mapping of the sediments and geomorphic features along the Rio Salado. Provenance studies could also be used for determining the source areas of the sediment, and consequently the chronology of drainage development. Clay minerology could be included in the provenance study. Radio carbon dating of organic debris, and tree ring dating could be used for dating particular features. Sites for this study should be selected downstream from major tributaries in order to identify the response of the Rio Salado to the development of additional drainage areas.

The area near Riley is a good choice for conducting such an investigation, largely due to the presence of terraces, flood plain deposits, tributary mouth fans, and organic debris within the sediments.

6.4 Surface-Water Modeling

The information and data bases developed during the present study could be used in conjunction with streamflow and sediment discharge/erosion modeling. The digitized topographic data base could be used in the quasi-deterministic runoff and sediment discharge numerical model of Gupta and Solomon (1977). The model uses digitized topographic data incorporated into a Universal Transverse Mercator (UTM) based grid. Each grid cell within the model carries information on elevation, flow direction, and the channel network, represented as numerical "levels".

A Geomorphologic Instantaneous Unit Hydrograph (GIUH) model (Rodriguez-Iturbe and Valdez, 1979) could be attempted using input parameters derived from the present study. The model could be calibrated using existing streamflow hydrographs (eg., Stephens, Cox, and Havlena, 1987).

Alternatively, a model could be developed which uses the channel network data base to investigate the chronology of sub-basin drainage in response to a uniform, instantaneous, basin-wide precipitation event. Such a model could use river distance to points on the drainage network as a surrogate for time.

6.5 Miscellaneous Work

Additional work could also include an analysis of the geographic distribution of the various basin parameters, including Horton numbers and hypsometric integrals, and an attempt to correlate the parameters with geologic, climatic, topographic, and soils information. Such an investigation may be possible with the data set produced from the present study.

REFERENCES

Barker, J. M., 1983, Preliminary investigation of the origin of the Riley Travertine, Socorro County, New Mexico: New Mexico Geological Society Guidebook 34, p. 269-276.

Begin, Z. B., and M. Inbar, 1984, A method for the determination of the discharge-frequency relationship in ungaged arid gravel streams: Journal of Hydrology, 69:163-172.

Bruning, J. E., 1973, Origin of the Popotosa Formation, north-central Socorro County, New Mexico: New Mexico Institute of Mining and Technology, unpublished Ph.D. dissertation, 132p.

Bull, W. B., 1984, Tectonic geomorphology: Journal of Geologic Education, v32, p. 310-324.

Callender, J. F., and R. E. Zillinski, 1976, Kinematics of Tertiary and Quaternary deformation along the eastern edge of the Lucero uplift, central New Mexico: New Mexico Geological Society Special Publication 6, p. 53-61.

Cather, S. M., 1982, Geology of the Table Mountain quadrangle: in Osburn, J. C., Geology and coal resources of three quadrangles in the central Datil Mountain coal field, Socorro County, New Mexico: New Mexico Bureau of Mines and Mineral Resources Open-file Report 164, 82 p.

Cather, S. M., and B. D. Johnson, 1984, Eocene tectonics and depositional setting of west-central New Mexico and eastern Arizona: New Mexico Bureau of Mines and Mineral Resources Circular 192, 33p.

Chamberlin, R. M., 1978, Geologic maps and cross sections of the Lemitar, Socorro, and north Chupadera Mountains: New Mexico Bureau of Mines and Mineral Resources Open-file Report 88.

------------------, 1983, Cenozoic domino-style crustal extension in the Lemitar Mountains, New Mexico: A Summary: New Mexico Geological Society Guidebook 34, p. 111-118.

Chapin, C. E., Sanford, A. R., White, D. W., Chamberlin, R. M., and G. R. Osburn, 1979, Geologic investigation of the Socorro geothermal area - final report: New Mexico Bureau of Mines and Mineral Resources Open-file Report 80, 70 p.

Chapin, C. E. and W. R. Seager, 1975, Evolution of the Rio Grande rift in the Socorro and Las Cruces areas: New Mexico Geological Society Guidebook 26, p. 297-321.

Cherkauer, D. S., 1972, Longitudinal profiles of ephemeral streams in southwestern Arizona: Geological Society of America Bulletin, v83, p. 353-366.

Chorley, R. J., Schumm, S. A., and D. E. Sugden, 1985, Geomorphology: New York, Methuen and Co., 607 p.

Coffin, G. C., 1981, Geology of the southwestern Gallinas Mountains, Socorro County, New Mexico: unpublished Masters Thesis, New Mexico Institute of Mining and Technology, Socorro, New Mexico.

Condie, K. C., 1976, Precambrian rocks of Ladron Mountains, Socorro County, New Mexico, New Mexico Bureau of Mines and Mineral Resources Geologic Map 38.

Dane, C. H., Wanek, A. A., and J. B. Reedside, Jr., 1957, Reinterpretation of section of Cretaceous rocks in Alamosa Creek Valley area, Catron and Socorro counties, New Mexico:

American Association of Petroleum Geologists Bulletin, v41, p. 181-196.

Denny, C. S., 1940, Tertiary geology of the San Acacia area, New Mexico: Journal of Geology, v48, p. 73-106.

--------------, 1949, Quaternary geology of the San Acacia area, New Mexico: Journal of Geology, v49, n3, p. 225-260.

Gabin, V. L., and L. E. Lesperance, 1977, New Mexico climatological data, precipitation, temperature, evaporation, and wind, monthly and annual means 1850-1975: Socorro, New Mexico, W. K. Summers and Assiciates, 436p.

Gile, L. H., Hawley, J. W., and R. B. Grossman, 1981, Soils and geomorphology in the Basin and Range area of southern New Mexico - guidebook to the Desert Project: New Mexico Bureau of Mines and Mineral Resources Memoir 39, 222p.

Givens, D. B., 1978, Geology of Dog Springs quadrangle, New Mexico: New Mexico Bureau of Mines and Mineral Resources Bulletin 58, 40 p.

Gregory, K. J., and D. E. Walling, 1973, Drainage basin form and process: A geomorphological approach: London, Edward Arnold, 456 p.

Gupta, S. K., and S. I. Solomon, 1977, Distributed numerical model for estimating runoff and sediment discharge of ungaged rivers 1. The information system: Water Resources Research, v13(3), p. 613-617.

--------------------------------------, 1977, Distributed numerical model for estimating runoff and sediment discharge of ungaged rivers 3. Comparison with other simple techniques: Water Resources Research, v13(3), p. 631-636.

Harrison, R. W., 1980, Geology of the northeast Datil Mountains, Socorro County, New Mexico: unpublished Masters Thesis, New Mexico Institute of Mining and Technology, Socorro, New Mexico.

Horton, R. E., 1945, Erosional development of streams and their drainage basins: hydrophysical approach to quantitative morphology: Geological Society of America Bulletin, v56. p. 275-370.

Hunt, C. B., 1978, Surficial geology of northwest New Mexico: New Mexico Bureau of Mines and Mineral Resources Geologic Map 43.

Jicha, H. L., 1958, Geology and mineral resources of Mesa del Oro quadrangle, Socorro and Valencia counties, New Mexico: New Mexico Bureau of Mines and Mineral Resources Bulletin 56, 67p.

Johansen, S., 1983, The thick-splay depositional style of the Crevasse Canyon Formation, Cretaceous of the west-central New Mexico: New Mexico Geological Society Guidebook 34, p. 173-178.

LaRoche, T. M., 1980, Geology of the Gallinas Peak area, Socorro County, New Mexico: unpublished Masters Thesis, New Mexico Institute of Mining and Technology, Socorro, New Mexico.

Larsen, S., and R. E. Reilinger, 1983, Recent measurements of crustal deformation related to the Socorro Magma Body, New Mexico: New Mexico Geological Society Guidebook 34, p. 119-121.

Larsen, S., Reilinger, R. E., and L. Brown, 1986, Evidence of ongoing crustal deformation related to magmatic activity near San Acacia, New Mexico: Journal of Geophysical Research, v91, no. B6, p. 6283-6292.
Leopold, L. B., and T. Maddock, 1953, The hydraulic geometry of stream channels and some physiographic implications: U.S.G.S. Professional Paper 252, 57 p.
Leopold, L. B., and J. P. Miller, 1956, Ephemeral streams: hydraulic factors and their relationship to the drainage net: U.S.G.S. Professional Paper 282-A, 37p.
Leopold, L. B., Wolman, M. G., and J. P. Miller, 1964, Fluvial Processes in Geomorphology: W. H. Freeman, San Francisco, Ca., 522p.
Love, D. W., 1979, Quaternary fluvial geomorphic adjustments in Chaco Canyon, New Mexico: in Adjustments of the Fluvial System - Proceedings of the 10th annual Geomorphology Symposia Series, held at Binghamton, New York, Sept. 21-22, 1979: Dubuque, Kendall/Hunt Publishing Co., p. 277-308.
Machette, M., 1977, Geologic map of San Acacia 7.5-minute quadrangle, Socorro County, New Mexico: U.S.G.S. Geologic Quadrangle Map GQ-1415.
Maker, H. J., Downs, J. M., and J. U. Anderson, 1985(?), Soil association and land classification for irrigation, Socorro County, New Mexico: New Mexico State University Agricultural Experimental Station Research Report 234.
Massingill, G. L., 1979, Geology of the Riley-Puertecito area, southeastern margin of the Colorado Plateau, Socorro County, New Mexico: unpublished Ph.D. dissertation, University of Texas (El Paso), 301 p.
Meyerson, D. L., 1979, Geology of the Corkscrew Canyon- Abbe Springs area, Socorro County, New Mexico: New Mexico Bureau of Mines and Mineral Resources Open-file Report 103.
Morisawa, M. E., 1957, Accuracy of determination of stream lengths from topographic maps: (EOS) Transactions of the American Geophysical Union, 38, 86-88.
-----------------, 1961, Reply to letter by W. J. Schneider: Journal of Geophysical Research, v66(10), p.3619.
Osburn, G. R., 1984, Socorro County Geologic Map: New Mexico Bureau of Mines and Mineral Resources Open-file Report 238.
Osburn, J. C., 1982a, Geology and coal resources of the Alamo Band Navajo Reservation, Socorro County, New Mexico: New Mexico Bureau of Mines and Mineral Resources Open-file Report 160, 60 p.
--------------, 1982b, Geology and coal resources of three quadrangles in the central Datil Mountain coal field, Socorro County, New Mexico: New Mexico Bureau of Mines and Mineral Resources Open-file Report 164.
-------------, 1983, Geology and coal resources of Pasture Canyon quadrangle, Catron County, New Mexico: New Mexico Bureau of Mines and Mineral Resources Open-file Report 182, 27 p.
-------------, 1984, Geology of Pueblo Viejo Mesa quadrangle, Socorro and Cibola Counties, New Mexico: New Mexico Bureau of Mines and Mineral Resources Geologic Map 55.
-------------, 1985, Geology and coal resources of Wild Horse

Canyon quadrangle, Catron and Cibola Counties, New Mexico: New Mexico Bureau of Mines and Mineral Resources Open-file Report 227, 28p.

--------------, 1986, Cretaceous rocks and coal resources of the Magdalena, New Mexico 1:100,000 sheet: New Mexico Bureau of Mines and Mineral Resources Open-file Report 254, 7 p.

Ouchi, S., 1983a, Effects of uplift on the Rio Grande over the Socorro magma body, New Mexico: New Mexico Geological Society Guidebook 34, p. 54-56.

----------, 1983b, Response of alluvial rivers to active tectonics: unpublished Ph.D. dissertation, Colorado State University, Fort Collins, Colorado, 205 p.

Reilinger, R. E., Oliver, J. E., Brown, L. D., Sanford, A. R., and E. I. Balaz, 1980, New measurements of crustal doming over the Socorro Magma Body: Geology, 8, p.291-295.

Robinson, B. R., 1981, Geology of the D-Cross Mountain quadrangle, Socorro County, New Mexico, New Mexico Bureau of Mines and Mineral Resources Open-file Report 147.

Rodriguez-Iturbe, I., and J. B. Valdez, 1979, The geomorphological structure of hydrologic response: Water Resources Research, v15(6), p. 1409-1420.

Rodriguez-Iturbe, I., Gonzales Sanabria, M., and R. L. Bras, 1982, A geomorphoclimatic theory of the instantaneous unit hydrograph: Water Resources Research, v18(4).

Sanford, A., 1983, Magma bodies in the Rio Grande rift in central New Mexico: New Mexico Geological Society Guidebook 34, p. 123-125.

Sanford, A., Jaksha, L., and D. Wieder, 1983, Seismicity of the Socorro area of the Rio Grande rift: New Mexico Geological Society Guidebook 34, p. 127-131.

Schneider, W. J., 1961, A note on the accuracy of drainage density computed from topographic maps: Journal of Geophysical Research, v66(10), p. 3617-3618.

Schumm, S. A., 1960, The shape of alluvial channels in relation to sediment type: U.S.G.S. Professional Paper 352-B, p. 17-30.

----------------, 1961, Efect of sediment characteristics on erosion and deposition in ephemeral-stream channels: U.S.G.S. Professional Paper 352-C, 70p.

Shreve, R. L., 1966, Statistical law of stream numbers: Journal of Geology, v74, p. 17-37.

Solomon, S. I., and S. K. Gupta, 1977, Distributed numerical model for estimating runoff and sediment discharge of ungaged rivers 2. Model development: Water Resources Research, v13(3), p. 619-629.

Spiegel, Z. E., 1955, Geology and ground-water resources of northwestern Socorro County, New Mexico: New Mexico Bureau of Mines and Mineral Resources Ground-Water Report 4, 99p.

Stephens, D. B., Cox, W., and J. Havlena, 1987, Field study of ephemeral stream infiltration and recharge: New Mexico Water Resources Research Institute Technical Completion Report, project nos. 1423655 and 1423658.

Strahler, A. N., 1952, Hypsometric (area-altitude) analysis of erosional topography: Geological Society of America Bulletin, v63, p. 1117-1142.

------------------, 1964, Quantitative geomorphology of drainage basins and channel networks: in V. T. Chow (ed.), Handbook of Applied Hydrology, New York, McGraw-Hill, Section 4-II.

Thomas, H. E., 1962, The meteorological phenomenon of drought in the southwest: U.S.G.S. Professional Paper 372-A, 43p.

Tonking, W. H., 1957, Geology of the Puertecito 15 minute quadrangle, Socorro County, New Mexico: New Mexico Bureau of Mines and Mineral Resources Bulletin 41, 67p.

U.S.D.A., 1985, Engineering field manual for conservation practices - New Mexico: Soil Conservation Service.

Valdez, J. B., Fiallo, Y., and I. Rodriguez-Iturbe, 1979, A rainfall-runoff analysis of the geomorphological IUH: Water Resources Research, v15(6), p. 1421-1434.

Werritty, A., 1972, Accuracy of stream lengths derived from maps: Water Resources Research, v8(5), p. 1255-1264.

Willard, M. E., and D. B. Givens, 1958, Reconnaissance geologic map of Datil thirty-minute quadrangle: New Mexico Bureau of Mines and Mineral Resources Geologic Map 5.

Winchester, D. E., 1920, Geology of the Alamosa Creek Valley, Socorro County, New Mexico, with special reference to the occurrence of oil and gas: U.S.G.S. Bulletin 716, 15p.

Wolman, M. G., 1955, The natural channel of Brandywine Creek, Pennsylvania: U.S.G.S. Professional Paper 271, 56p.

Wright, H. E., 1946, Tertiary and Quaternary history and geology of the lower Rio Puerco, New Mexico: Geological Society of America Bulletin, v57, p. 383-456.

HYDROGEOLOGIC PARAMETERS OF AN EPHEMERAL STREAM: THE RIO SALADO OF CENTRAL NEW MEXICO

VOLUME II

APPENDICES

Submitted by

Jeff Havlena

in partial fulfillment of the requirements of Hydrology 590

Spring 1988

VOLUME II: Appendices

APPENDIX A: Normalized Longitudinal Profiles, Magnitude Input, and Hypsometric Curves.

EXPLANATION

Solid lines: Longitudinal profile, normalized according to:

x =(distance from source)/(total length)

y =(elevation - minimum channel elevation)/
(total channel relief)

Long dashed lines: Shreve Magnitude Input. Normalized According to:

x =(distance from source)/(total length)

y = 1-(magnitude)/(total magnitude)

Short dashed lines: Hypsometric curves, normalized according to procedures described in section 2.3.2.

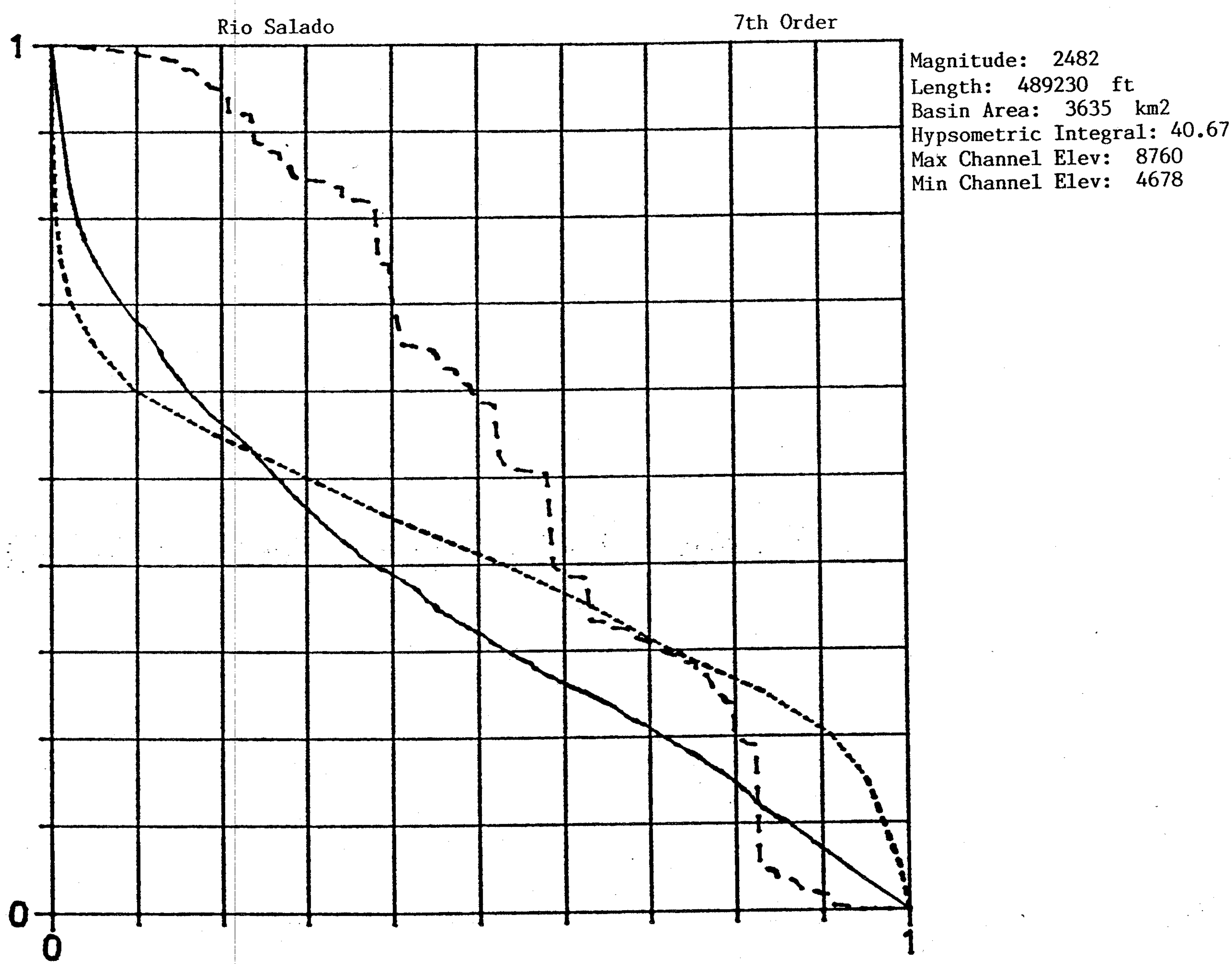
Rio Salado
7th Order
1
0
0
1
Magnitude: 2482
Length: 489230 ft
Basin Area: 3635 km2
Hypsometric Integral: 40.67
Max Channel Elev: 8760
Min Channel Elev: 4678

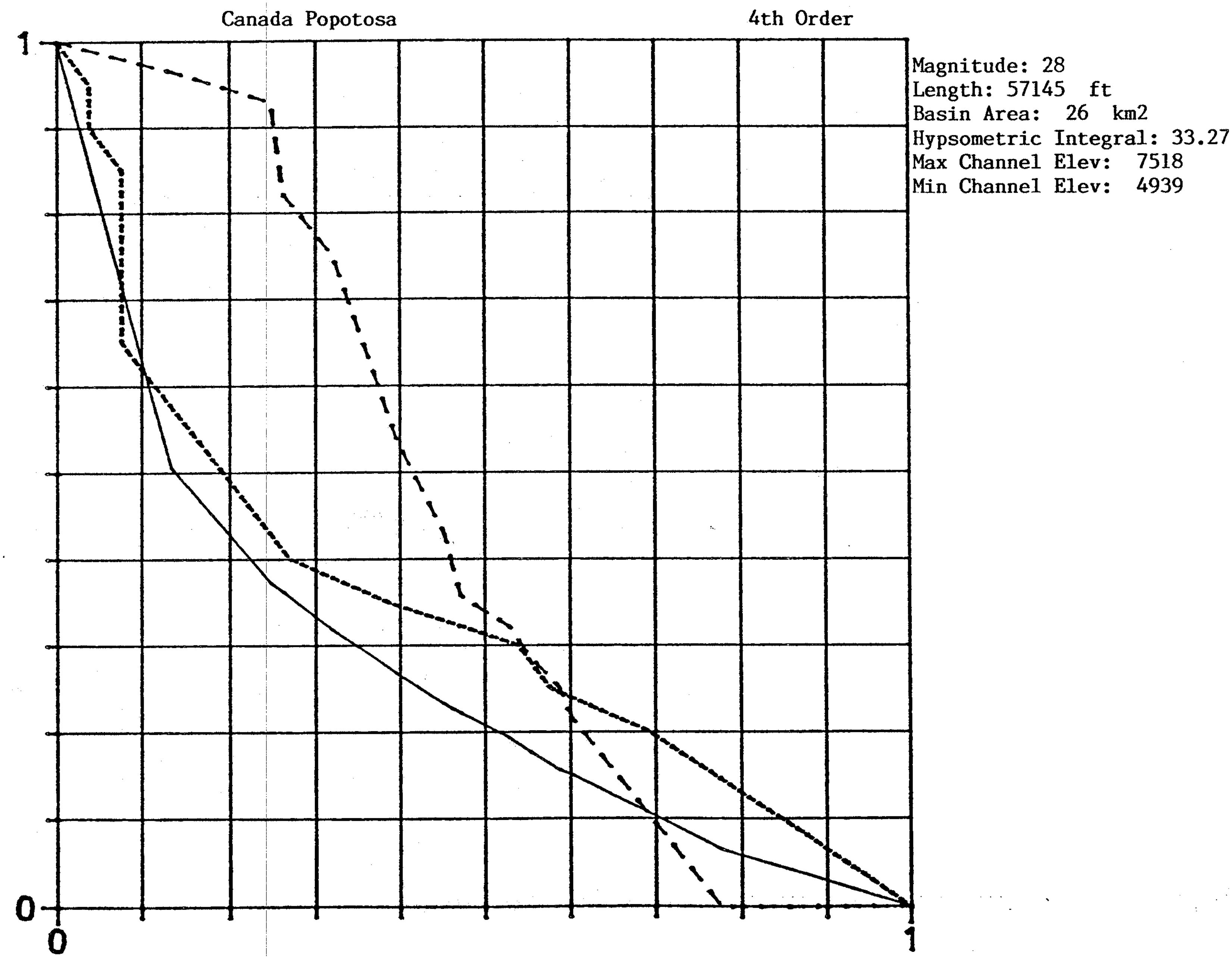
Canada Popotosa
4th Order
1
0
0
1
Magnitude: 28
Length: 57145 ft
Basin Area: 26 km2
Hypsometric Integral: 33.27
Max Channel Elev: 7518
Min Channel Elev: 4939

Silver Creek 4th Order

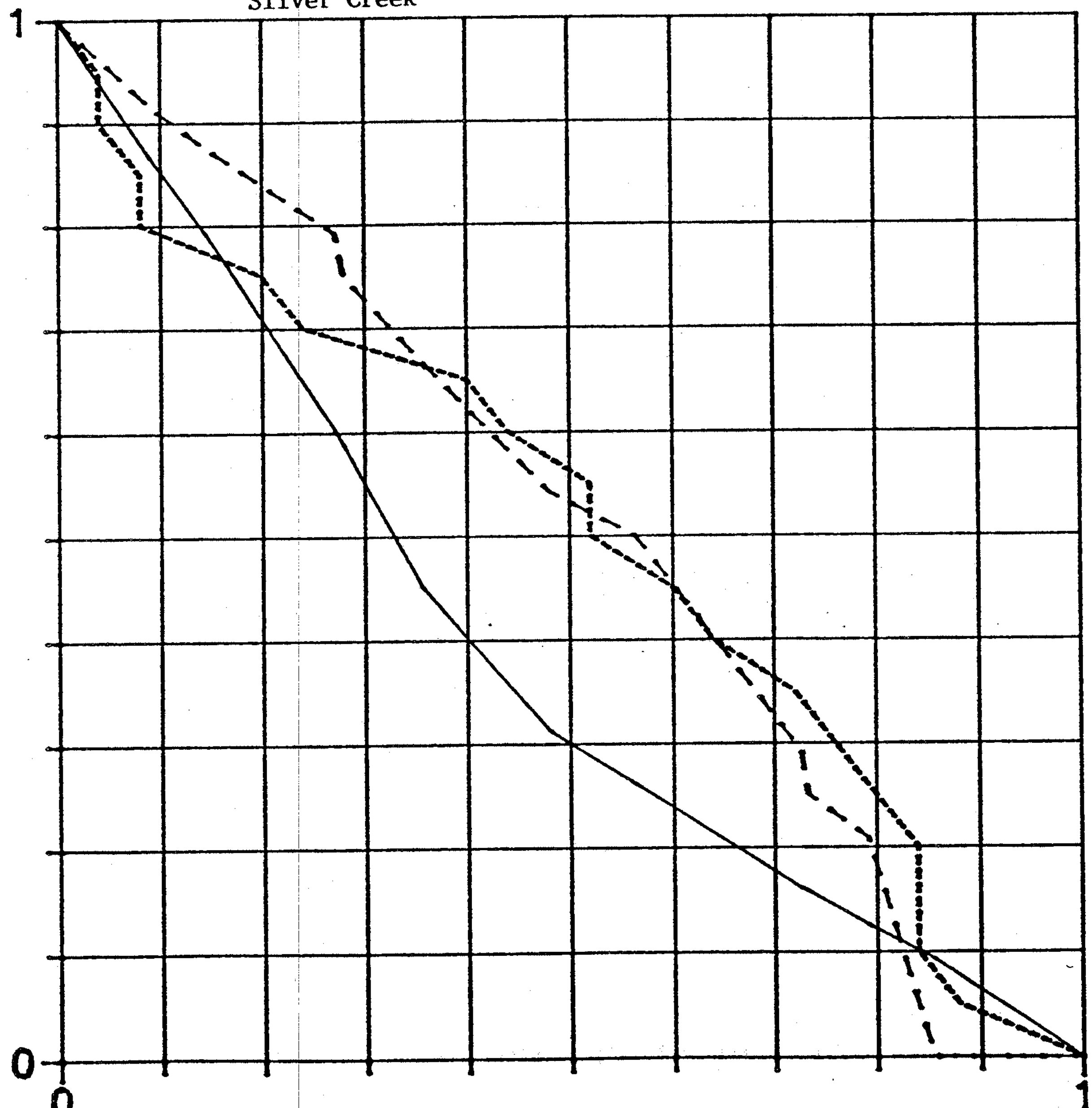

Magnitude: 24
Length: 35940 ft
Basin Area: 25 km2
Hypsometric Integral: 49.90
Max Channel Elev: 5748
Min Channel Elev: 5036

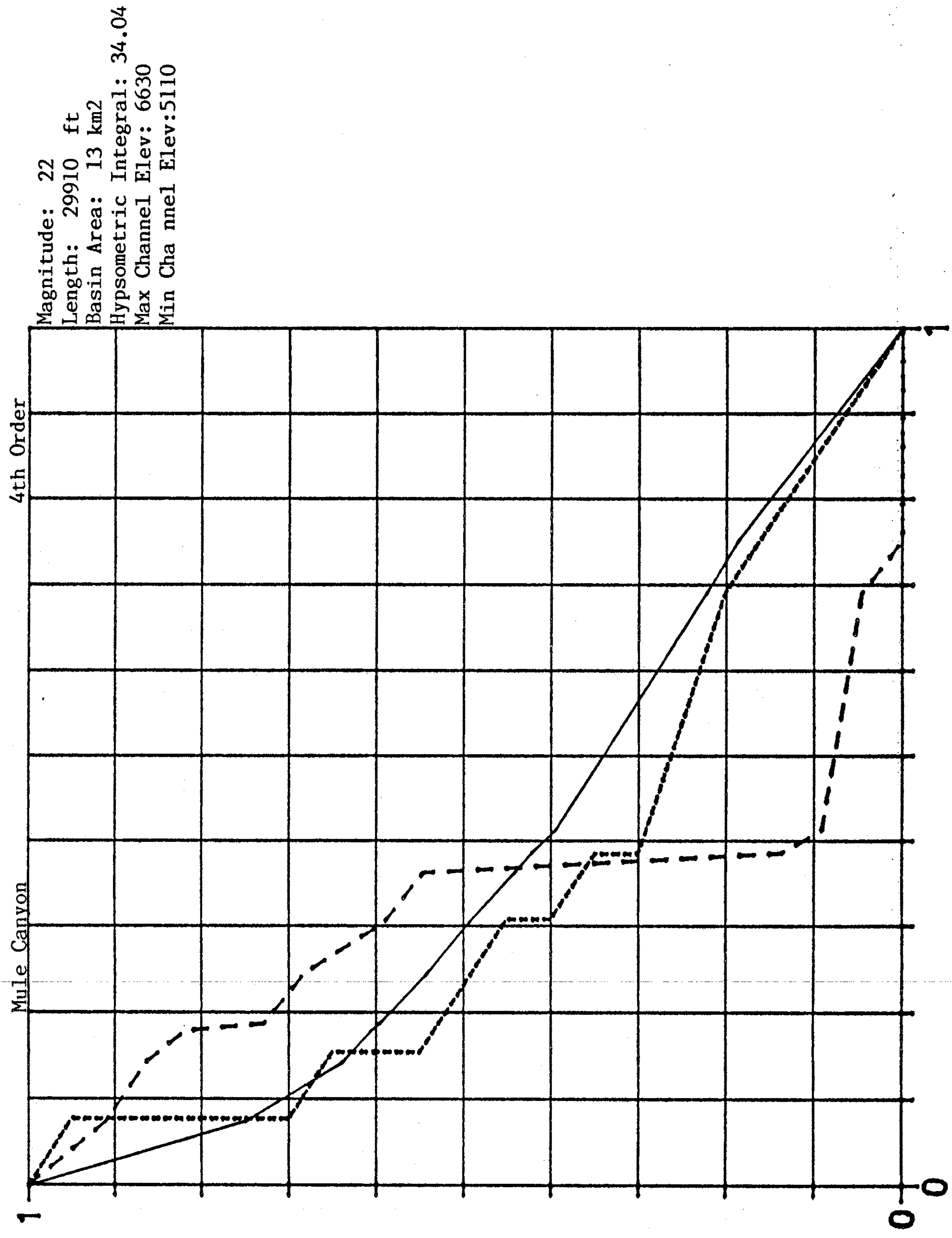
Mule Canyon
4th Order
Magnitude: 22
Length: 29910 ft
Basin Area: 13 km2
Hypsometric Integral: 34.04
Max Channel Elev: 6630
Min Cha nnel Elev:5110
1
0
0
1

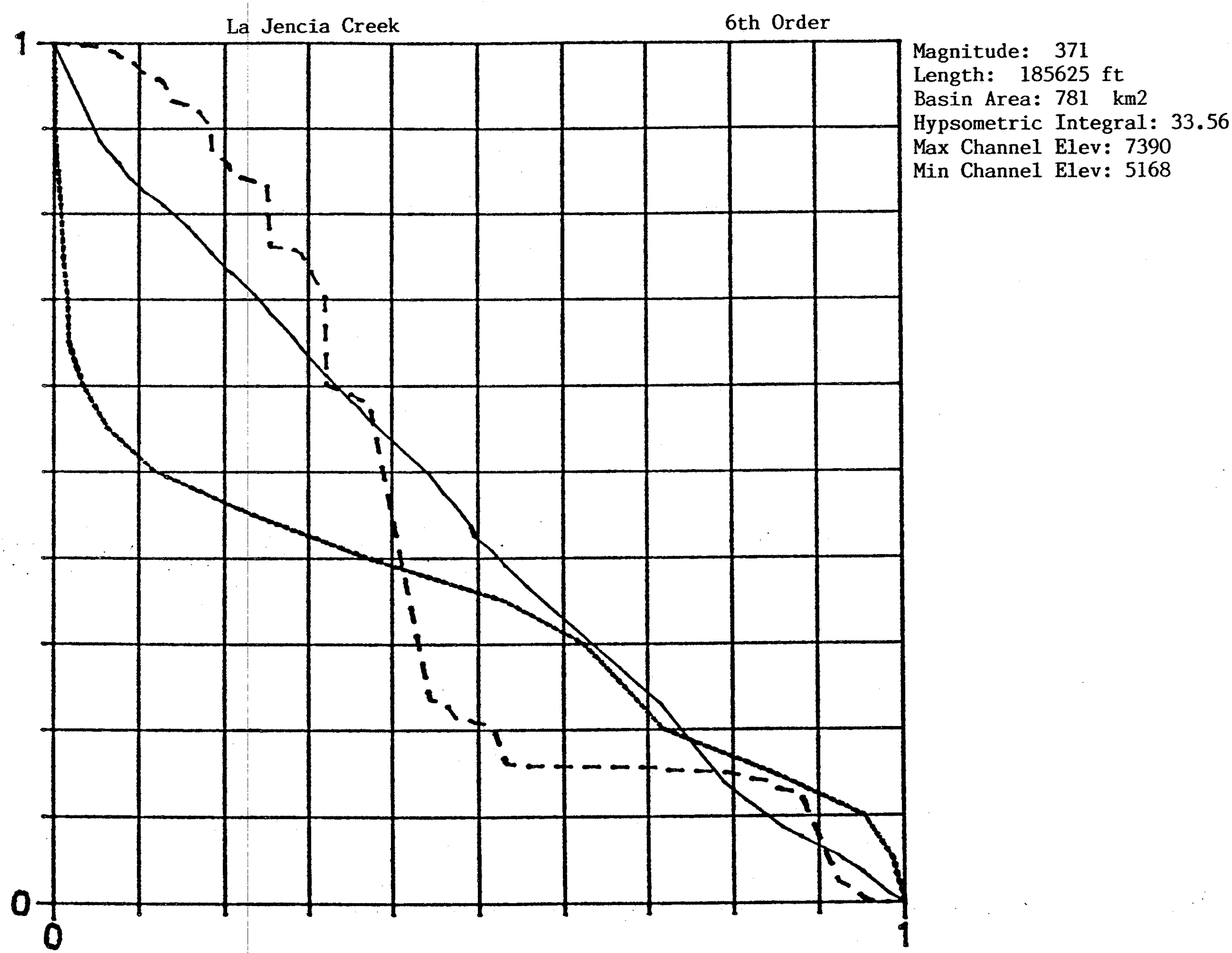
La Jencia Creek
6th Order
Magnitude: 371
Length: 185625 ft
Basin Area: 781 km2
Hypsometric Integral: 33.56
Max Channel Elev: 7390
Min Channel Elev: 5168
1
0
0
1

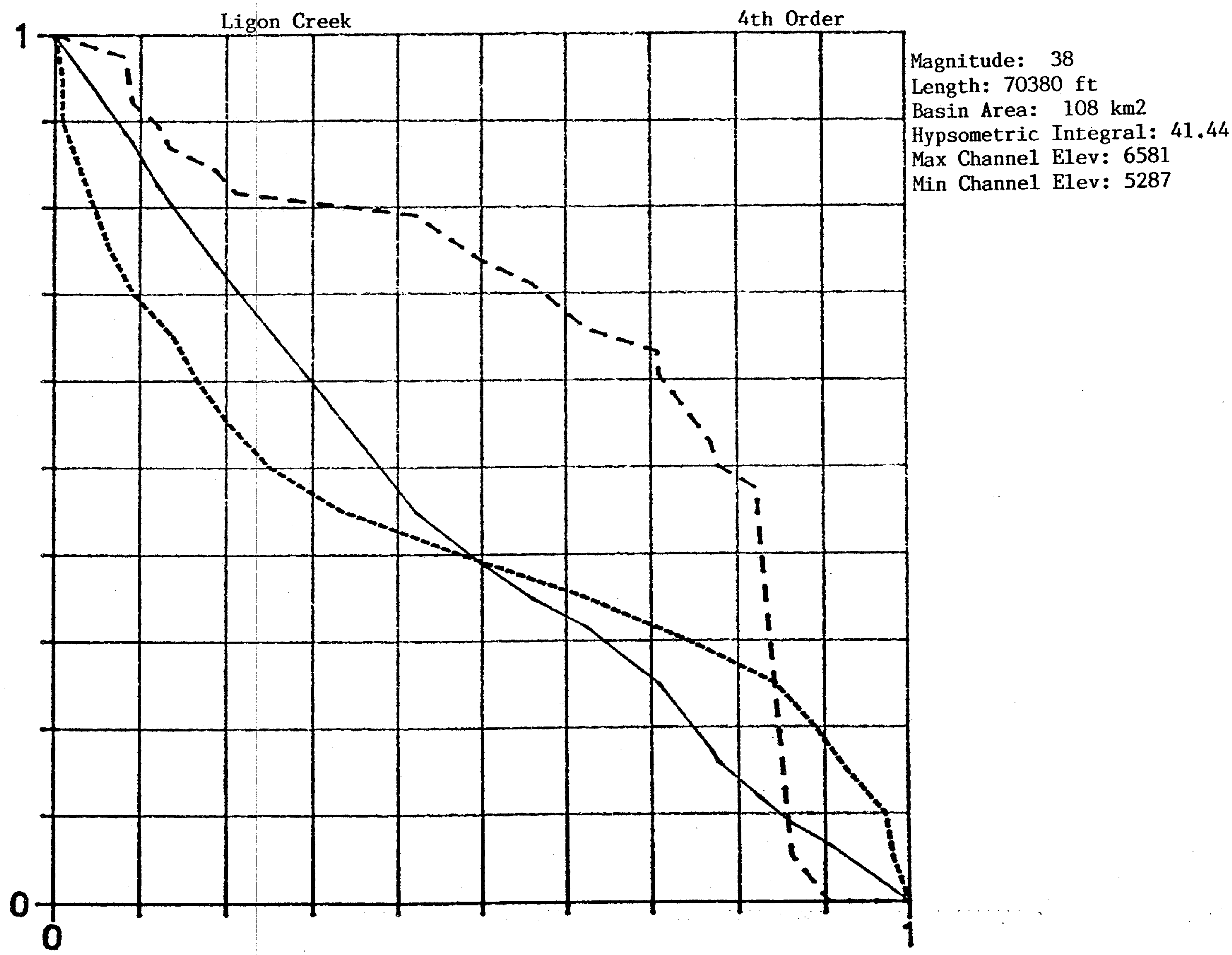
Ligon Creek
4th Order
Magnitude: 38
Length: 70380 ft
Basin Area: 108 km2
Hypsometric Integral: 41.44
Max Channel Elev: 6581
Min Channel Elev: 5287
1
0
0
1

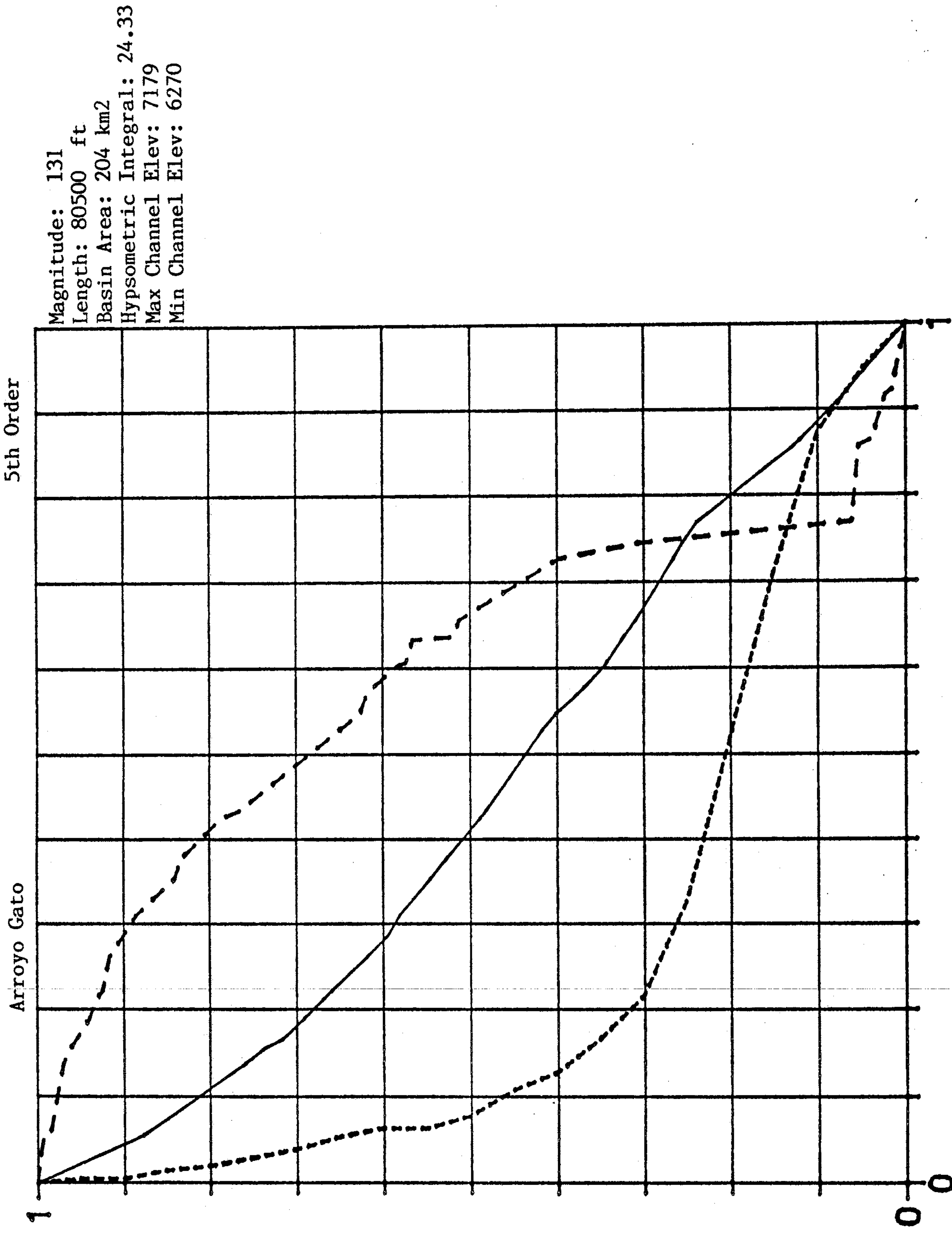
Arroyo Gato
5th Order
Magnitude: 131
Length: 80500 ft
Basin Area: 204 km2
Hypsometric Integral: 24.33
Max Channel Elev: 7179
Min Channel Elev: 6270
1
0
0
1

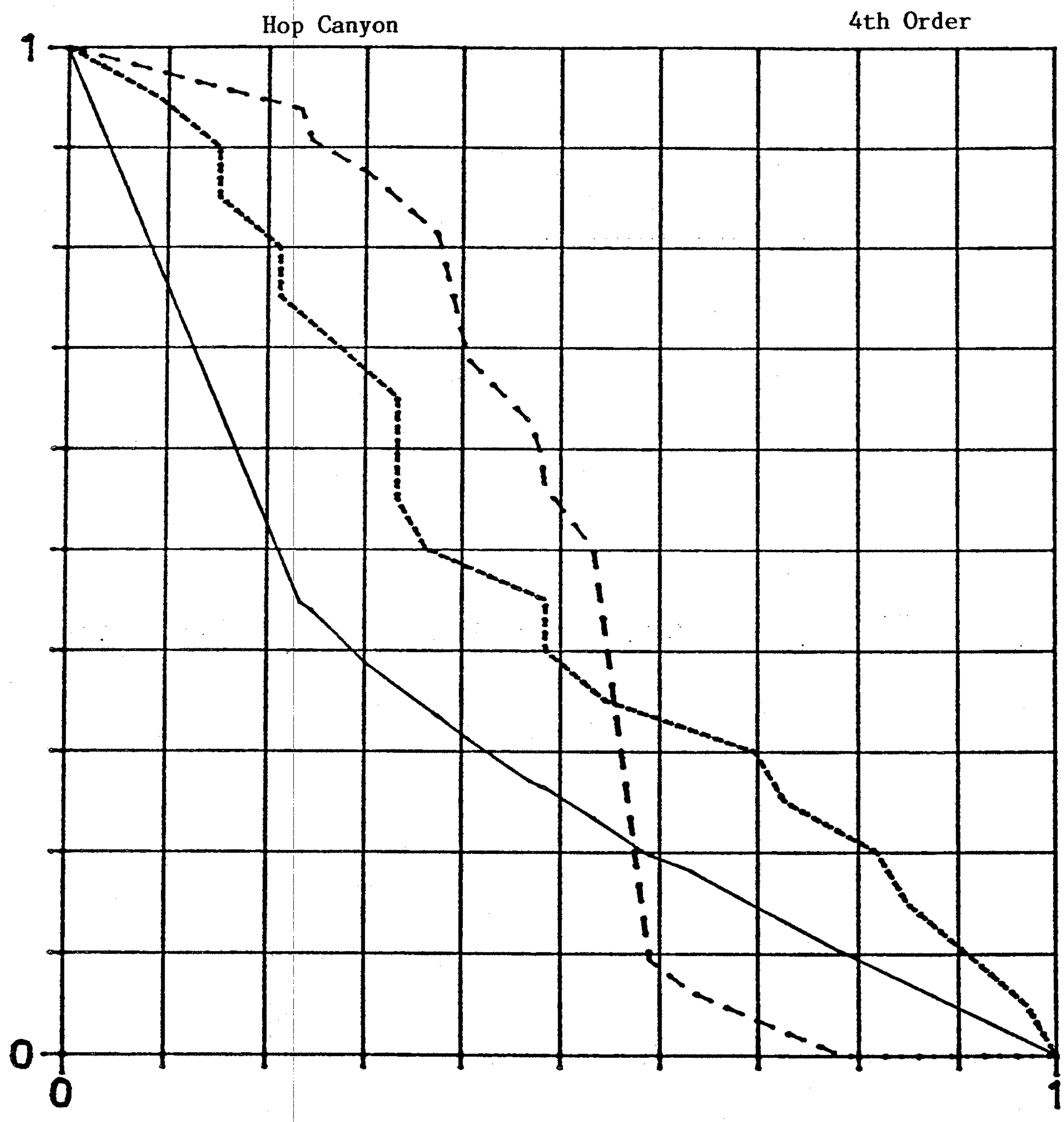

Magnitude: 32
Length: 35135 ft
Basin Area: 33 km2
Hypsometric Integral: 47.20
Max Channel Elev: 8318
Min Channel Elev: 6486

Arroyo Gato

4th Order

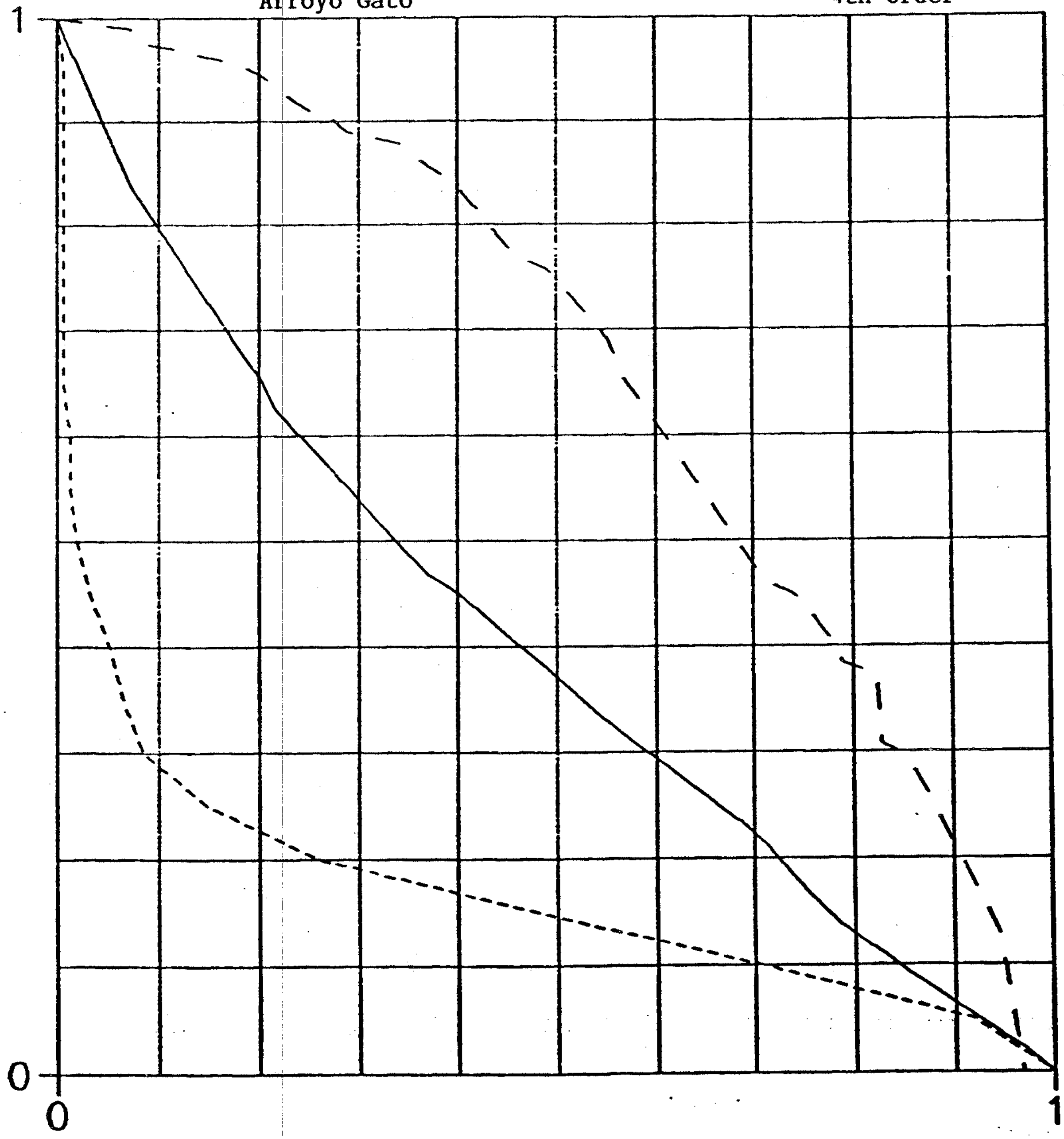

Magnitude: 91
Length: 61940 ft
Basin Area: 154 km2
Hypsometric Integral: 16.69
Max Channel Elev: 7179
Min Channel Elev: 6486

La Jencia Creek   5th Order

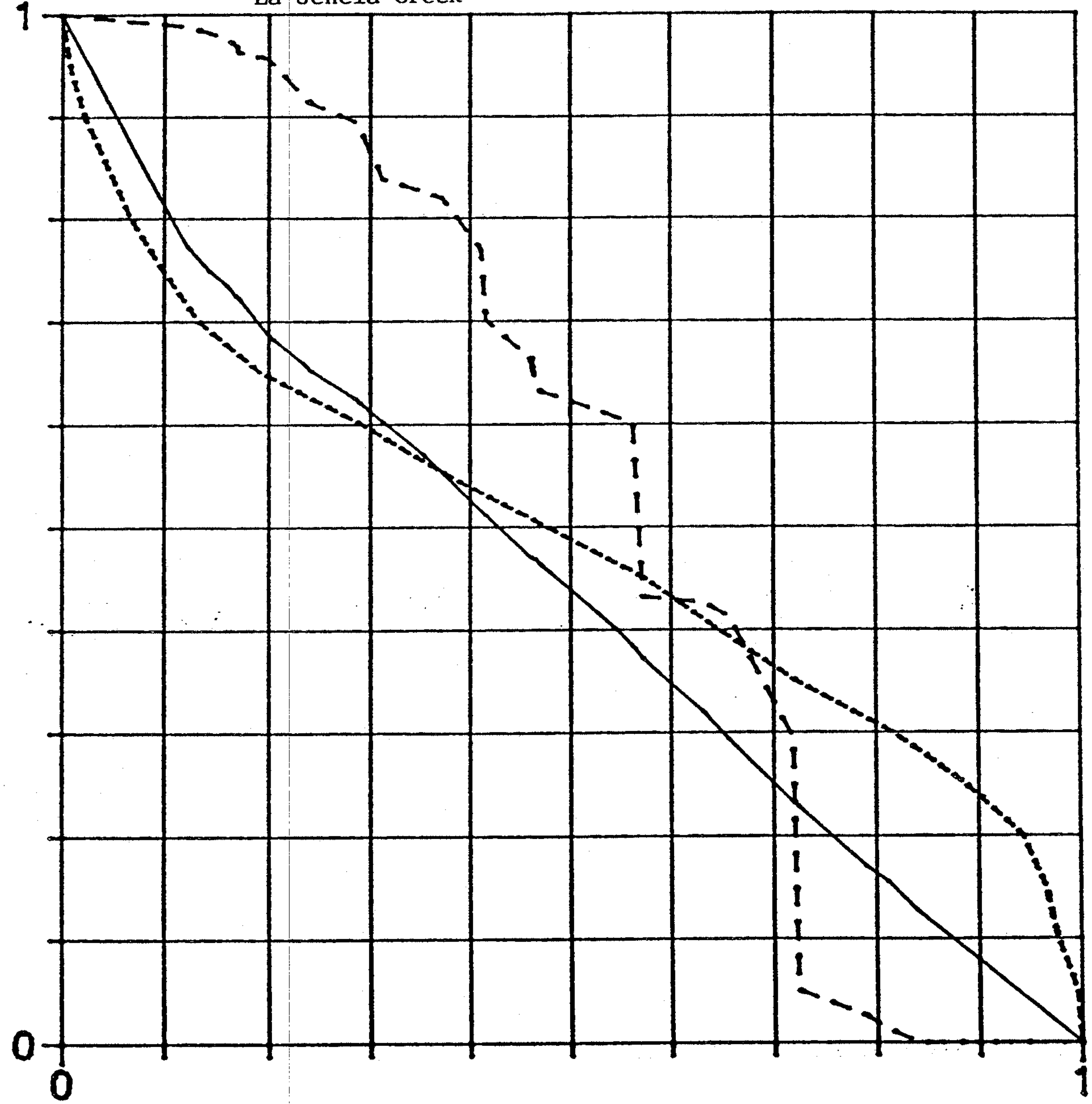

Magnitude: 160
Length: 82555 ft
Basin Area: 265 km2
Hypsometric Integral: 48.67
Max Channel Elev: 7390
Min Channel Elev: 6270

Arroyo Montosa

4th Order

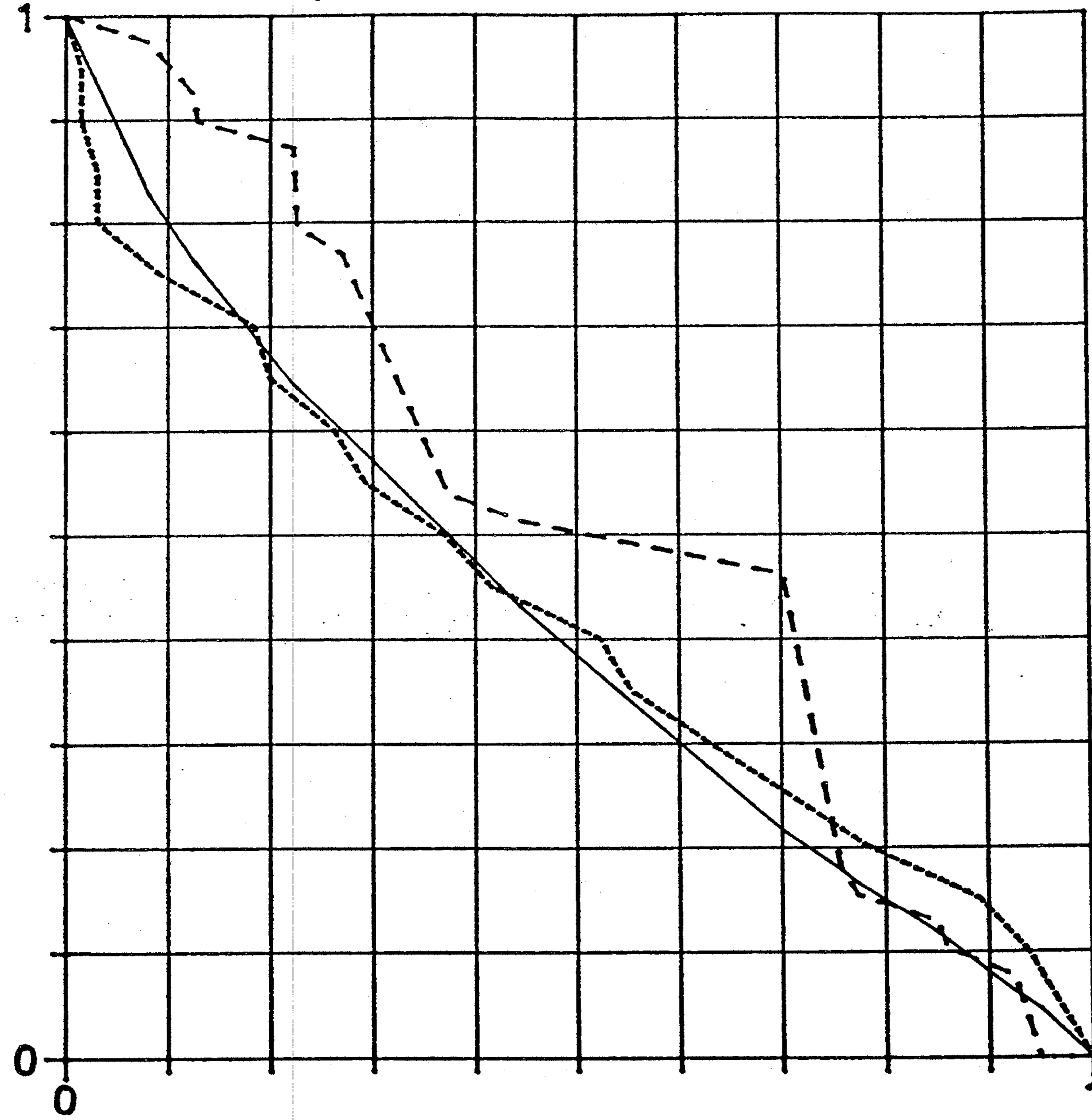

Magnitude: 39
Length: 55840 ft
Basin Area: 65 km2
Hypsometric Integral: 42.04
Max Channel Elev: 7440
Min Channel Elev: 6526

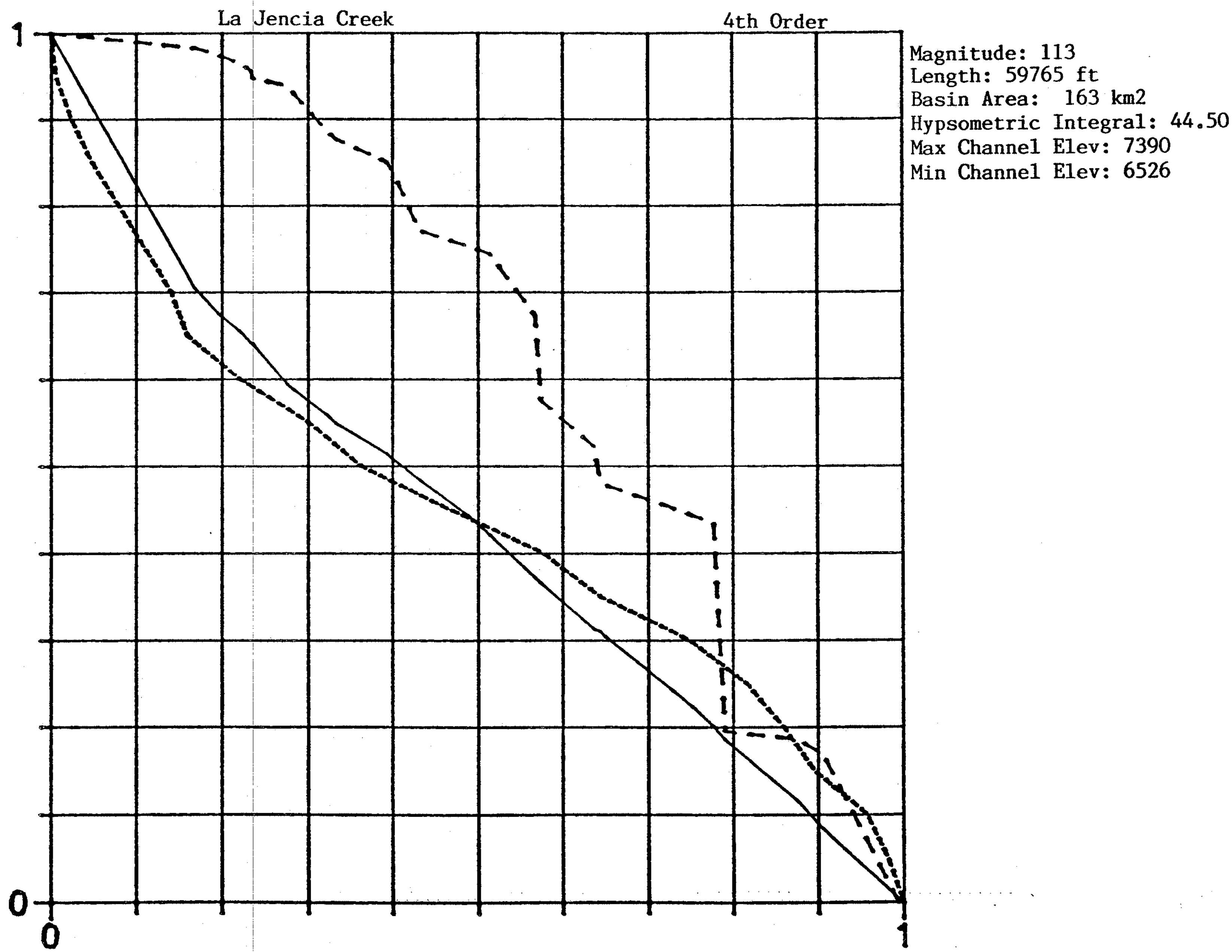
La Jencia Creek
4th Order
Magnitude: 113
Length: 59765 ft
Basin Area: 163 km2
Hypsometric Integral: 44.50
Max Channel Elev: 7390
Min Channel Elev: 6526
1
0
0
1

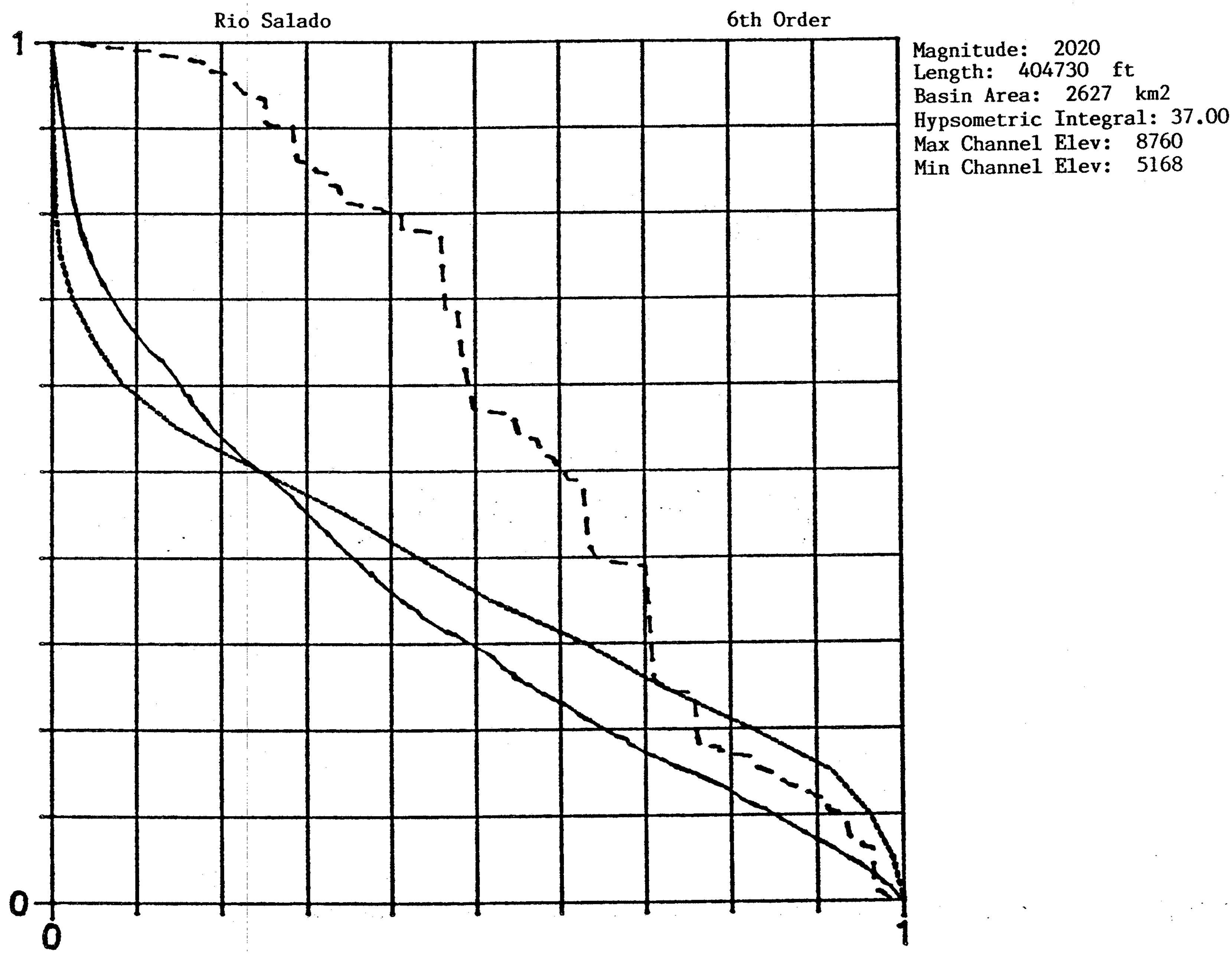
Rio Salado
6th Order
Magnitude: 2020
Length: 404730 ft
Basin Area: 2627 km2
Hypsometric Integral: 37.00
Max Channel Elev: 8760
Min Channel Elev: 5168
1
0
0
1

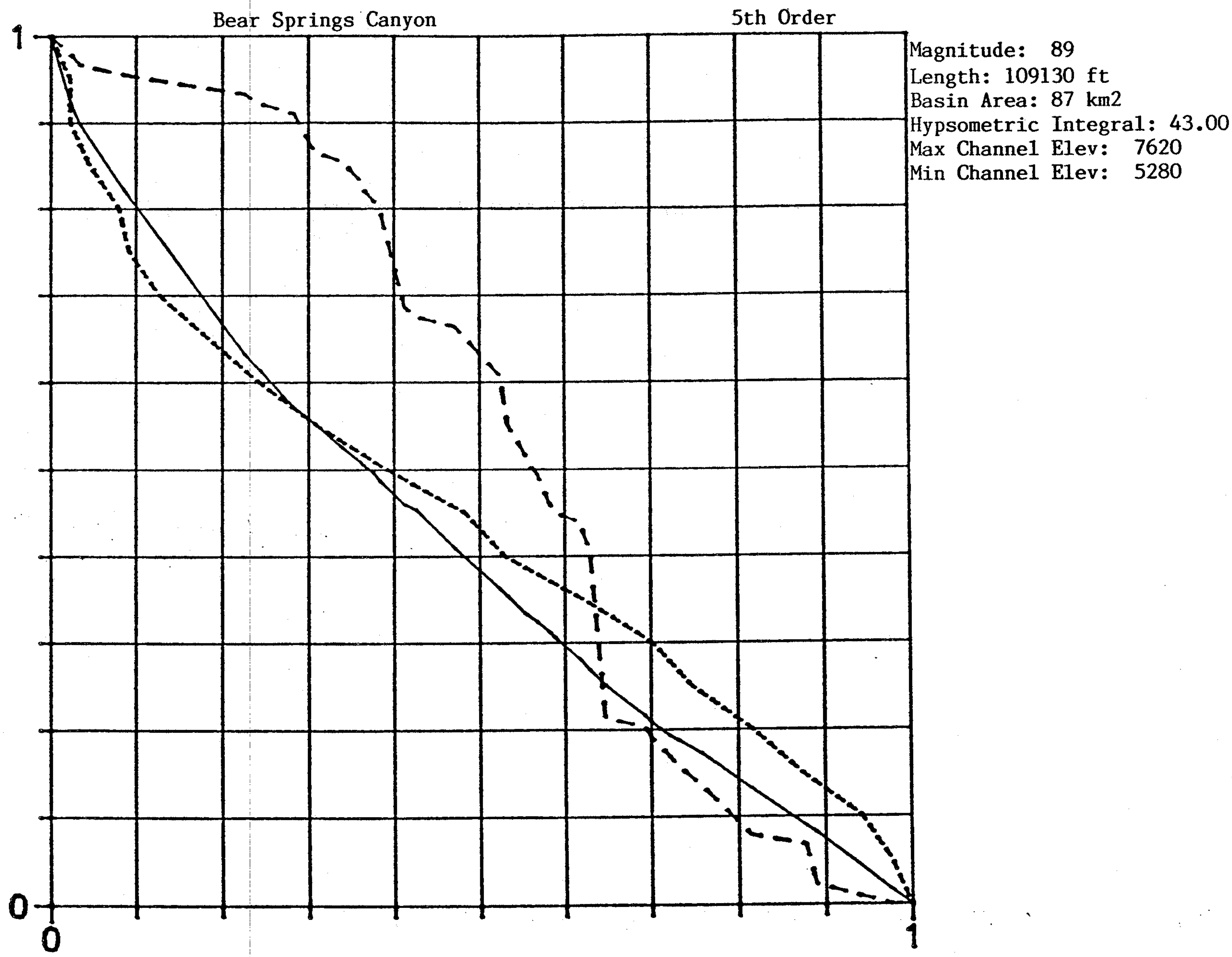

Bear Springs Canyon
5th Order
1
0
0
1
Magnitude: 89
Length: 109130 ft
Basin Area: 87 km2
Hypsometric Integral: 43.00
Max Channel Elev: 7620
Min Channel Elev: 5280

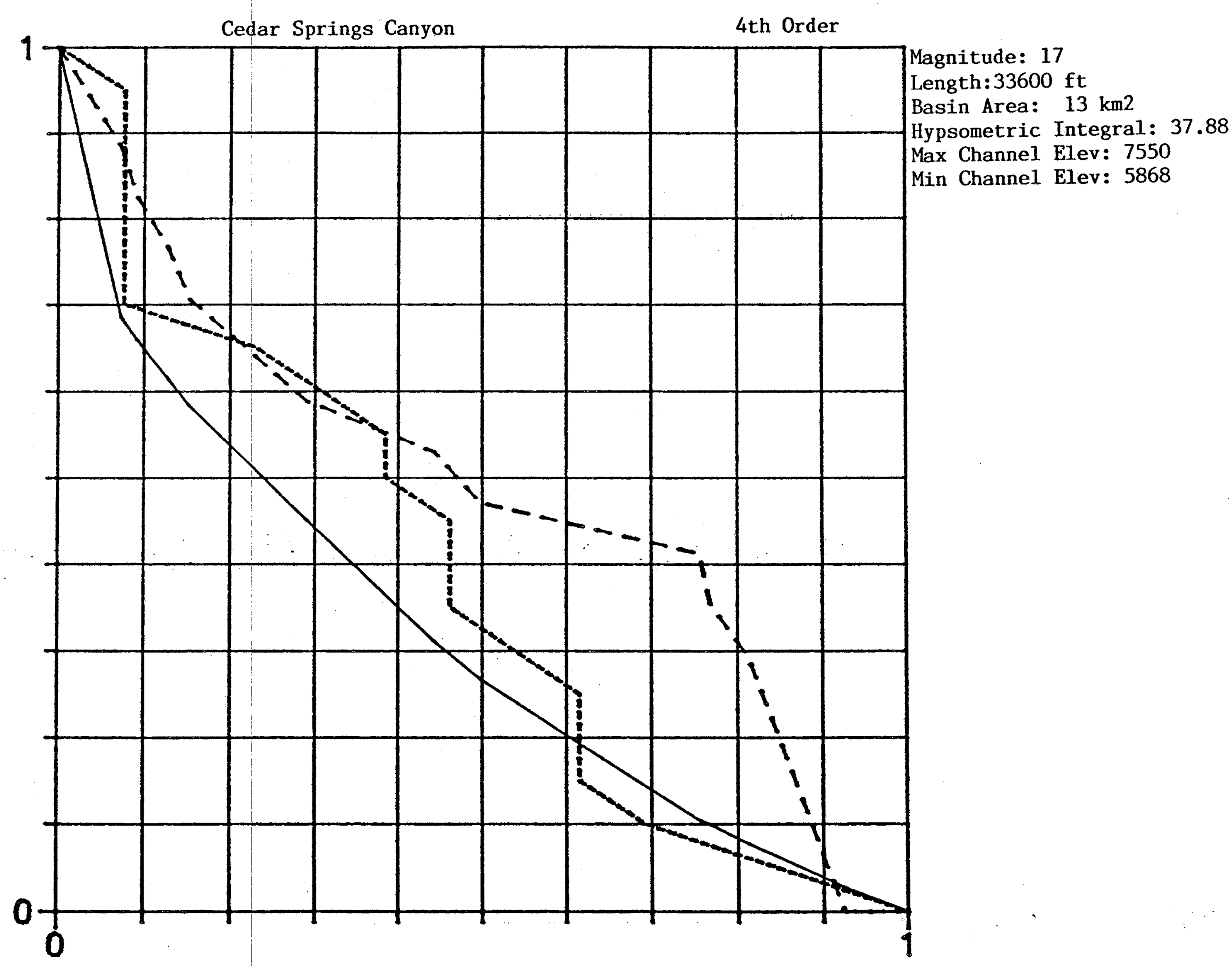
Cedar Springs Canyon
4th Order
Magnitude: 17
Length:33600 ft
Basin Area: 13 km2
Hypsometric Integral: 37.88
Max Channel Elev: 7550
Min Channel Elev: 5868
1
0
0
1

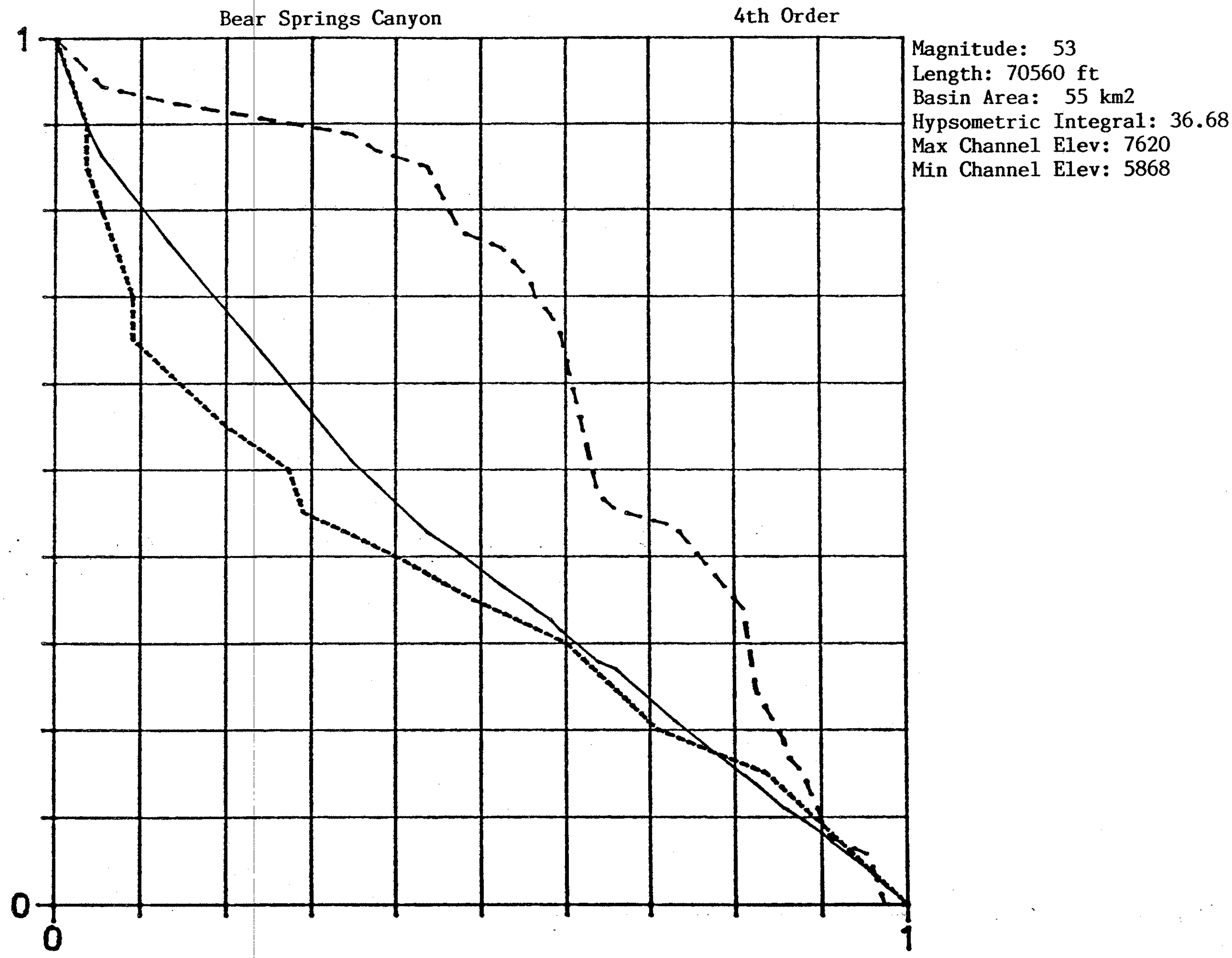
Bear Springs Canyon
4th Order
1
0
0
1
Magnitude: 53
Length: 70560 ft
Basin Area: 55 km2
Hypsometric Integral: 36.68
Max Channel Elev: 7620
Min Channel Elev: 5868

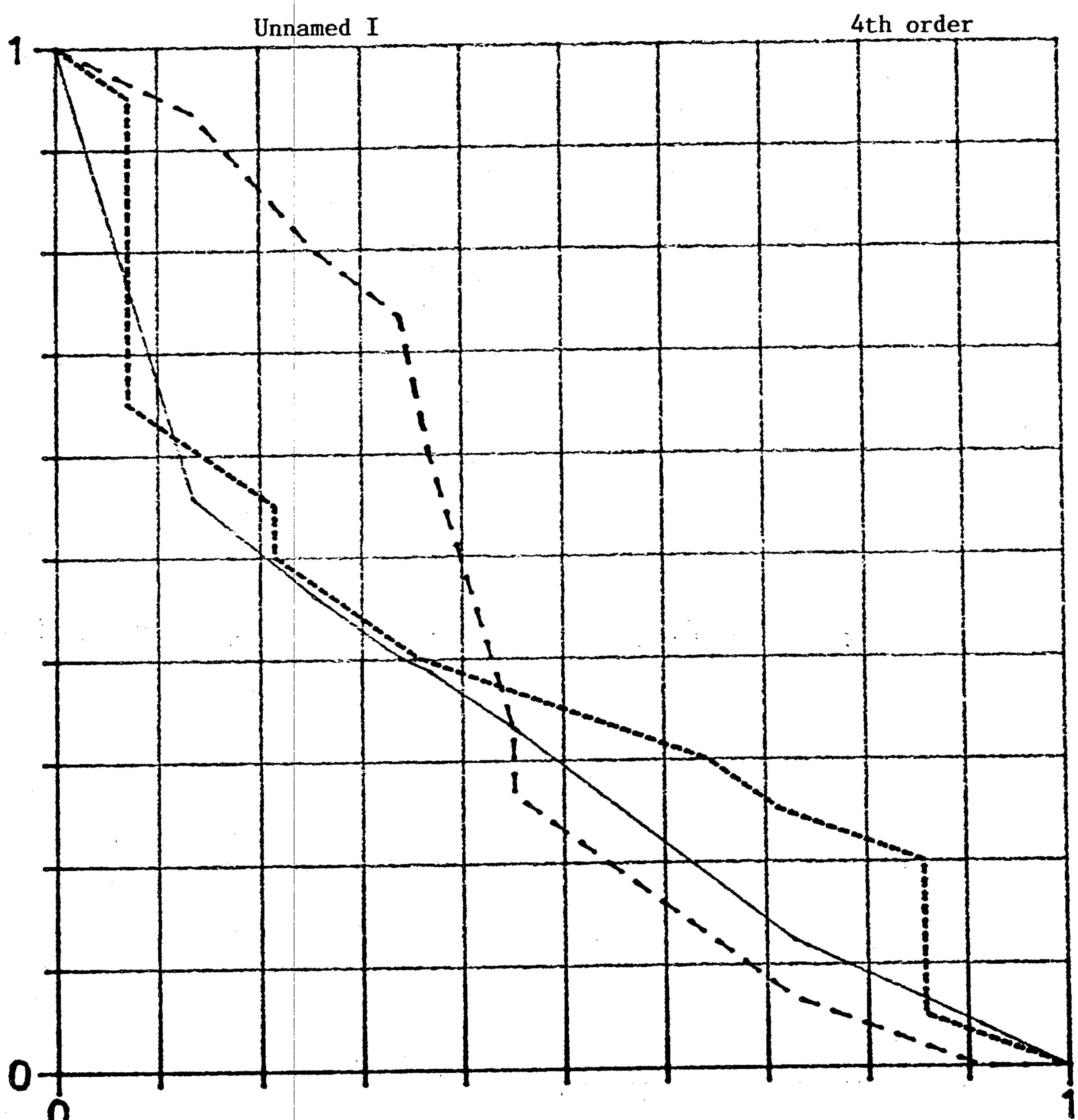

Magnitude: 14
Length: 32460 ft
Basin Area: 14 km2
Hypsometric Integral: 37.50
Max Channel Elev: 7040
Min Channel Elev: 5308

Canon de las Cabras

4th Order

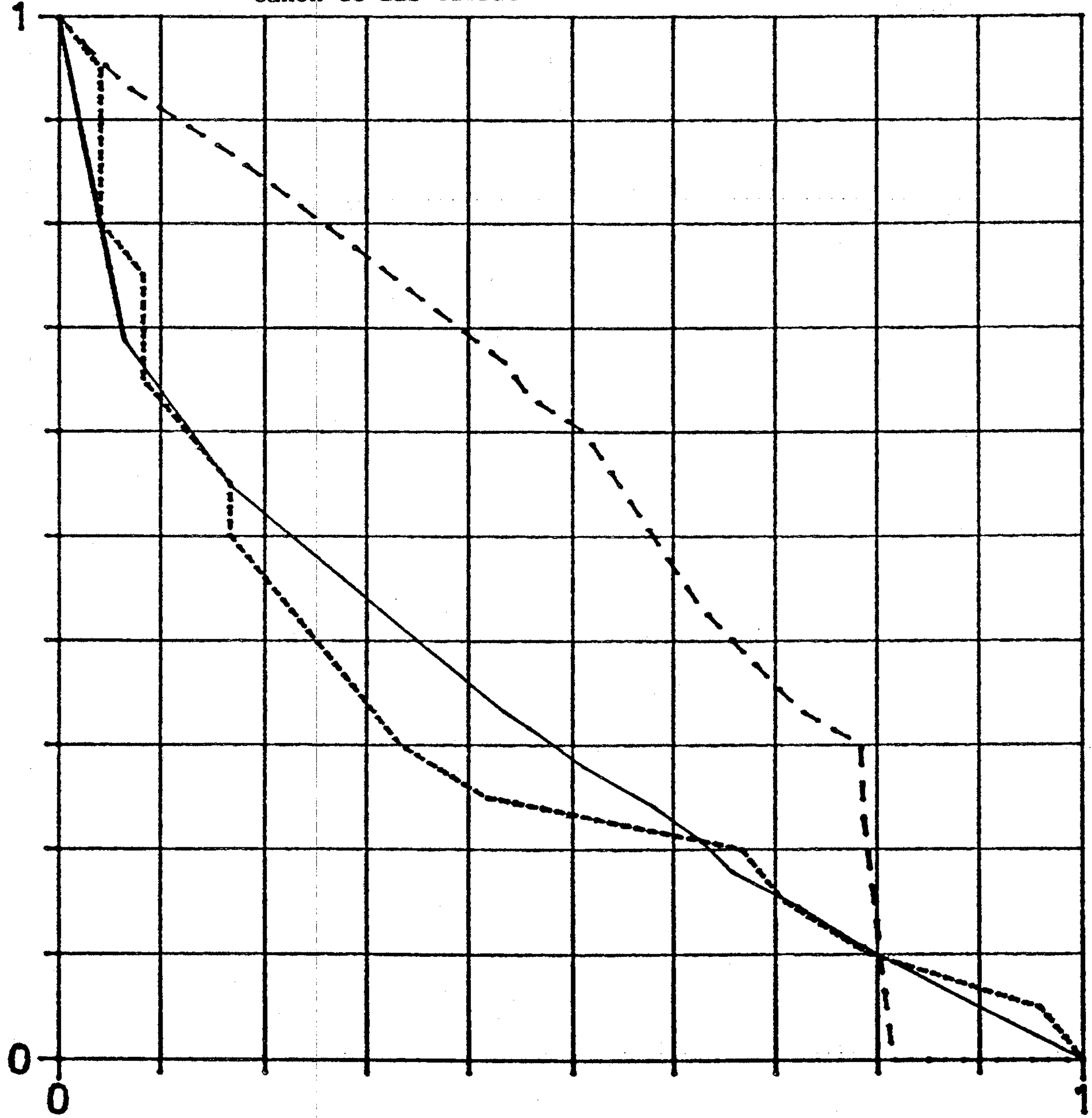

Magnitude: 30
Length: 49570 ft
Basin Area: 24 km2
Hypsometric Integral: 30.00
Max Channel Elev: 7040
Min Channel Elev: 5340

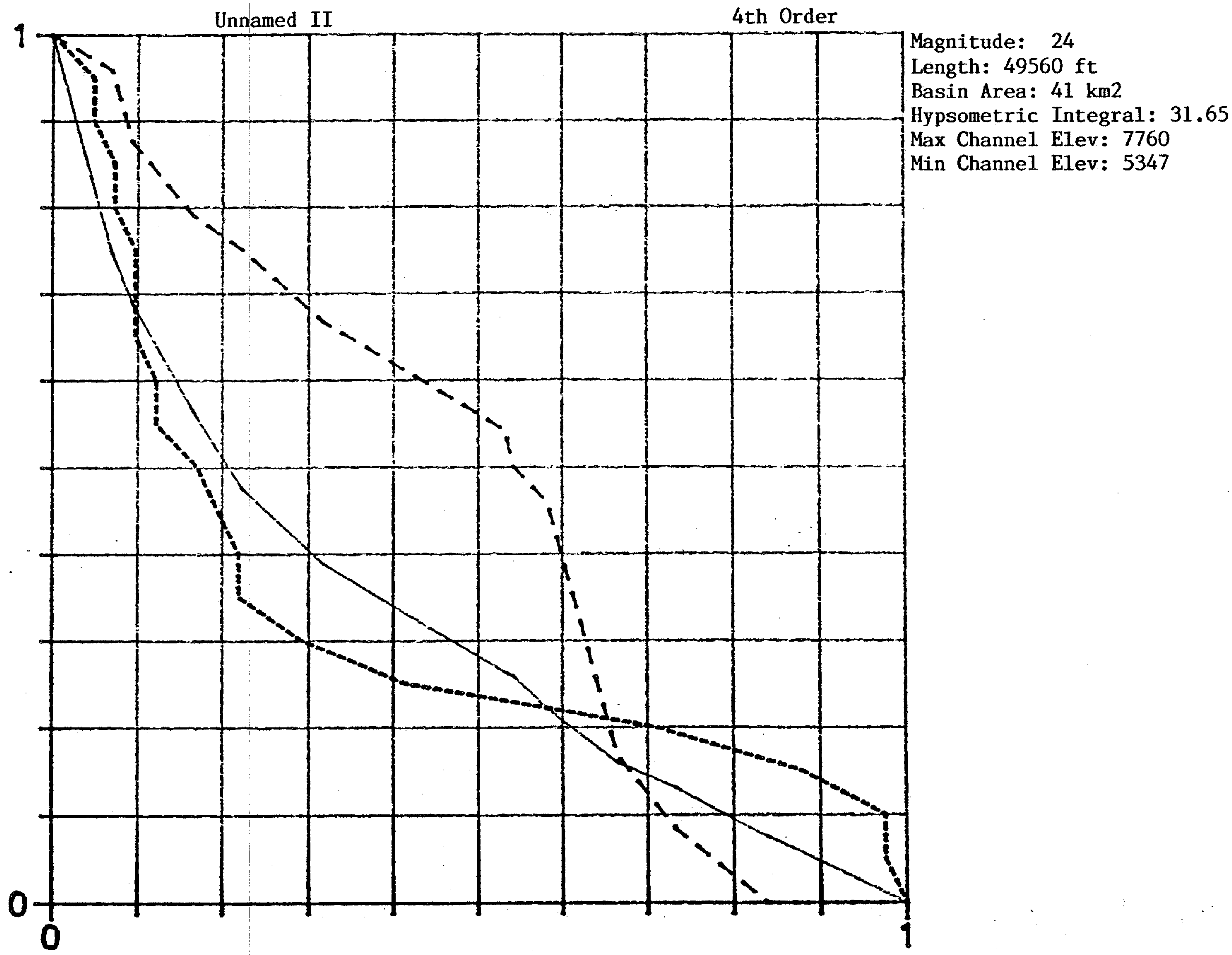
Unnamed II
4th Order
Magnitude: 24
Length: 49560 ft
Basin Area: 41 km2
Hypsometric Integral: 31.65
Max Channel Elev: 7760
Min Channel Elev: 5347
1
0
0
1

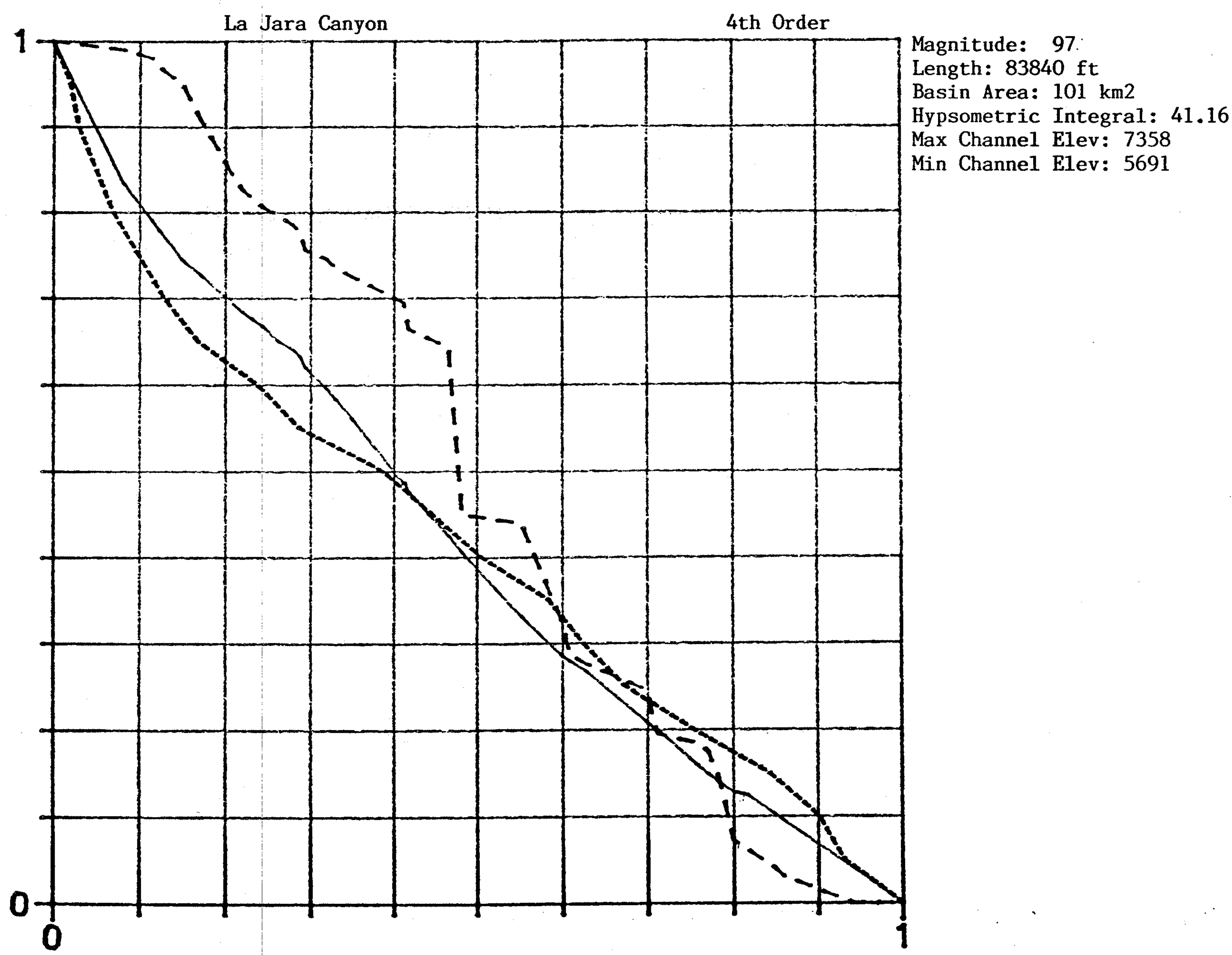

La Jara Canyon
4th Order
1
0
0
1
Magnitude: 97
Length: 83840 ft
Basin Area: 101 km2
Hypsometric Integral: 41.16
Max Channel Elev: 7358
Min Channel Elev: 5691

Canada Bonita 5th Order

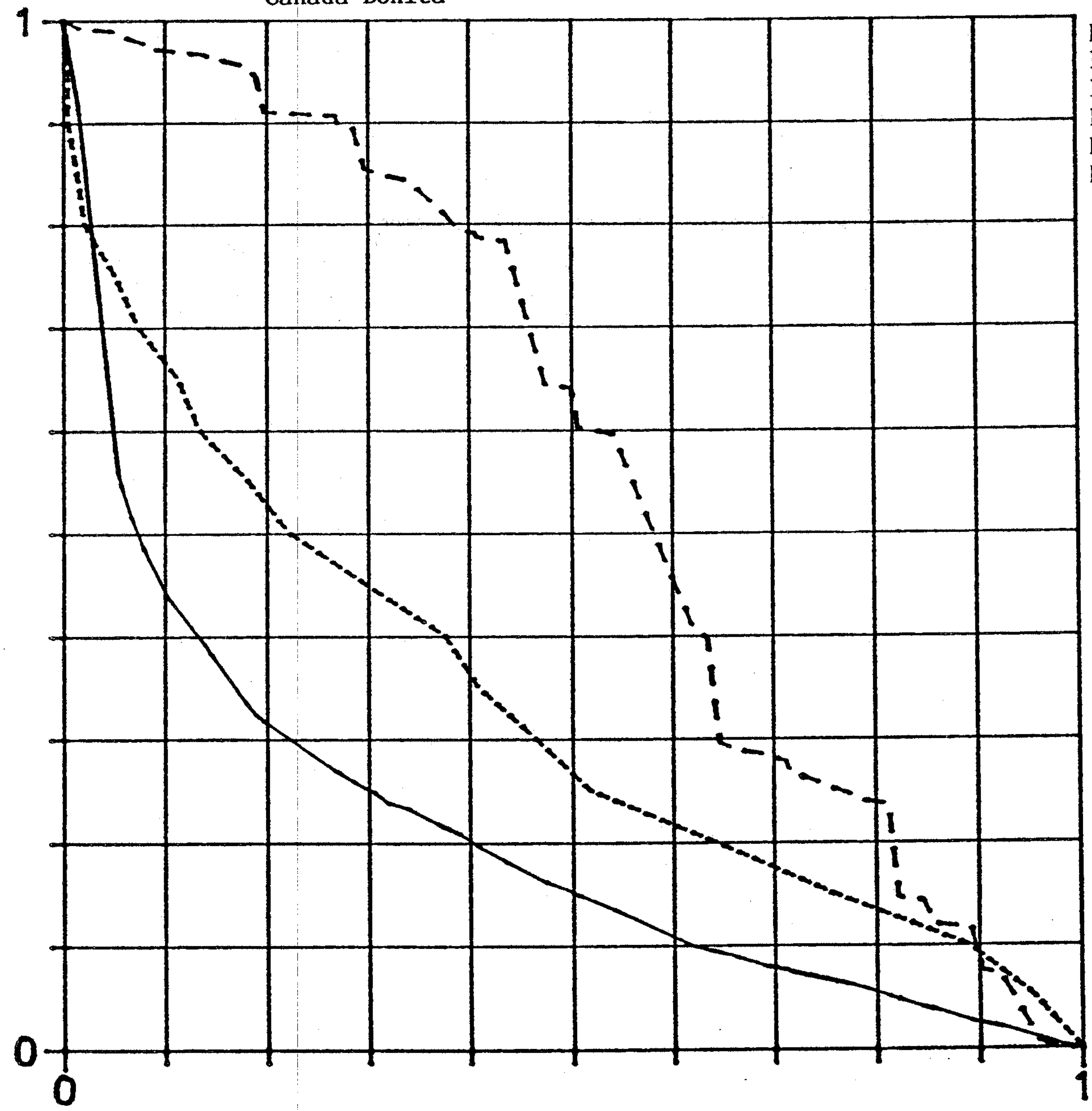

Magnitude: 267
Length: 133840 ft
Basin Area: 433 km2
Hypsometric Integral: 33.14
Max Channel Elev: 7420
Min Channel Elev: 5771

Juan de Dios Creek 4th Order

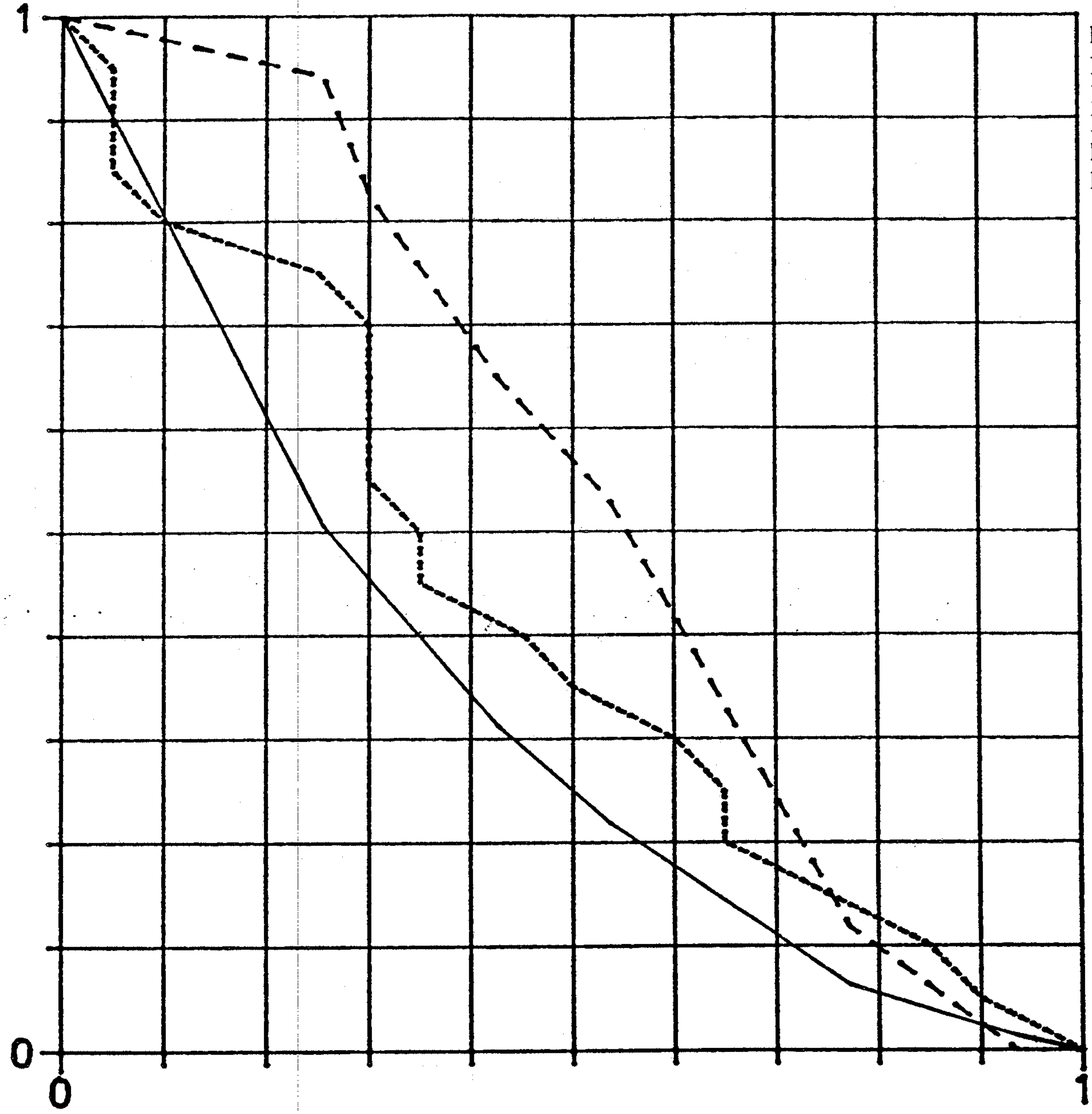

Magnitude: 17
Length: 41260 ft
Basin Area: 20 km2
Hypsometric Integral: 41.25
Max Channel Elev: 6733
Min Channel Elev: 5787

Field Ranch Creek 4th Order

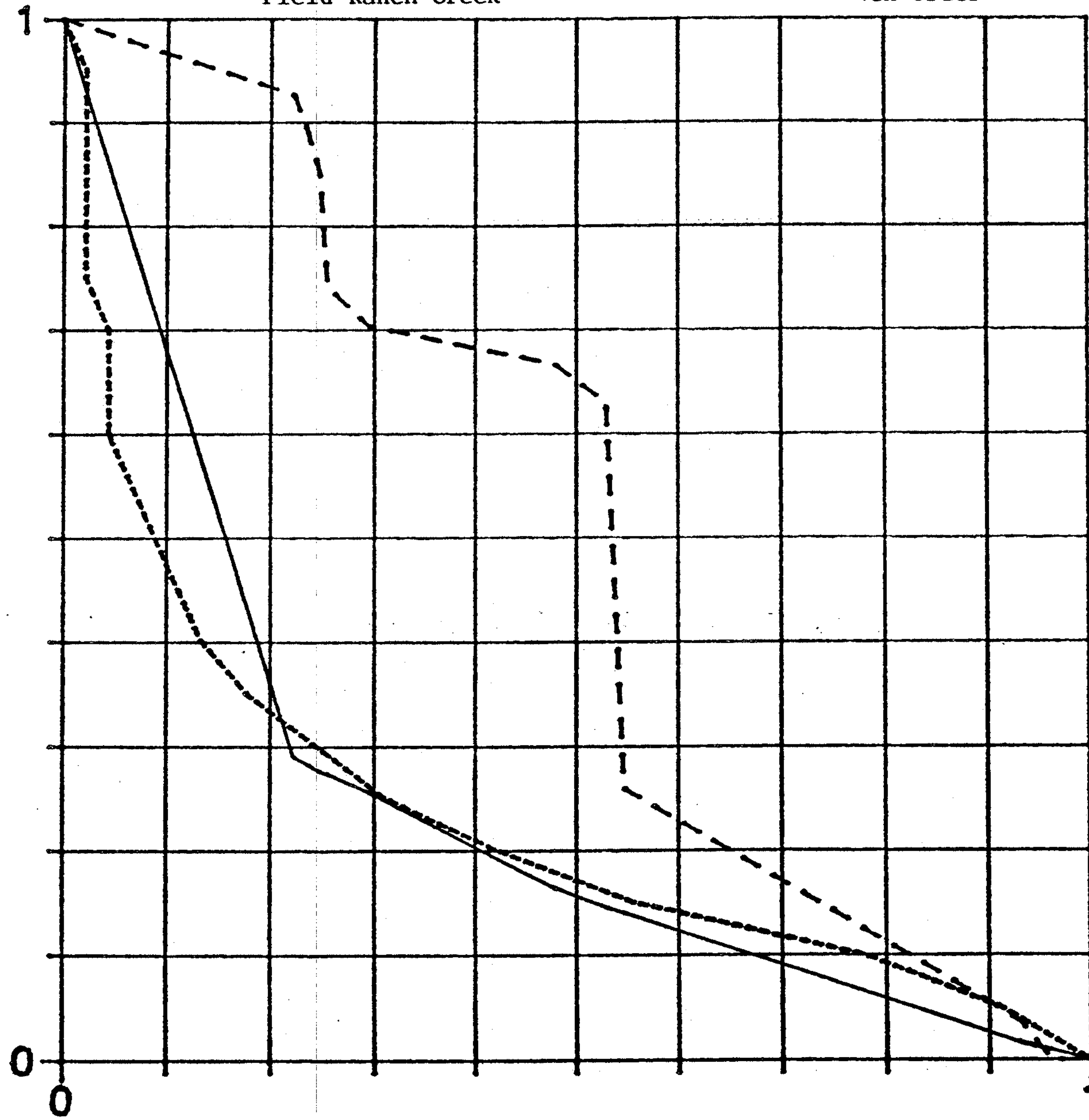

Magnitude: 27
Length: 44975 ft
Basin Area: 45 km2
Hypsometric Integral: 22.72
Max Channel Elev: 6662
Min Channel Elev: 5924

Waterbury Draw 4th Order

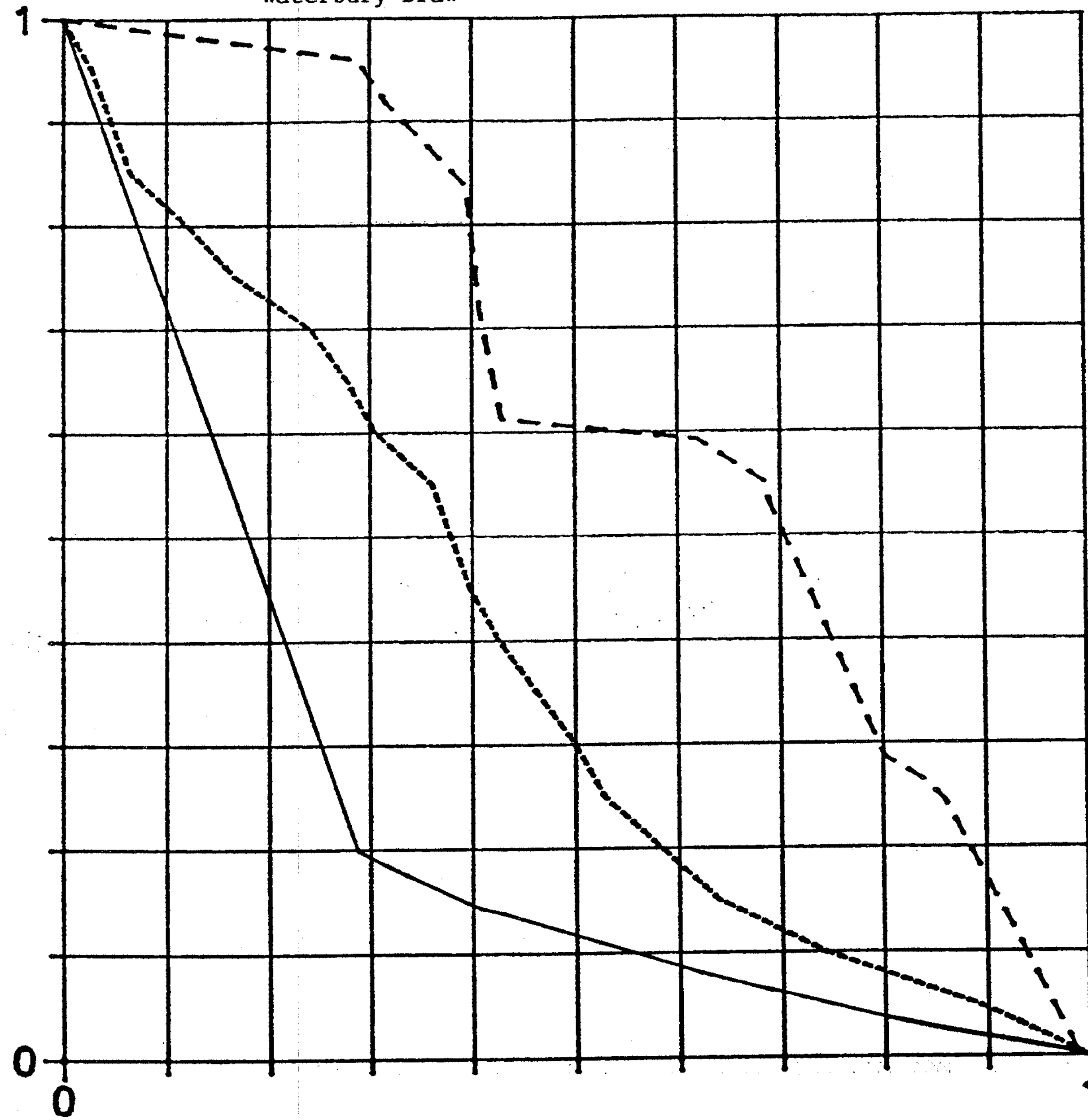

Magnitude: 49
Length: 57630 ft
Basin Area: 108 km2
Hypsometric Integral: 38.29
Max Channel Elev: 7365
Min Channel Elev: 5934

Chicken Mountain Draw 4th Order

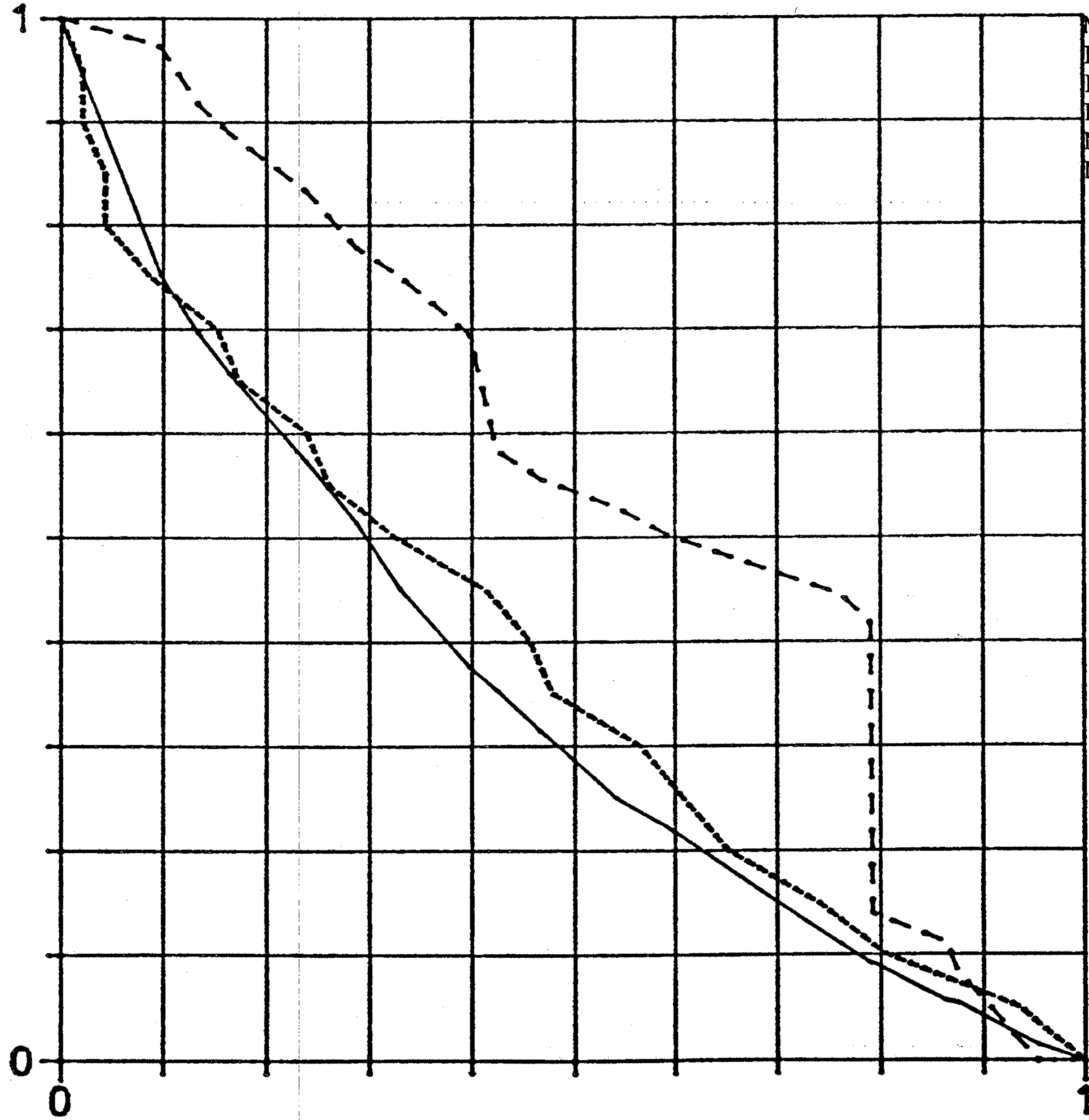

Magnitude: 36
Length: 56240 ft
Basin Area: 46 km2
Hypsometric Integral: 37.61
Max Channel Elev: 7506
Min Channel Elev: 6037

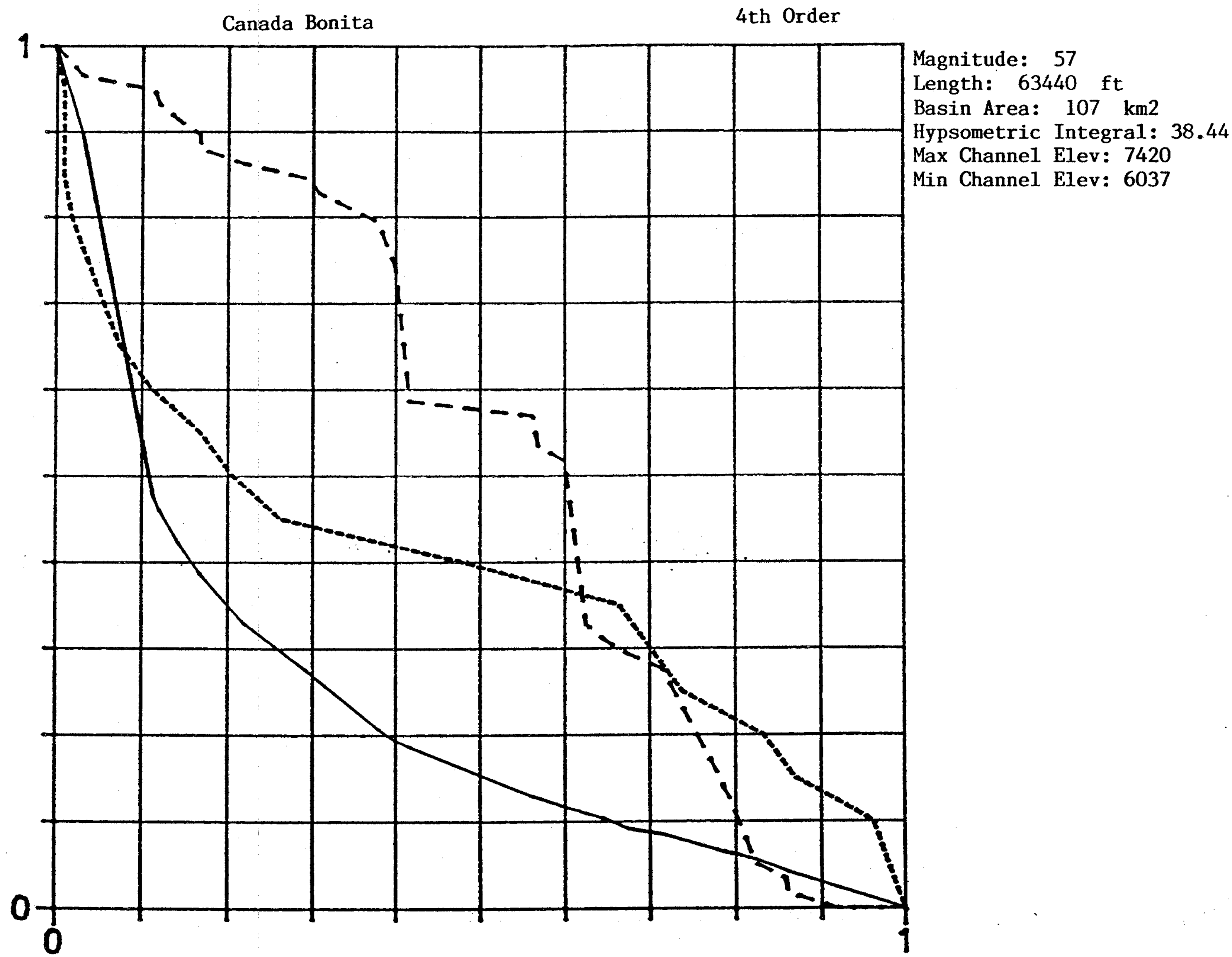
Canada Bonita
4th Order
Magnitude: 57
Length: 63440 ft
Basin Area: 107 km2
Hypsometric Integral: 38.44
Max Channel Elev: 7420
Min Channel Elev: 6037
1
0
0
1

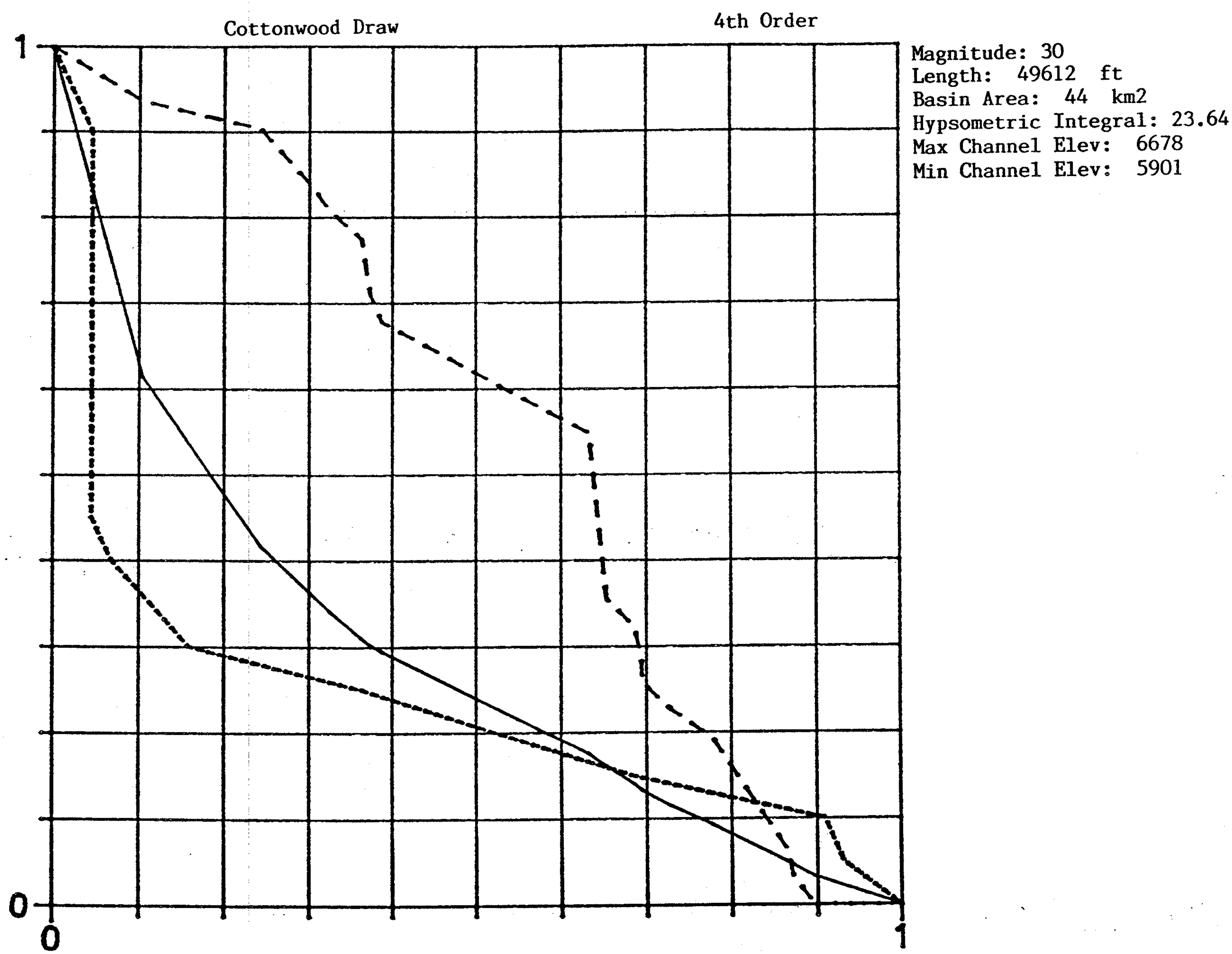
Cottonwood Draw
4th Order
1
0
0
1
Magnitude: 30
Length: 49612 ft
Basin Area: 44 km2
Hypsometric Integral: 23.64
Max Channel Elev: 6678
Min Channel Elev: 5901

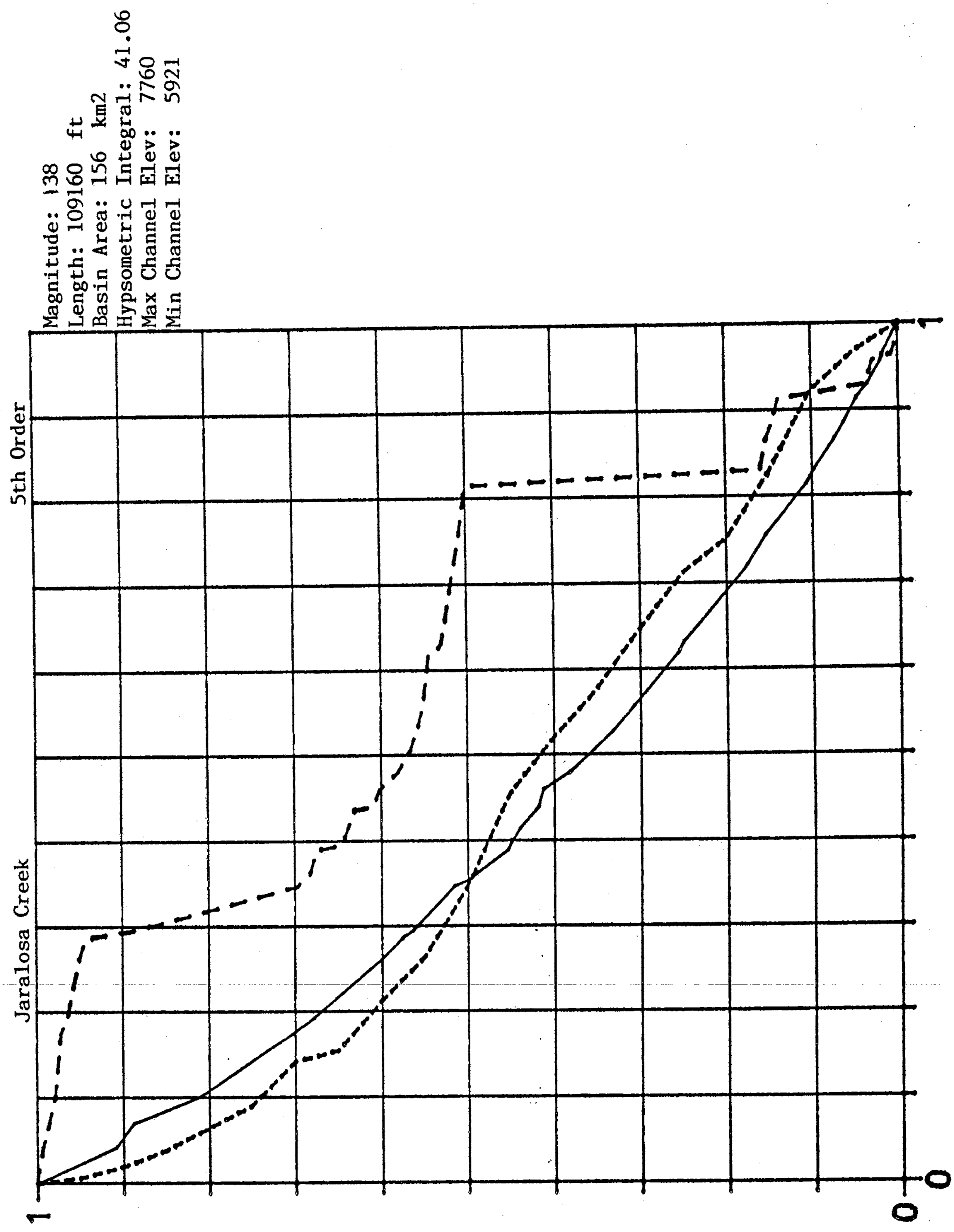
Jaralosa Creek
5th Order
Magnitude: 138
Length: 109160 ft
Basin Area: 156 km2
Hypsometric Integral: 41.06
Max Channel Elev: 7760
Min Channel Elev: 5921
1
0
0
1

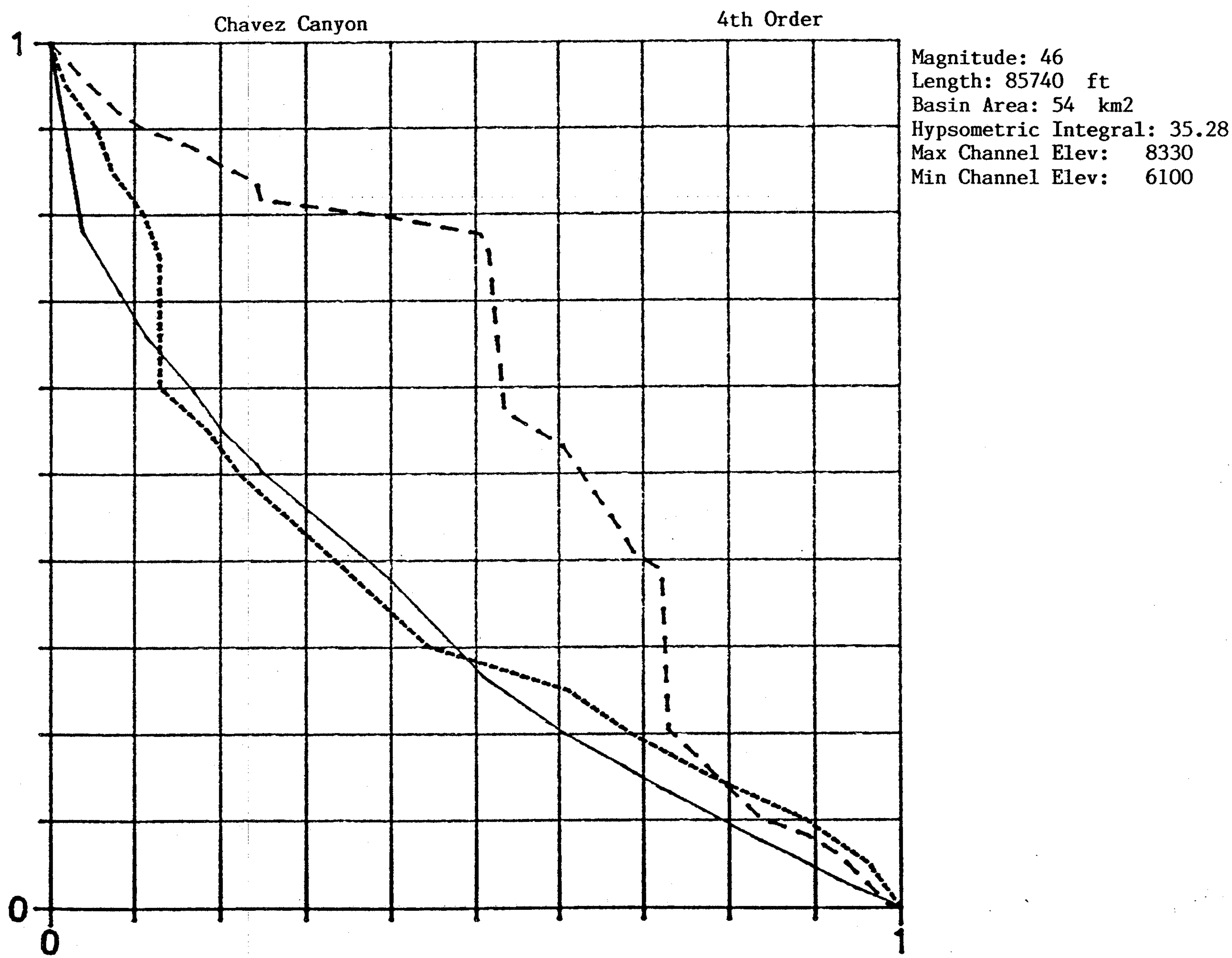
Chavez Canyon
4th Order
1
0
0
1
Magnitude: 46
Length: 85740 ft
Basin Area: 54 km2
Hypsometric Integral: 35.28
Max Channel Elev: 8330
Min Channel Elev: 6100

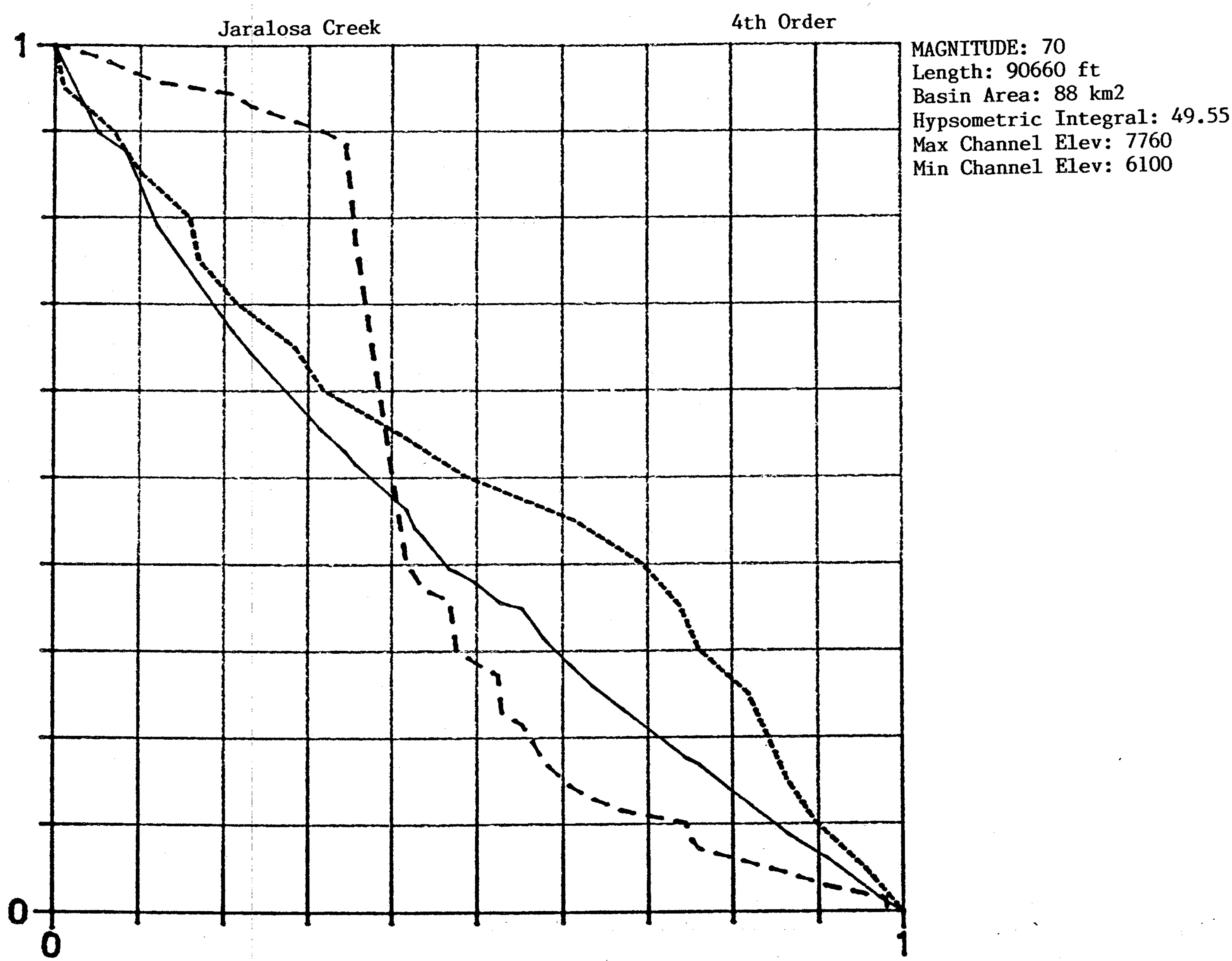
Jaralosa Creek
4th Order
MAGNITUDE: 70
Length: 90660 ft
Basin Area: 88 km2
Hypsometric Integral: 49.55
Max Channel Elev: 7760
Min Channel Elev: 6100
1
0
0
1

Alamo Creek 4th Order

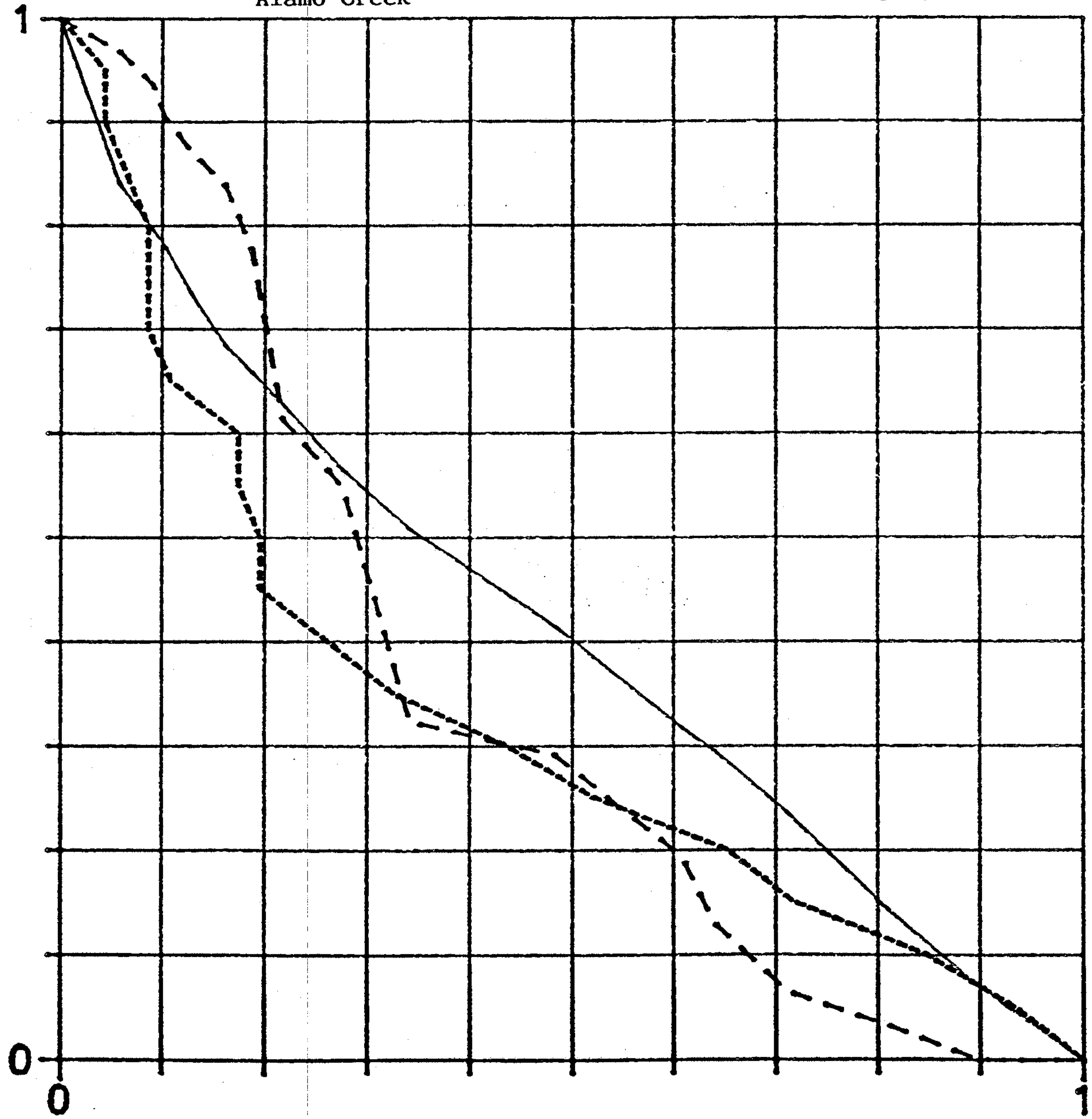

Magnitude: 31
Length: 48180 ft
Basin Area: 46 km2
Hypsometric Integral: 32.28
Max Channel Elev: 6830
Min Channel Elev: 5998

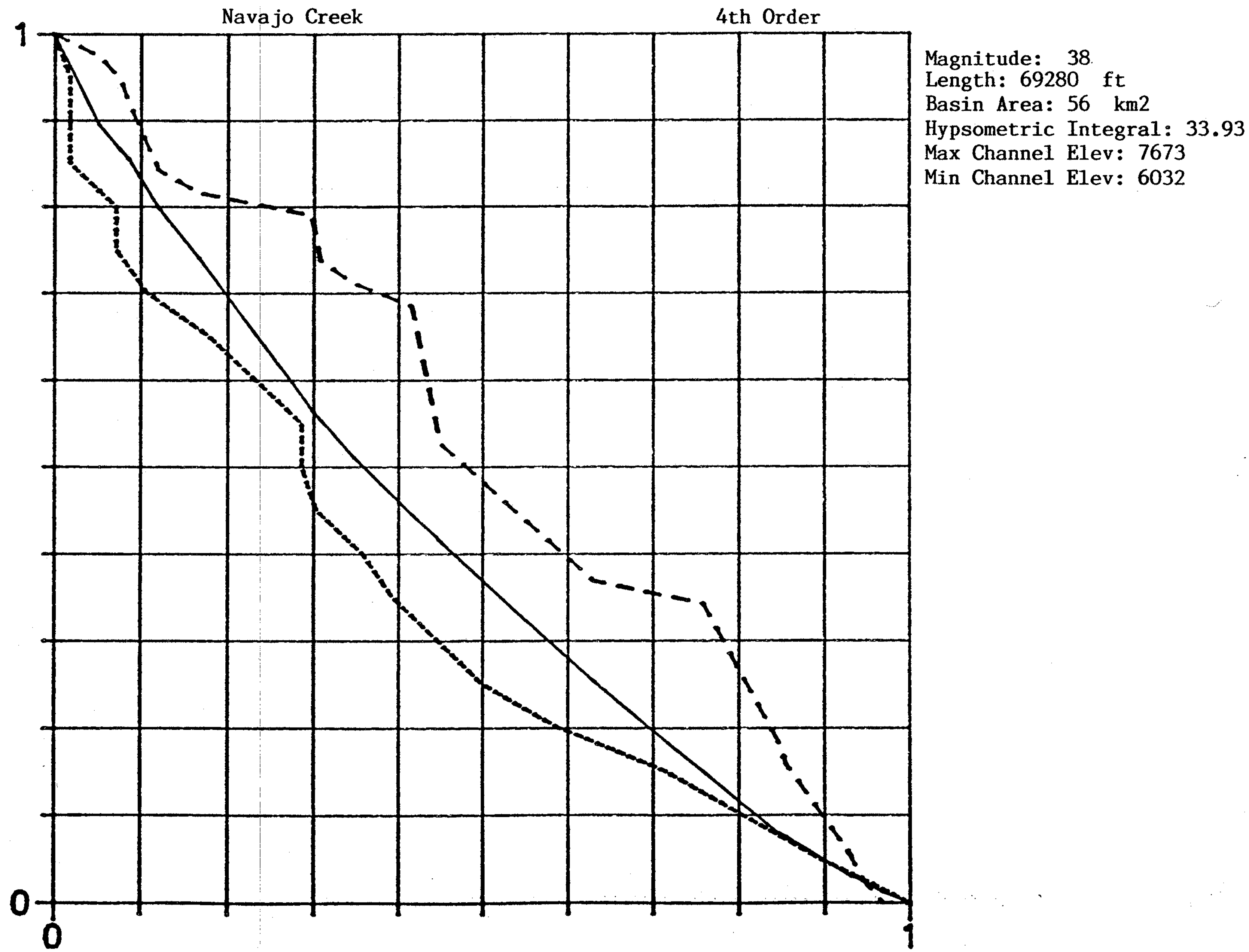
Navajo Creek
4th Order
1
0
0
1
Magnitude: 38
Length: 69280 ft
Basin Area: 56 km2
Hypsometric Integral: 33.93
Max Channel Elev: 7673
Min Channel Elev: 6032

Jaramillo Canyon 4th Order

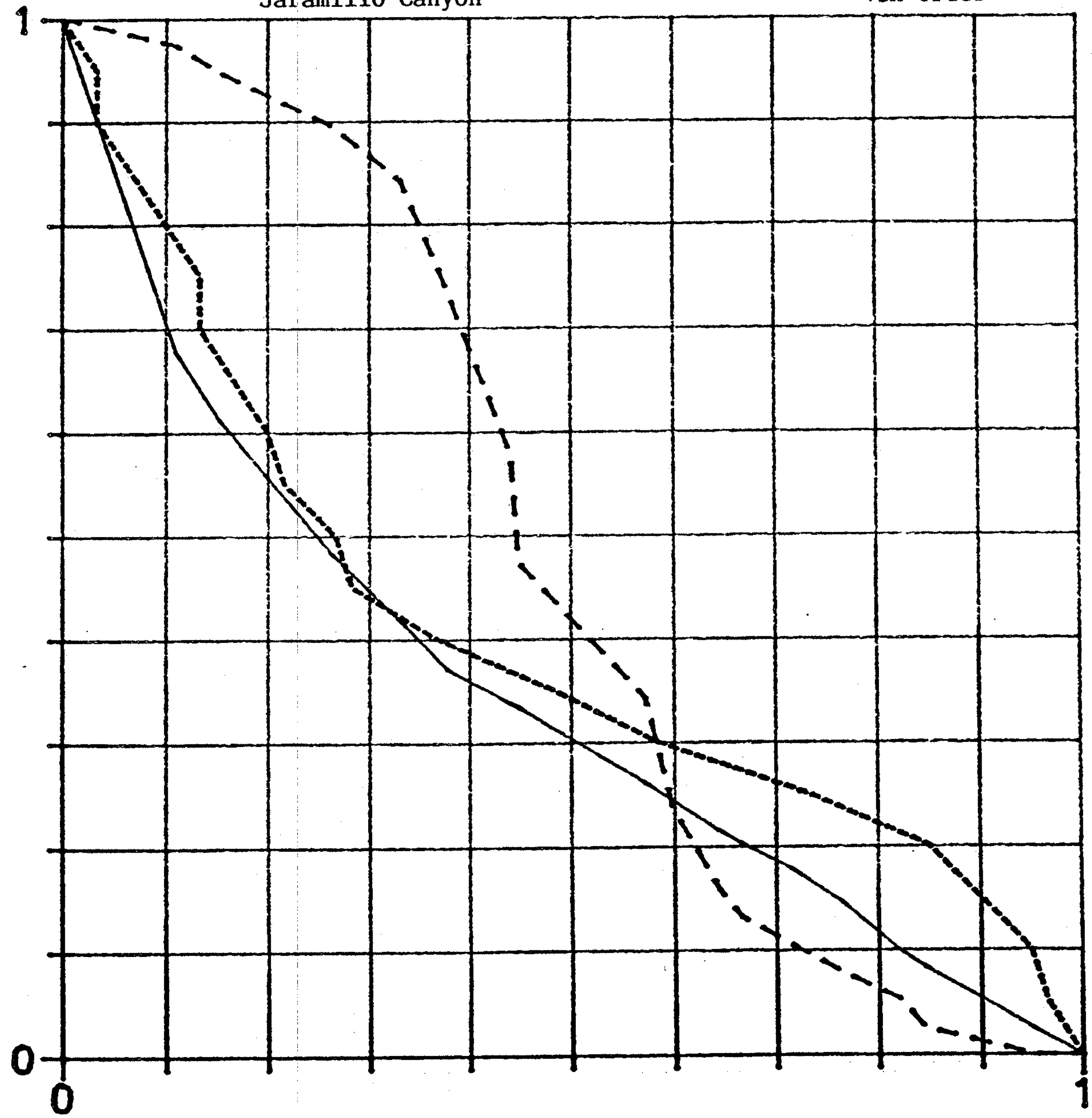

Magnitude: 38
Length: 50025 ft
Basin Area: 60 km2
Hypsometric Integral: 39.83
Max Channel Elev: 7170
Min Channel Elev: 6089

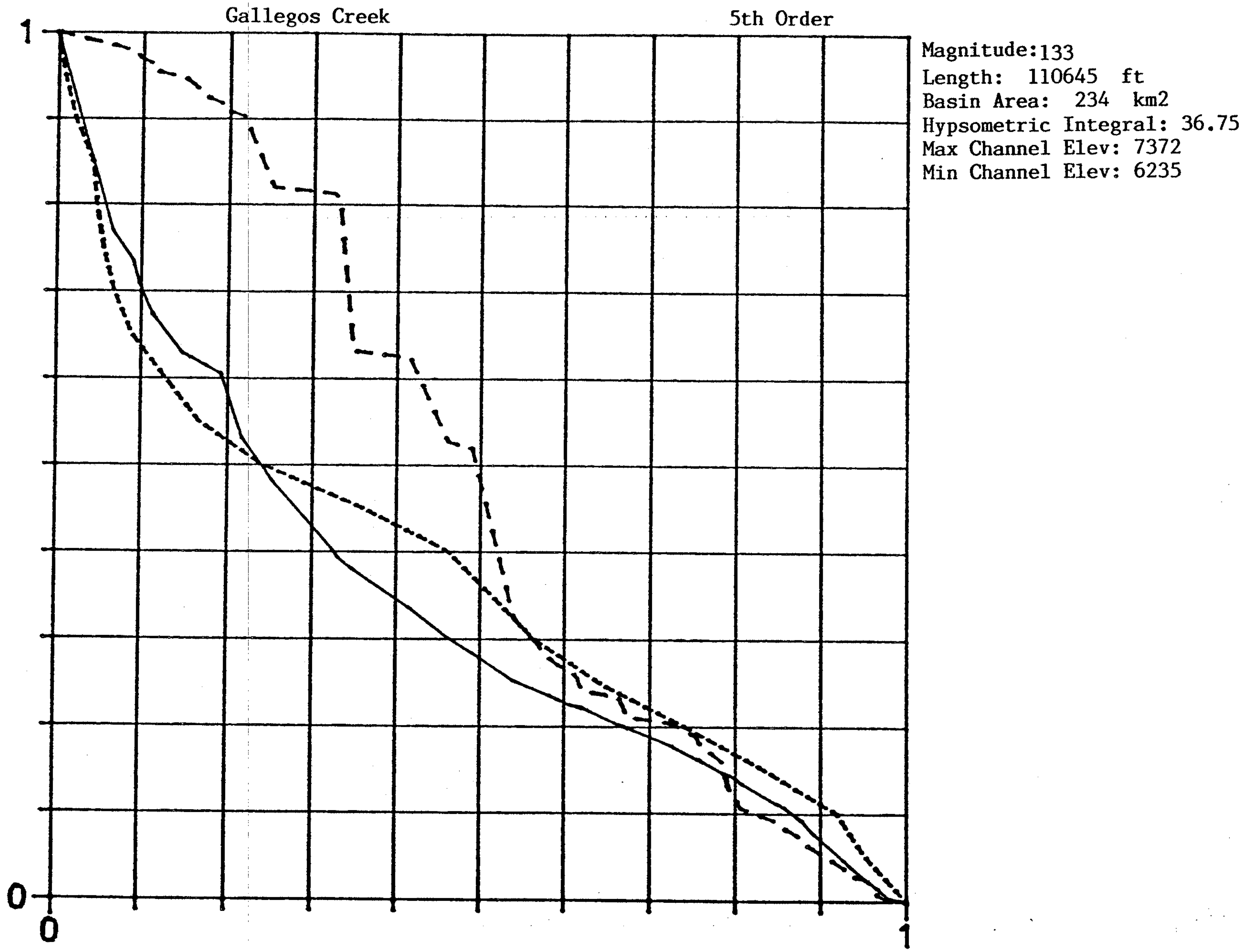
Gallegos Creek
5th Order
1
0
0
1
Magnitude:133
Length: 110645 ft
Basin Area: 234 km2
Hypsometric Integral: 36.75
Max Channel Elev: 7372
Min Channel Elev: 6235

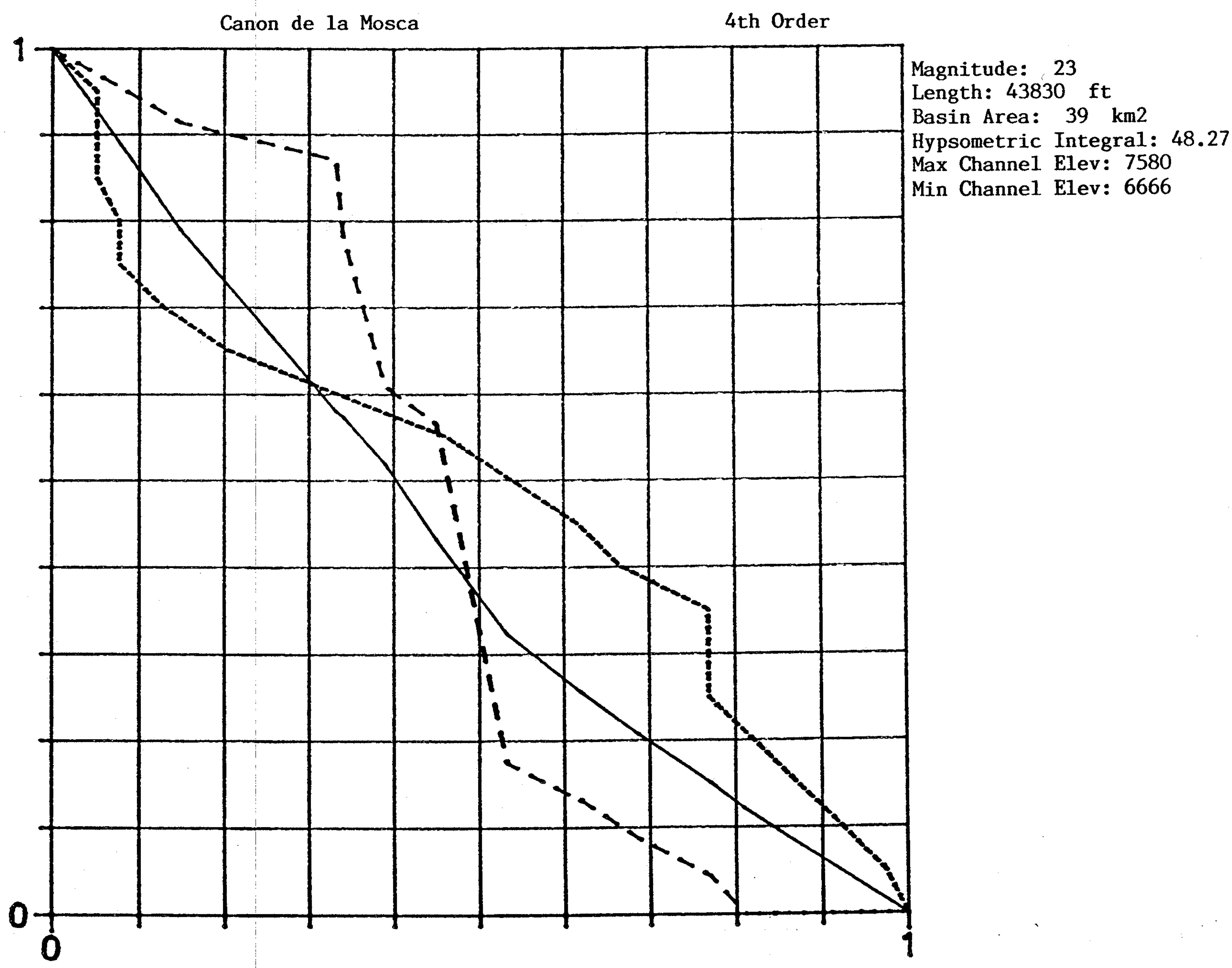

Canon de la Mosca
4th Order
1
0
0
1
Magnitude: 23
Length: 43830 ft
Basin Area: 39 km2
Hypsometric Integral: 48.27
Max Channel Elev: 7580
Min Channel Elev: 6666

Gallegos Creek 4th Order

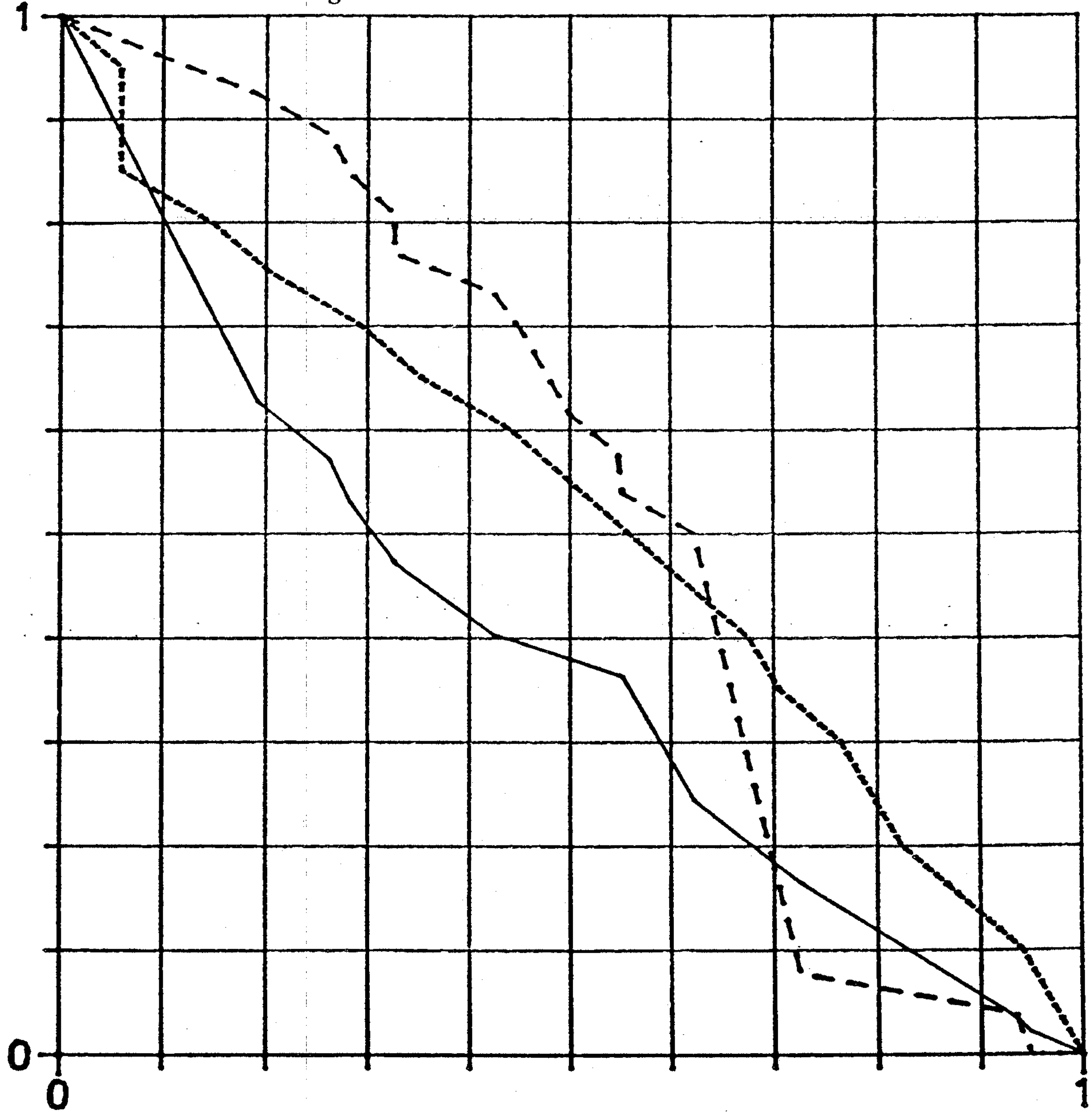

Magnitude: 25
Length: 38510 ft
Basin Area: 34 km2
Hypsometric Integral: 51.76
Max Channel Elev: 7372
Min Channel Elev: 6666

Dog Springs Canyon

5th Order

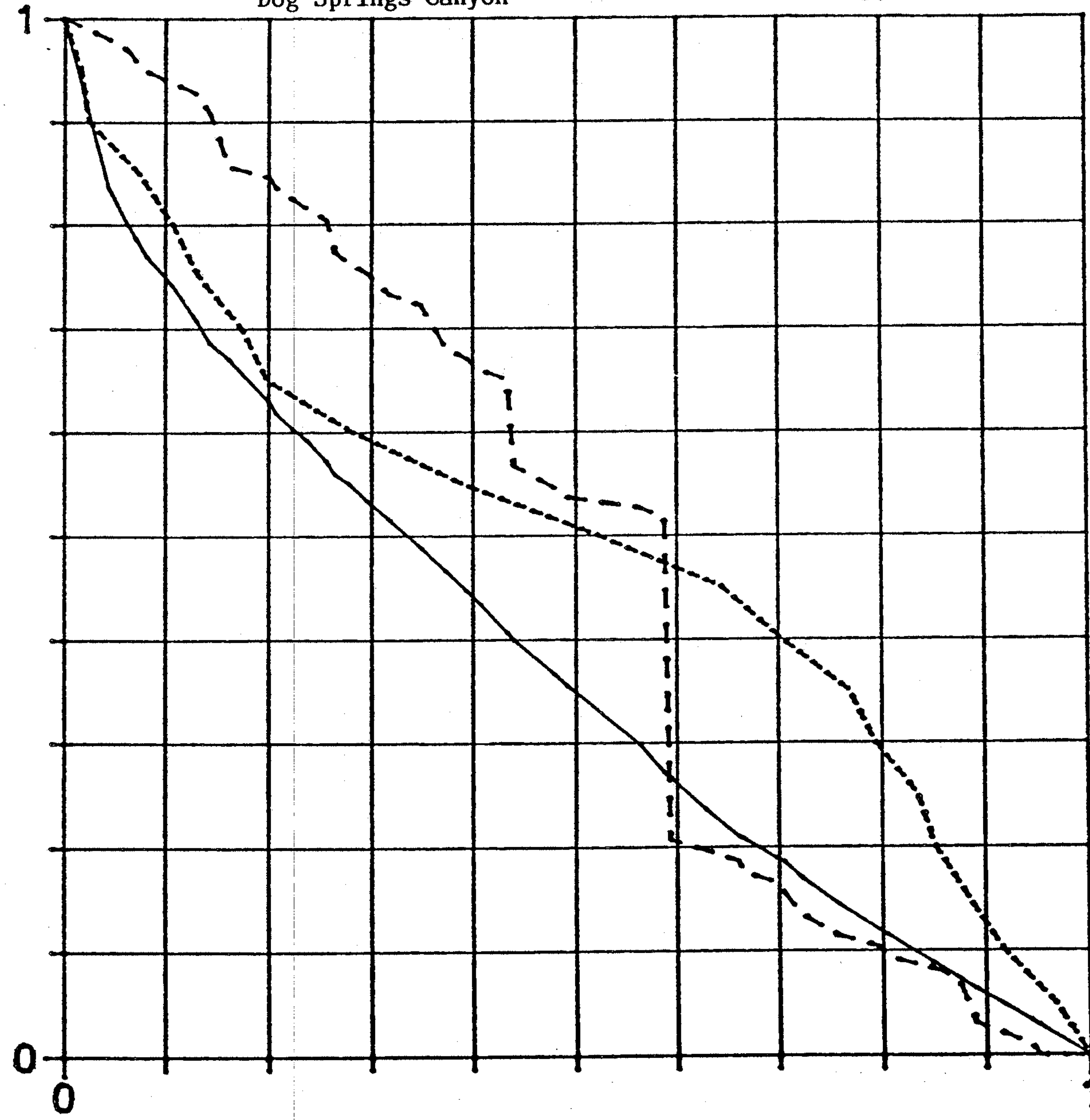

Magnitude: 97
Length: 104086 ft
Basin Area: 121 km2
Hypsometric Integral: 48.90
Max Channel Elev: 8510
Min Channel Elev: 6262

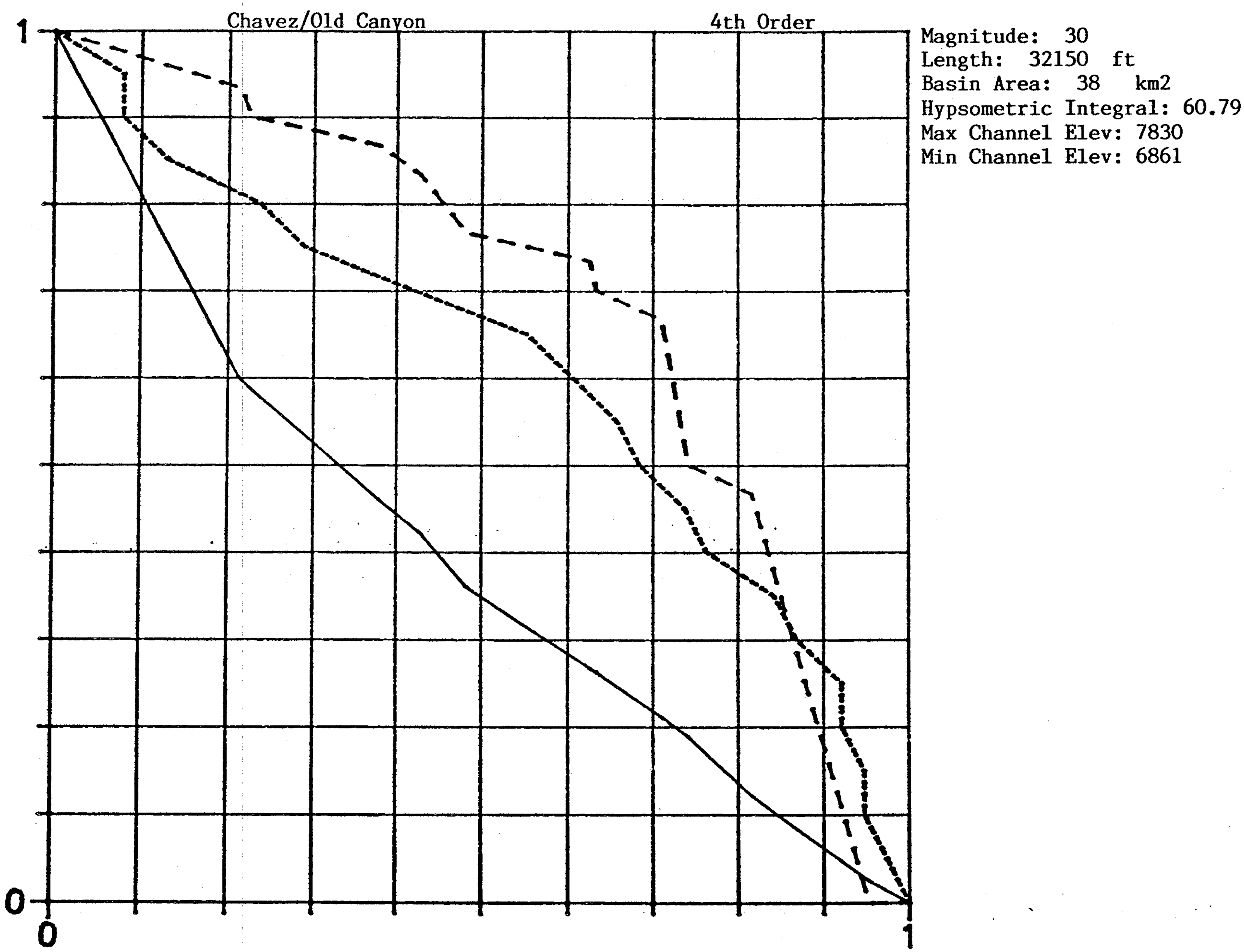
Chavez/Old Canyon
4th Order
1
0
0
1
Magnitude: 30
Length: 32150 ft
Basin Area: 38 km2
Hypsometric Integral: 60.79
Max Channel Elev: 7830
Min Channel Elev: 6861

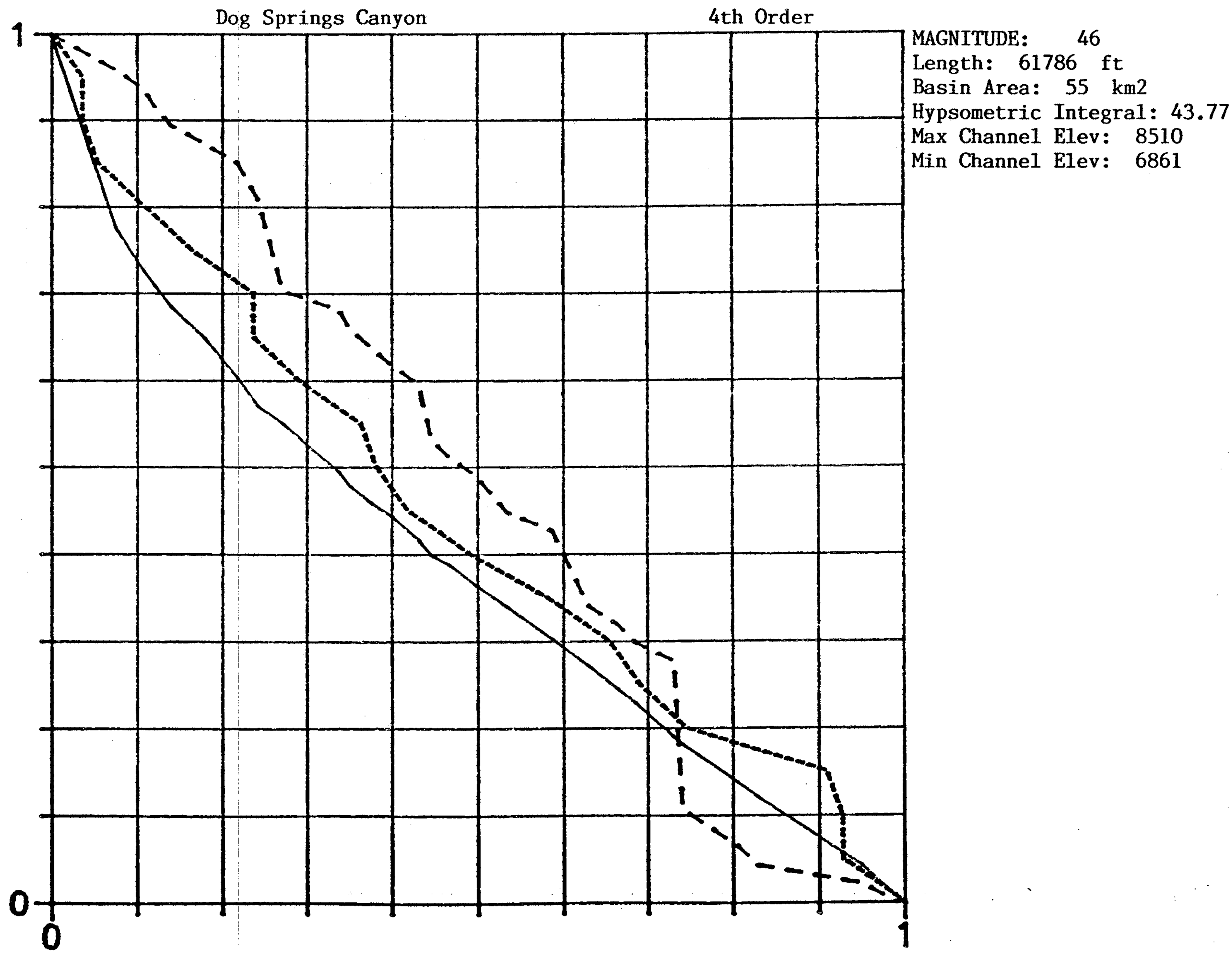
Dog Springs Canyon
4th Order
1
0
0
1
MAGNITUDE: 46
Length: 61786 ft
Basin Area: 55 km2
Hypsometric Integral: 43.77
Max Channel Elev: 8510
Min Channel Elev: 6861

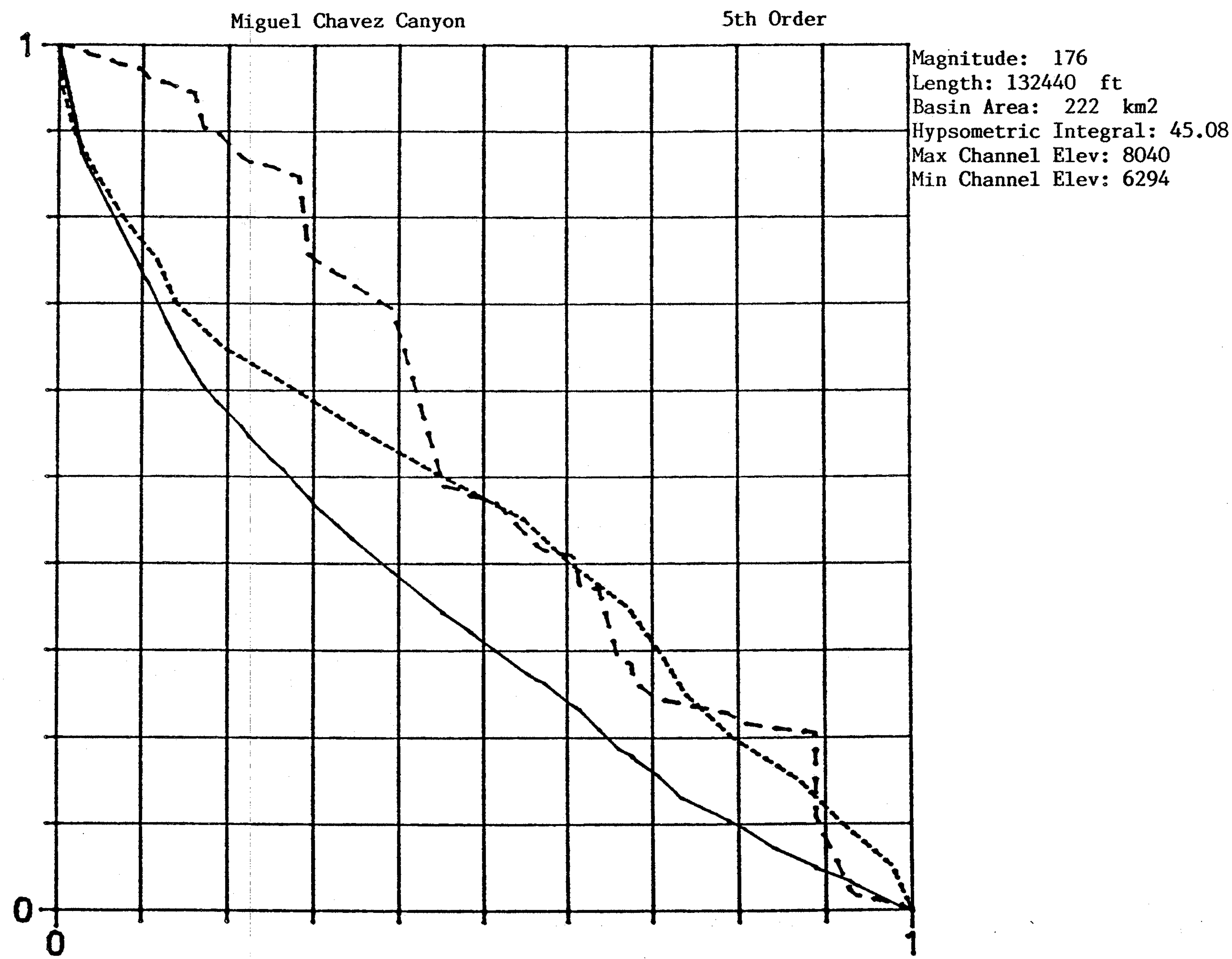
Miguel Chavez Canyon
5th Order
Magnitude: 176
Length: 132440 ft
Basin Area: 222 km2
Hypsometric Integral: 45.08
Max Channel Elev: 8040
Min Channel Elev: 6294
1
0
0
1

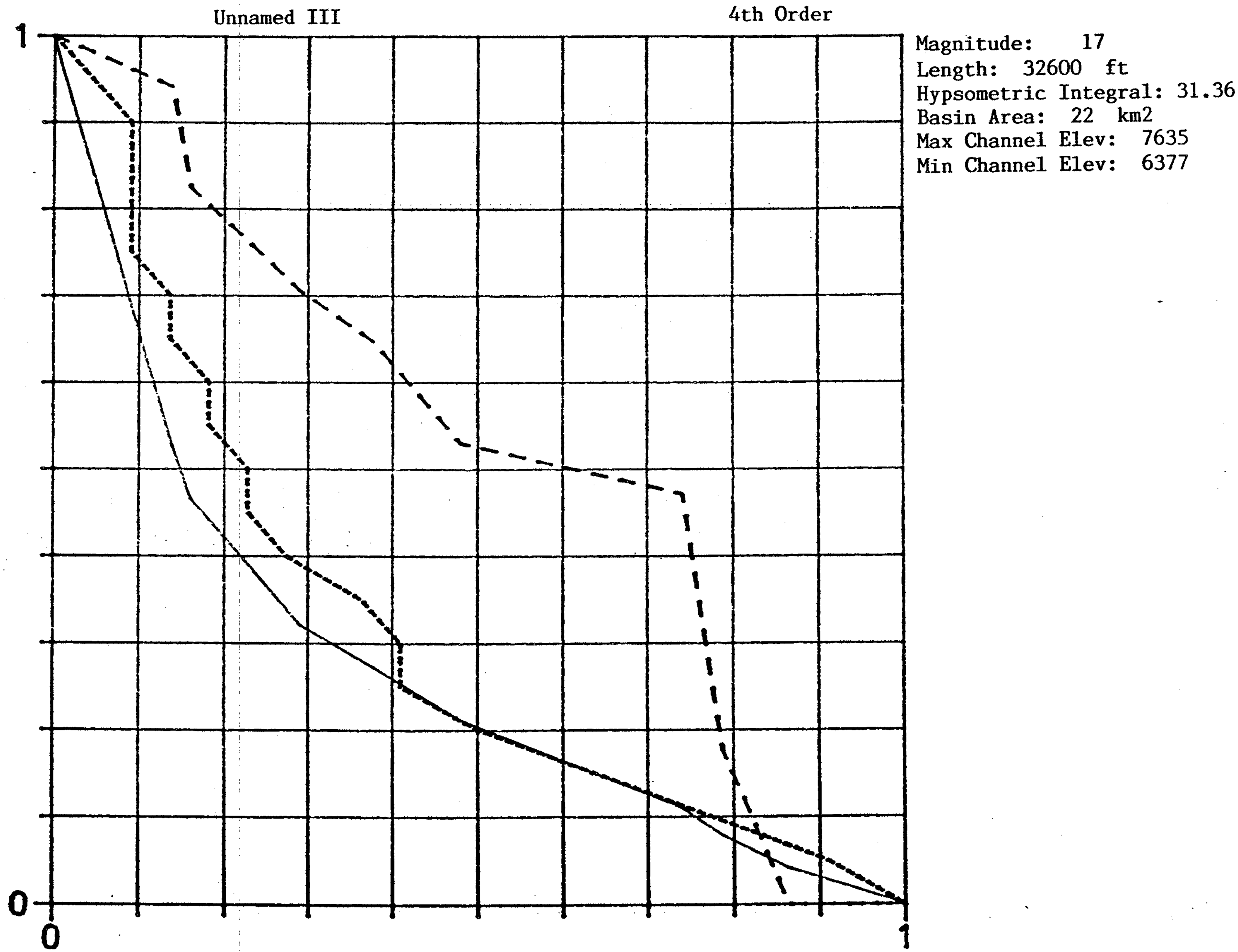
Unnamed III
4th Order
1
0
0
1
Magnitude: 17
Length: 32600 ft
Hypsometric Integral: 31.36
Basin Area: 22 km2
Max Channel Elev: 7635
Min Channel Elev: 6377

Pine Springs Canyon

4th Order

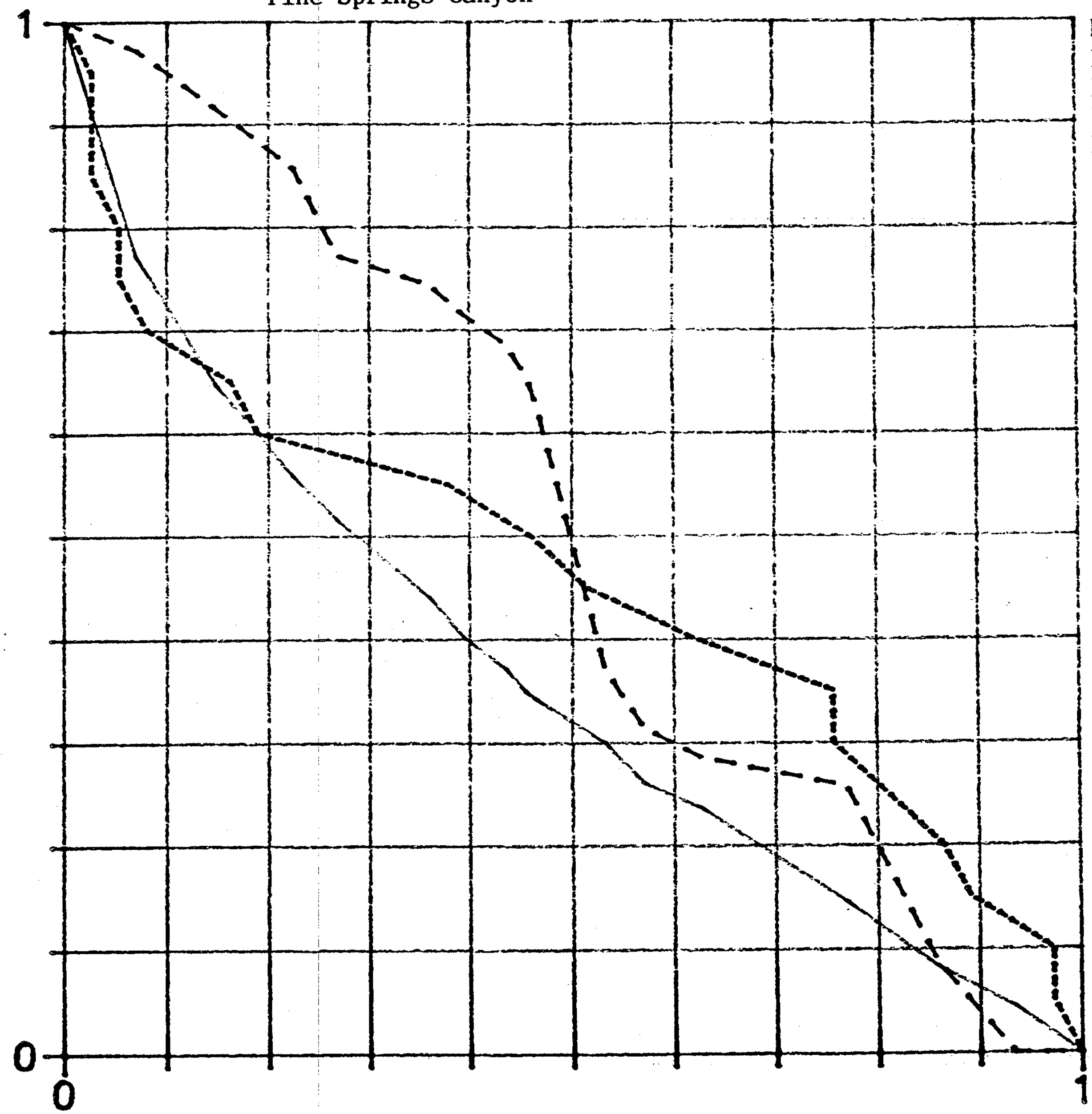

Magnitude: 35
Length: 36320 ft
Basin Area: 37 km2
Hypsometric Integral: 45.61
Max Channel Elev: 7680
Min Channel Elev: 6894

Wild Horse Canyon 4th Order

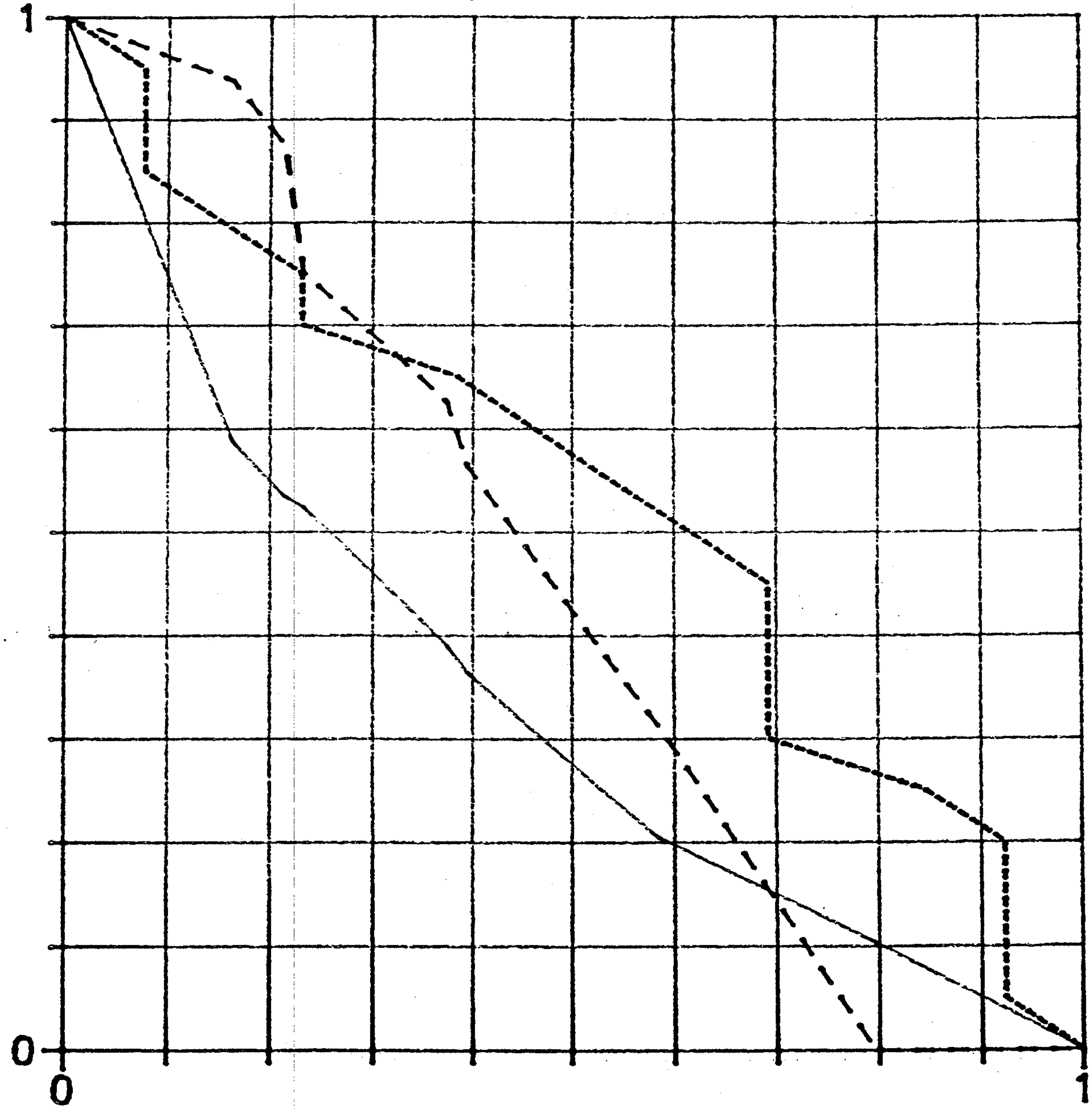

Magnitude: 16
Length: 19640 ft
Basin Area: 13 km2
Hypsometric Integral: 53.27
Max Channel Elev: 7780
Min Channel Elev: 7125

Miguel Chavez Canyon

4th Order

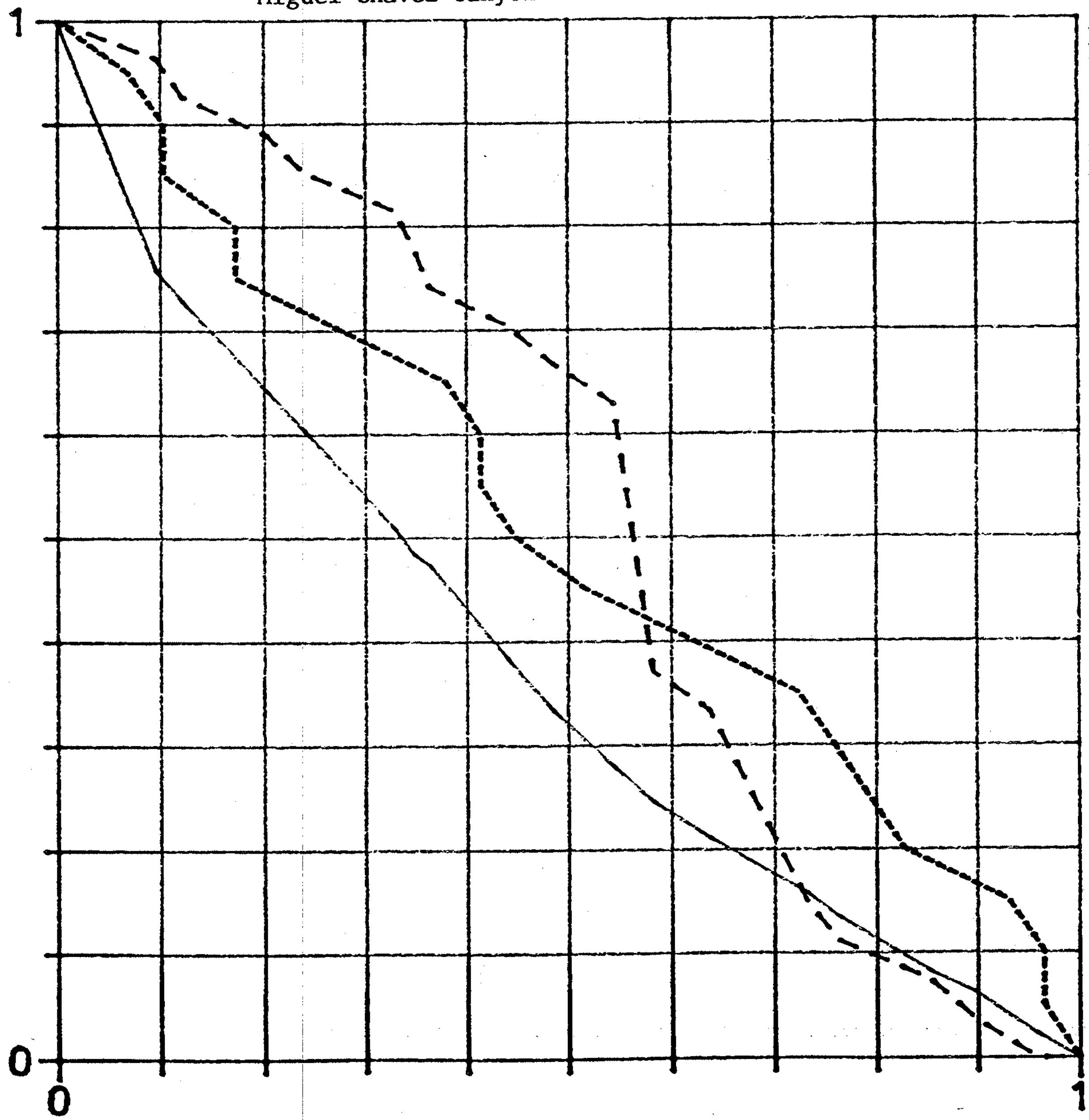

Magnitude: 26
Length: 38990 ft
Basin Area: 29 km2
Hypsometric Integral: 50.76
Max Channel Elev: 8040
Min Channel Elev: 7125

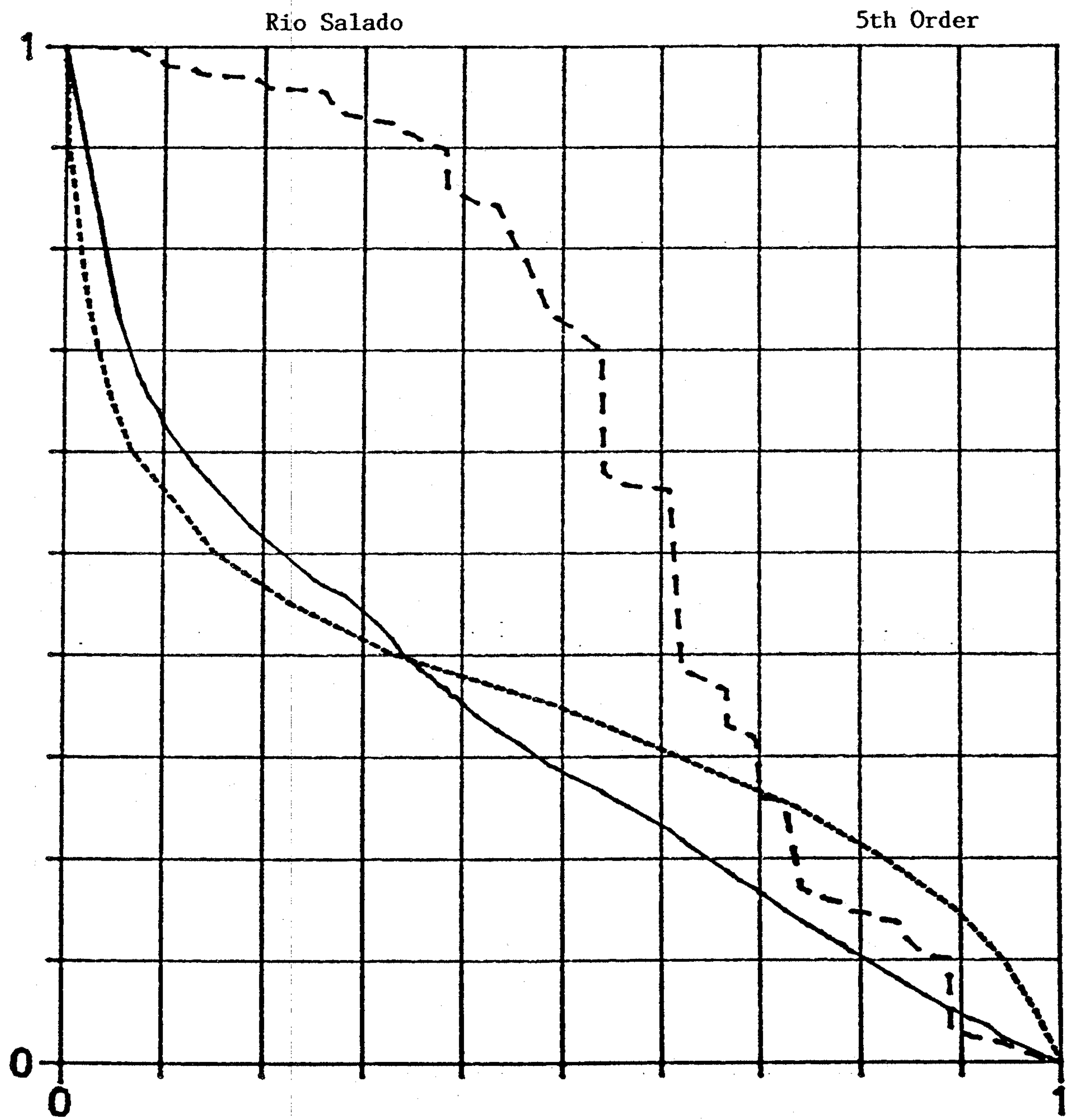

Magnitude: 447
Length: 188130 ft
Basin Area: 554 km2
Hypsometric Integral: 35.03
Max Channel Elev: 8760
Min Channel Elev: 6294

Rock Tank Canyon 4th Order

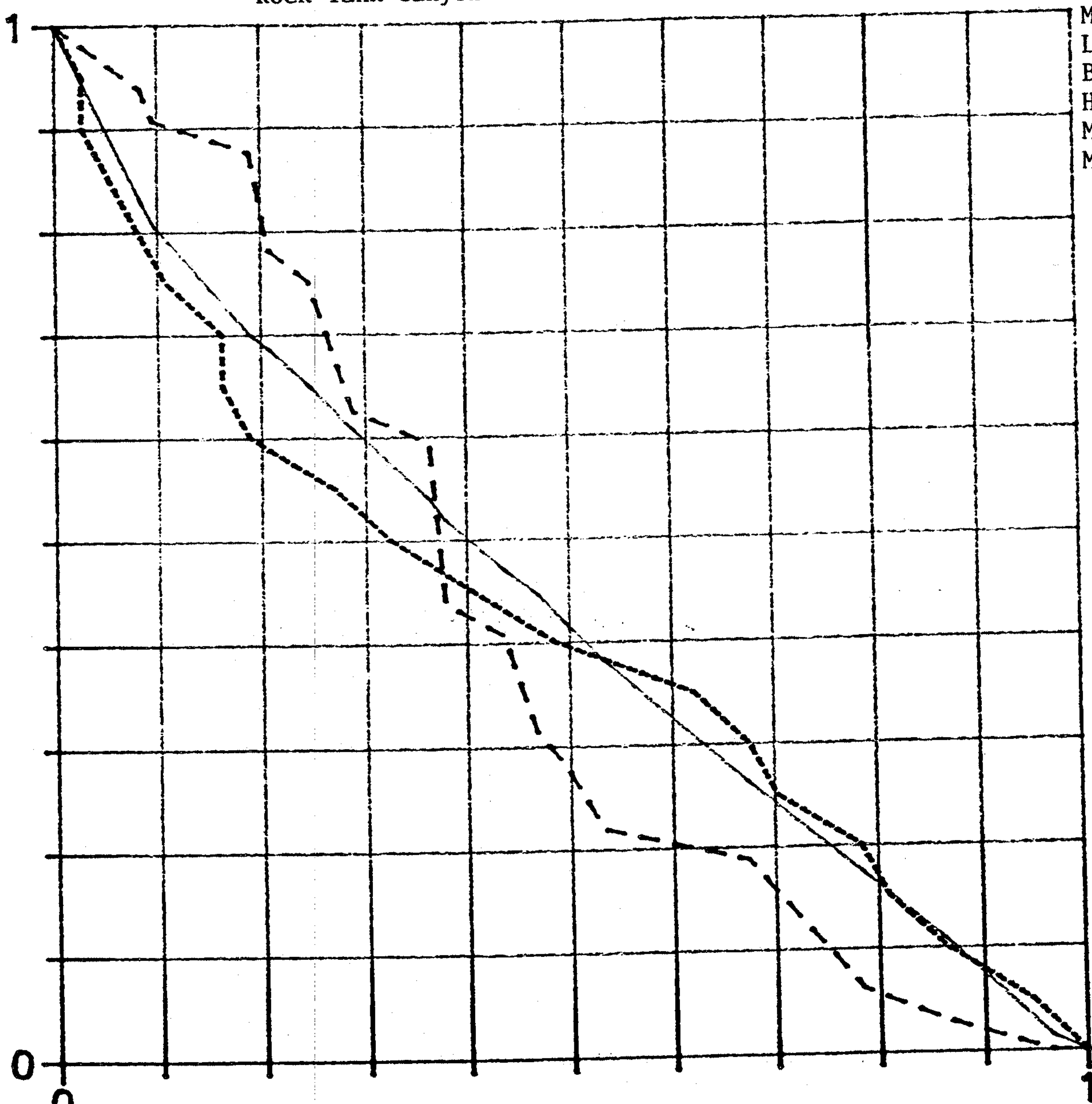

Magnitude: 32
Length: 65755 ft
Basin Area: 37 km2
Hypsometric Integral: 41.01
Max Channel Elev: 7758
Min Channel Elev: 6421

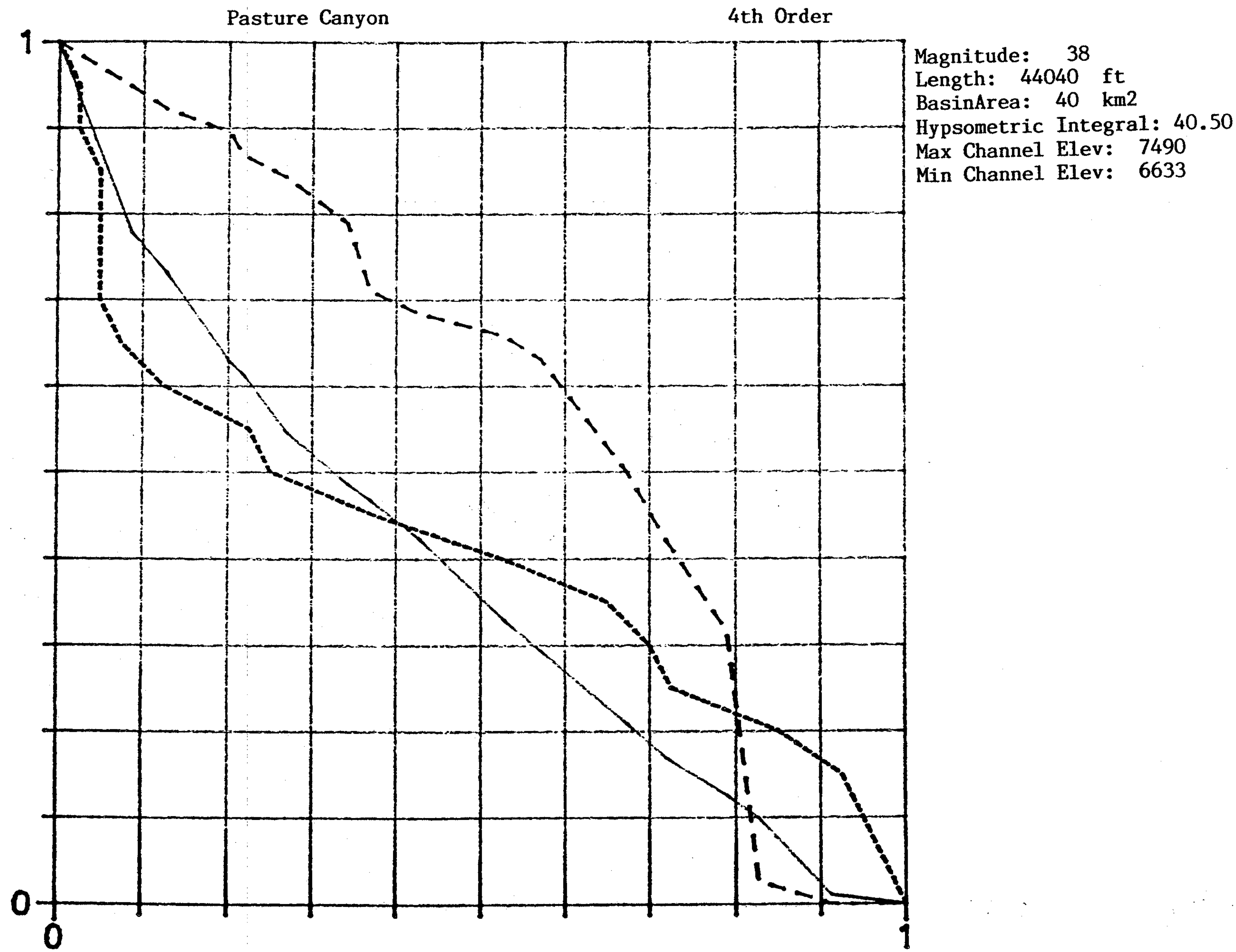
Pasture Canyon
4th Order
1
0
0
1
Magnitude: 38
Length: 44040 ft
BasinArea: 40 km2
Hypsometric Integral: 40.50
Max Channel Elev: 7490
Min Channel Elev: 6633

Rock House Canyon

4th Order

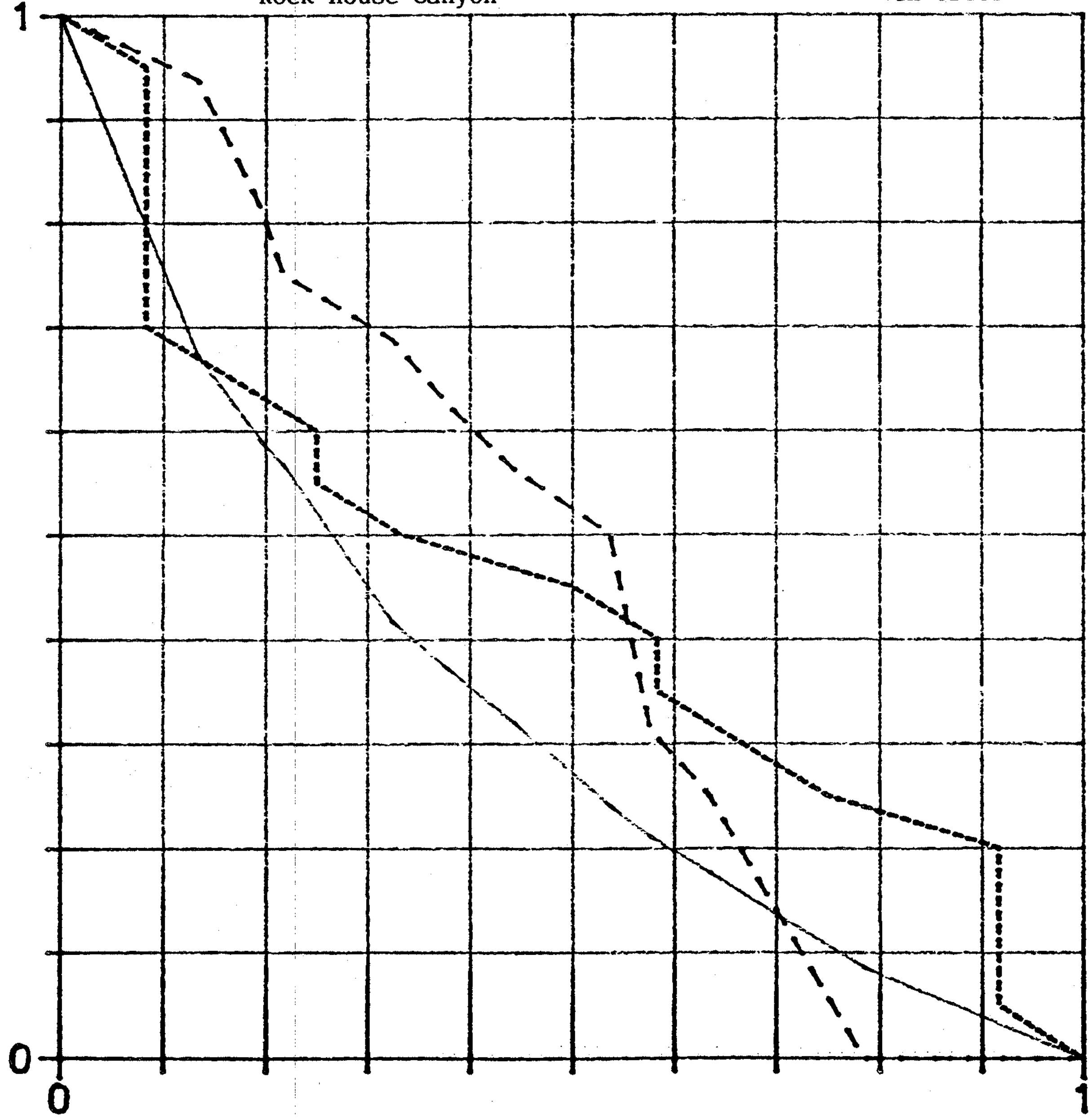

Magnitude: 16
Length: 29600 ft
Basin Area: 12 km2
Max Channel Elev: 7395
Min Channel Elev: 6755
Hypsometric Integral: 43.75

Red Canyon 4th Order

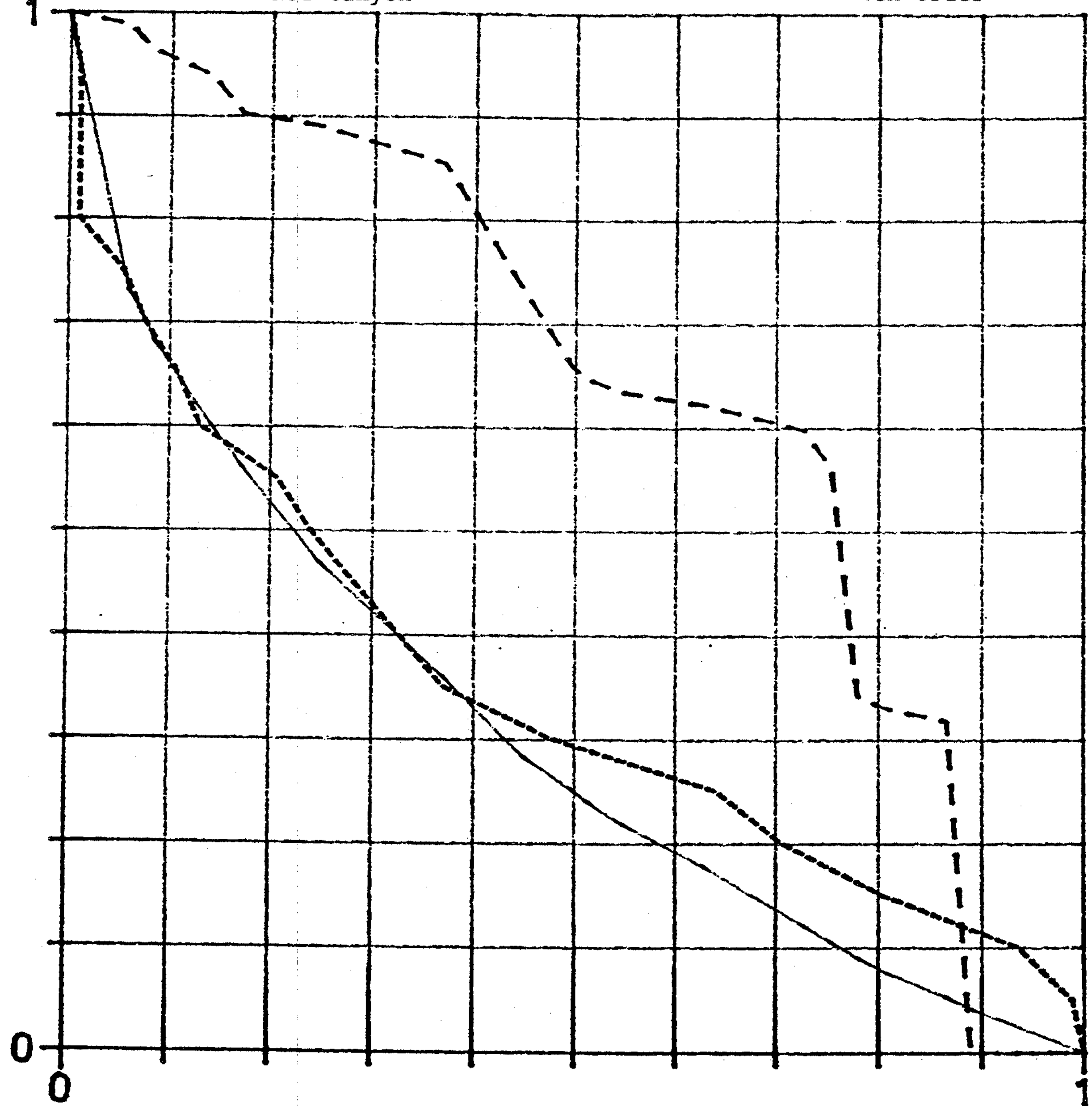

Magnitude: 81
Length: 55720 ft
Basin Area: 92 km2
Hypsometric Integral: 34.46
Max Channel Elev: 8341
Min Channel Elev: 6831

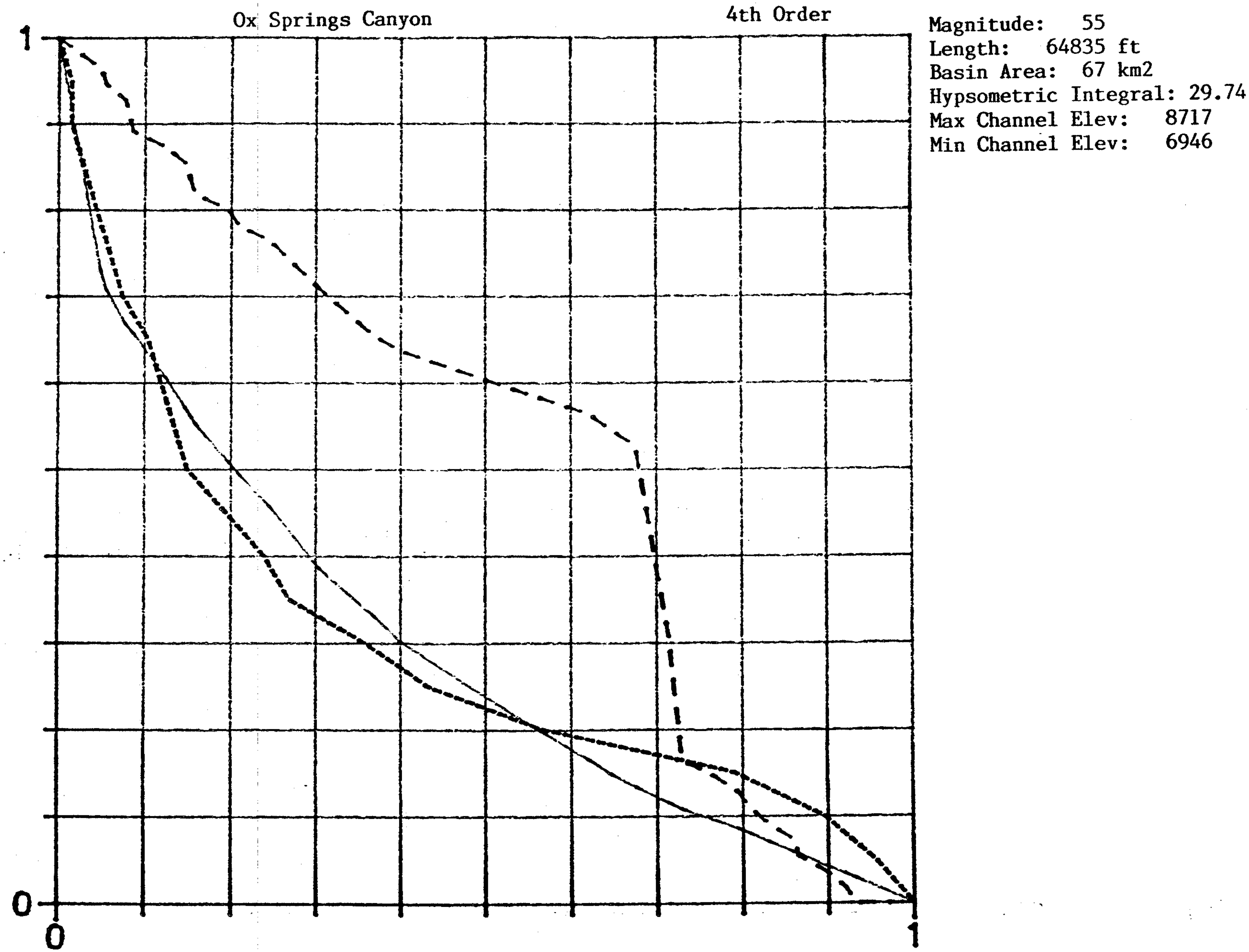

Ox Springs Canyon
4th Order
1
0
0
1
Magnitude: 55
Length: 64835 ft
Basin Area: 67 km2
Hypsometric Integral: 29.74
Max Channel Elev: 8717
Min Channel Elev: 6946

Harrington Canyon 4th Order

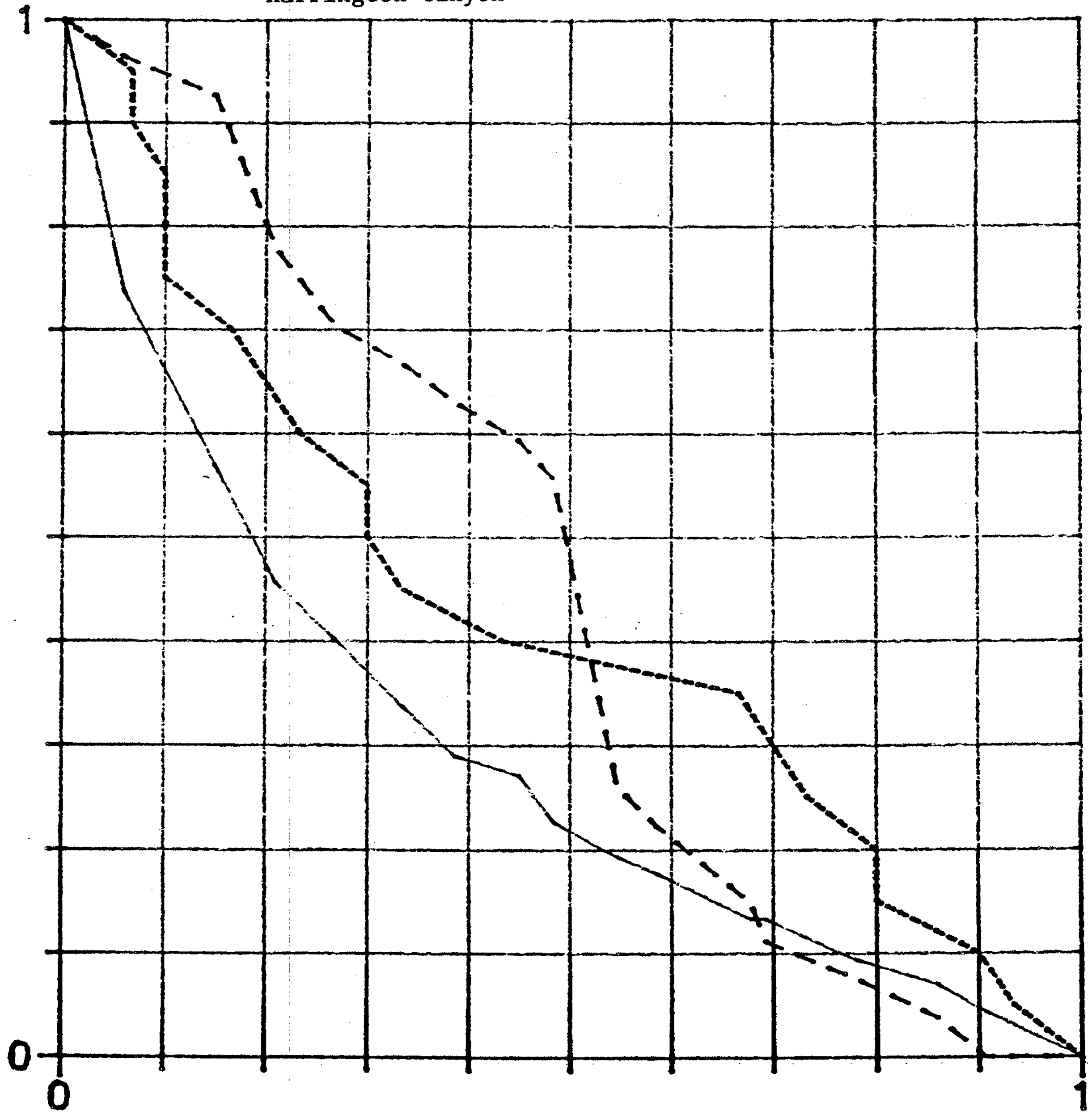

Magnitude: 27
Length: 44120
Basin Area: 30 km2
Hypsometric Integral: 42.17
Max Channel Elev: 7940
Min Channel Elev: 7012

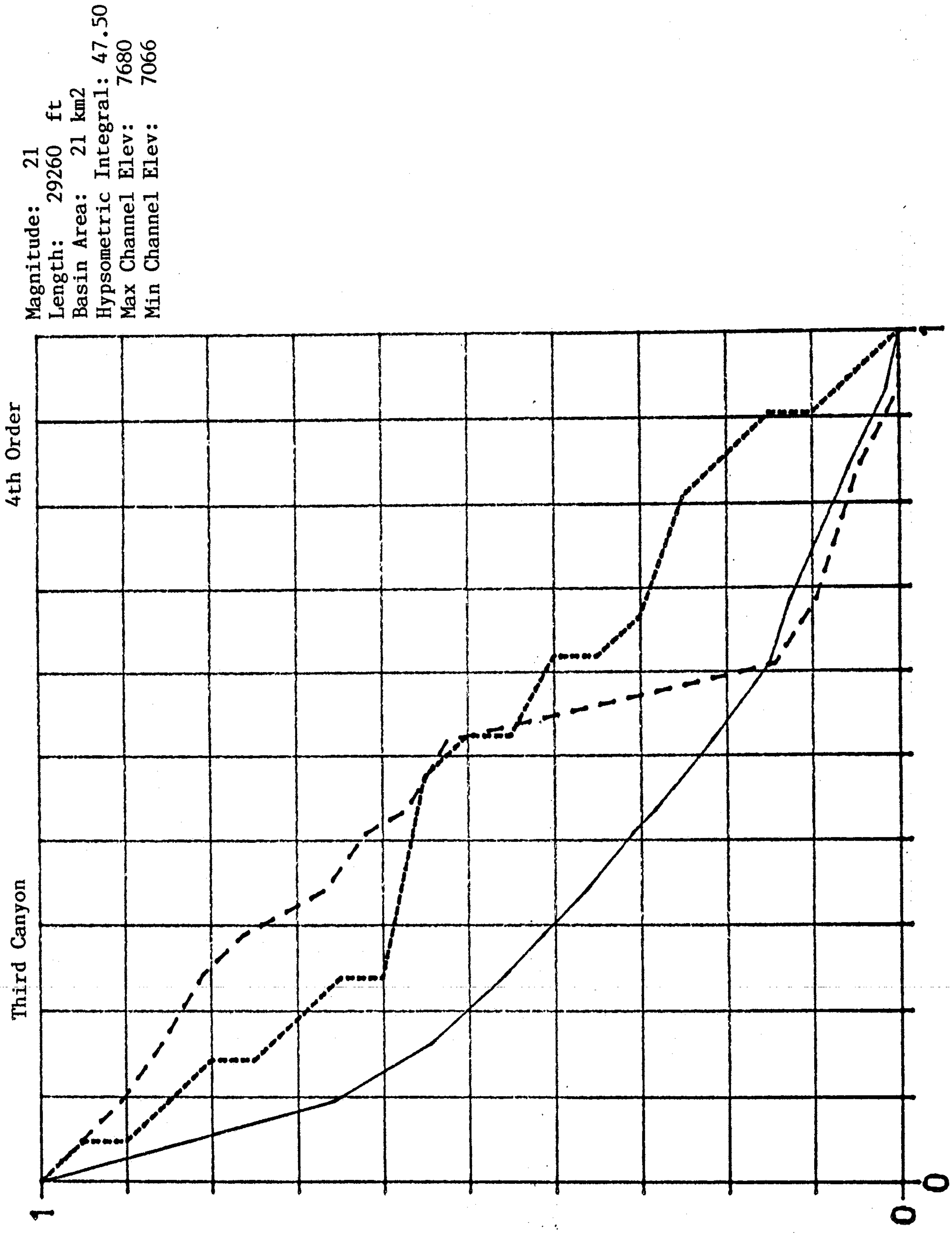
Third Canyon
4th Order
Magnitude: 21
Length: 29260 ft
Basin Area: 21 km2
Hypsometric Integral: 47.50
Max Channel Elev: 7680
Min Channel Elev: 7066
1
0
0
1

W H Canyon 4th Order

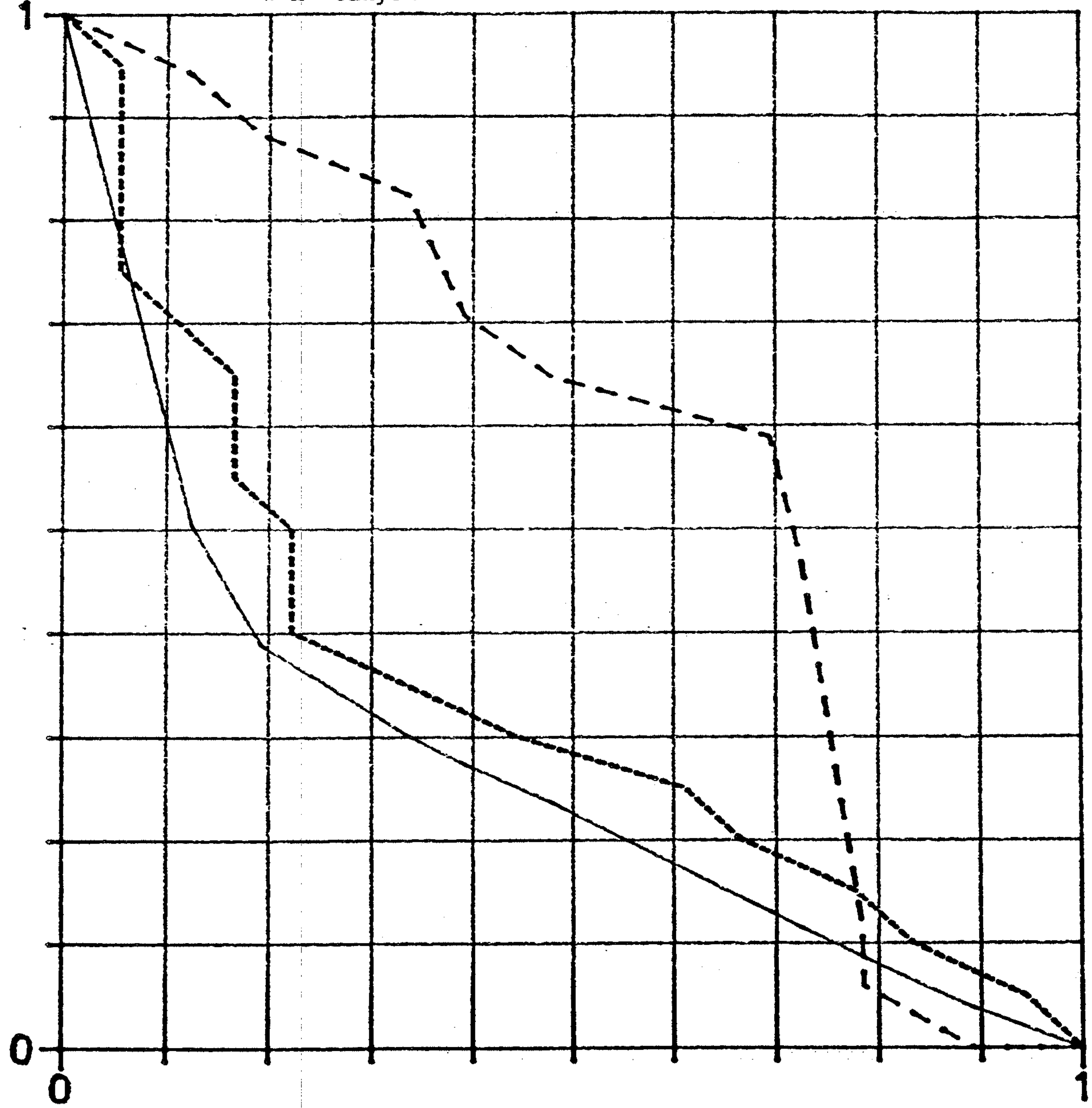

Magnitude: 17
Length: 33610 ft
Basin Area: 18 km2
Hypsometric Integral: 33.33
Max Channel Elev: 8230
Min Channel Elev: 7198

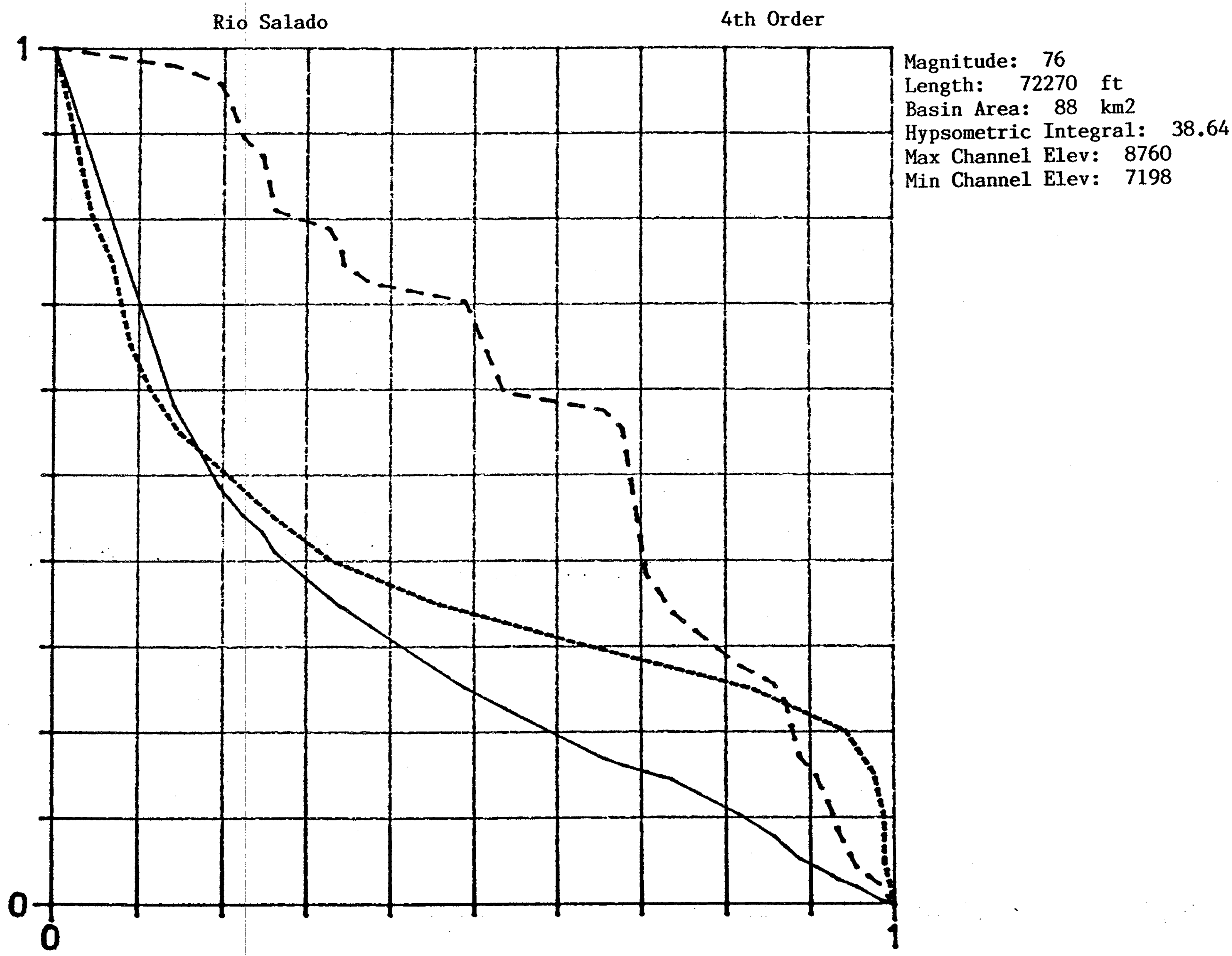
Rio Salado
4th Order
1
0
0
1
Magnitude: 76
Length: 72270 ft
Basin Area: 88 km2
Hypsometric Integral: 38.64
Max Channel Elev: 8760
Min Channel Elev: 7198

APPENDIX B: Working Maps

Appendix B consists of the working USGS topographic maps, which are included under separate cover.

NOT INCLUDED IN THIS DISTRIBUTION COPY

Blank

APPENDIX C: Channel Cross Sections

EXPLANATION

Cross sections plotted looking upstream, the left bank is taken as the origin.

Dashed line depicts the approximate location of the high-water surface, based on observed high water marks.

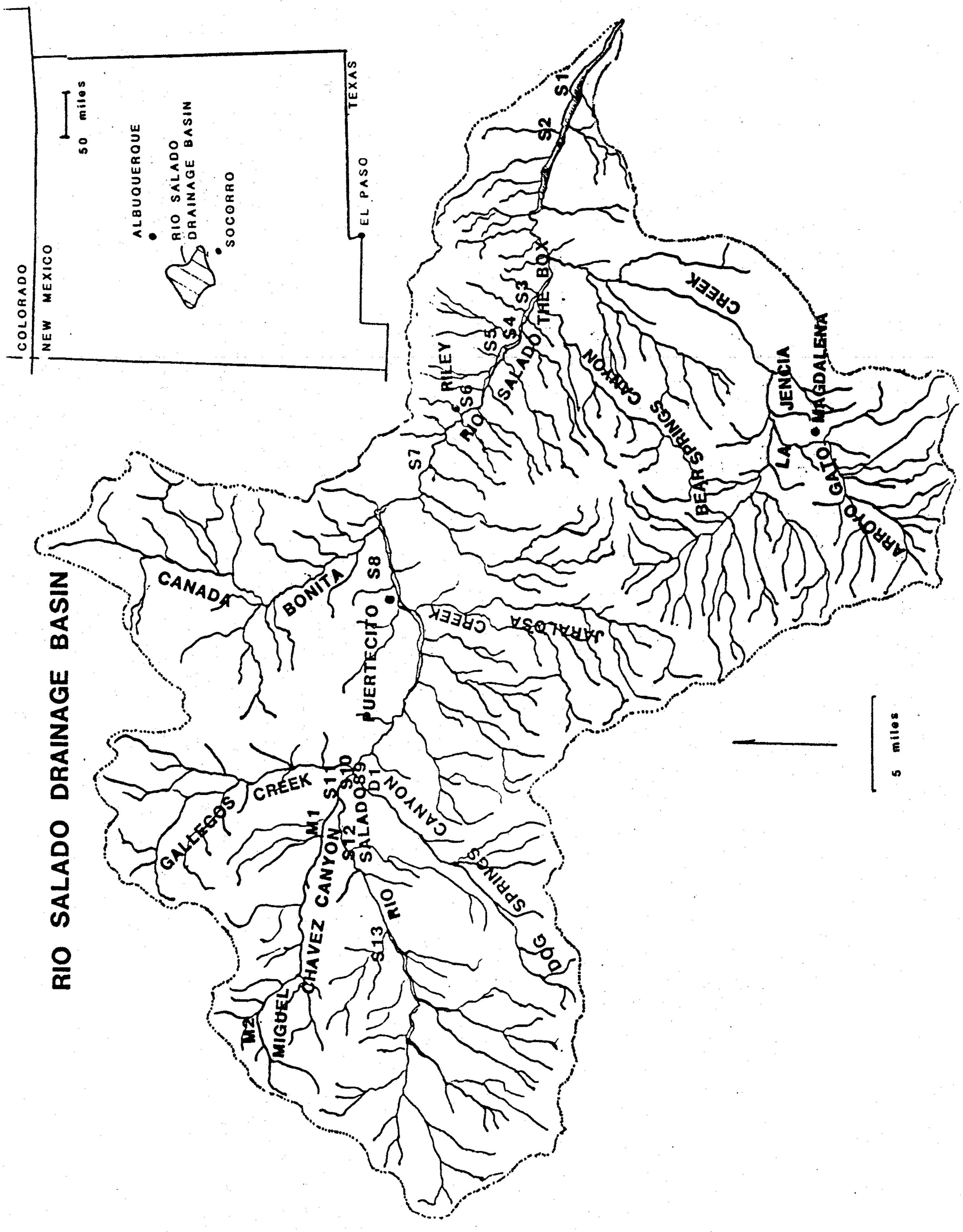
RIO SALADO DRAINAGE BASIN
COLORADO
NEW MEXICO
TEXAS
ALBUQUERQUE
RIO SALADO DRAINAGE BASIN
SOCORRO
EL PASO
50 miles
CANADA
BONITA
S8
PUERTECITO
JARALOSA CREEK
GALLEGOS
CREEK
S11
S10
S9
D1
M1
S12
SALADO
CANYON
CHAVEZ CANYON
RIO
S13
DOG SPRINGS
MIGUEL
M2
S7
RIO
S6
RILEY
SALADO
S5
S4
S3
THE BOX
S2
S1
BEAR SPRINGS CANYON
CREEK
LA JENCIA
MAGDALENA
GATO
ARROYO
5 miles

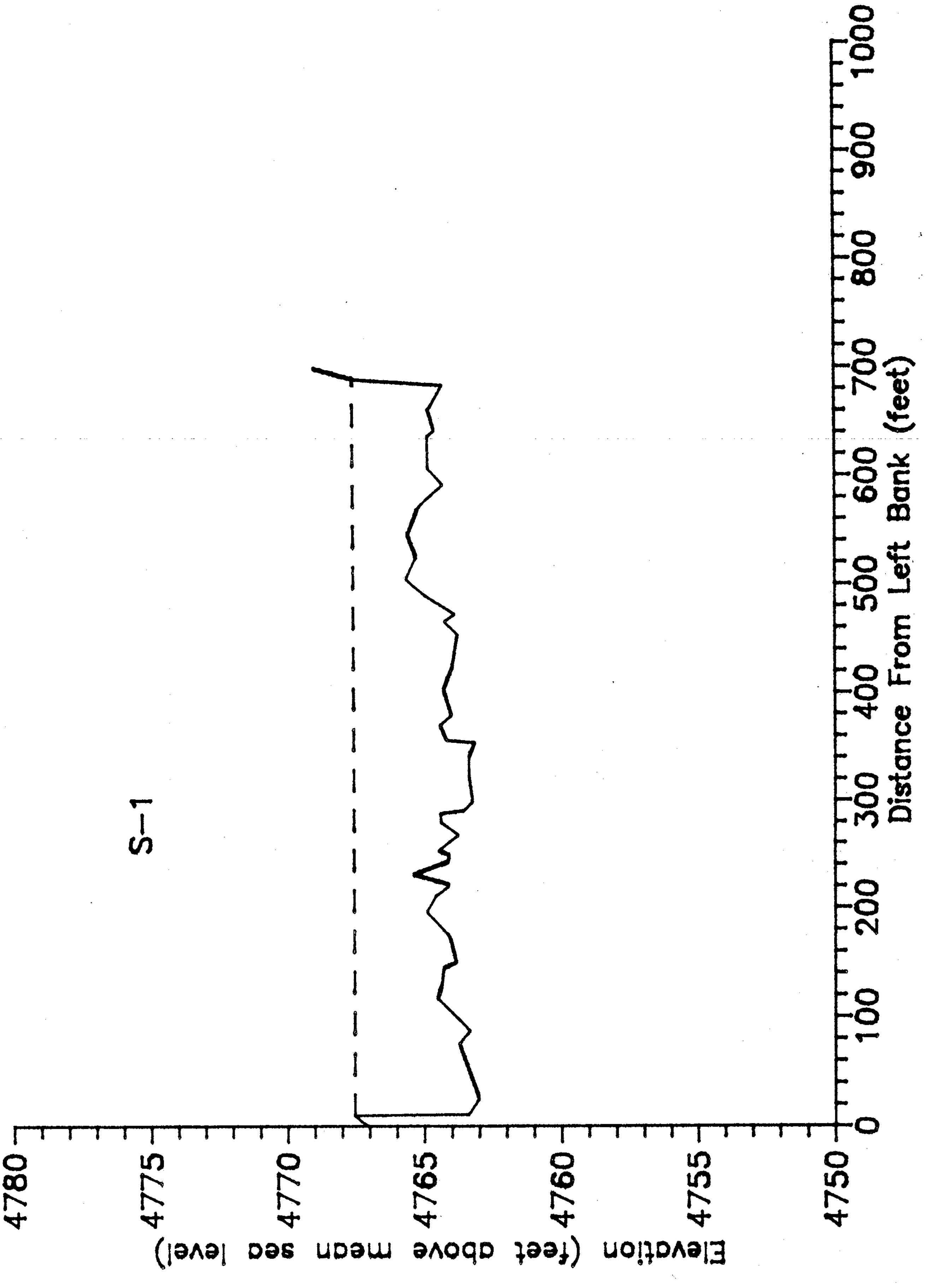
S–1
Elevation (feet above mean sea level)
4750
4755
4760
4765
4770
4775
4780
Distance From Left Bank (feet)
0
100
200
300
400
500
600
700
800
900
1000

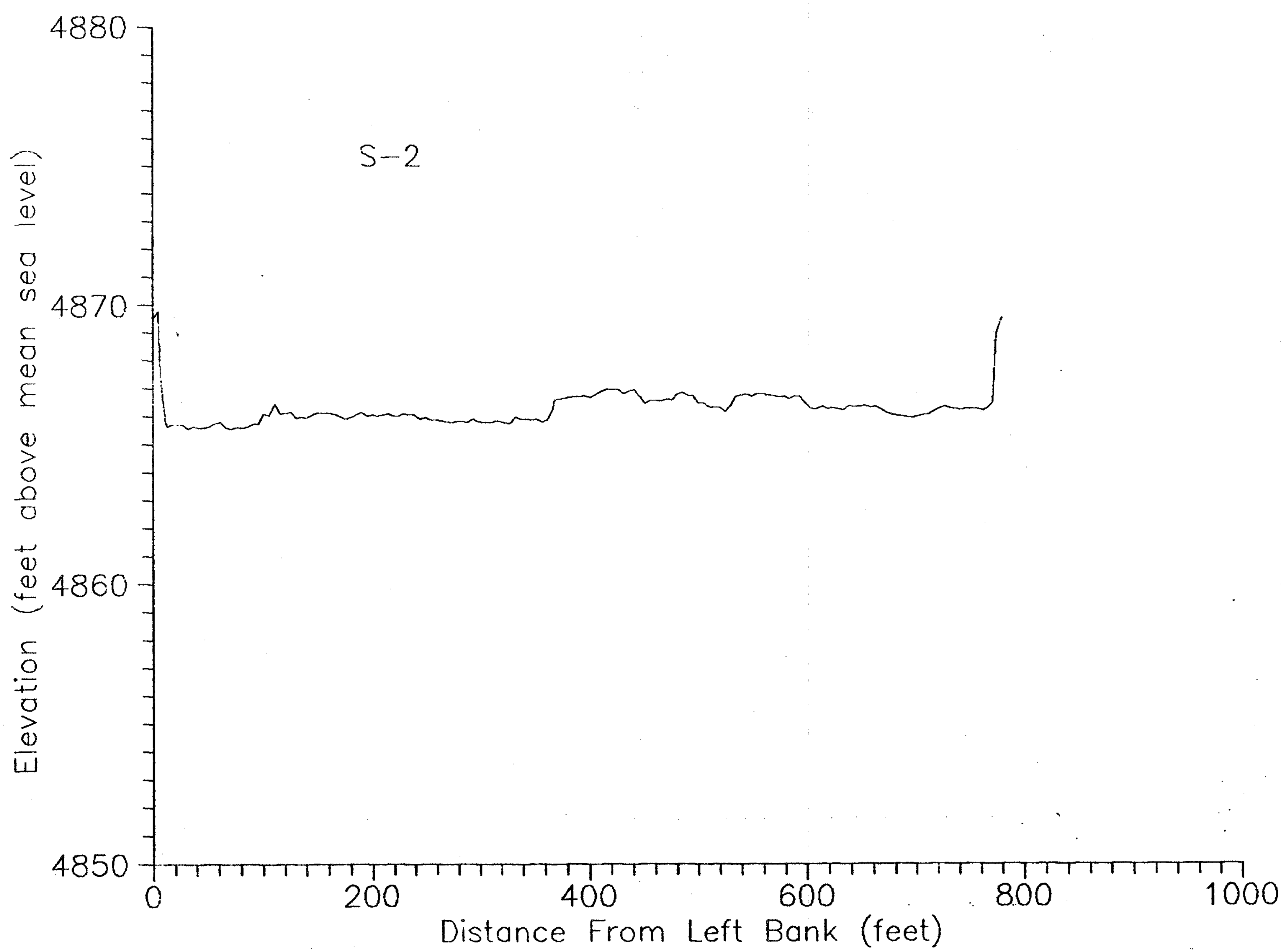
S-2
Elevation (feet above mean sea level)
4880
4870
4860
4850
0
200
400
600
800
1000
Distance From Left Bank (feet)

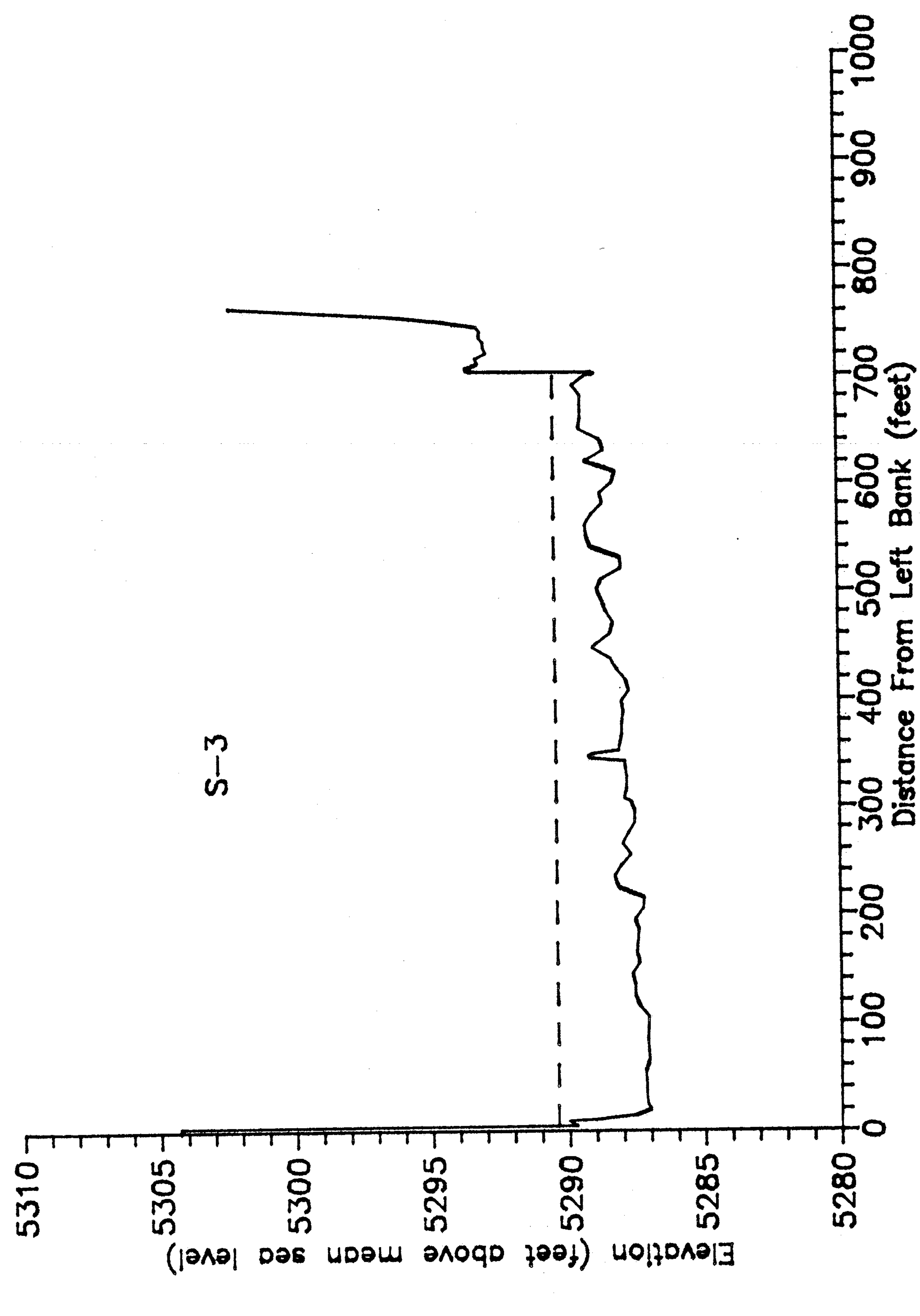
S-3
Elevation (feet above mean sea level)
5280
5285
5290
5295
5300
5305
5310
Distance From Left Bank (feet)
0
100
200
300
400
500
600
700
800
900
1000

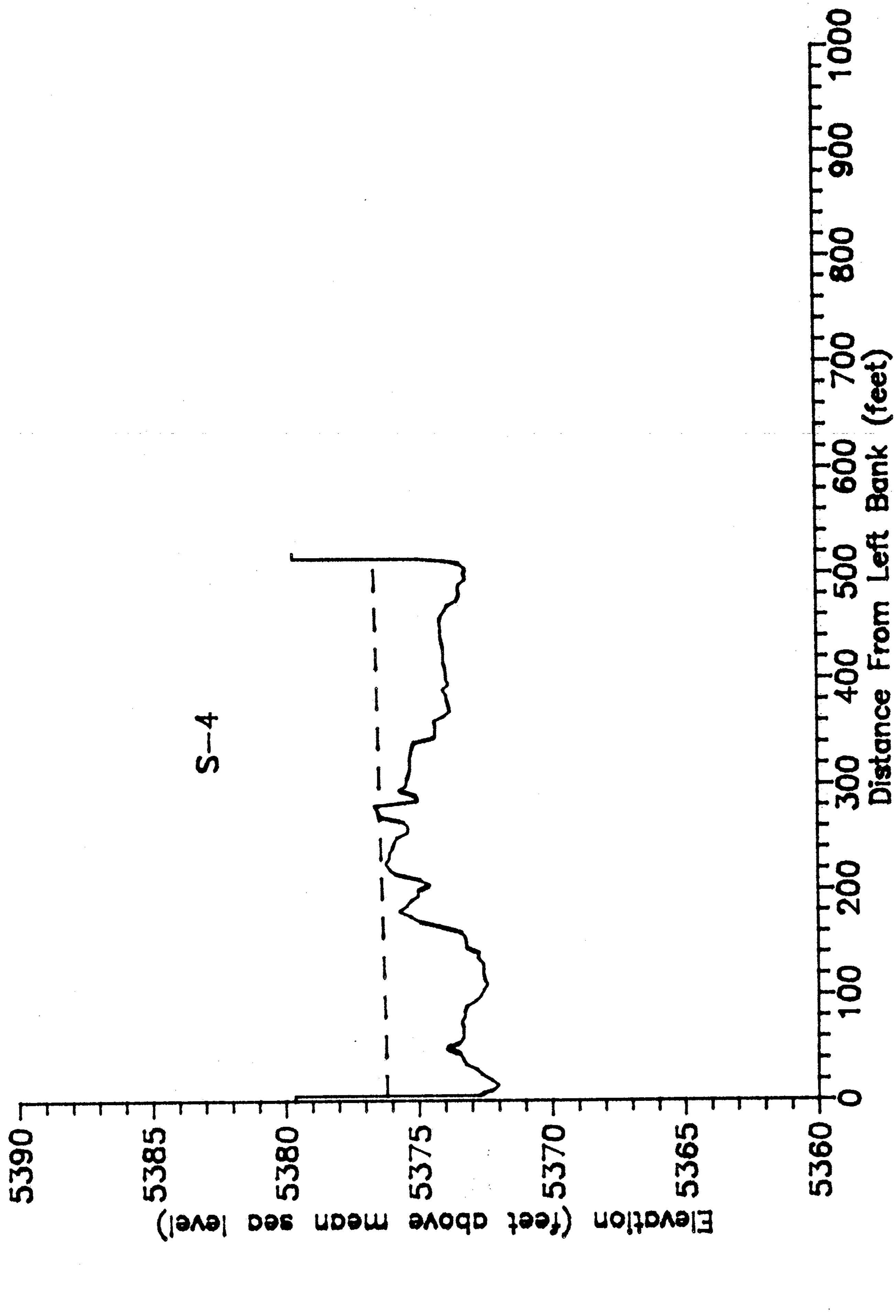

S—4
Elevation (feet above mean sea level)
5390
5385
5380
5375
5370
5365
5360
Distance From Left Bank (feet)
0
100
200
300
400
500
600
700
800
900
1000

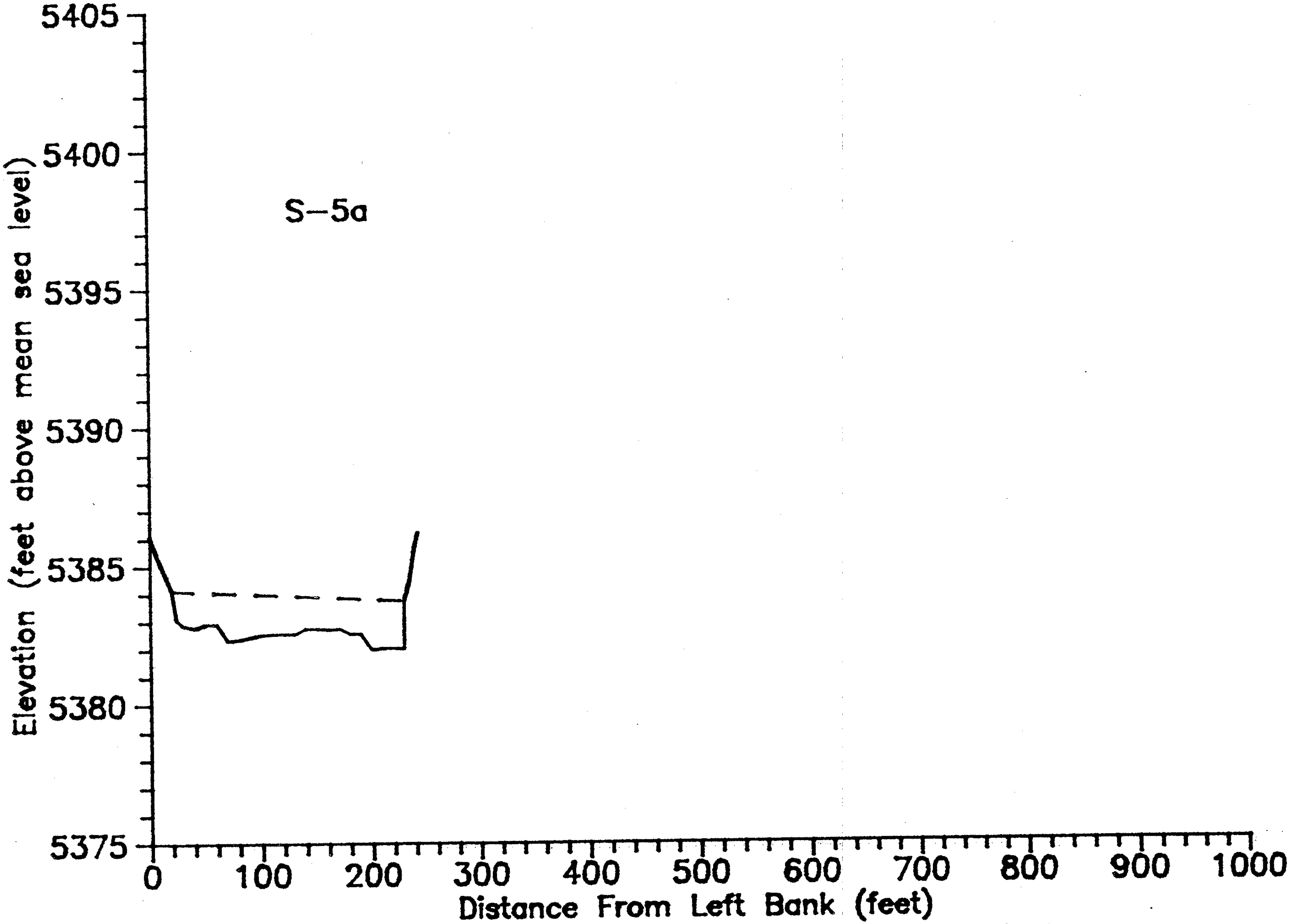
S–5a
Elevation (feet above mean sea level)
5405
5400
5395
5390
5385
5380
5375
0
100
200
300
400
500
600
700
800
900
1000
Distance From Left Bank (feet)

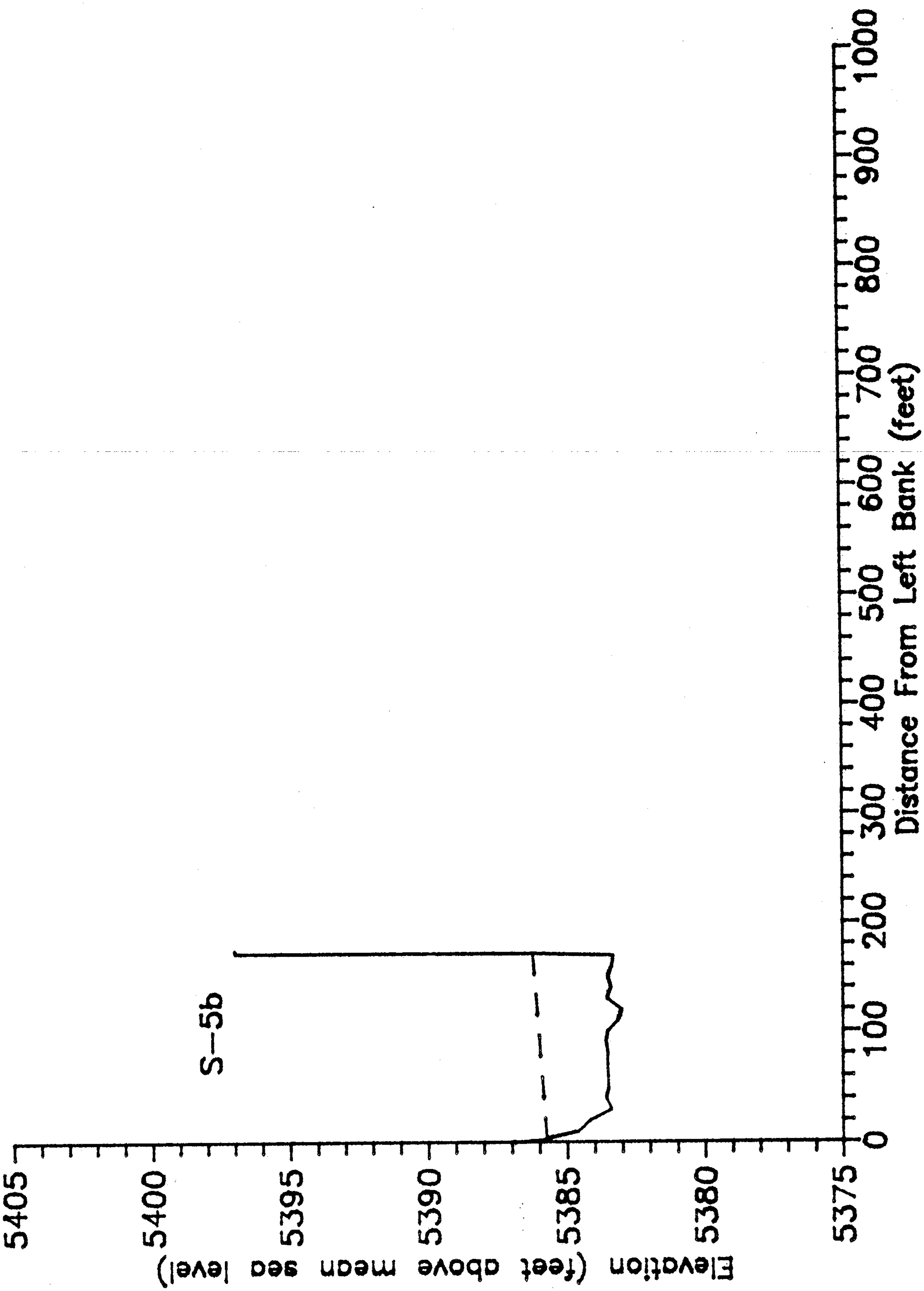
S—5b
Elevation (feet above mean sea level)
5405
5400
5395
5390
5385
5380
5375
Distance From Left Bank (feet)
0
100
200
300
400
500
600
700
800
900
1000

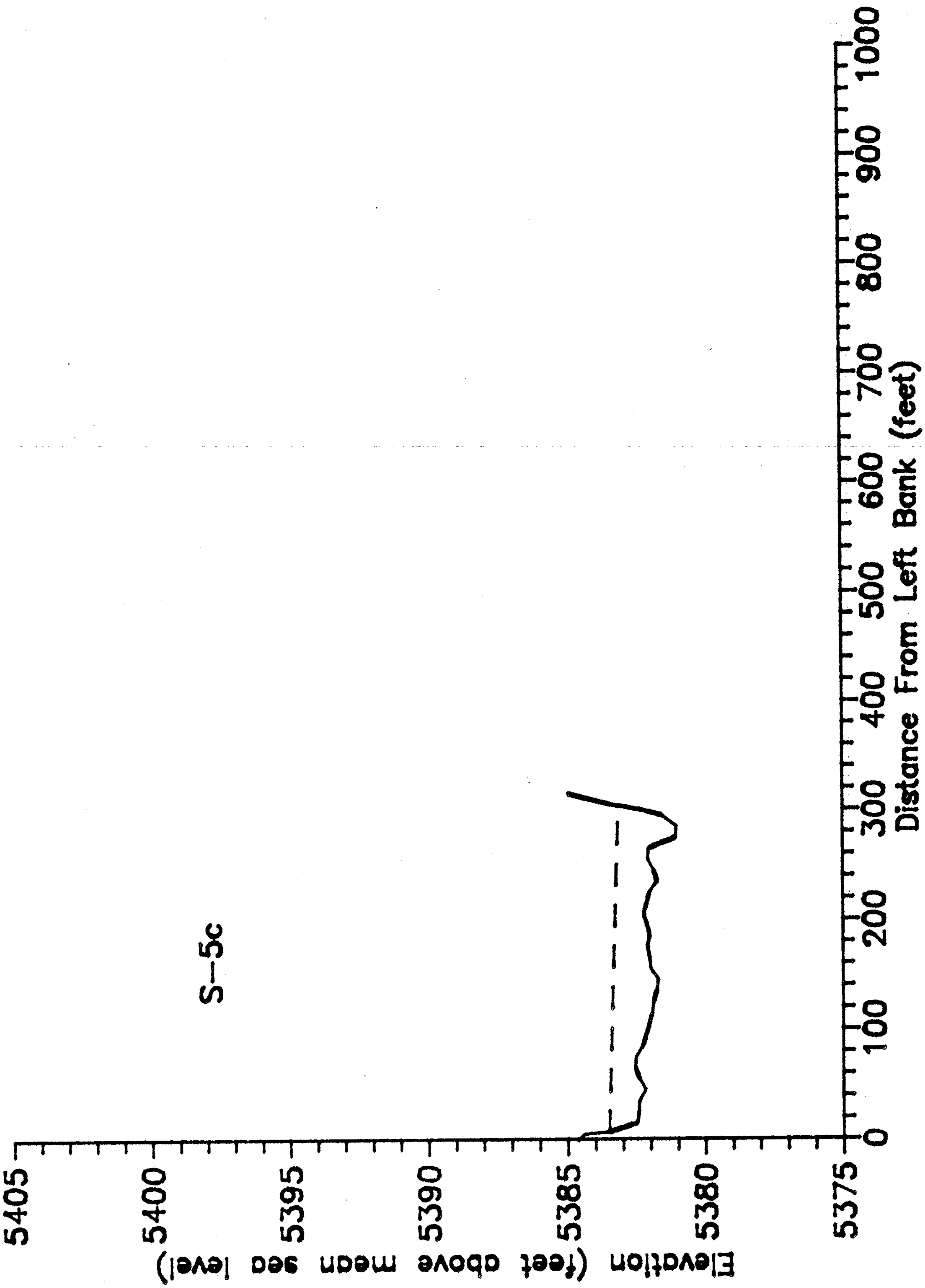

S—5c
Elevation (feet above mean sea level)
5405
5400
5395
5390
5385
5380
5375
Distance From Left Bank (feet)
0
100
200
300
400
500
600
700
800
900
1000

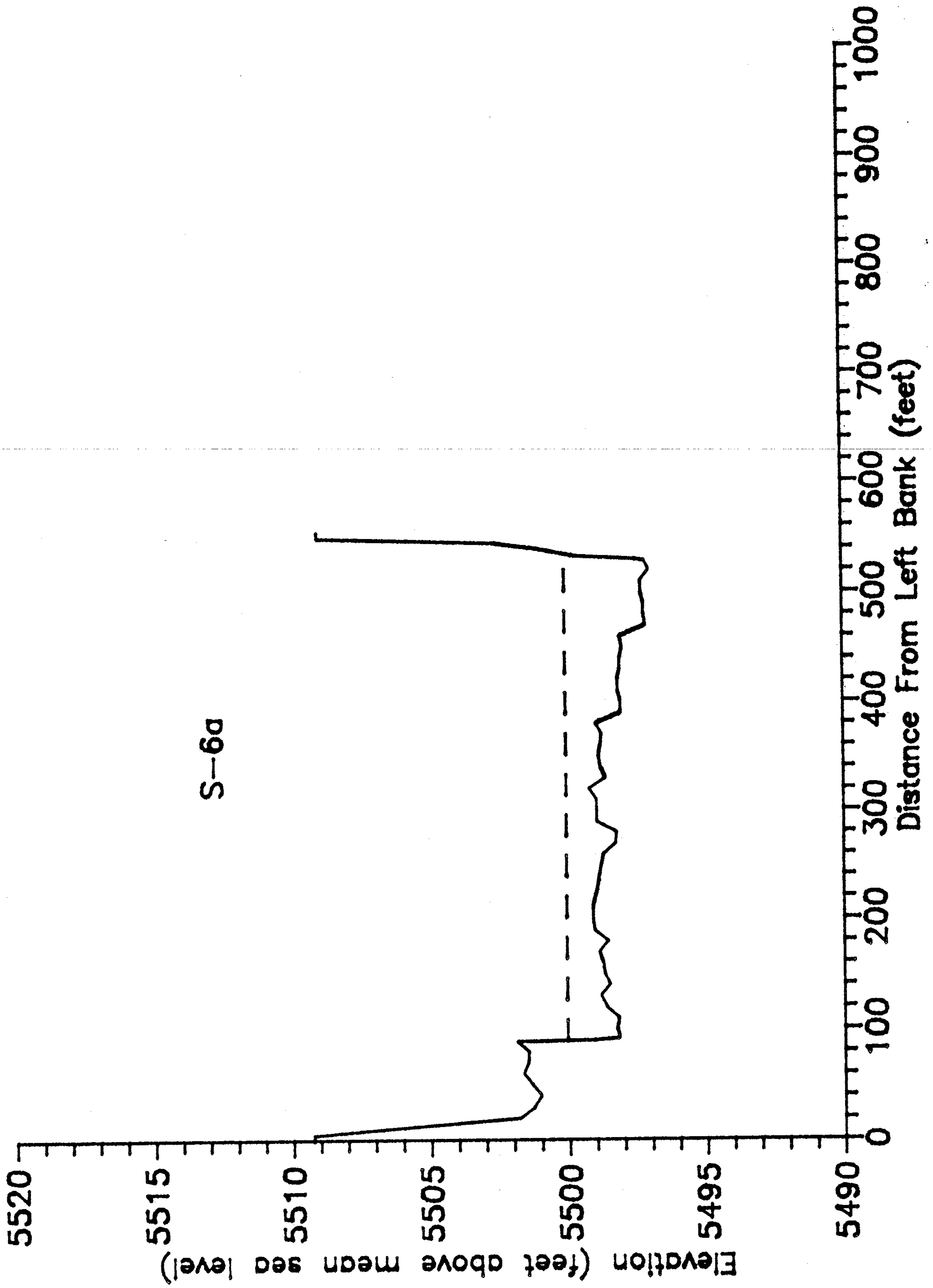
S—6a
Elevation (feet above mean sea level)
5490
5495
5500
5505
5510
5515
5520
0
100
200
300
400
500
600
700
800
900
1000
Distance From Left Bank (feet)

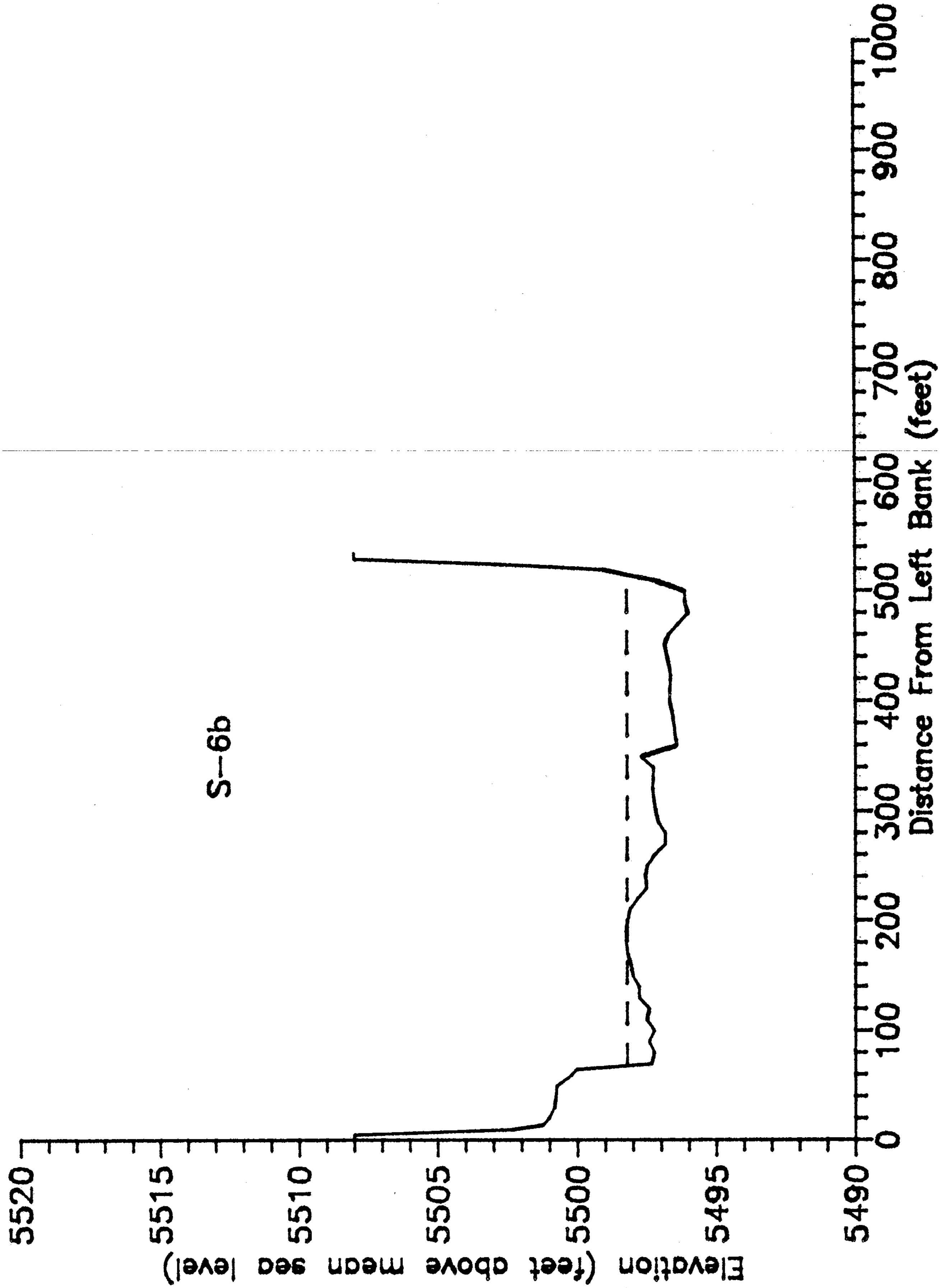
S—6b
Elevation (feet above mean sea level)
5520
5515
5510
5505
5500
5495
5490
Distance From Left Bank (feet)
0
100
200
300
400
500
600
700
800
900
1000

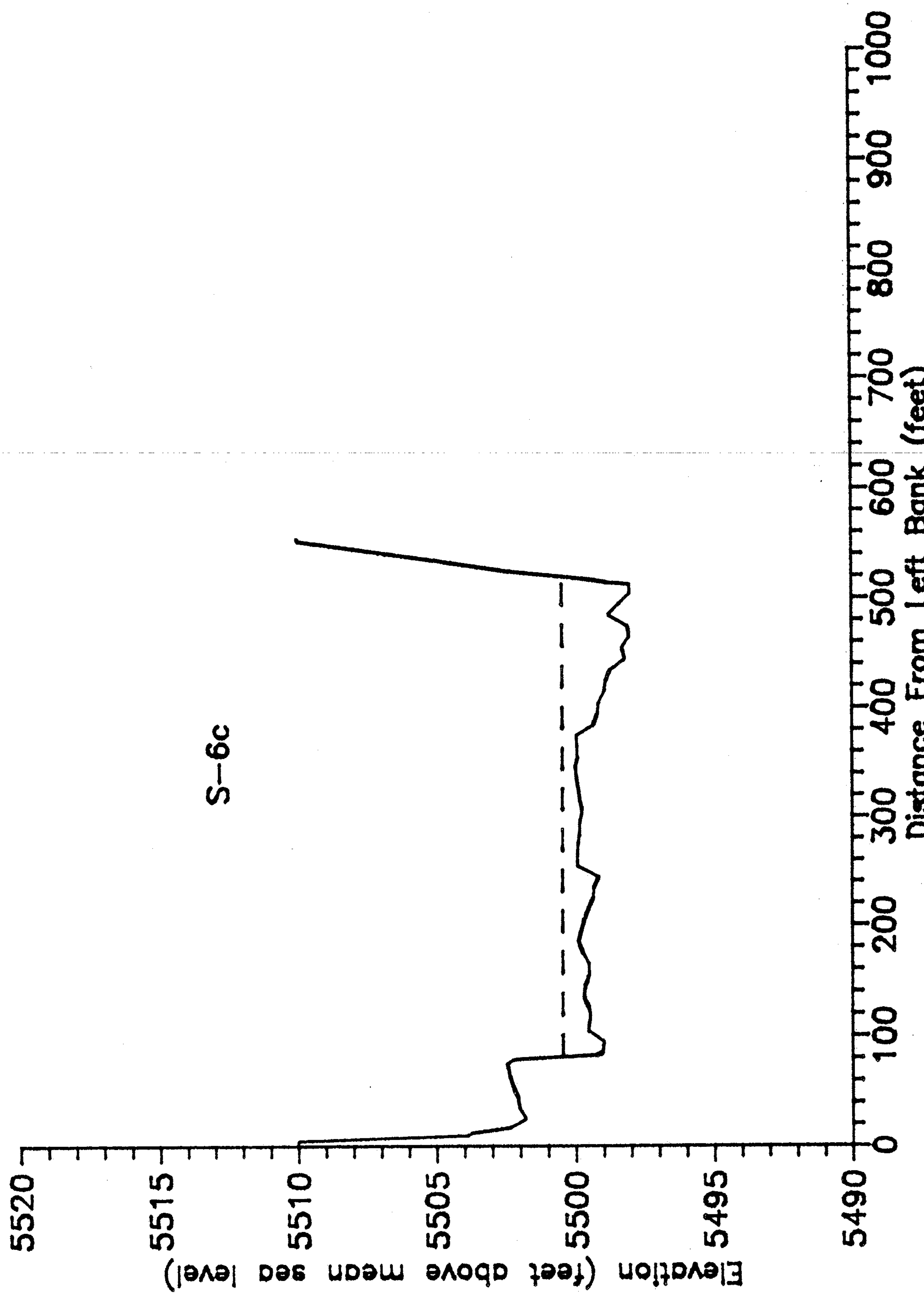
S–6c
Elevation (feet above mean sea level)
5490
5495
5500
5505
5510
5515
5520
Distance From Left Bank (feet)
0
100
200
300
400
500
600
700
800
900
1000

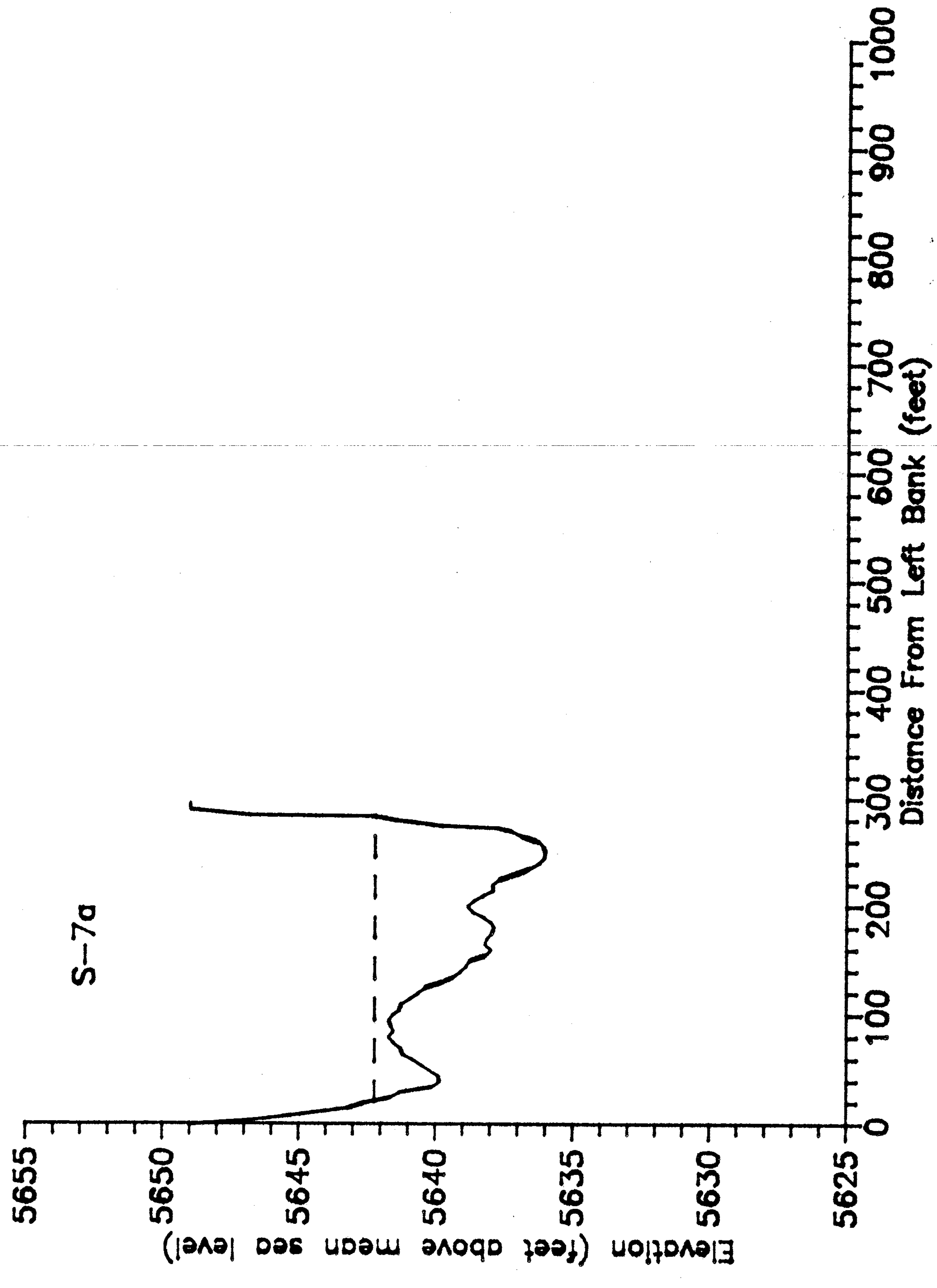
S—7a
Elevation (feet above mean sea level)
5655
5650
5645
5640
5635
5630
5625
Distance From Left Bank (feet)
0
100
200
300
400
500
600
700
800
900
1000

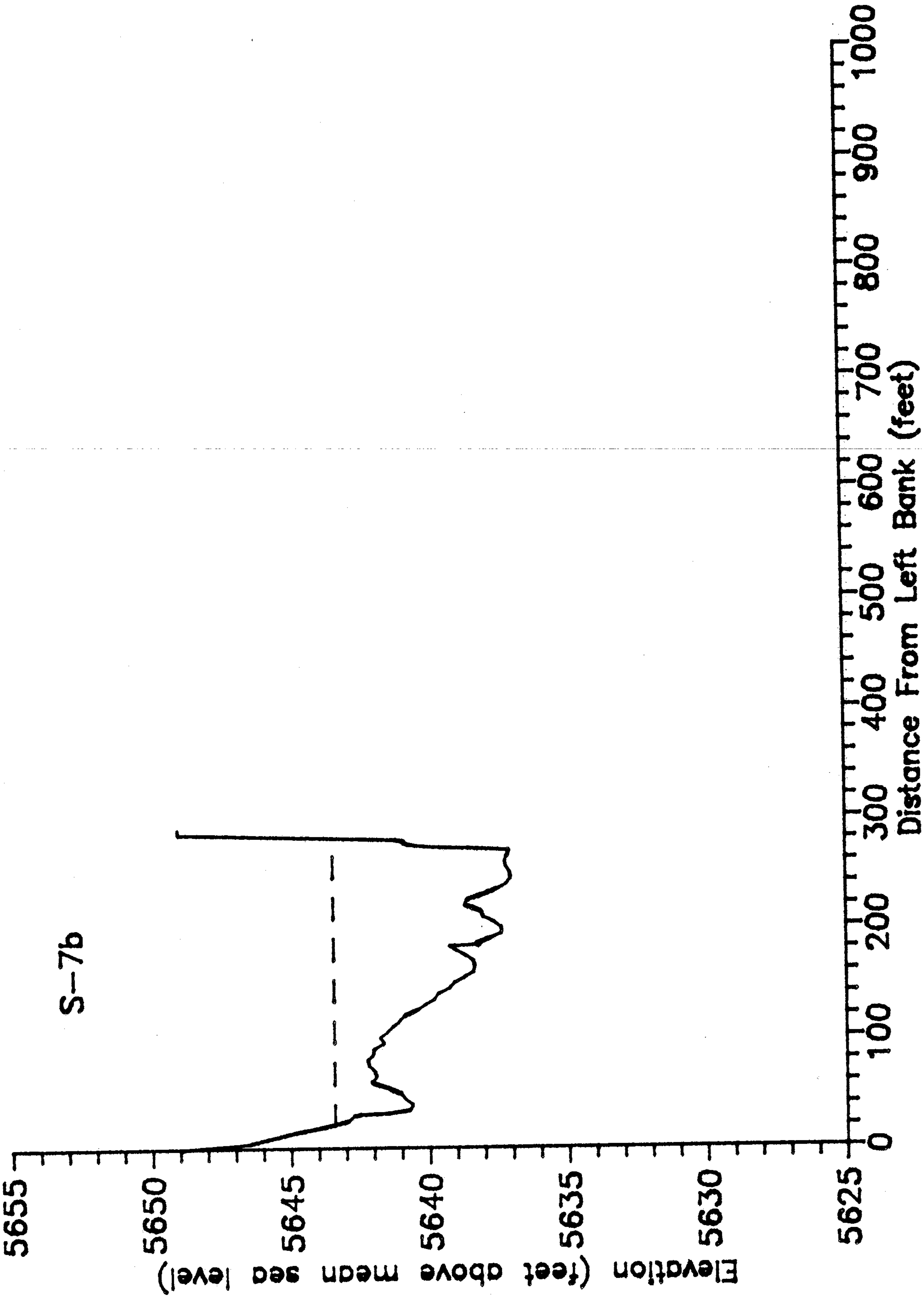
S-7b
Elevation (feet above mean sea level)
5625
5630
5635
5640
5645
5650
5655
Distance From Left Bank (feet)
0
100
200
300
400
500
600
700
800
900
1000

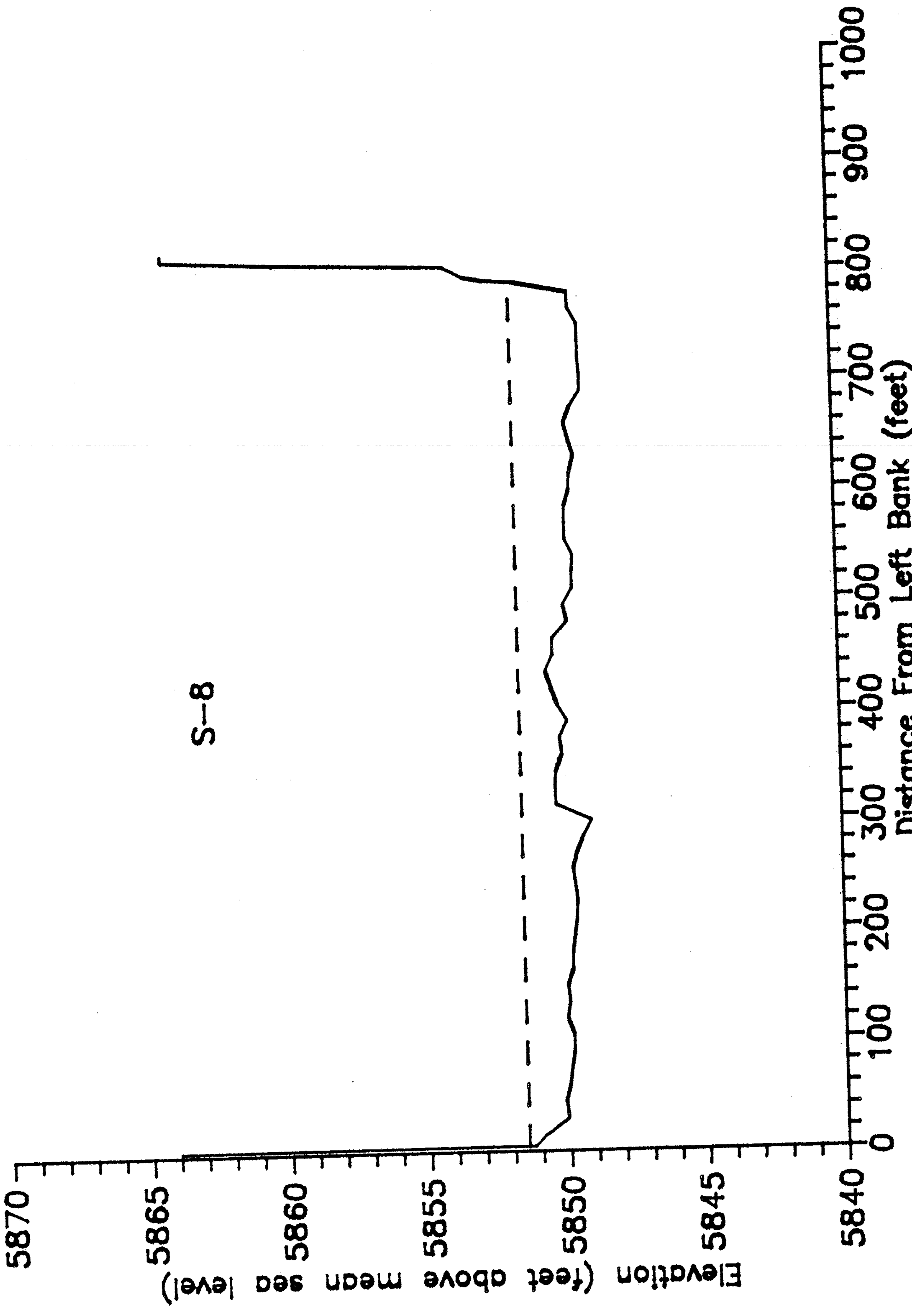
S-8
Elevation (feet above mean sea level)
5840
5845
5850
5855
5860
5865
5870
Distance From Left Bank (feet)
0
100
200
300
400
500
600
700
800
900
1000

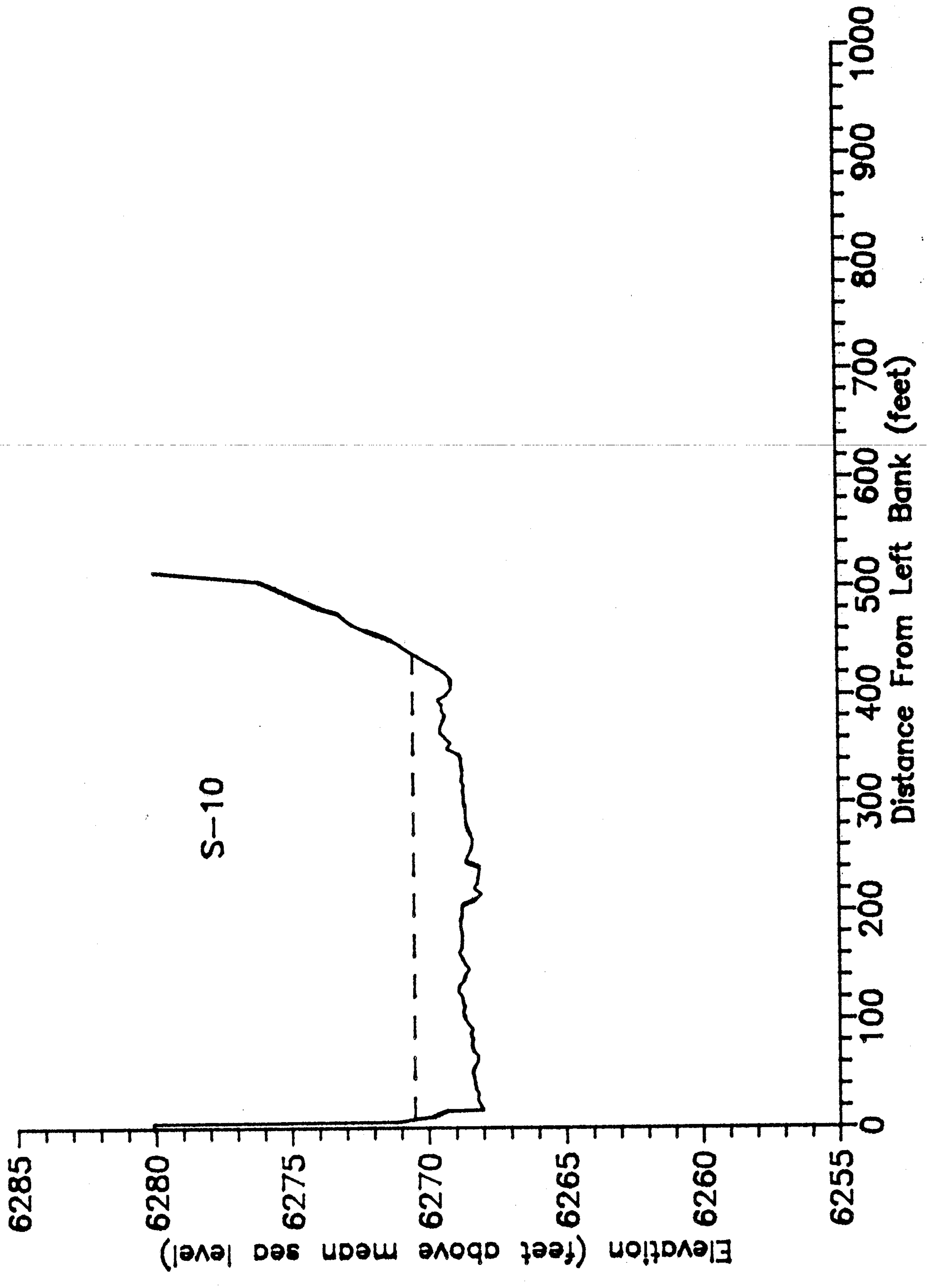
S–10
Elevation (feet above mean sea level)
6285
6280
6275
6270
6265
6260
6255
Distance From Left Bank (feet)
0
100
200
300
400
500
600
700
800
900
1000

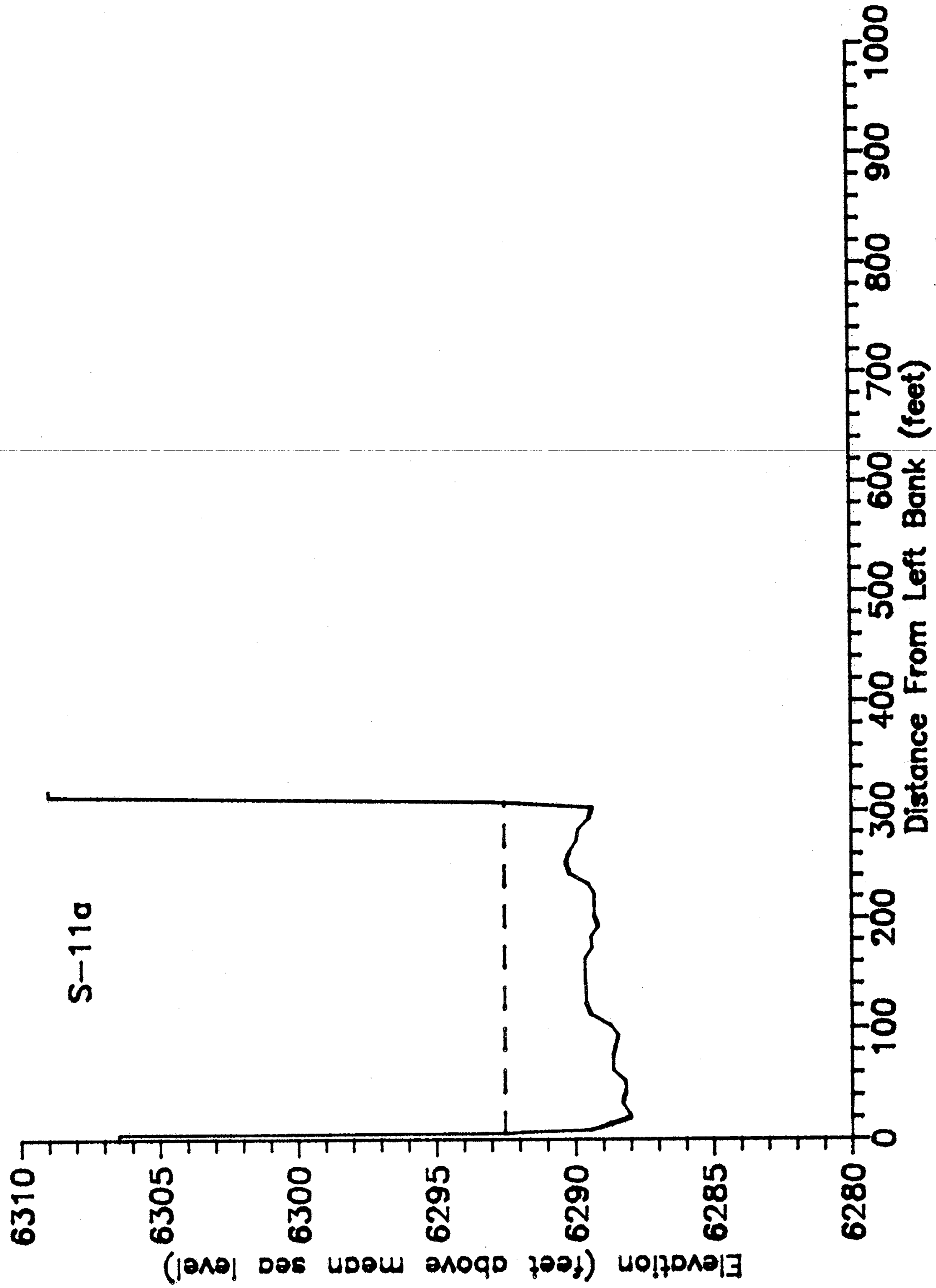
S—11a
6310
6305
6300
6295
6290
6285
6280
Elevation (feet above mean sea level)
0
100
200
300
400
500
600
700
800
900
1000
Distance From Left Bank (feet)

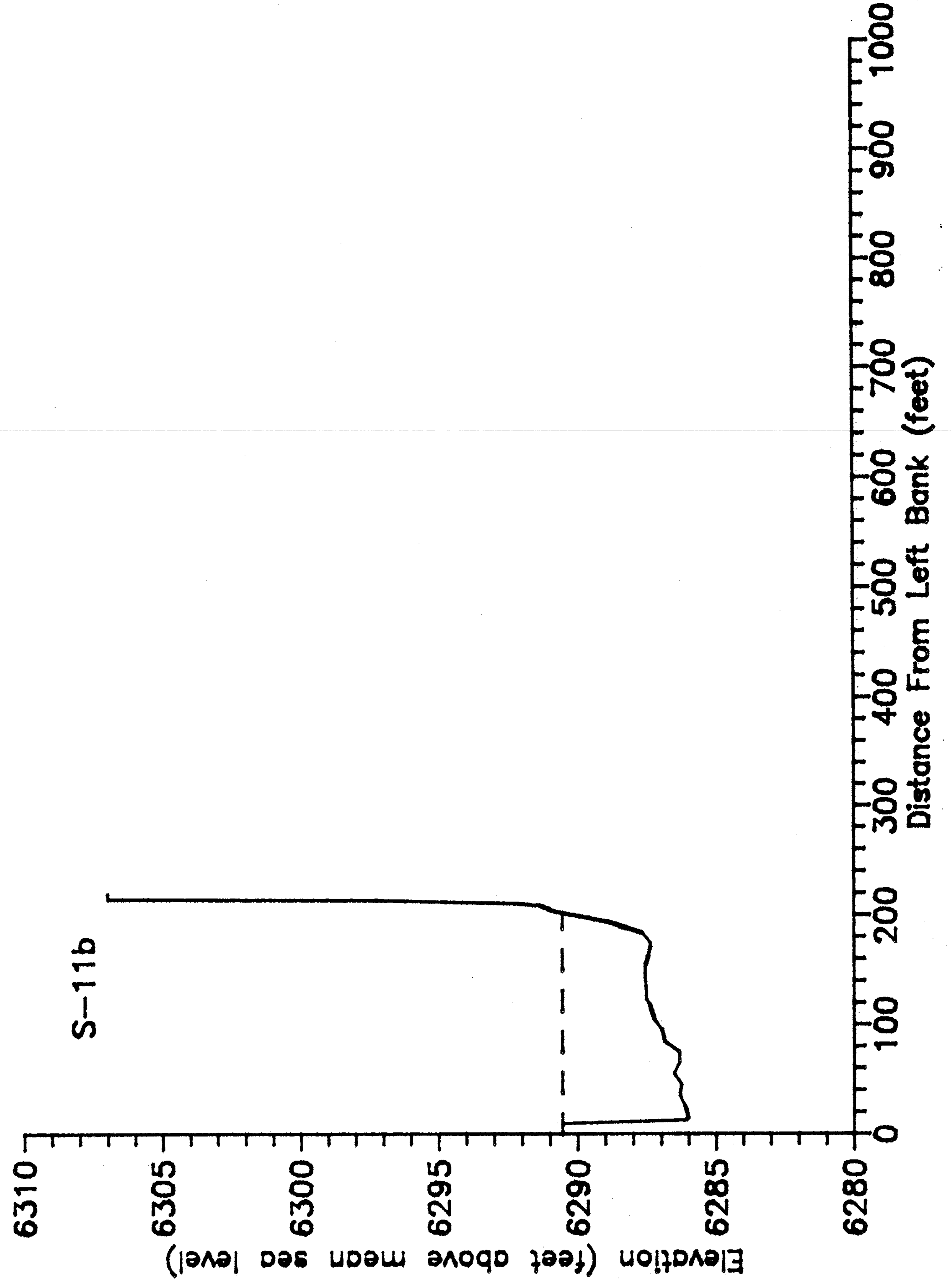
S—11b
Elevation (feet above mean sea level)
6310
6305
6300
6295
6290
6285
6280
Distance From Left Bank (feet)
0
100
200
300
400
500
600
700
800
900
1000

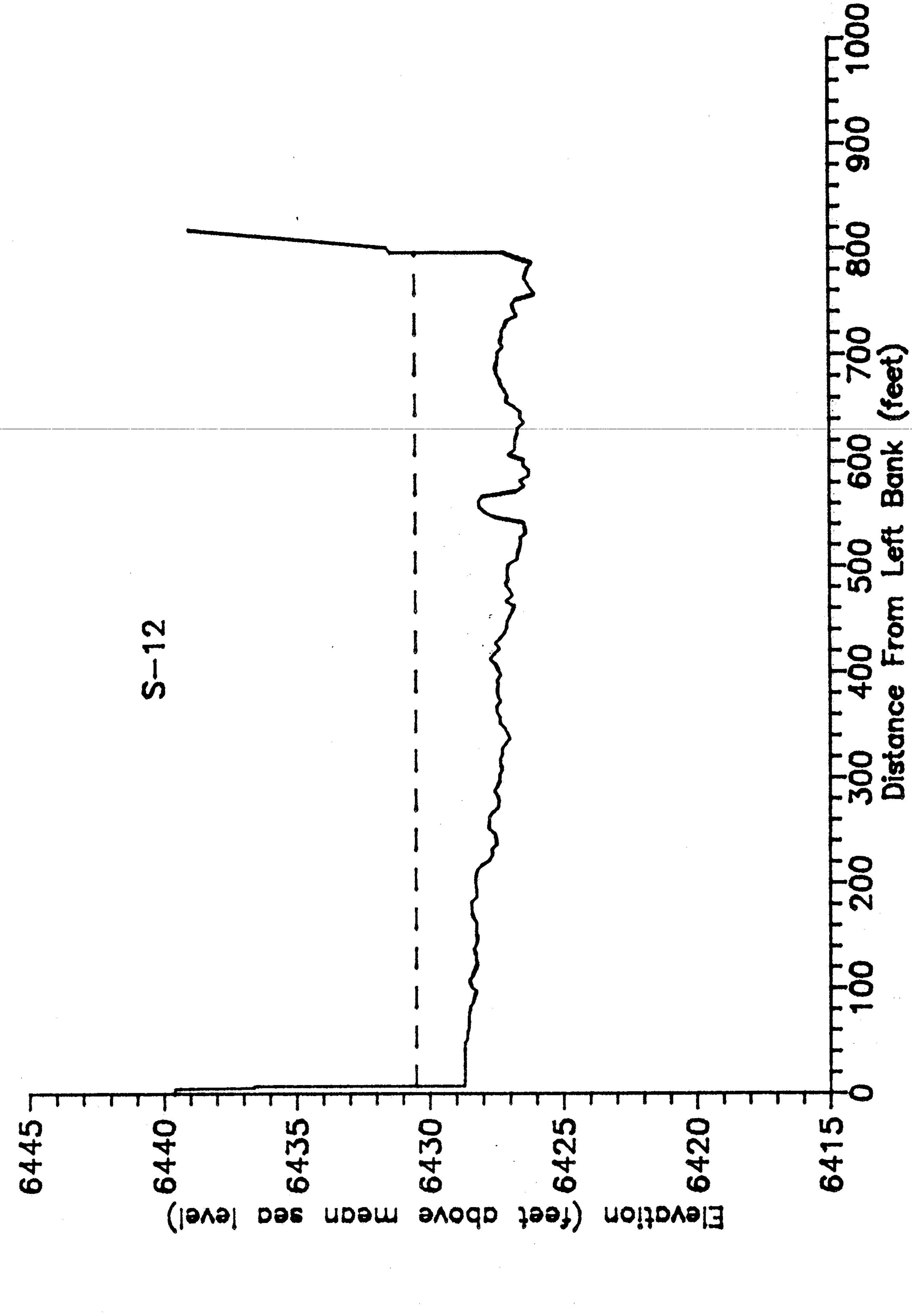

S–12
Elevation (feet above mean sea level)
6445
6440
6435
6430
6425
6420
6415
Distance From Left Bank (feet)
0
100
200
300
400
500
600
700
800
900
1000

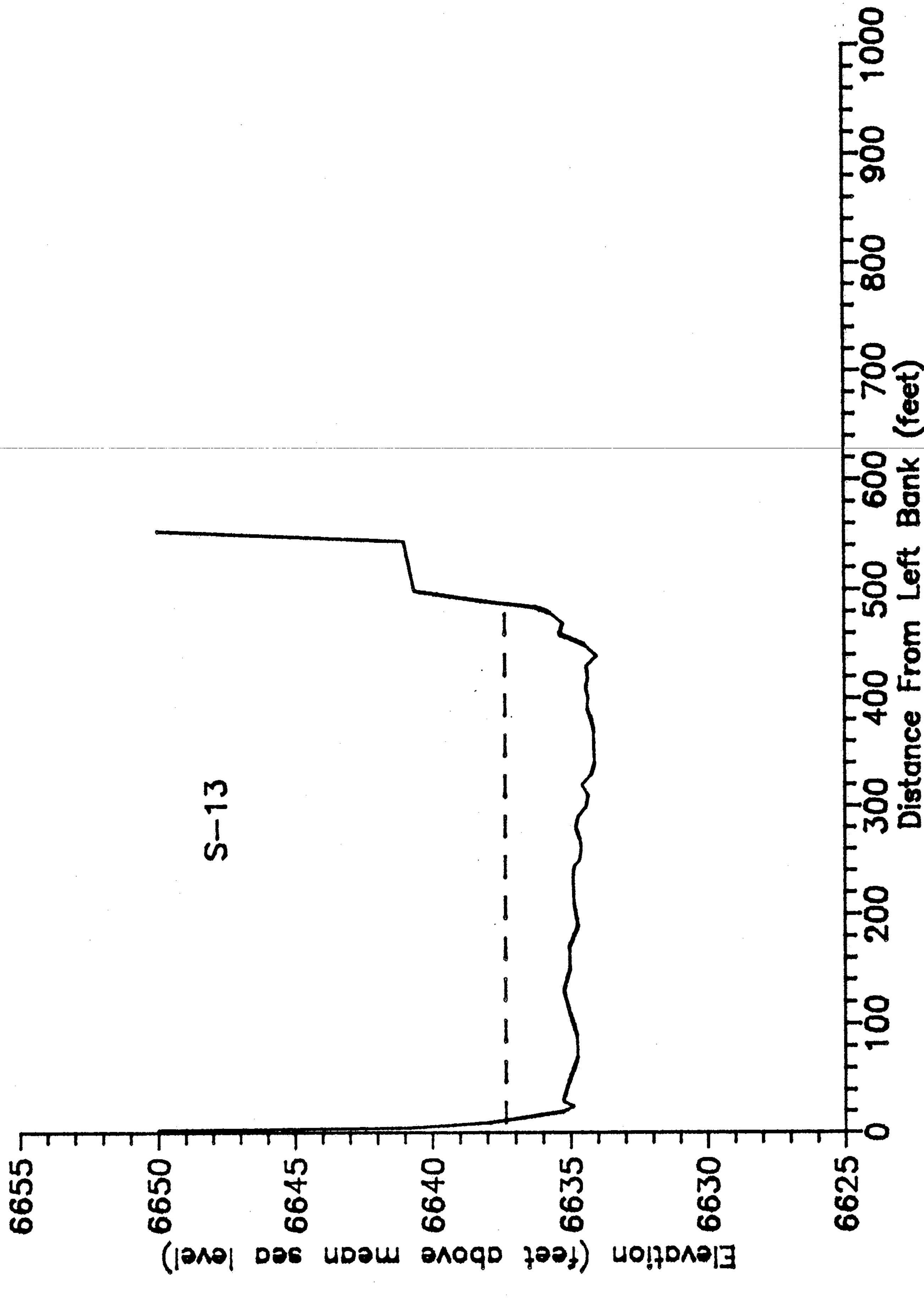
S–13
Elevation (feet above mean sea level)
6625
6630
6635
6640
6645
6650
6655
Distance From Left Bank (feet)
0
100
200
300
400
500
600
700
800
900
1000

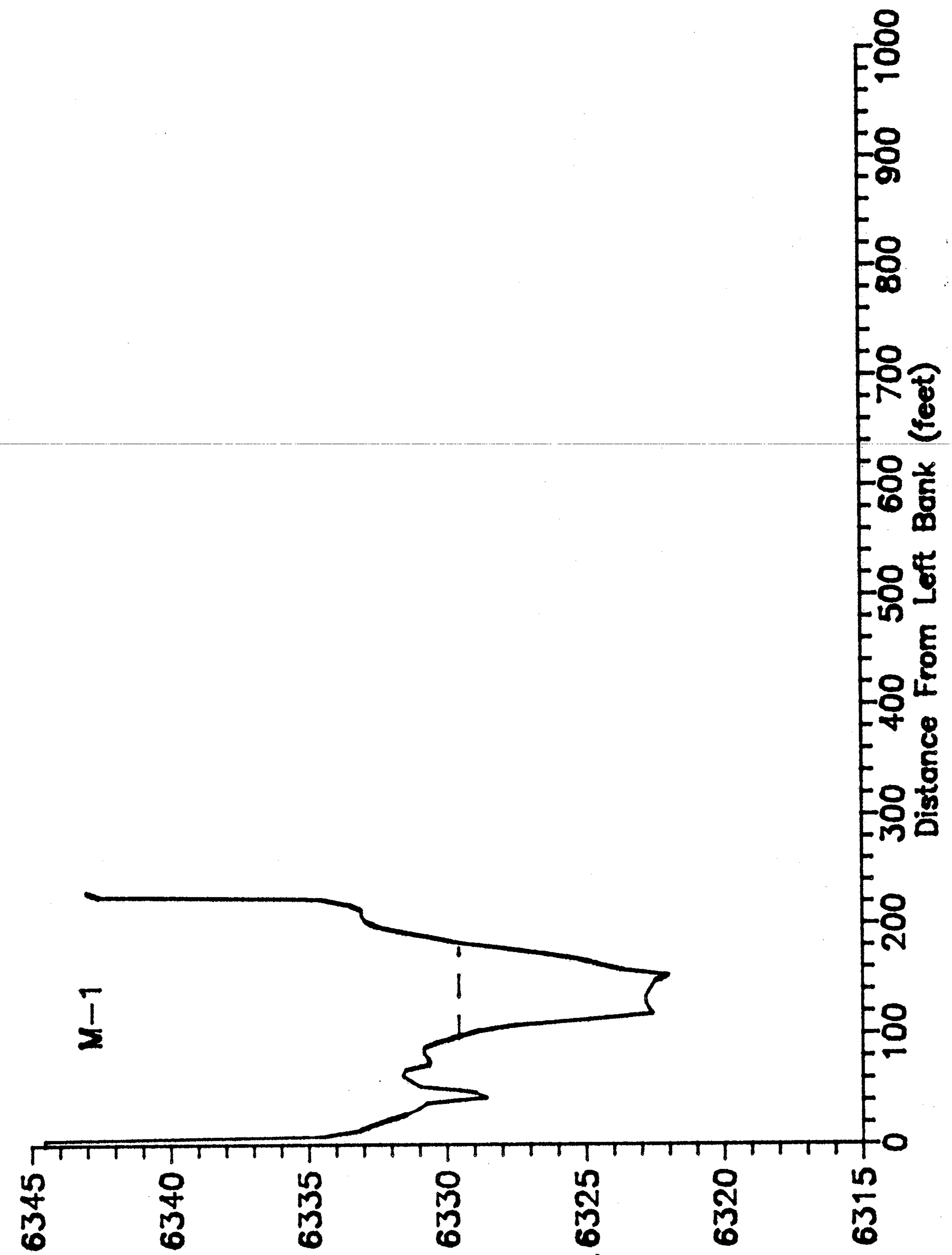
M—1
6345
6340
6335
6330
6325
6320
6315
Elevation (feet above mean sea level)
0
100
200
300
400
500
600
700
800
900
1000
Distance From Left Bank (feet)

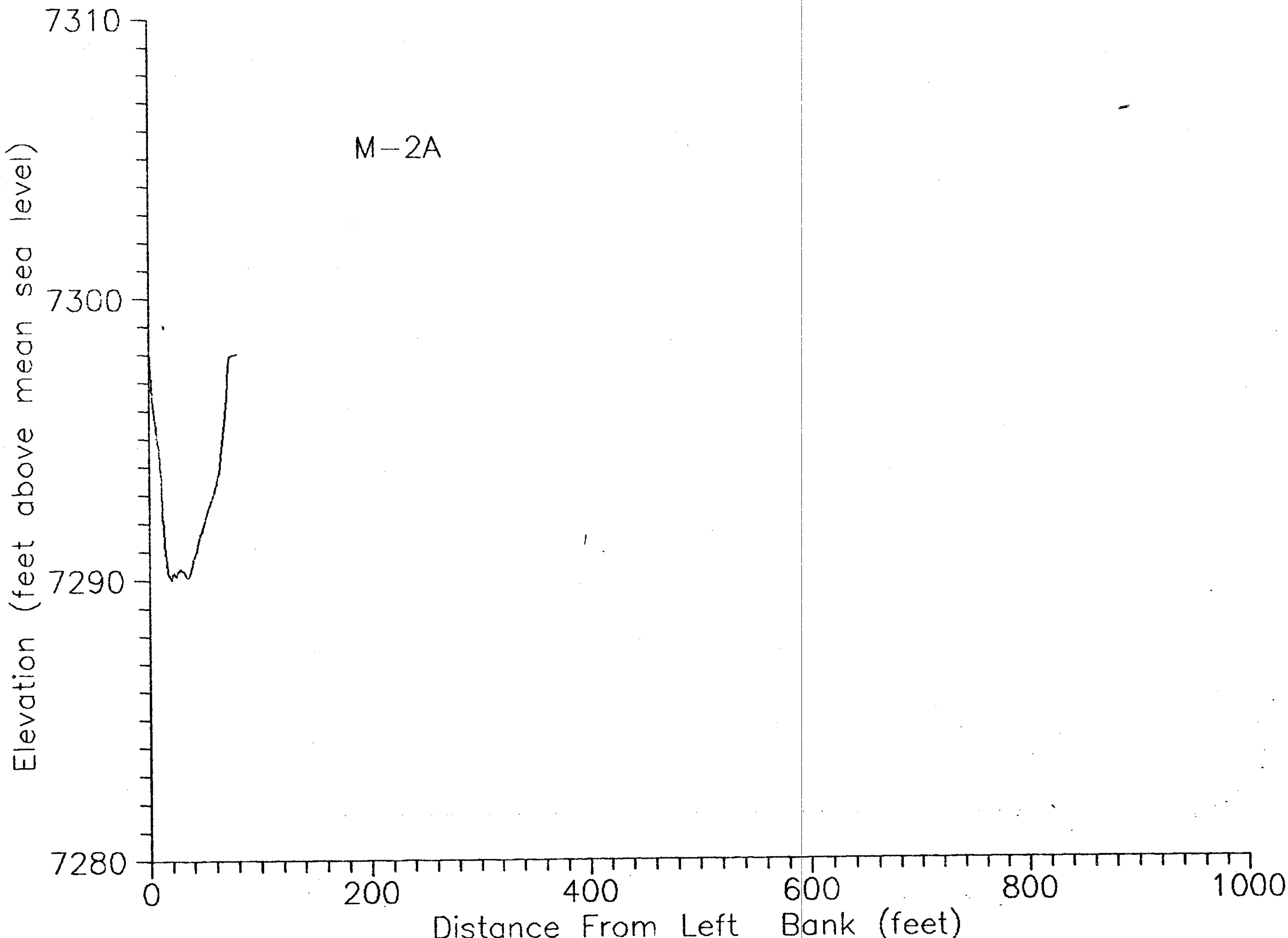
M-2A
Elevation (feet above mean sea level)
7310
7300
7290
7280
0
200
400
600
800
1000
Distance From Left Bank (feet)

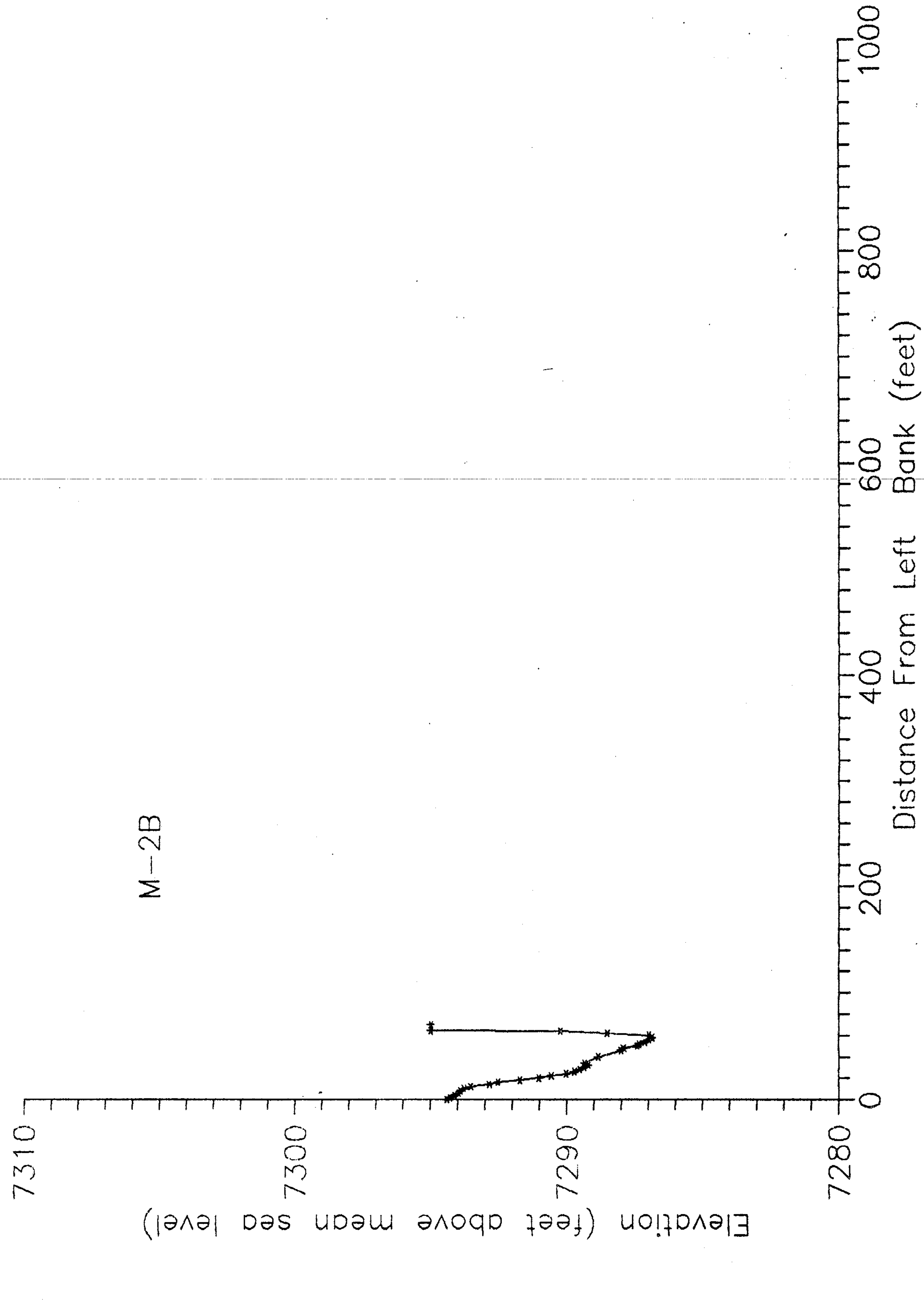
M—2B
Distance From Left Bank (feet)
Elevation (feet above mean sea level)
0
200
400
600
800
1000
7280
7290
7300
7310

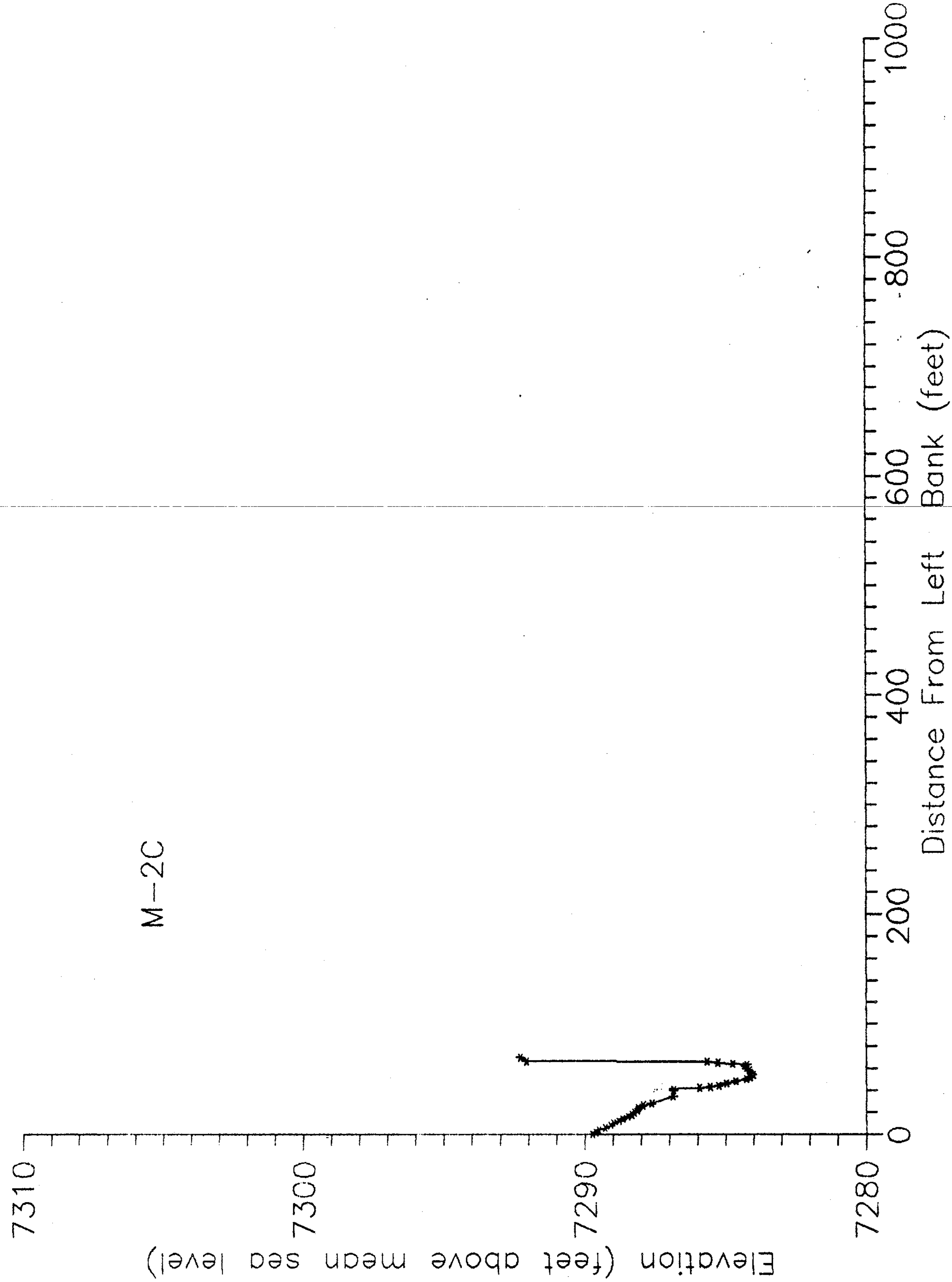
M--2C
Elevation (feet above mean sea level)
7310
7300
7290
7280
Distance From Left Bank (feet)
0
200
400
600
800
1000

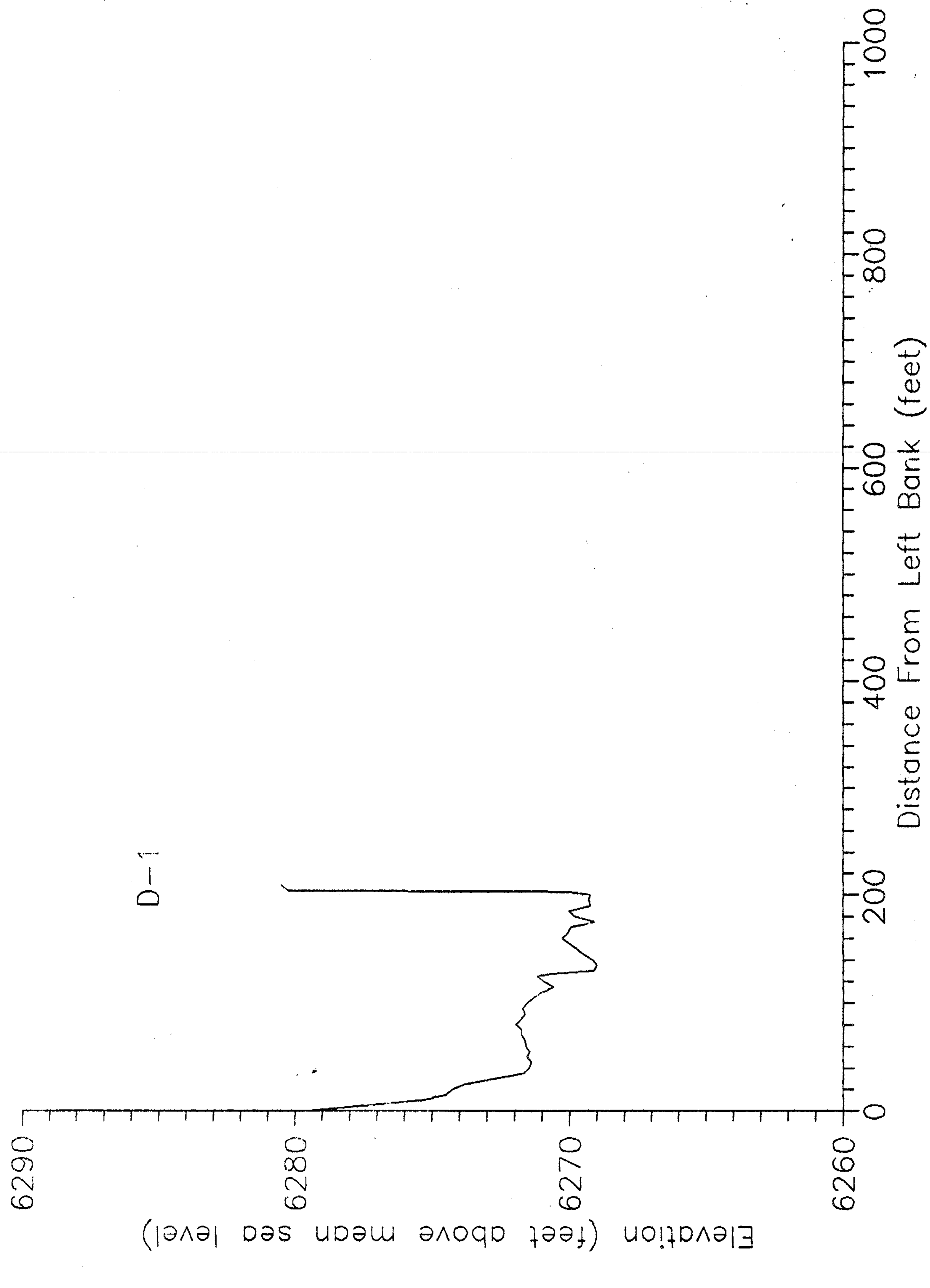
D—1
Distance From Left Bank (feet)
Elevation (feet above mean sea level)
0
200
400
600
800
1000
6260
6270
6280
6290

APPENDIX D: Particle Size Distribution Plots

EXPLANATION

Sample Numbers: Station Number + Identifier

where Identifier = RC: Random Channel
Th: Low-Flow Channel
B: Overbank
EB: East Overbank
WB: West Overbank
NB: North Overbank
SB: South Overbank

θi = Mean Particle Diameter = [(d16+d50+d84)/3]

Cu = Uniformity Coefficient = (d60/d10)

Cc = Coefficient of Curvature = $[(d30)^2/d10 \times d60]$

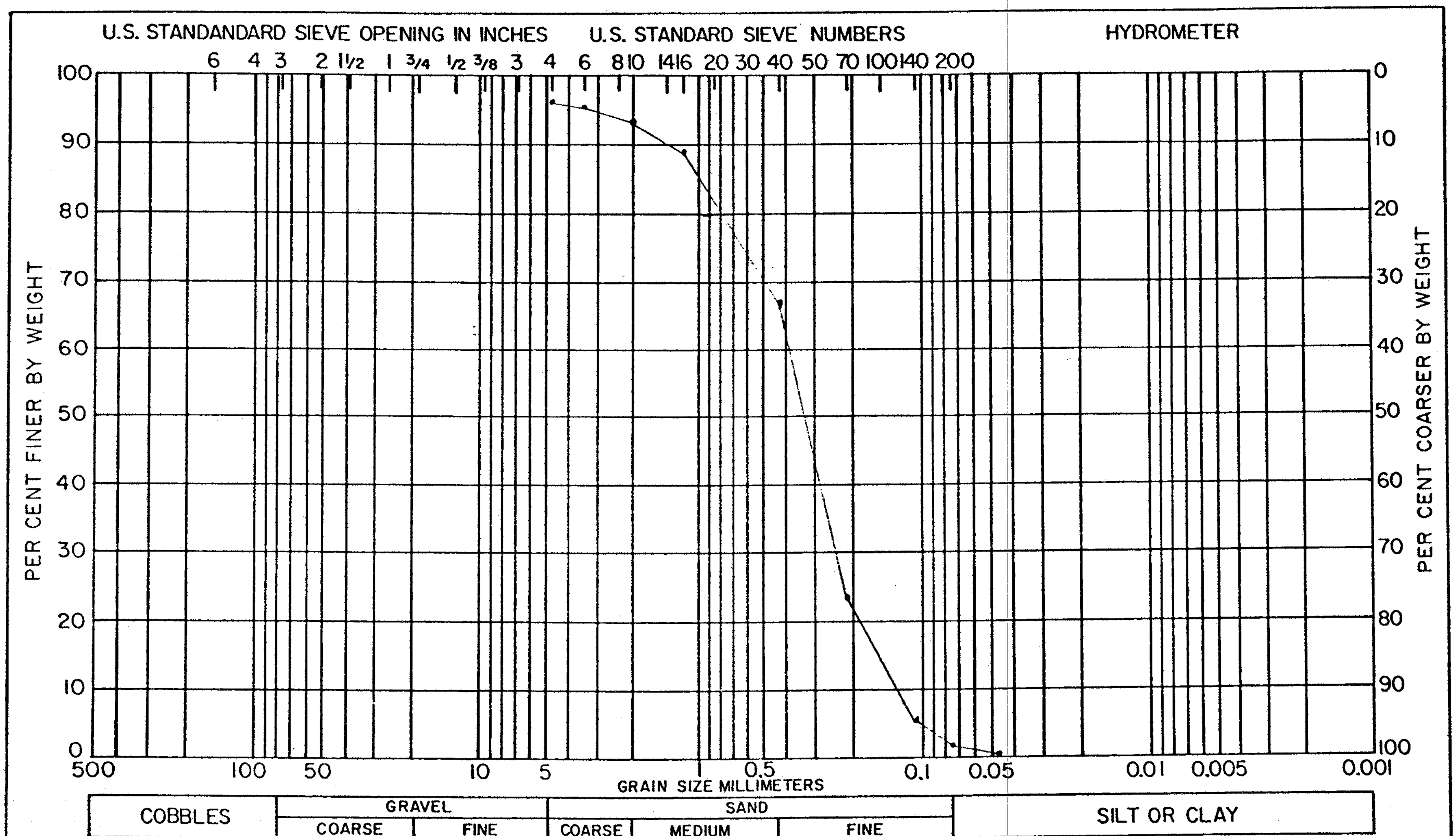

SAMPLE NO.	DEPTH	CLASSIFICATION (USDA TEXTURE TRIANGLE)	θ_i	d_{10}	d_{50}	d_{60}	C_u	C_c
S1-RC			0.49	0.14	0.34	0.39	2.79	1.14

d30	d16	d84
0.25	0.17	0.95

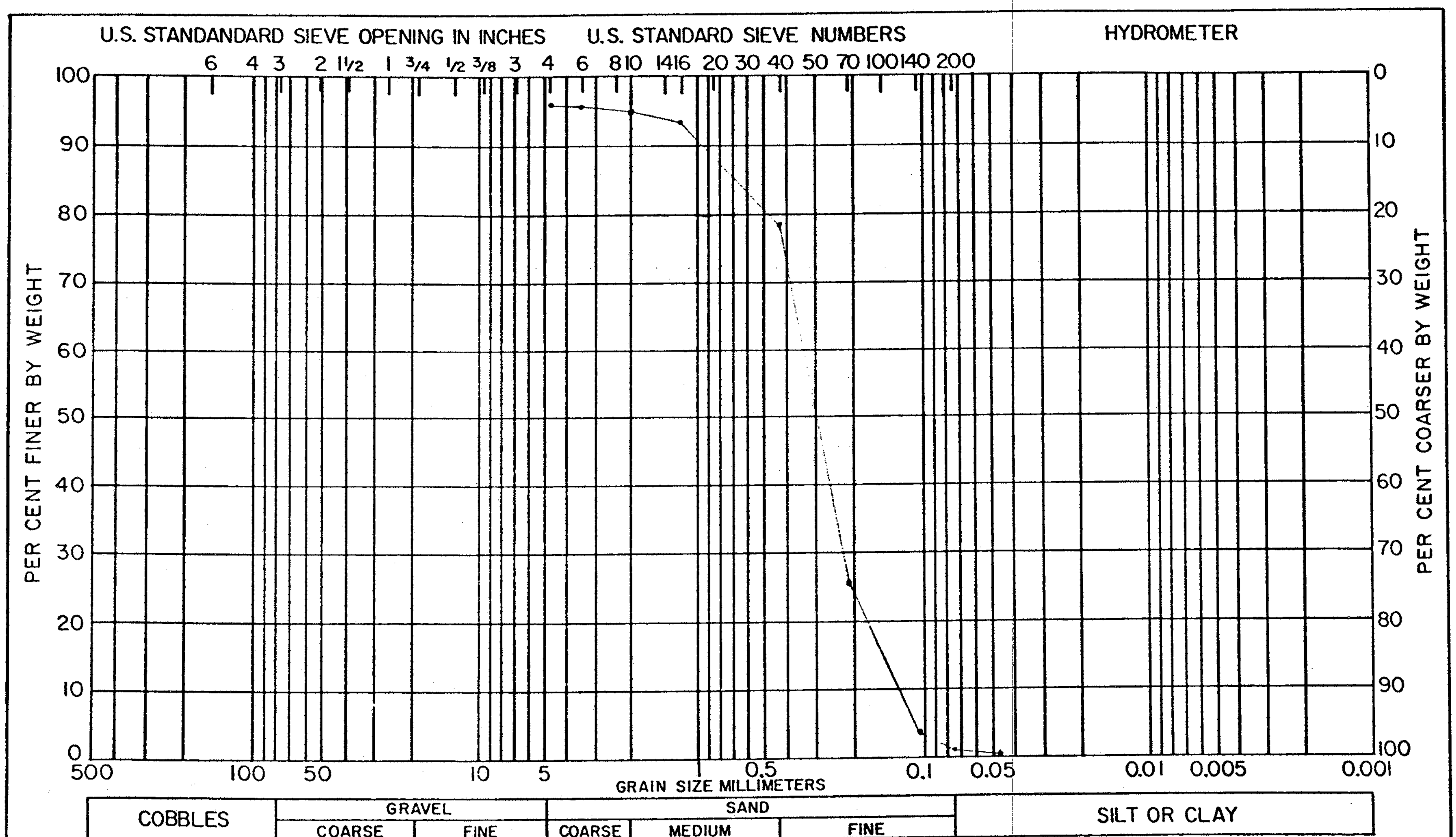

SAMPLE NO.	DEPTH	CLASSIFICATION (USDA TEXTURE TRIANGLE)	θ_i	d_{10}	d_{50}	d_{60}	C_u	C_c
S1-Th			0.38	0.14	0.30	0.34	2.43	1.11

d30	d16	d84
0.23	0.17	0.68

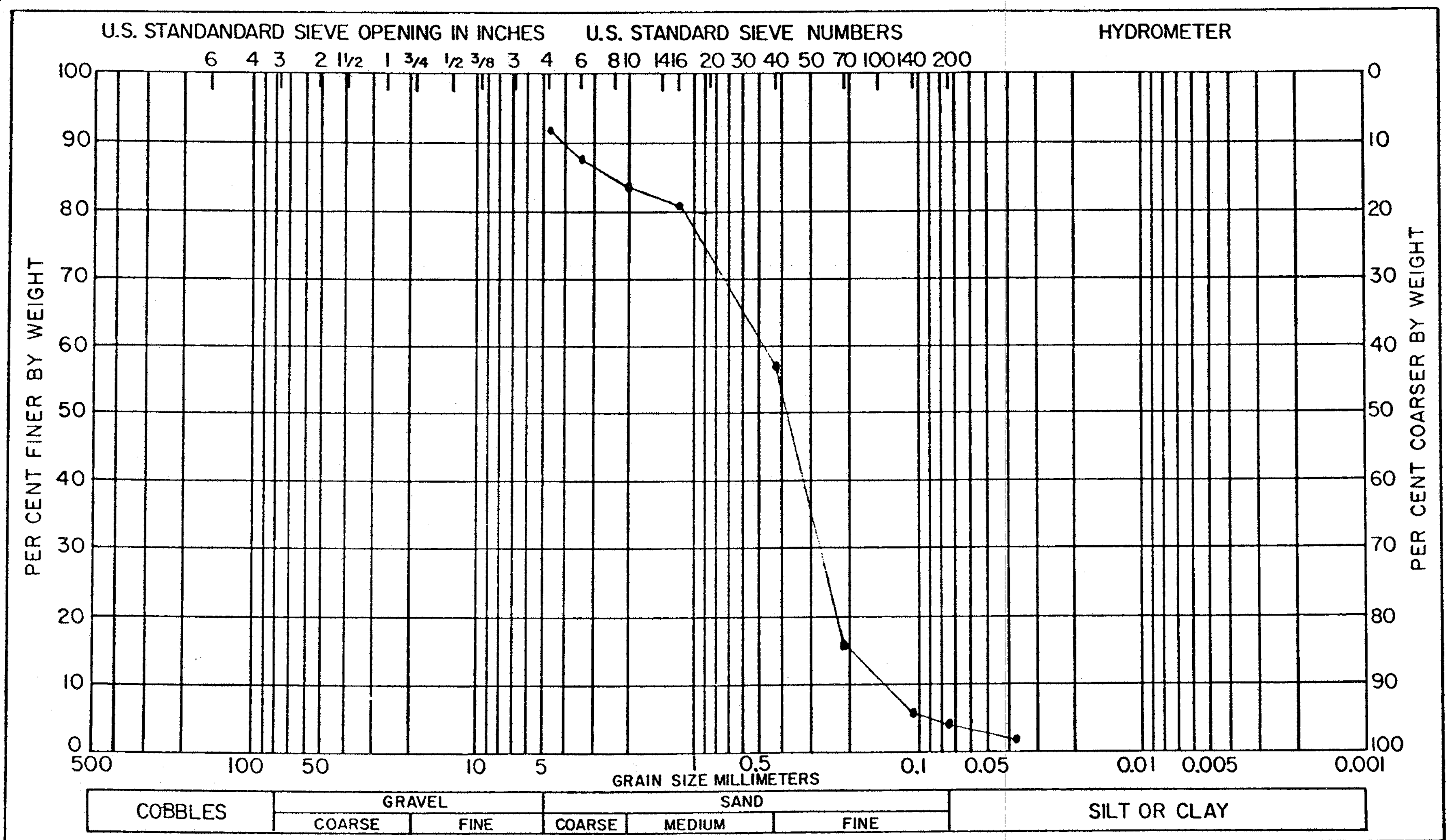

SAMPLE NO.	DEPTH	CLASSIFICATION (USDA TEXTURE TRIANGLE)	θ_i	d_{10}	d_{50}	d_{60}	C_u	C_c
S3-RC			0.87	0.15	0.38	0.48	3.20	1.01

d30	d16	d84
0.27	0.22	2.00

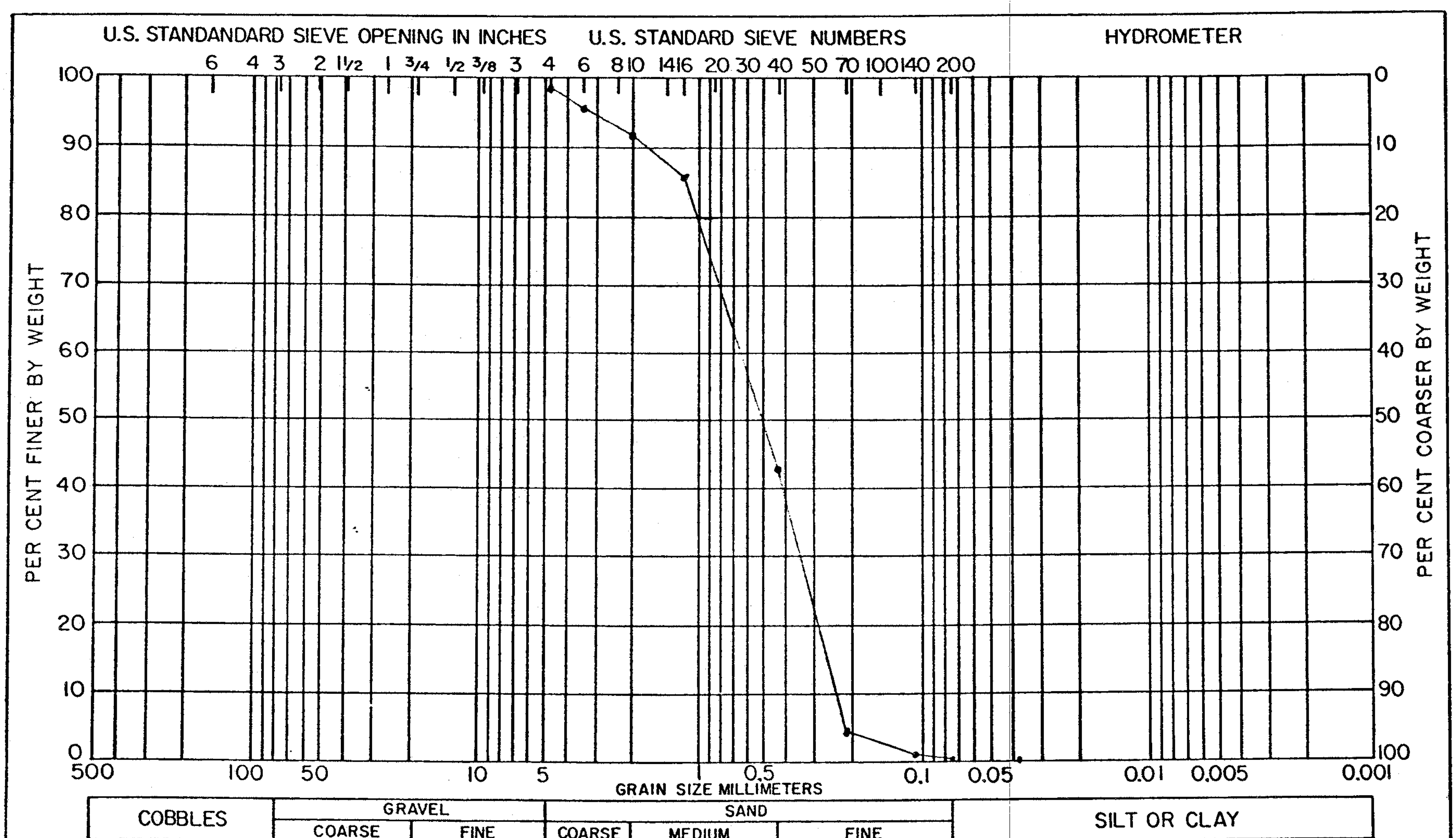

SAMPLE NO.	DEPTH	CLASSIFICATION (USDA TEXTURE TRIANGLE)	θ_i	d_{10}	d_{50}	d_{60}	C_u	C_c
S3-Th			0.66	0.24	0.50	0.65	2.71	0.78

d30 0.35 d16 0.27 d84 1.20

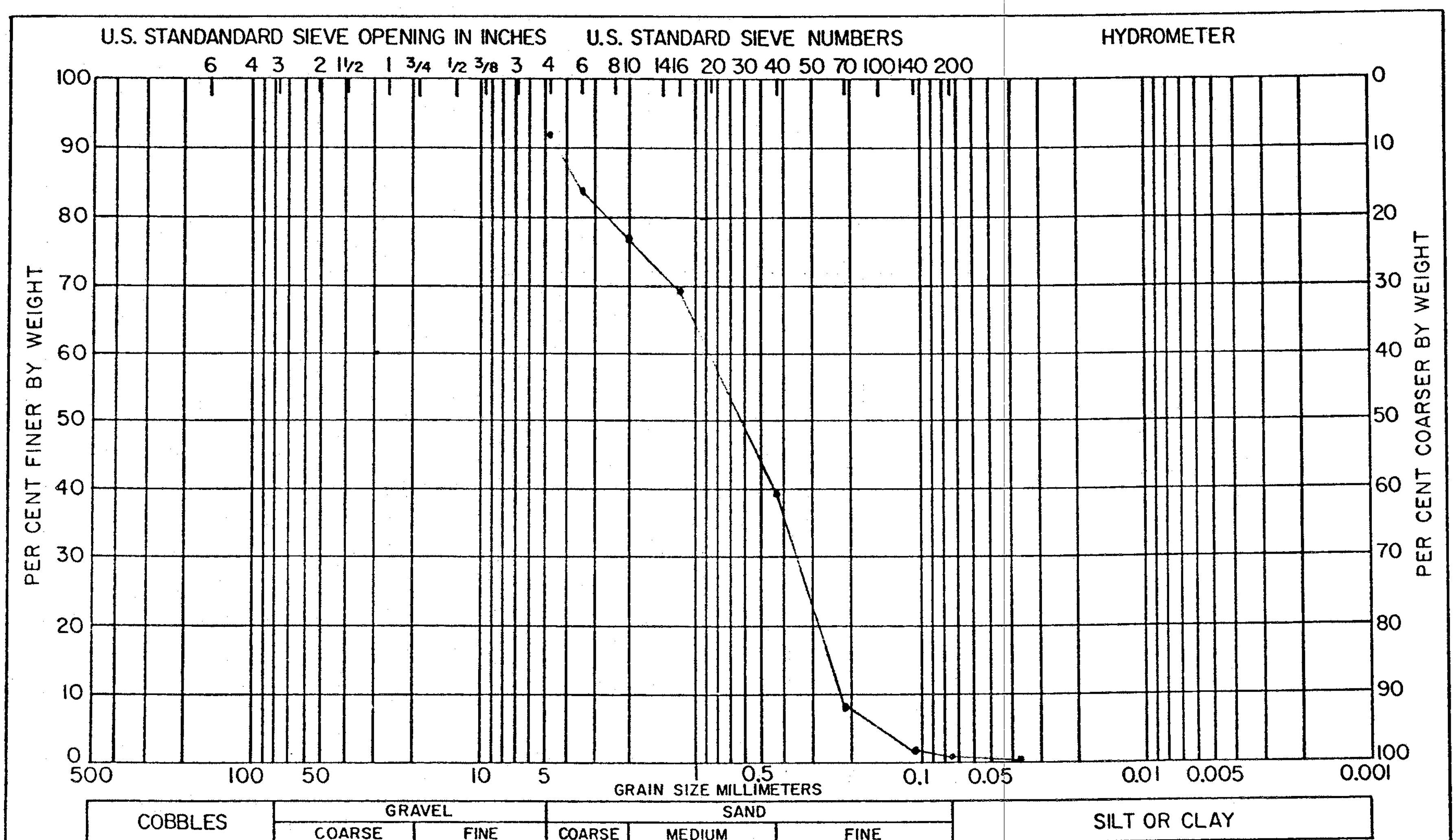

SAMPLE NO.	DEPTH	CLASSIFICATION (USDA TEXTURE TRIANGLE)	θ_i	d_{10}	d_{50}	d_{60}	C_u	C_c
S4-RC			1.46	0.23	0.63	0.88	3.83	0.61
			d30 0.35	d16 0.26	d84 3.50			

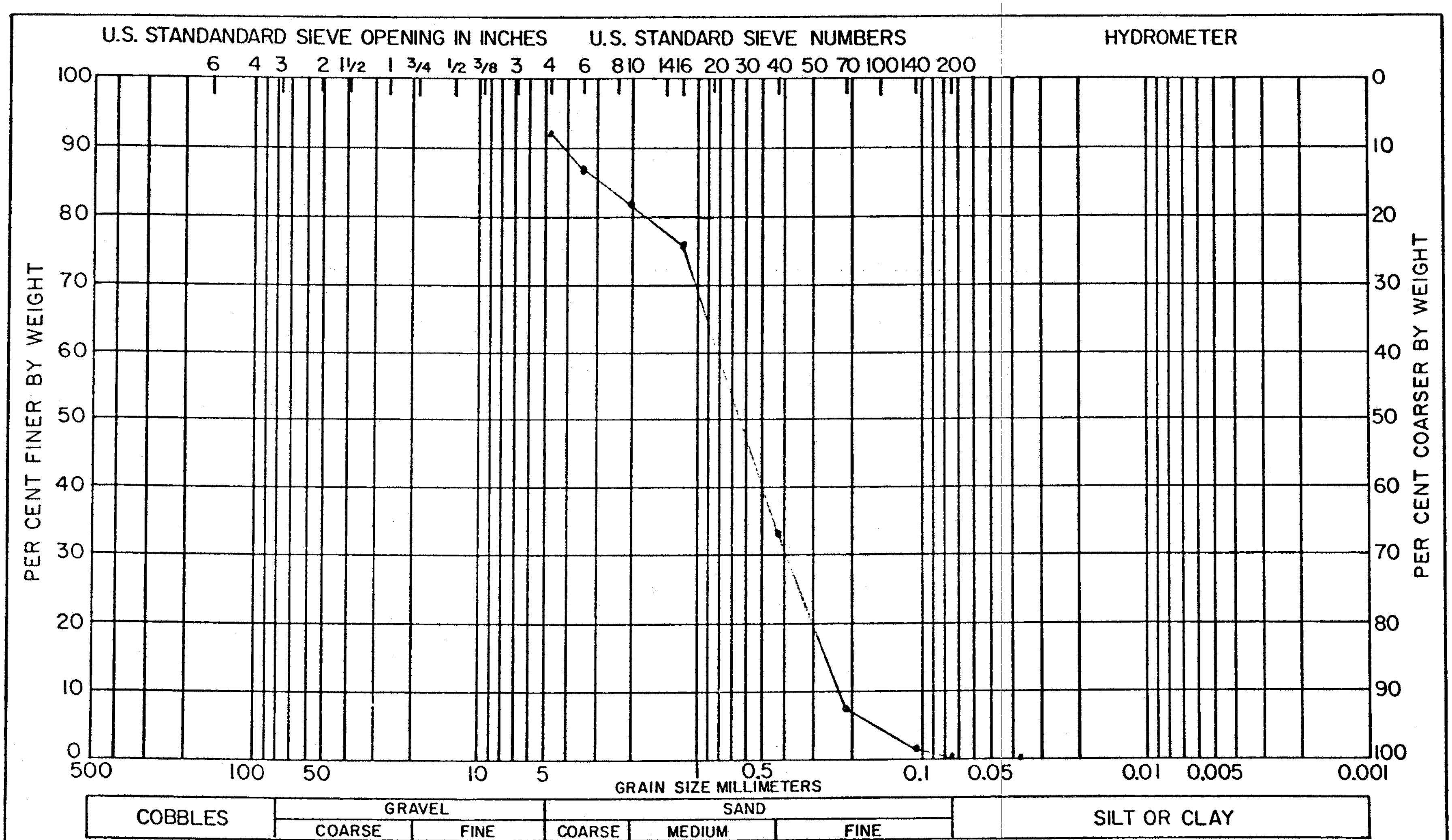

SAMPLE NO.	DEPTH	CLASSIFICATION (USDA TEXTURE TRIANGLE)	θ_i	d_{10}	d_{50}	d_{60}	C_u	C_c
S4-Th			1.17	0.23	0.65	0.80	3.48	0.87

d30 0.40 | d16 0.27 | d84 2.60

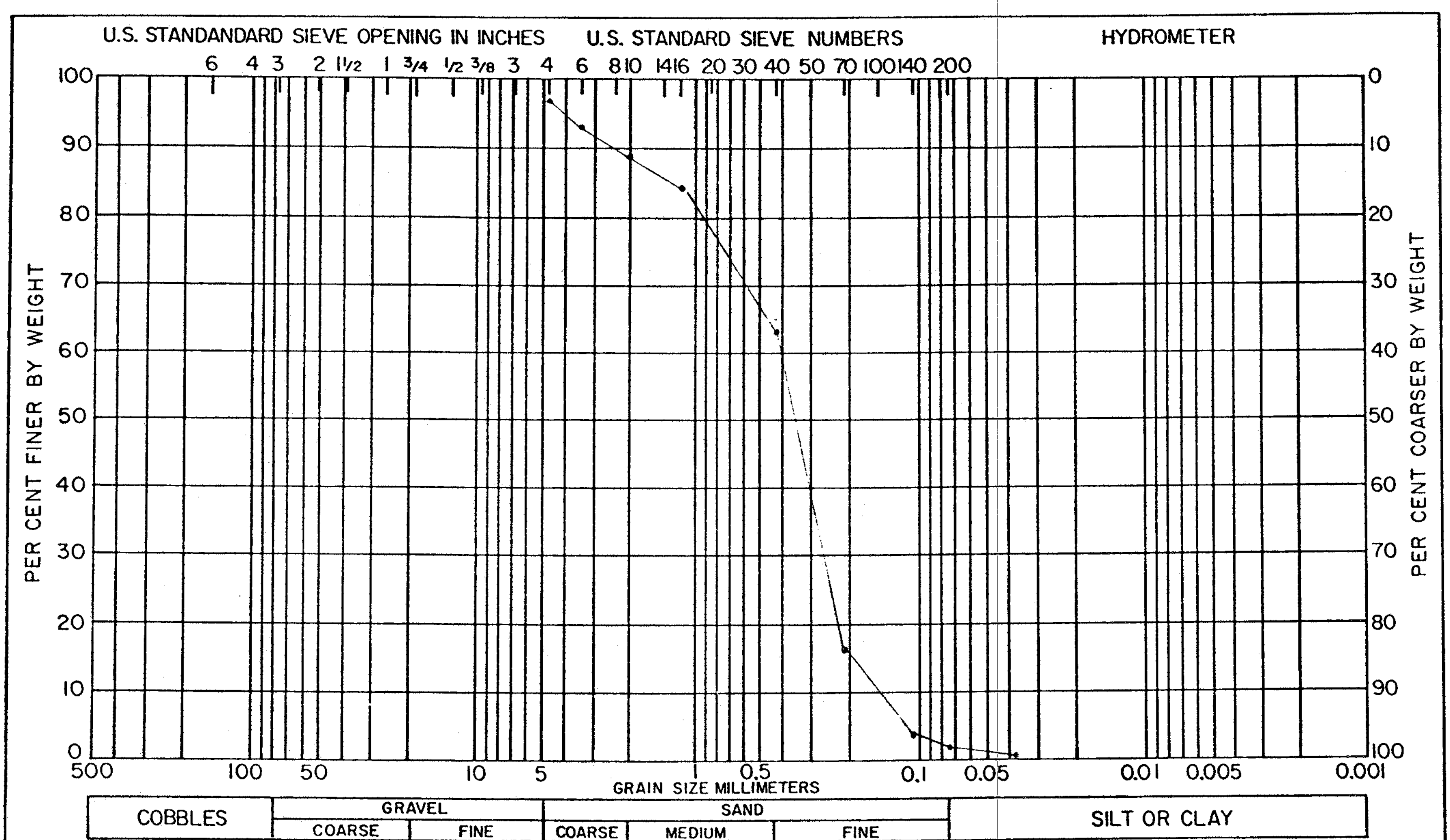

SAMPLE NO.	DEPTH	CLASSIFICATION (USDA TEXTURE TRIANGLE)	θ_i	d_{10}	d_{50}	d_{60}	C_u	C_c
S5-RC			0.58	0.15	0.35	0.40	2.67	1.13

d30	d16	d84
0.26	0.20	1.20

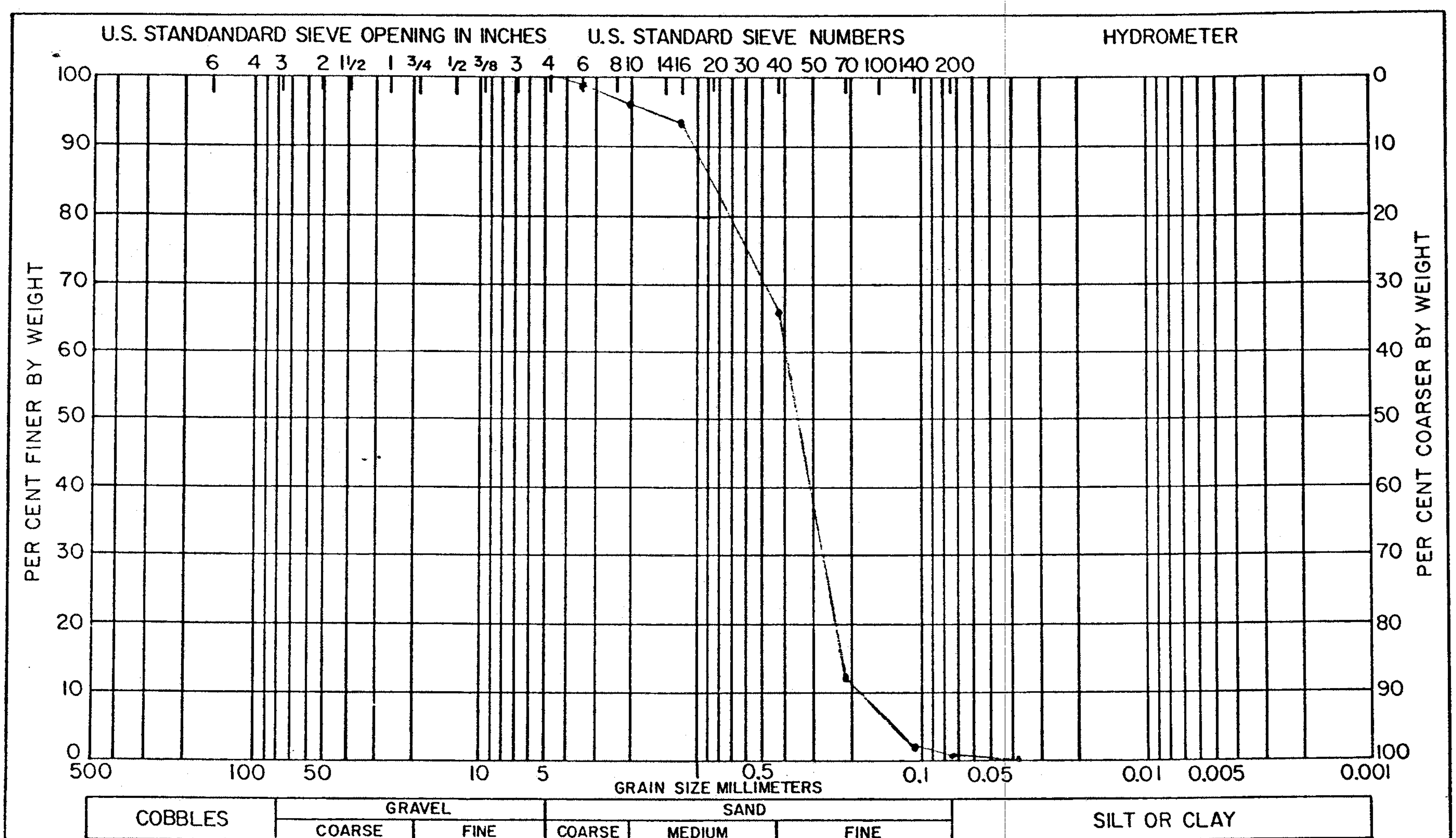

SAMPLE NO.	DEPTH	CLASSIFICATION (USDA TEXTURE TRIANGLE)	θ_i	d_{10}	d_{50}	d_{60}	C_u	C_c
S5–Th			0.47	0.19	0.35	0.40	2.11	0.96

d30 0.27 d16 0.23 d84 0.84

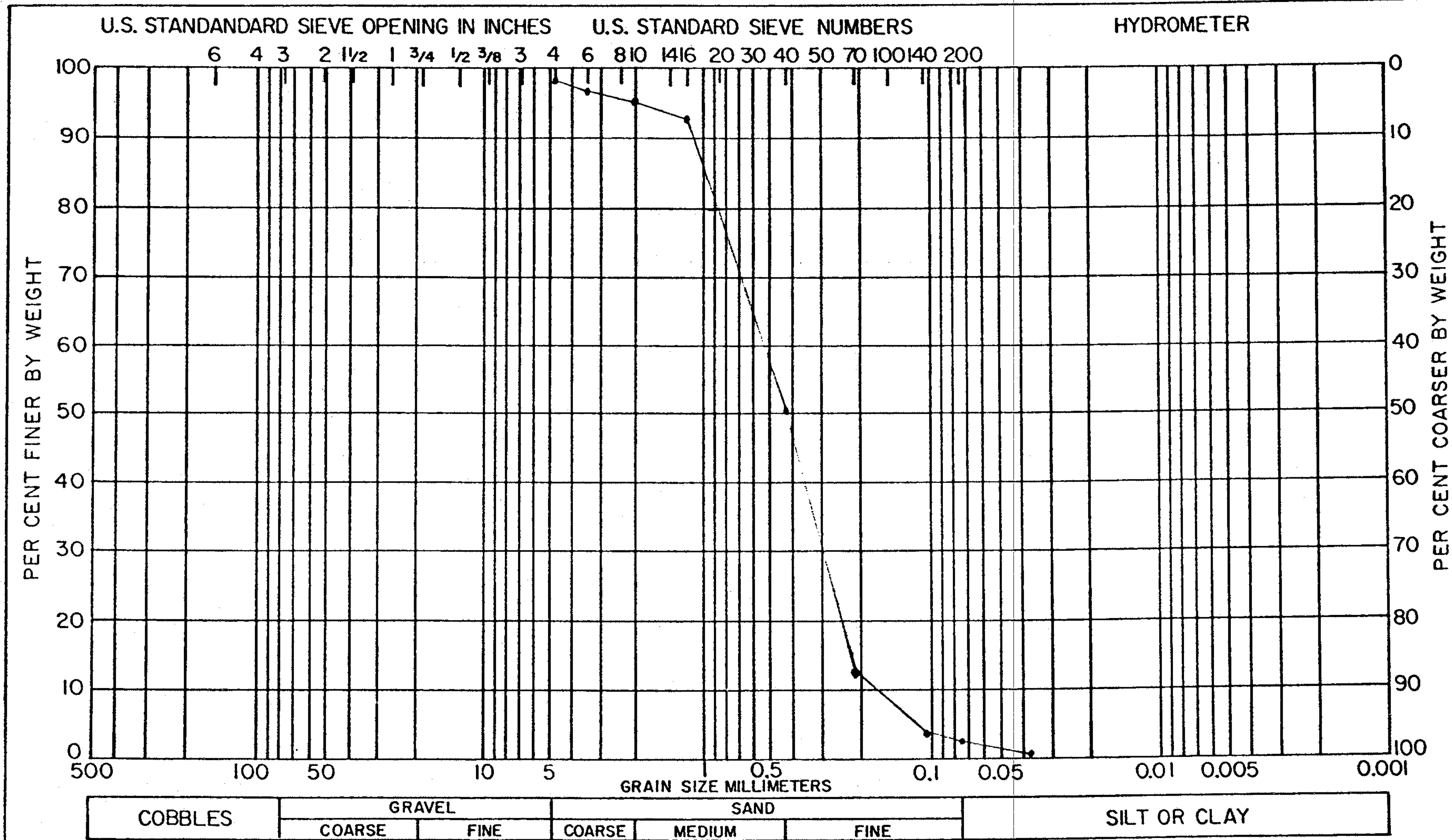

SAMPLE NO.	DEPTH	CLASSIFICATION (USDA TEXTURE TRIANGLE)	θ_i	d_{10}	d_{50}	d_{60}	C_u	C_c
S5-B			0.54	0.17	0.42	0.53	3.12	1.00

d30	d16	d84
0.30	0.23	0.98

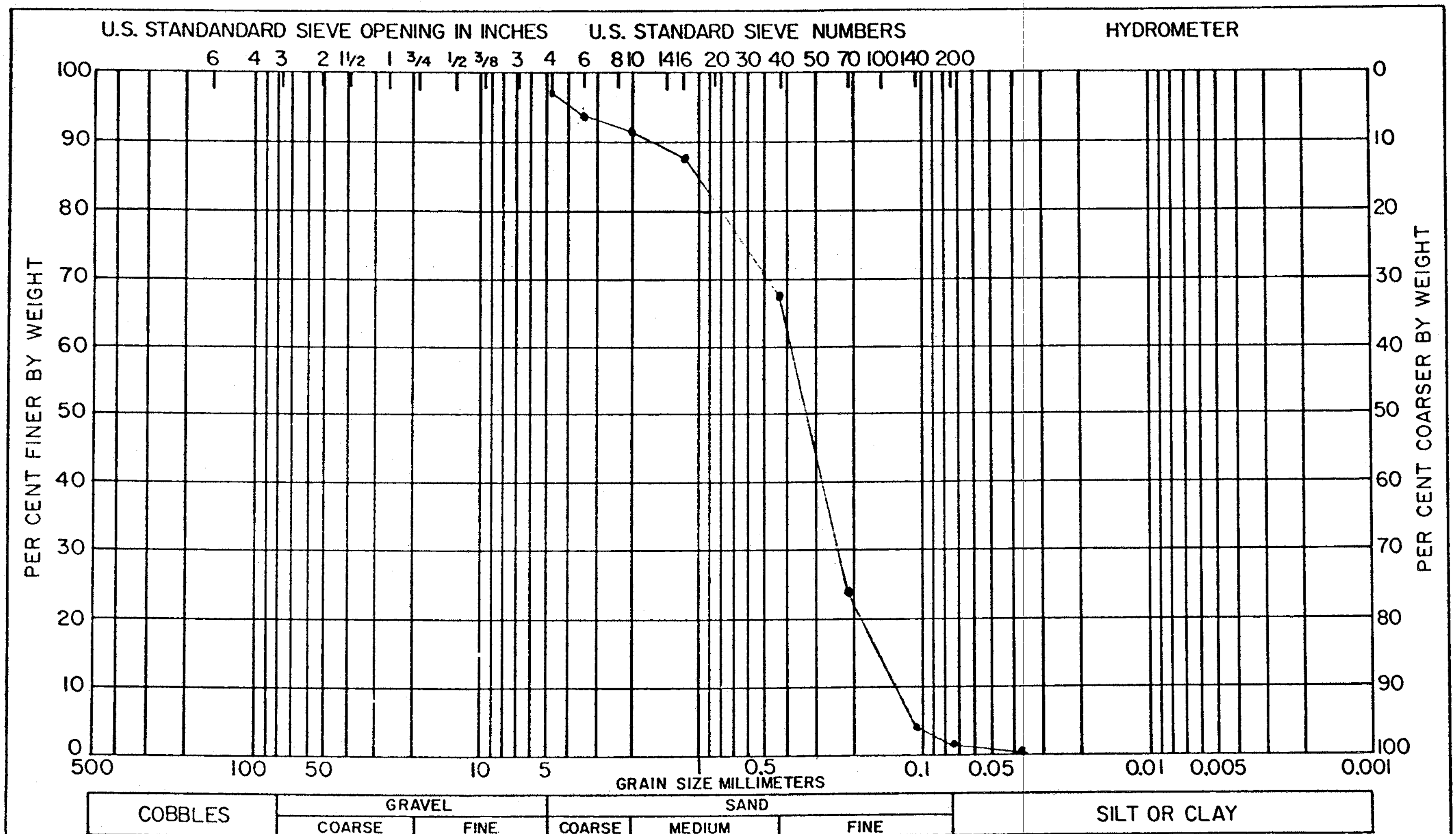

SAMPLE NO.	DEPTH	CLASSIFICATION (USDA TEXTURE TRIANGLE)	θ_i	d_{10}	d_{50}	d_{60}	C_u	C_c
S6-RC			0.49	0.14	0.33	0.39	2.79	1.05
			d30	d16	d84			
			0.24	0.17	0.98			

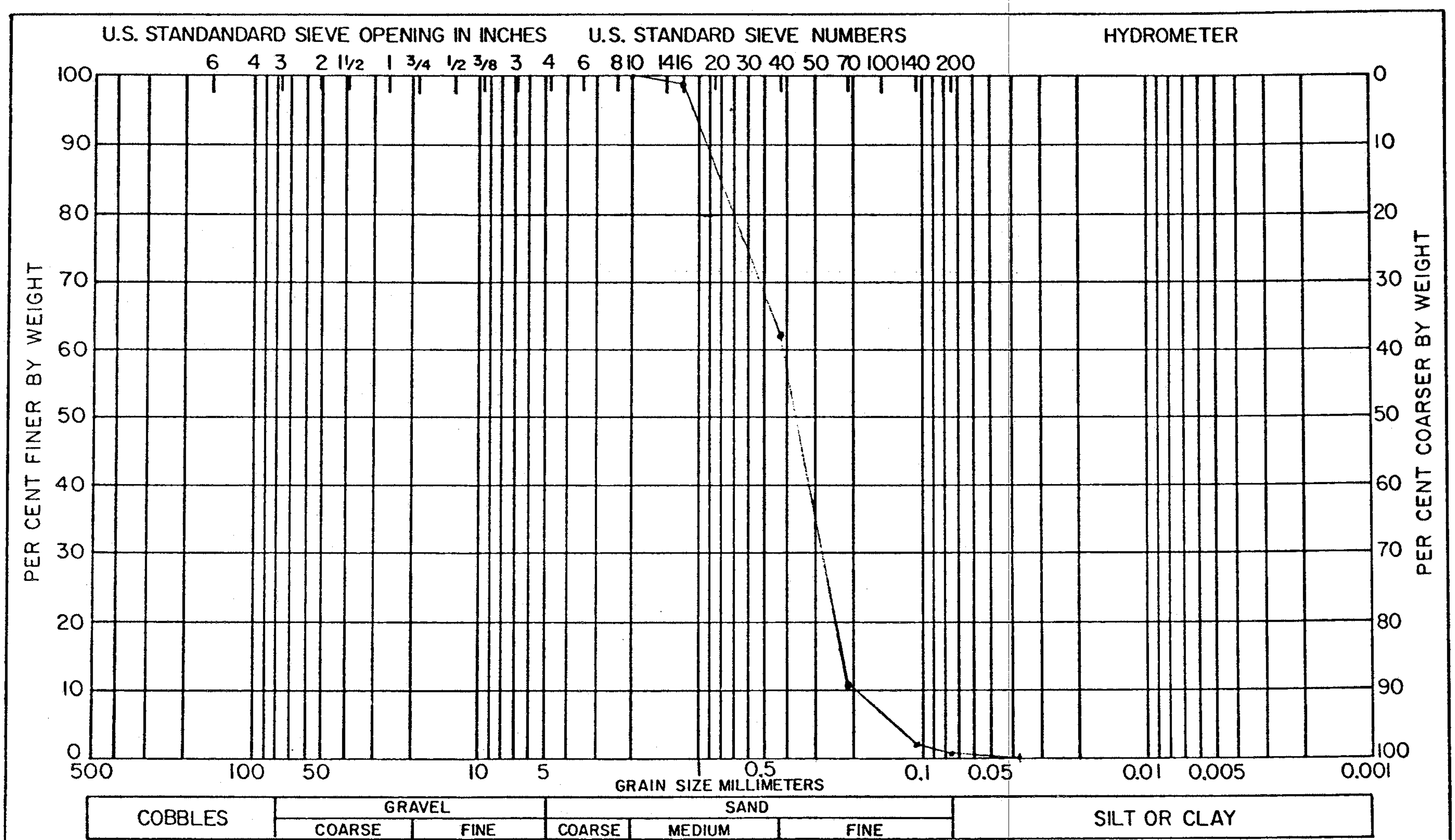

SAMPLE NO.	DEPTH	CLASSIFICATION (USDA TEXTURE TRIANGLE)	θ_i	d_{10}	d_{50}	d_{60}	C_u	C_c
S6-Th			0.47	0.20	0.37	0.42	2.10	0.93

d_{30}	d_{16}	d_{84}
0.28	0.23	0.80

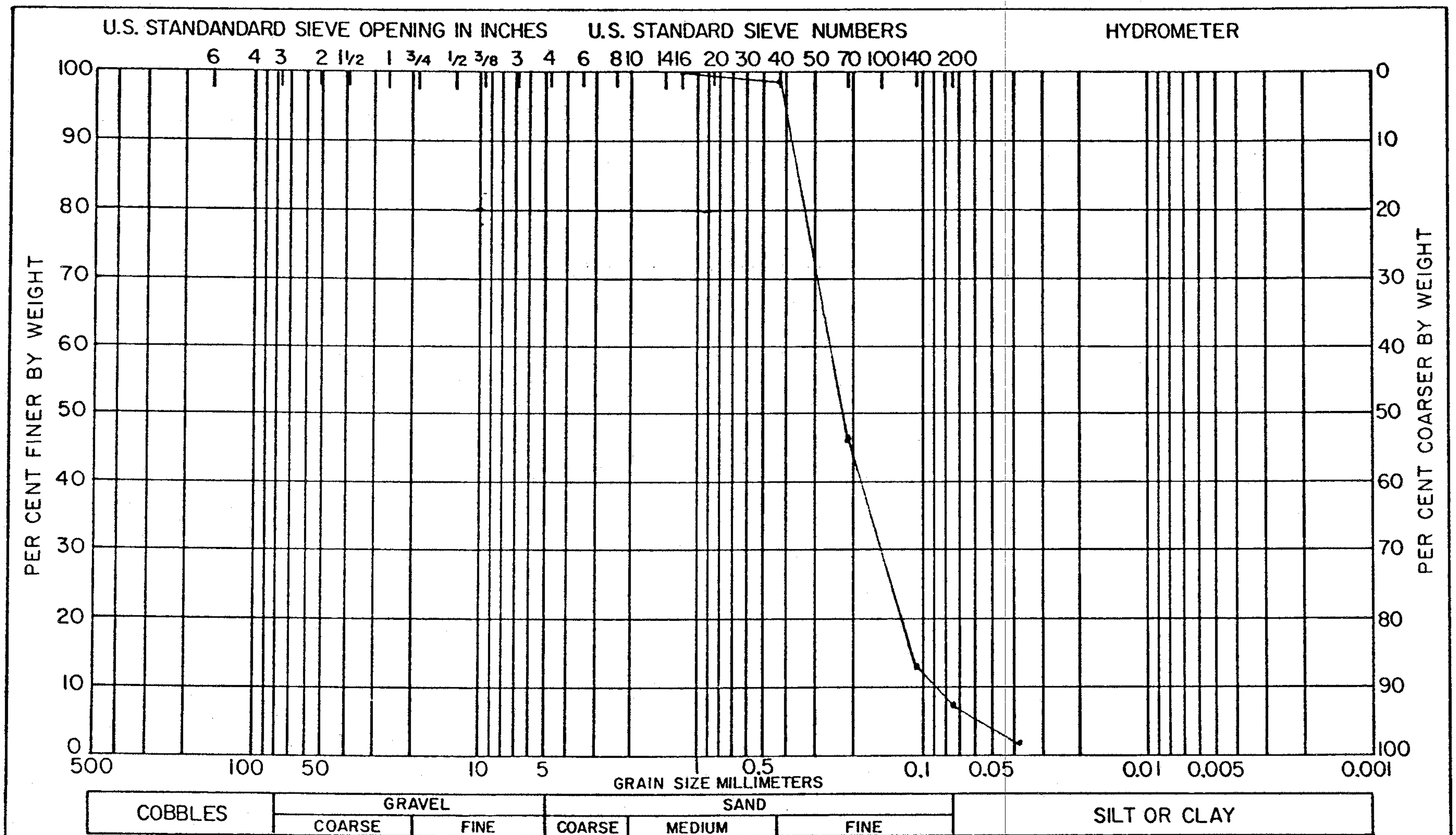

SAMPLE NO.	DEPTH	CLASSIFICATION (USDA TEXTURE TRIANGLE)	θ_i	d_{10}	d_{50}	d_{60}	C_u	C_c
S6 WB			0.23	0.089	0.23	0.26	2.92	1.11

d30	d16	d84
0.16	0.12	0.35

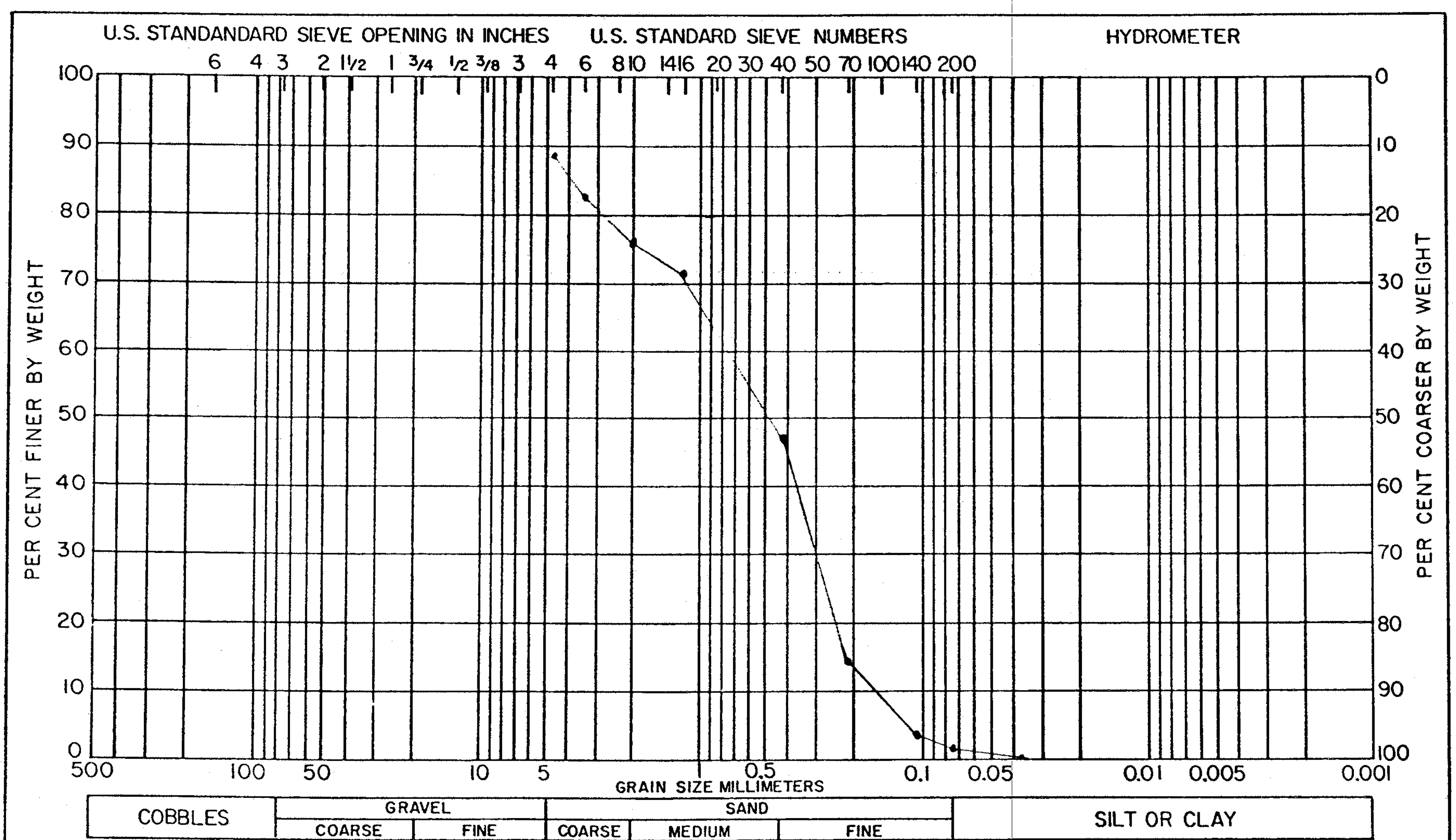

SAMPLE NO.	DEPTH	CLASSIFICATION (USDA TEXTURE TRIANGLE)	θ_i	d_{10}	d_{50}	d_{60}	C_u	C_c
S7-RC			1.50	0.16	0.48	0.75	4.69	0.75

d30	d16	d84
0.30	0.22	3.80

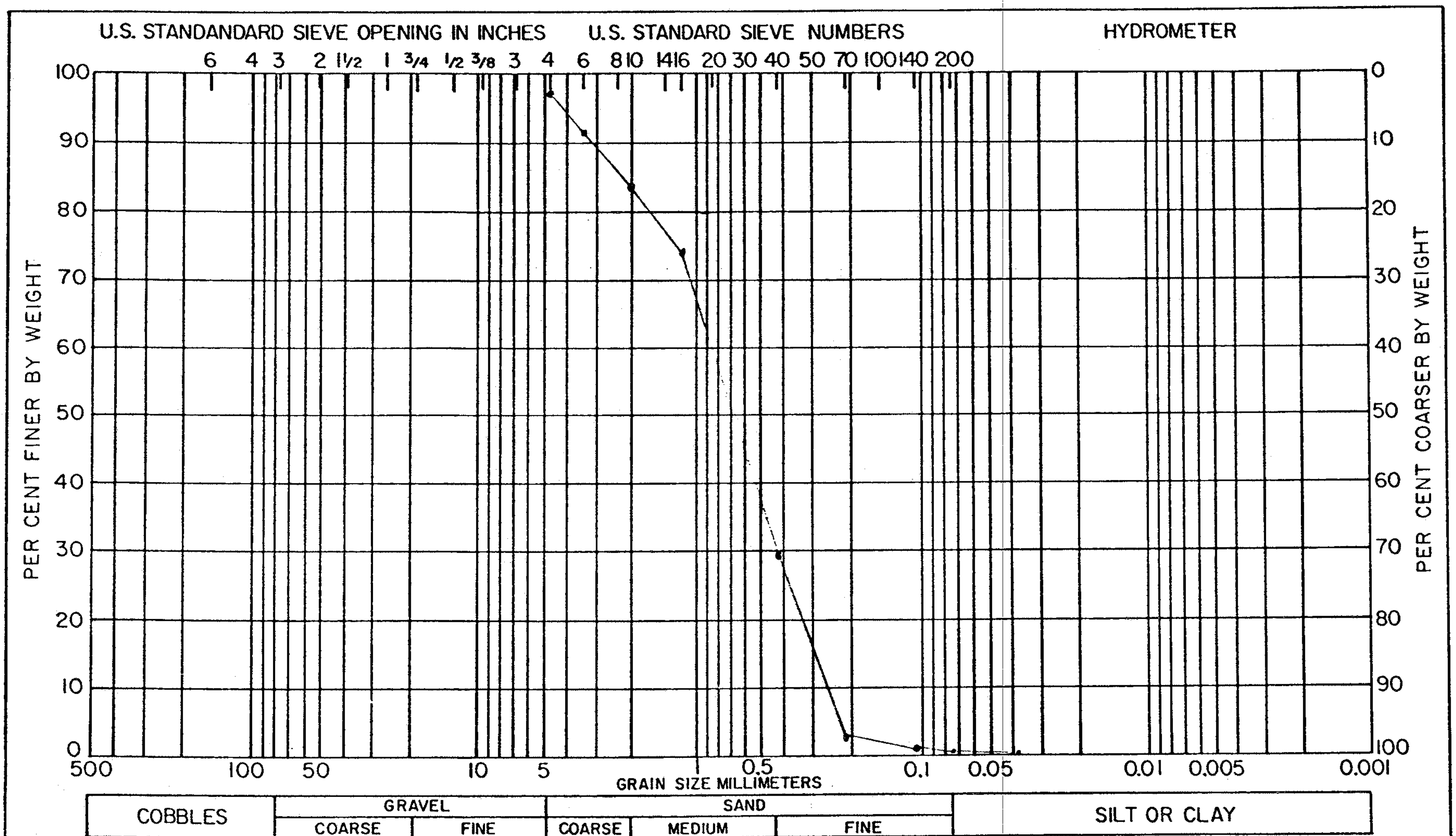

SAMPLE NO.	DEPTH	CLASSIFICATION (USDA TEXTURE TRIANGLE)	θ_i	d_{10}	d_{50}	d_{60}	C_u	C_c
S7-Th			0.99	0.26	0.69	0.86	3.31	0.83
				d30	d16	d84		
				0.43	0.29	2.00		

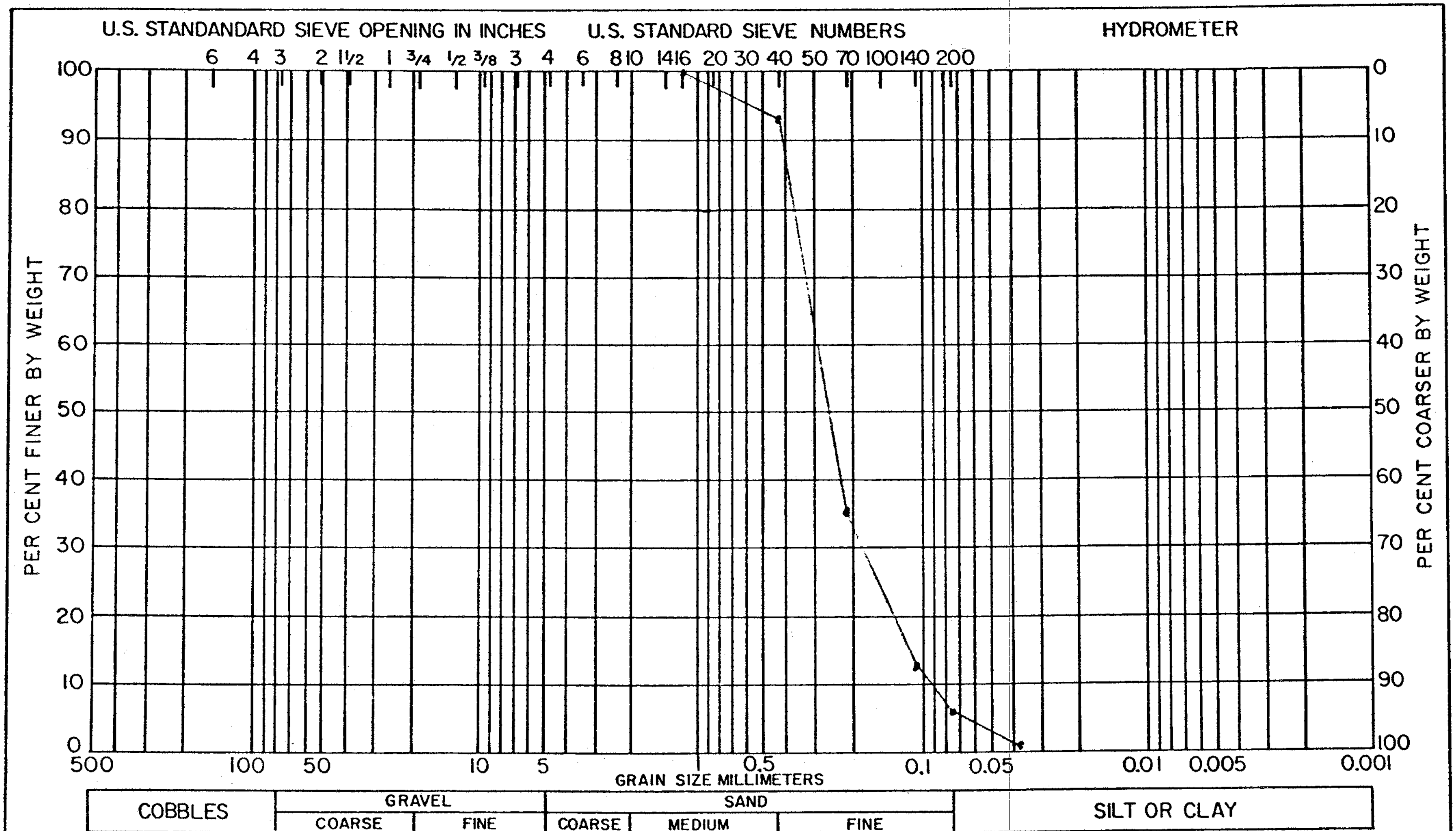

SAMPLE NO.	DEPTH	CLASSIFICATION (USDA TEXTURE TRIANGLE)	θ_i	d_{10}	d_{50}	d_{60}	C_u	C_c
S7-B			0.26	0.093	0.26	0.29	3.12	1.34
				d30 0.19	d16 0.13	d84 0.38		

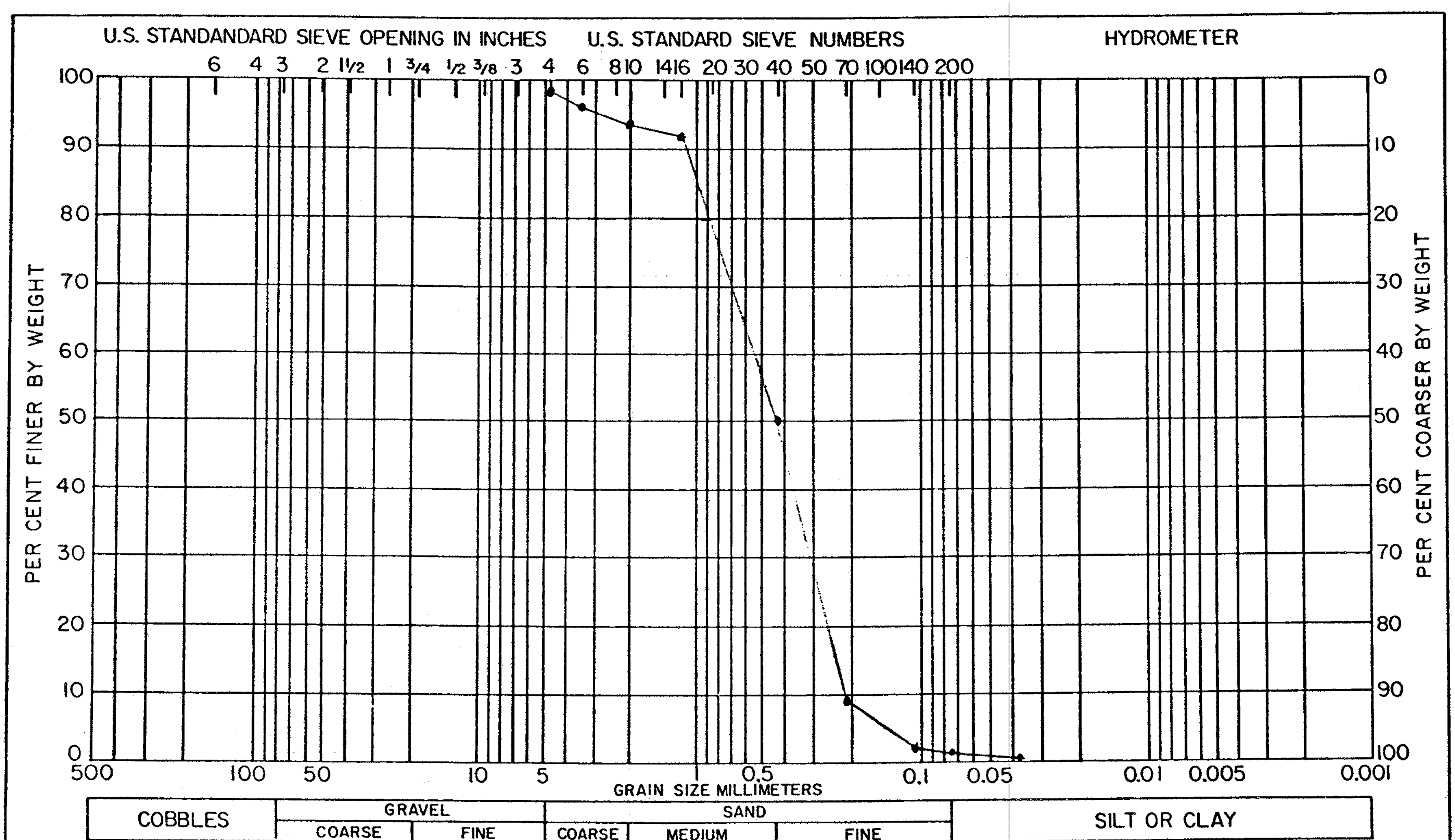

SAMPLE NO.	DEPTH	CLASSIFICATION (USDA TEXTURE TRIANGLE)	θ_i	d_{10}	d_{50}	d_{60}	C_u	C_c
S8-RC			0.54	0.22	0.42	0.55	2.50	0.79
				d30	d16	d84		
				0.31	0.24	0.97		

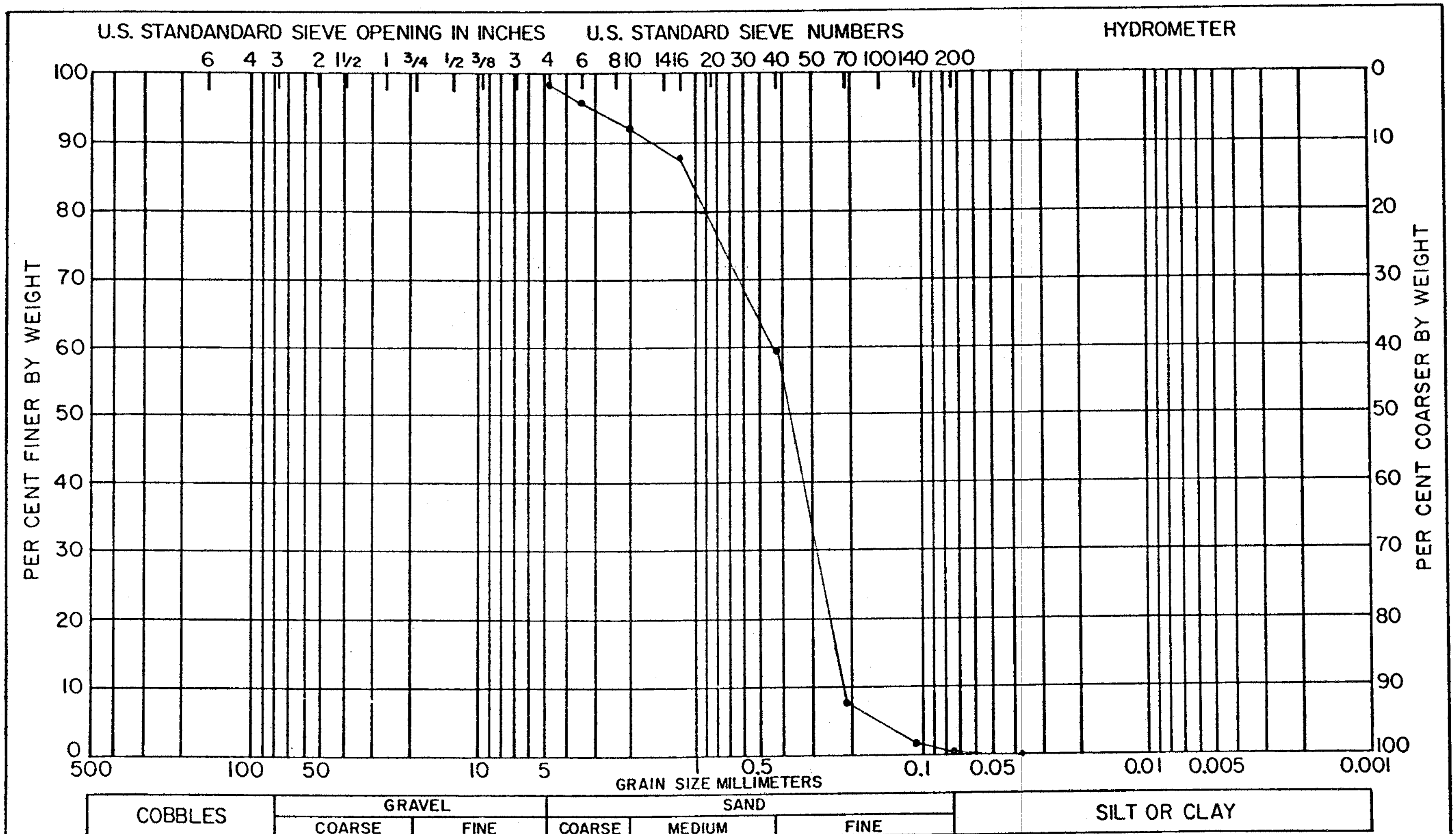

SAMPLE NO.	DEPTH	CLASSIFICATION (USDA TEXTURE TRIANGLE)	θ_i	d_{10}	d_{50}	d_{60}	C_u	C_c
S8-Th			0.57	0.22	0.38	0.45	2.05	0.85

d30	d16	d84
0.29	0.24	1.10

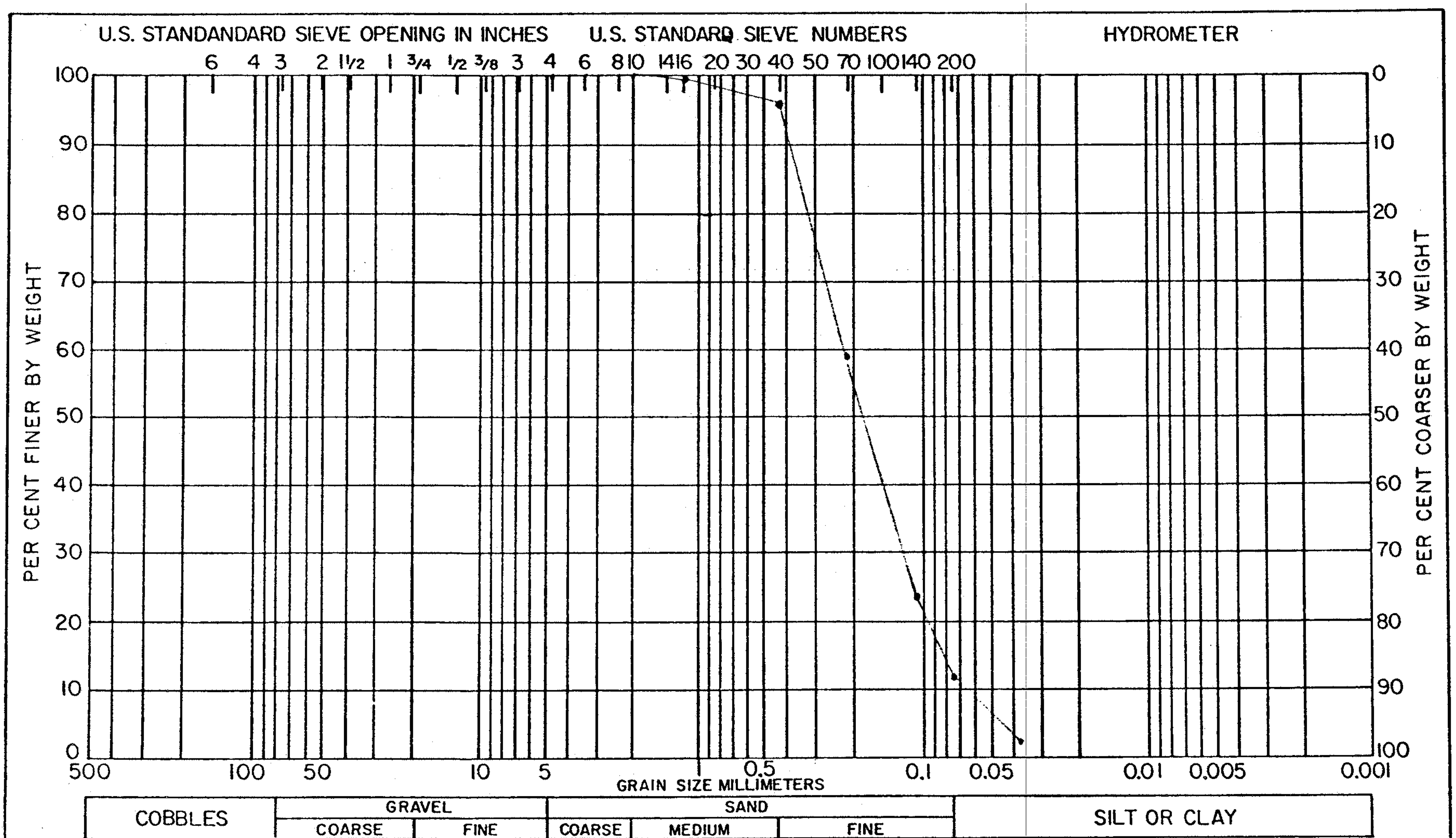

SAMPLE NO.	DEPTH	CLASSIFICATION (USDA TEXTURE TRIANGLE)	θ_i	d_{10}	d_{50}	d_{60}	C_u	C_c
S8–NB			0.21	0.065	0.19	0.23	3.54	1.13
				d30 0.13	d16 0.085	d84 0.35		

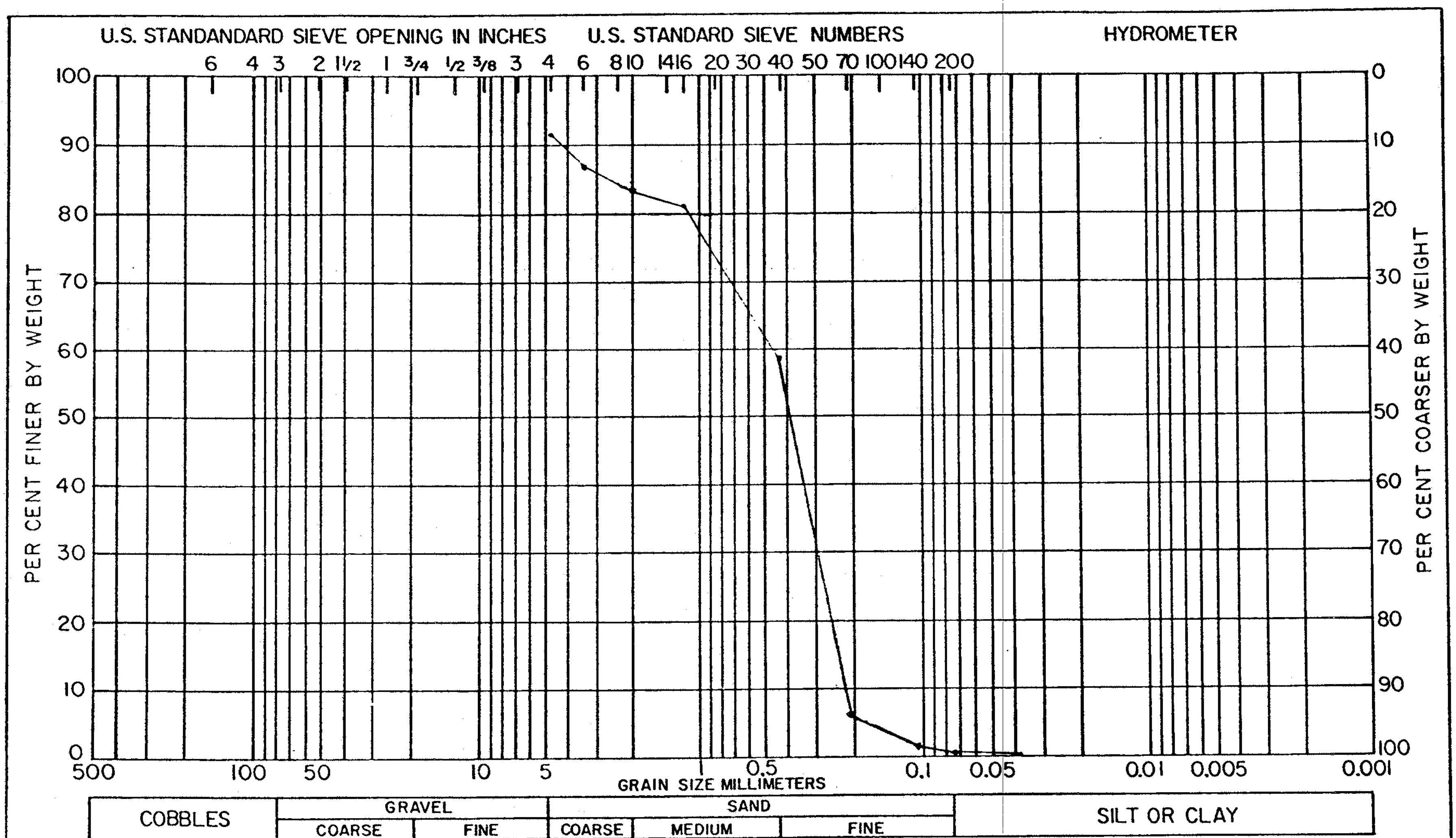

SAMPLE NO.	DEPTH	CLASSIFICATION (USDA TEXTURE TRIANGLE)	θ_i	d_{10}	d_{50}	d_{60}	C_u	C_c
S9-RC			0.93	0.22	0.39	0.46	2.09	0.89

d30	d16	d84
0.30	0.25	2.15

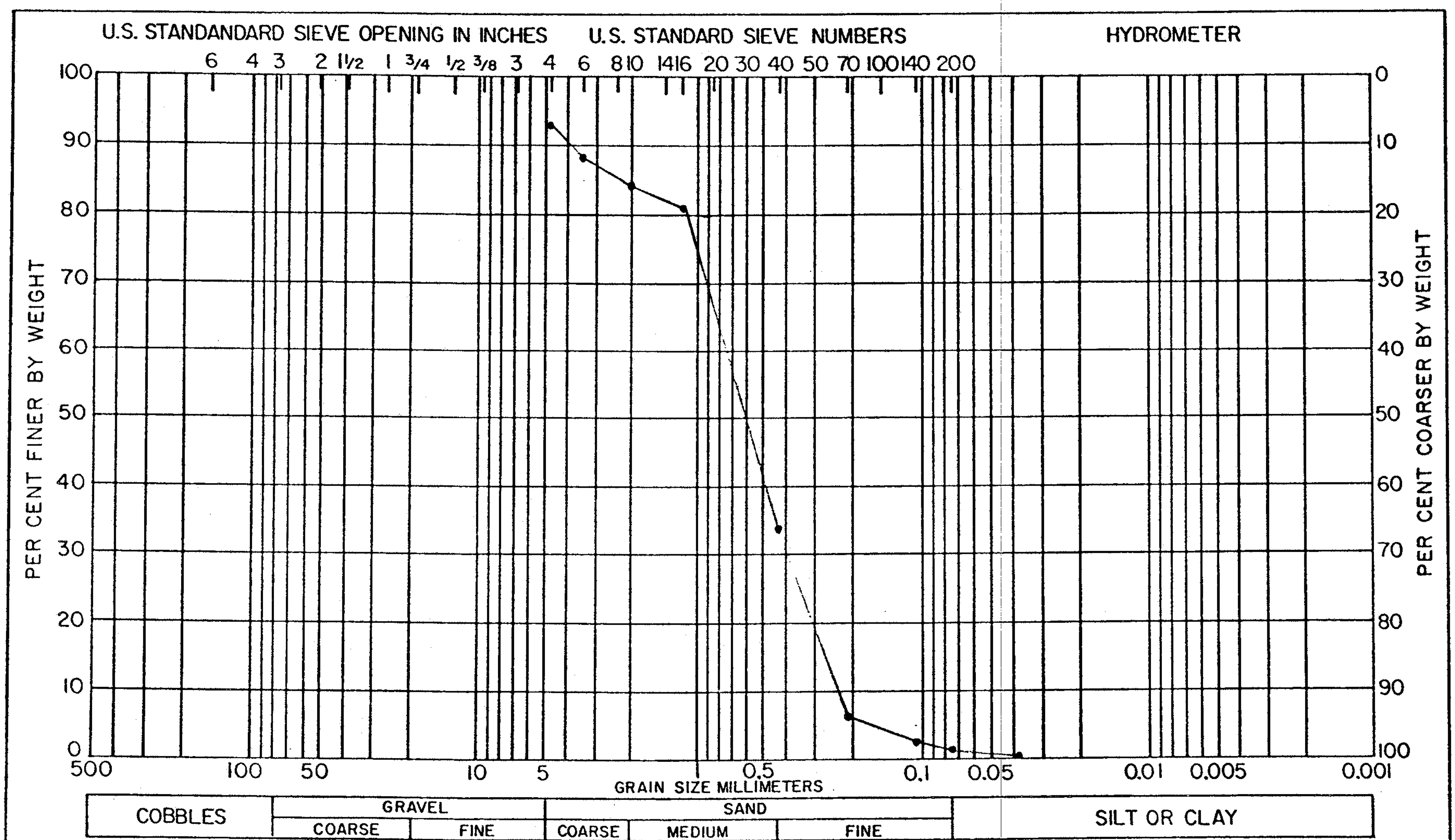

SAMPLE NO.	DEPTH	CLASSIFICATION (USDA TEXTURE TRIANGLE)	θ_i	d_{10}	d_{50}	d_{60}	C_u	C_c
S10-RC			0.96	0.24	0.60	0.75	3.12	0.89
				d30	d16	d84		
				0.40	0.27	2.00		

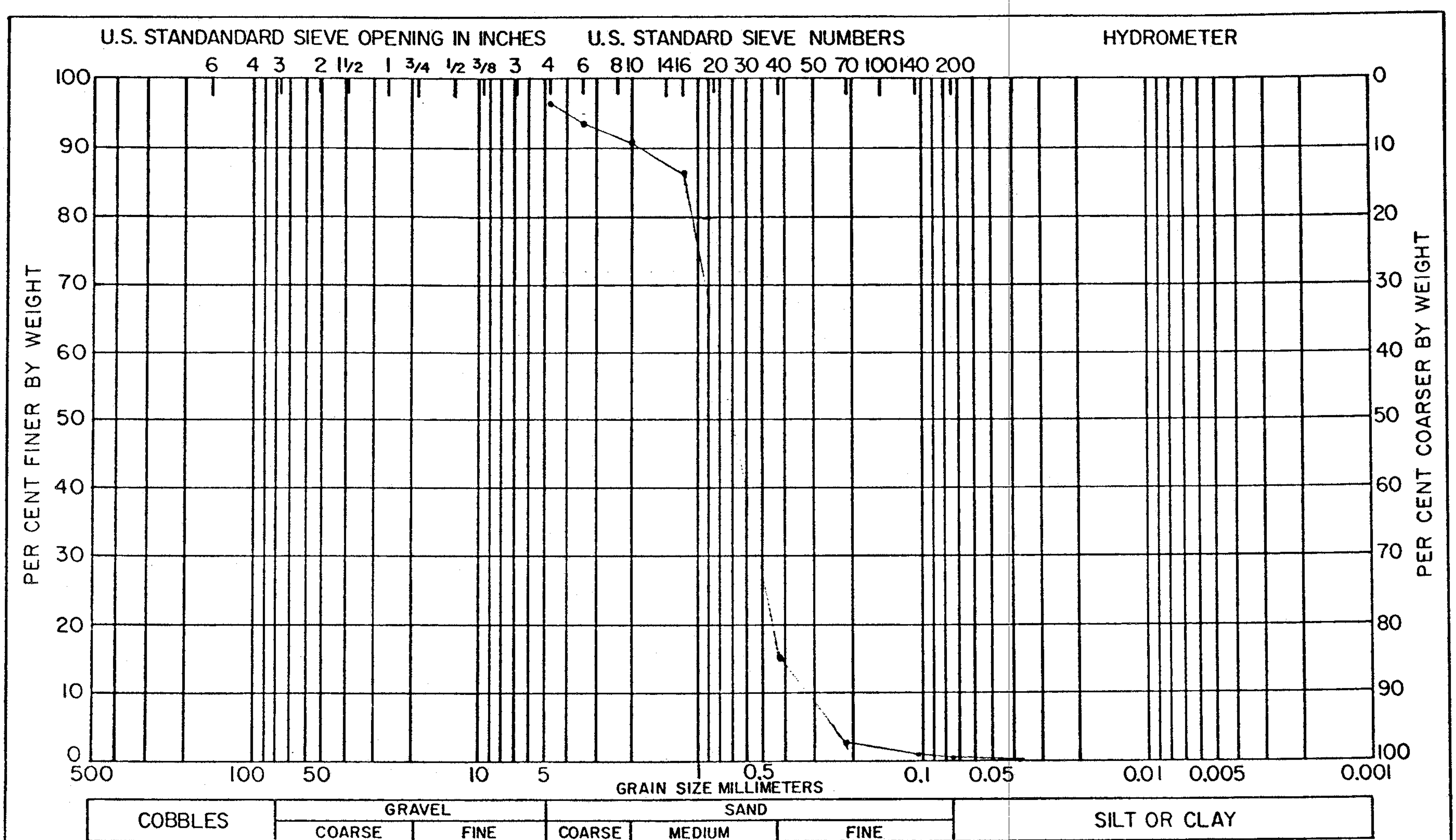

SAMPLE NO.	DEPTH	CLASSIFICATION (USDA TEXTURE TRIANGLE)	θ_i	d_{10}	d_{50}	d_{60}	C_u	C_c
S10-Th			0.78	0.33	0.70	0.81	2.45	1.05
				d30 0.53	d16 0.44	d84 1.20		

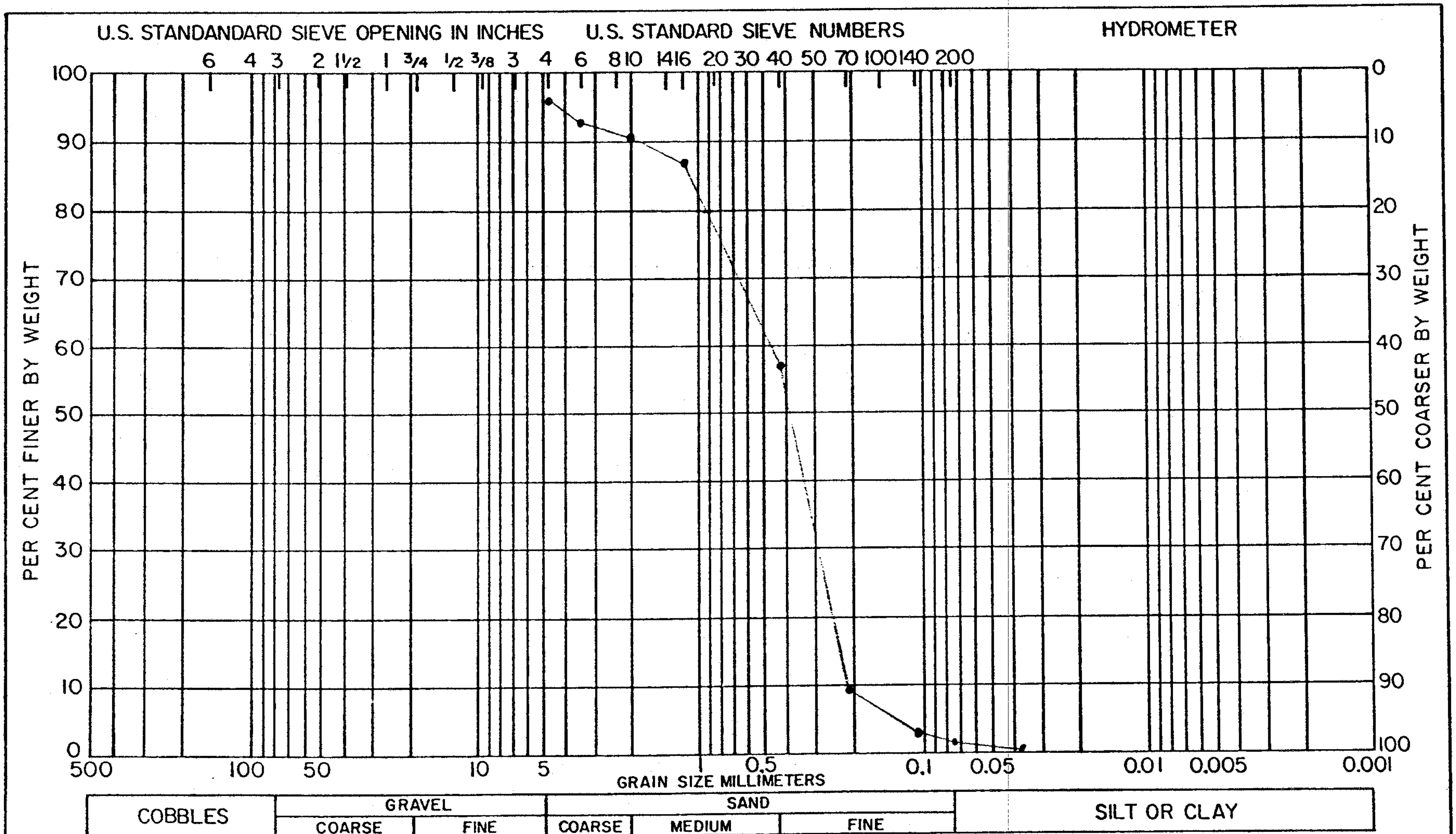

SAMPLE NO.	DEPTH	CLASSIFICATION (USDA TEXTURE TRIANGLE)	θ_i	d_{10}	d_{50}	d_{60}	C_u	C_c
S11-RC			0.58	0.22	0.39	0.47	2.14	0.81
				d30	d16	d84		
				0.29	0.24	1.10		

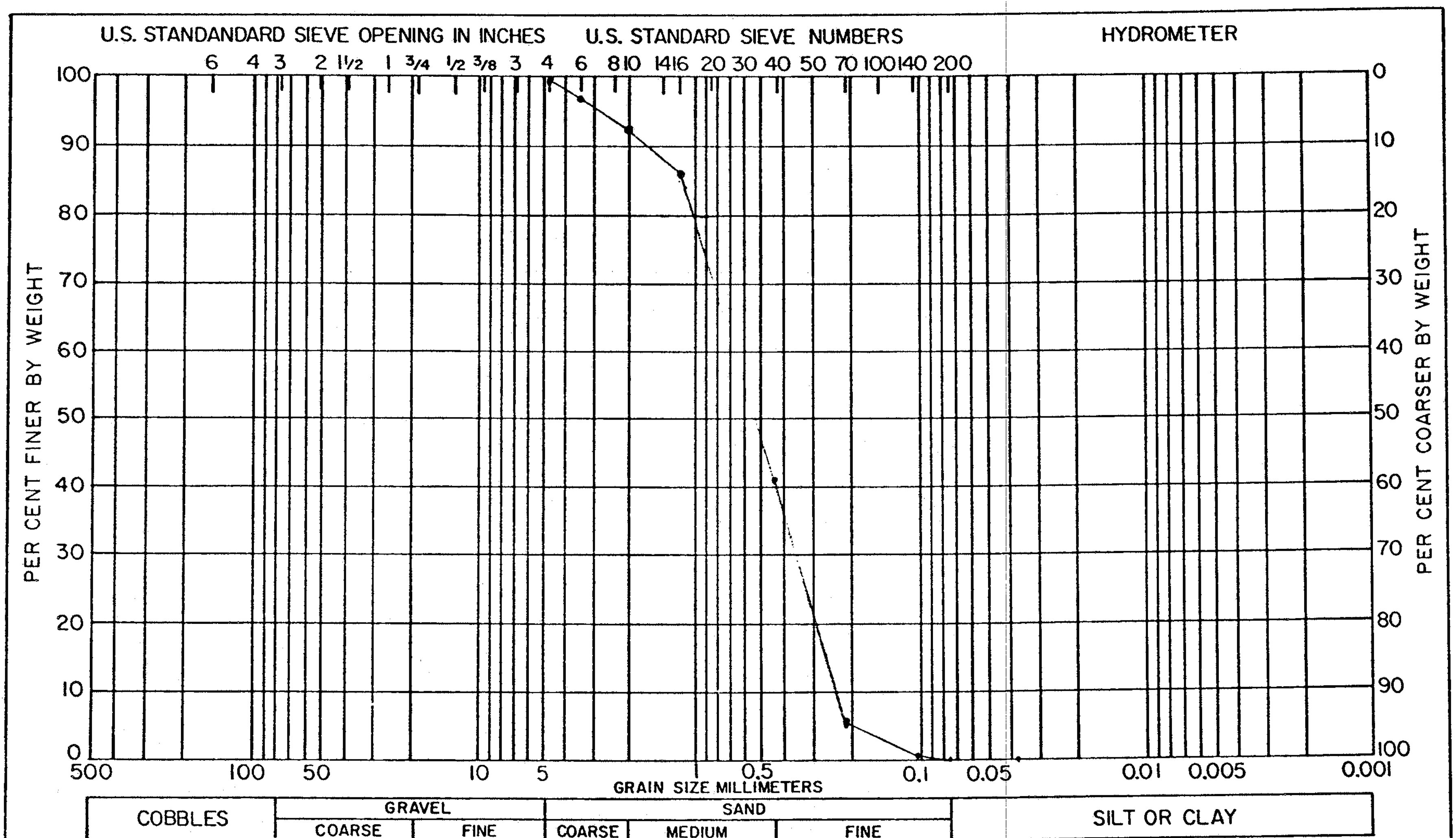

SAMPLE NO.	DEPTH	CLASSIFICATION (USDA TEXTURE TRIANGLE)	θ_i	d_{10}	d_{50}	d_{60}	C_u	C_c
S11-Th			0.66	0.24	0.54	0.68	2.83	0.79
				d30	d16	d84		
				0.36	0.27	1.18		

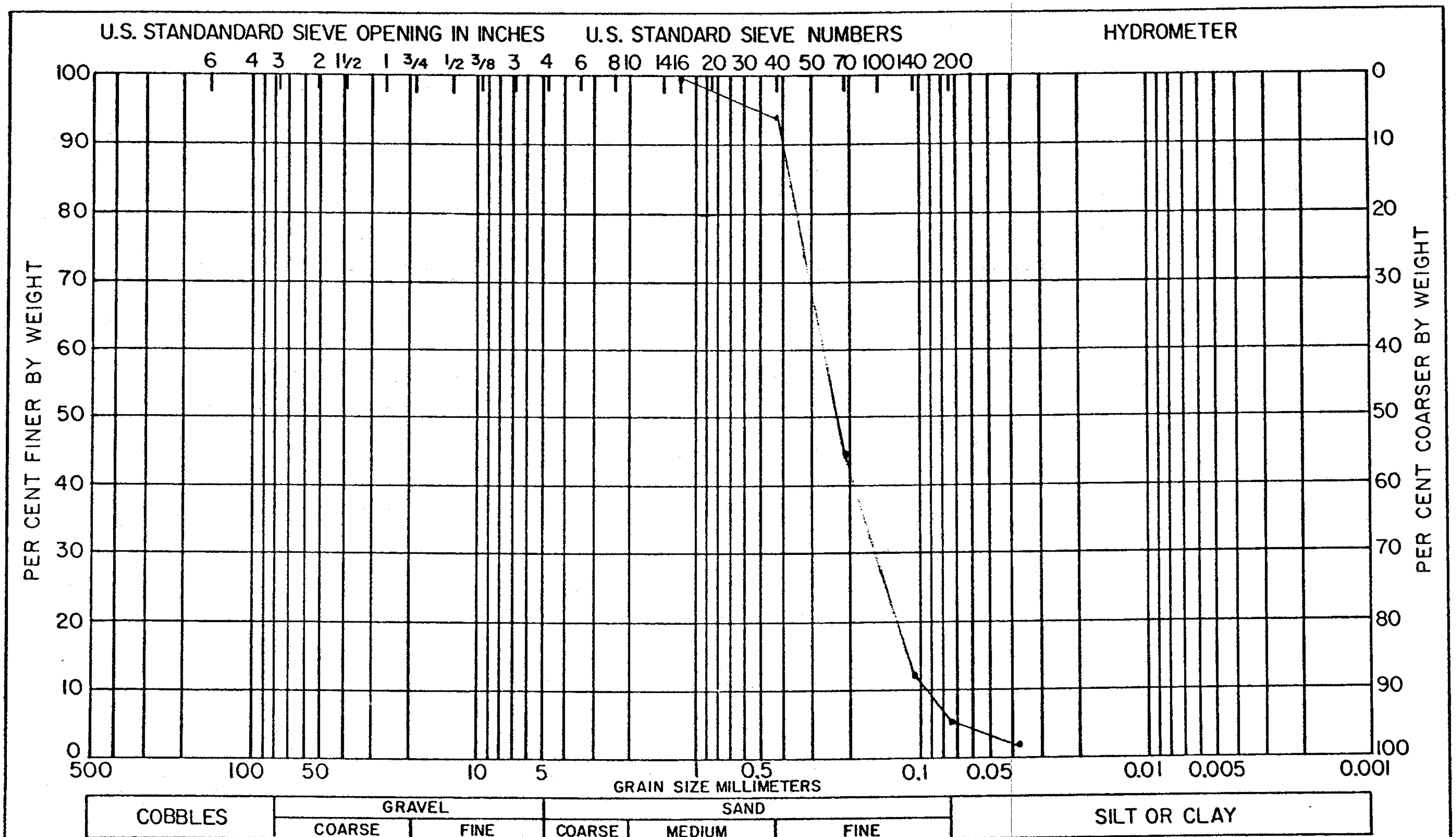

SAMPLE NO.	DEPTH	CLASSIFICATION (USDA TEXTURE TRIANGLE)	θ_i	d_{10}	d_{50}	d_{60}	C_u	C_c
S11-B			0.24	0.095	0.23	0.27	2.84	1.13
				d30 0.17	d16 0.12	d84 0.37		

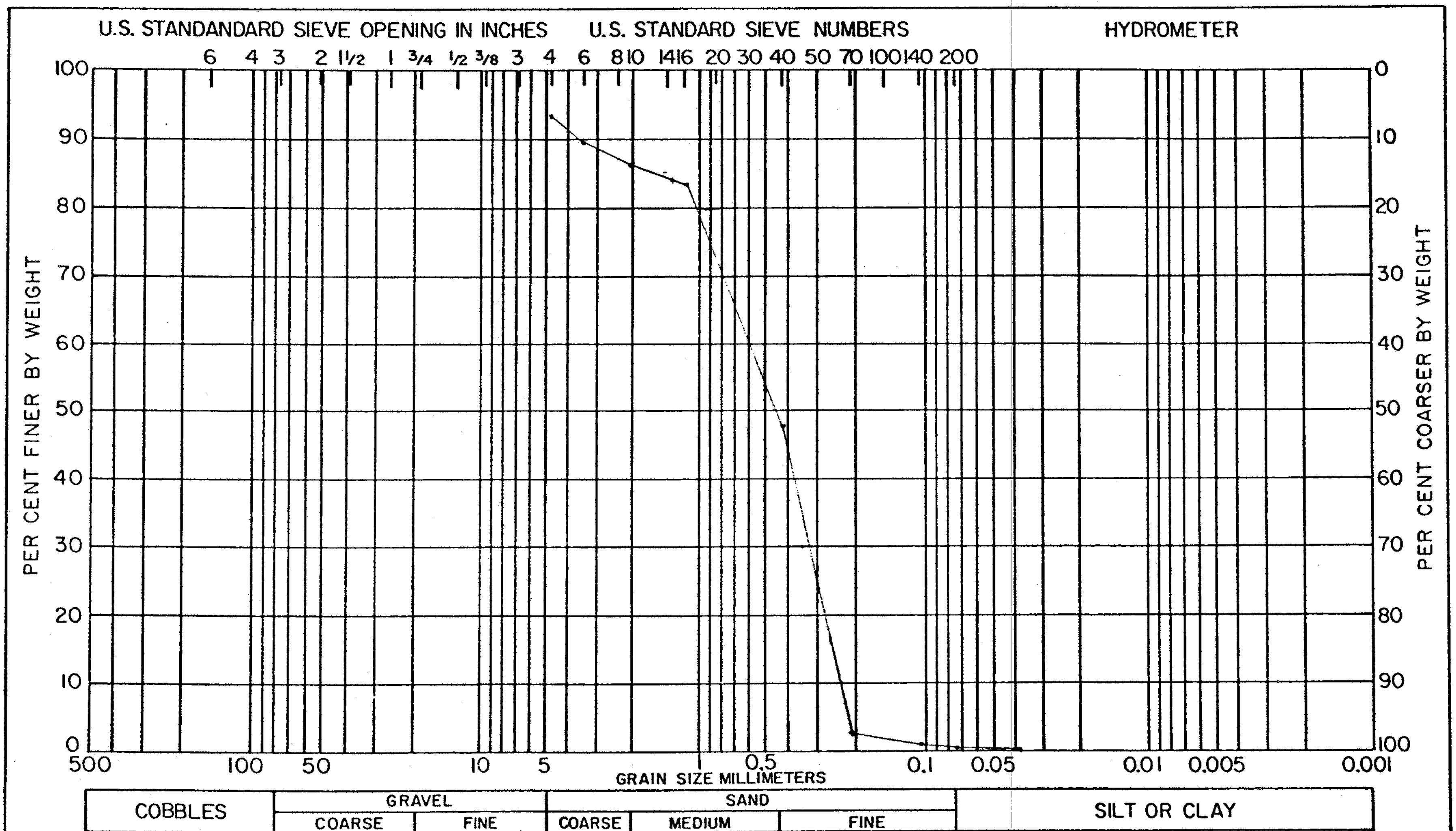

SAMPLE NO.	DEPTH	CLASSIFICATION (USDA TEXTURE TRIANGLE)	θ_i	d_{10}	d_{50}	d_{60}	C_u	C_c
S12-RC			0.72	0.24	0.45	0.59	2.46	0.77
				d30 0.33	d16 0.27	d84 1.45		

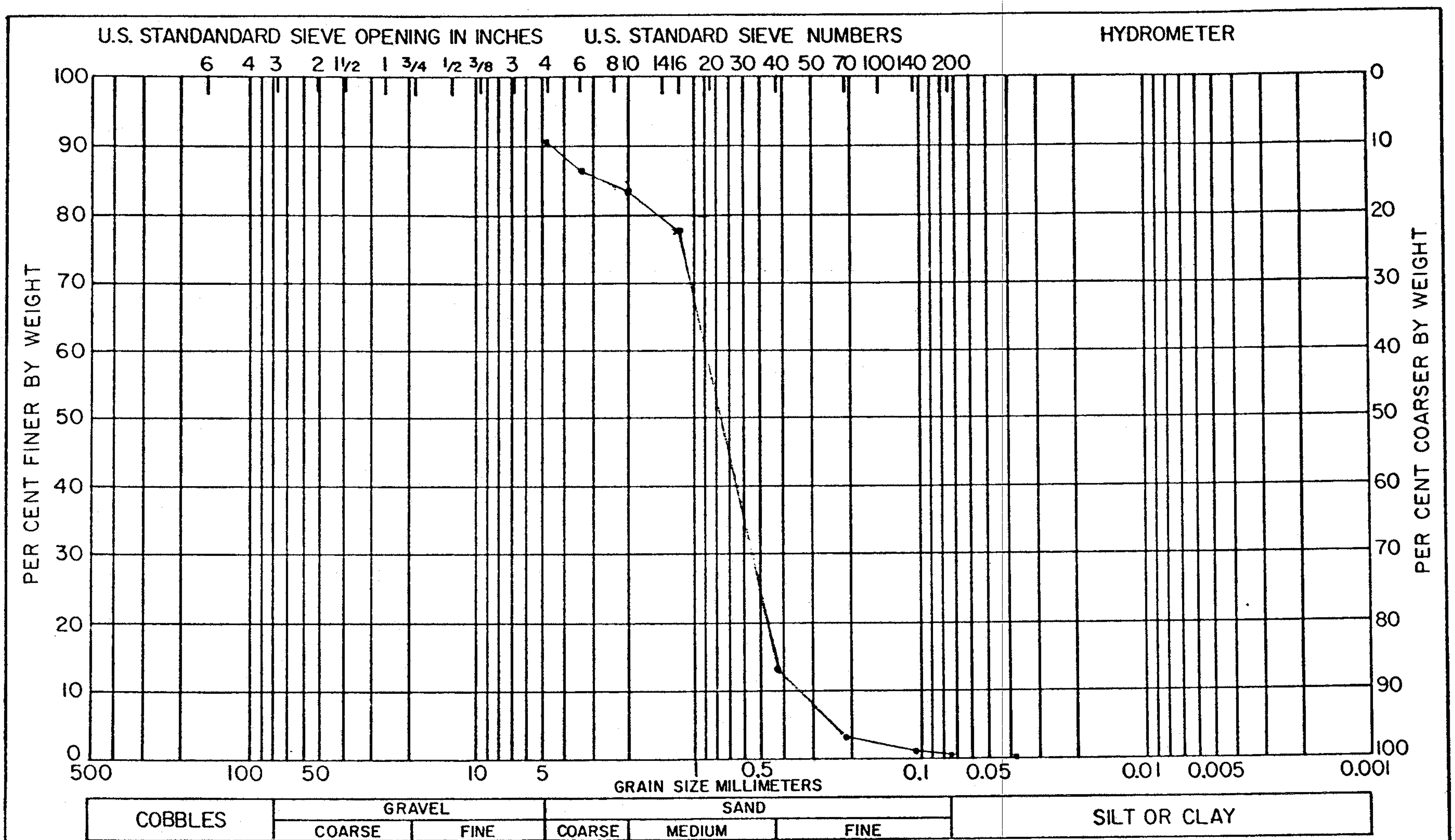

SAMPLE NO.	DEPTH	CLASSIFICATION (USDA TEXTURE TRIANGLE)	θ_i	d_{10}	d_{50}	d_{60}	C_u	C_c
S12-Th			1.10	0.35	0.76	0.90	2.57	0.96

d30 0.55

d16 0.44

d84 2.10

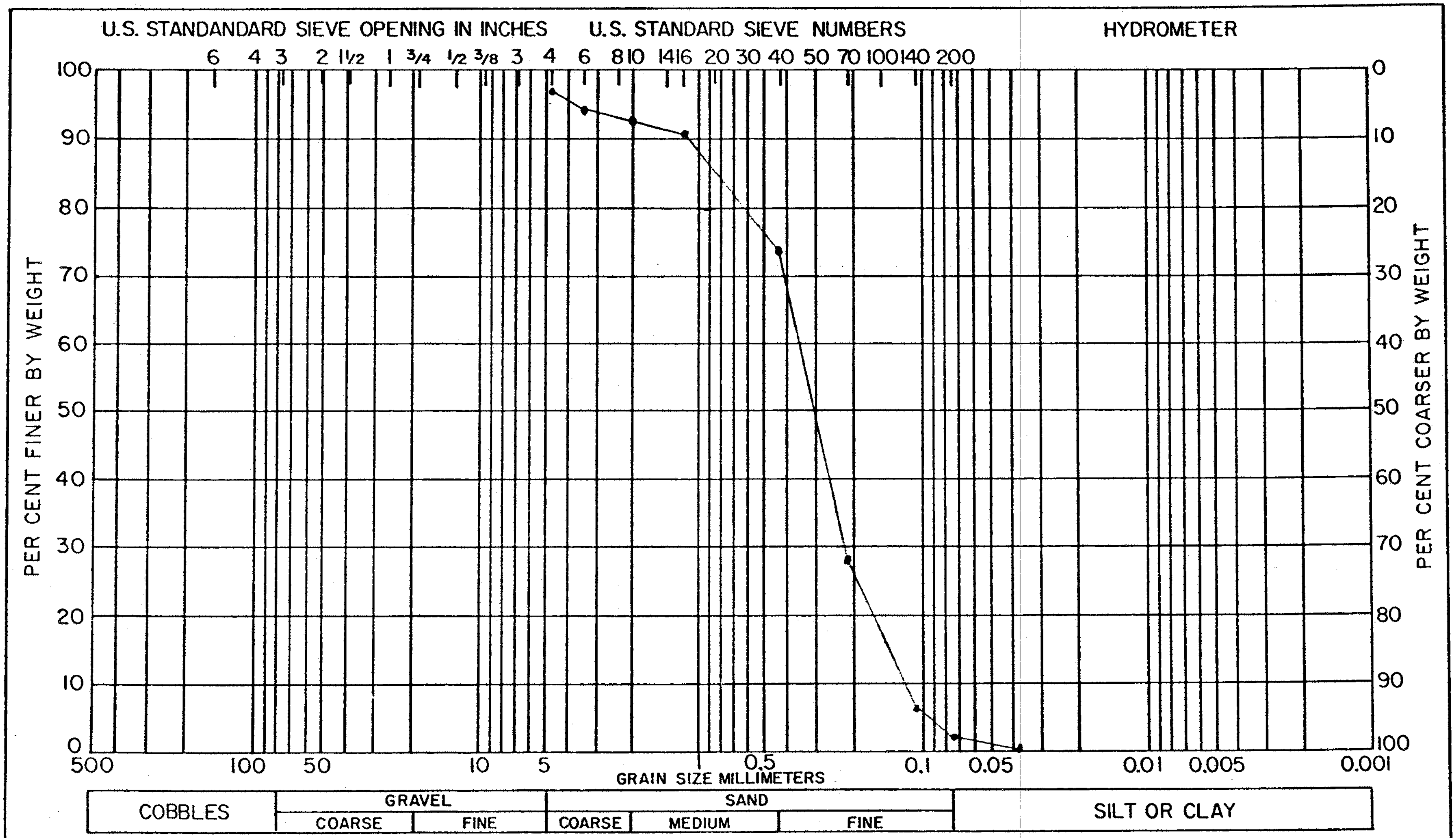

SAMPLE NO.	DEPTH	CLASSIFICATION (USDA TEXTURE TRIANGLE)	θ_i	d_{10}	d_{50}	d_{60}	C_u	C_c
S13-RC			0.42	0.13	0.31	0.36	2.77	1.13
				d30 0.23	d16 0.16	d84 0.80		

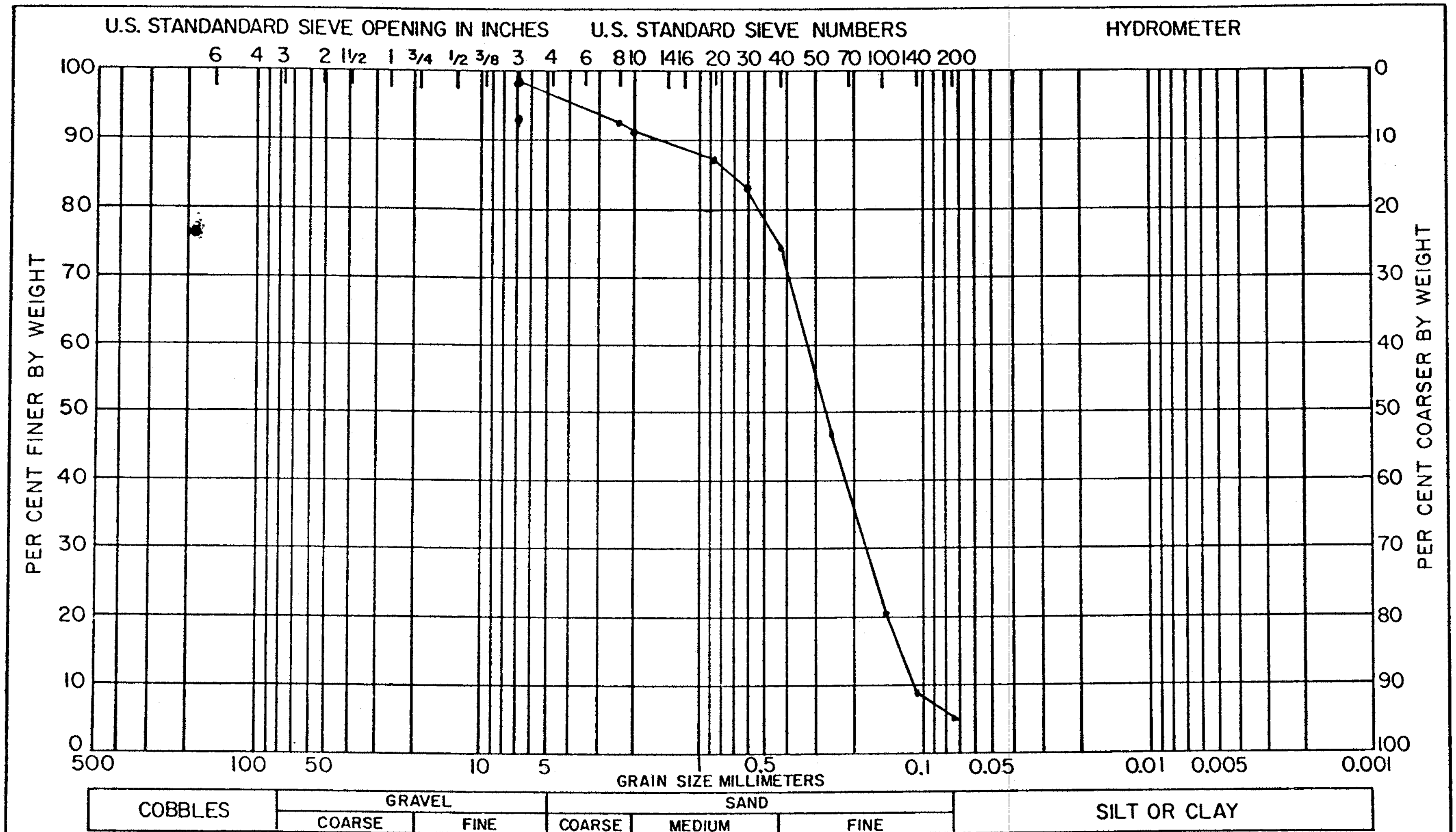

SAMPLE NO.	DEPTH	CLASSIFICATION (USDA TEXTURE TRIANGLE)	θ_i	d_{10}	d_{50}	d_{60}	C_u	C_c
S13-Th			0.36	0.12	0.27	0.32	2.67	0.84
				d30	d16	d84		
				0.18	0.13	0.68		

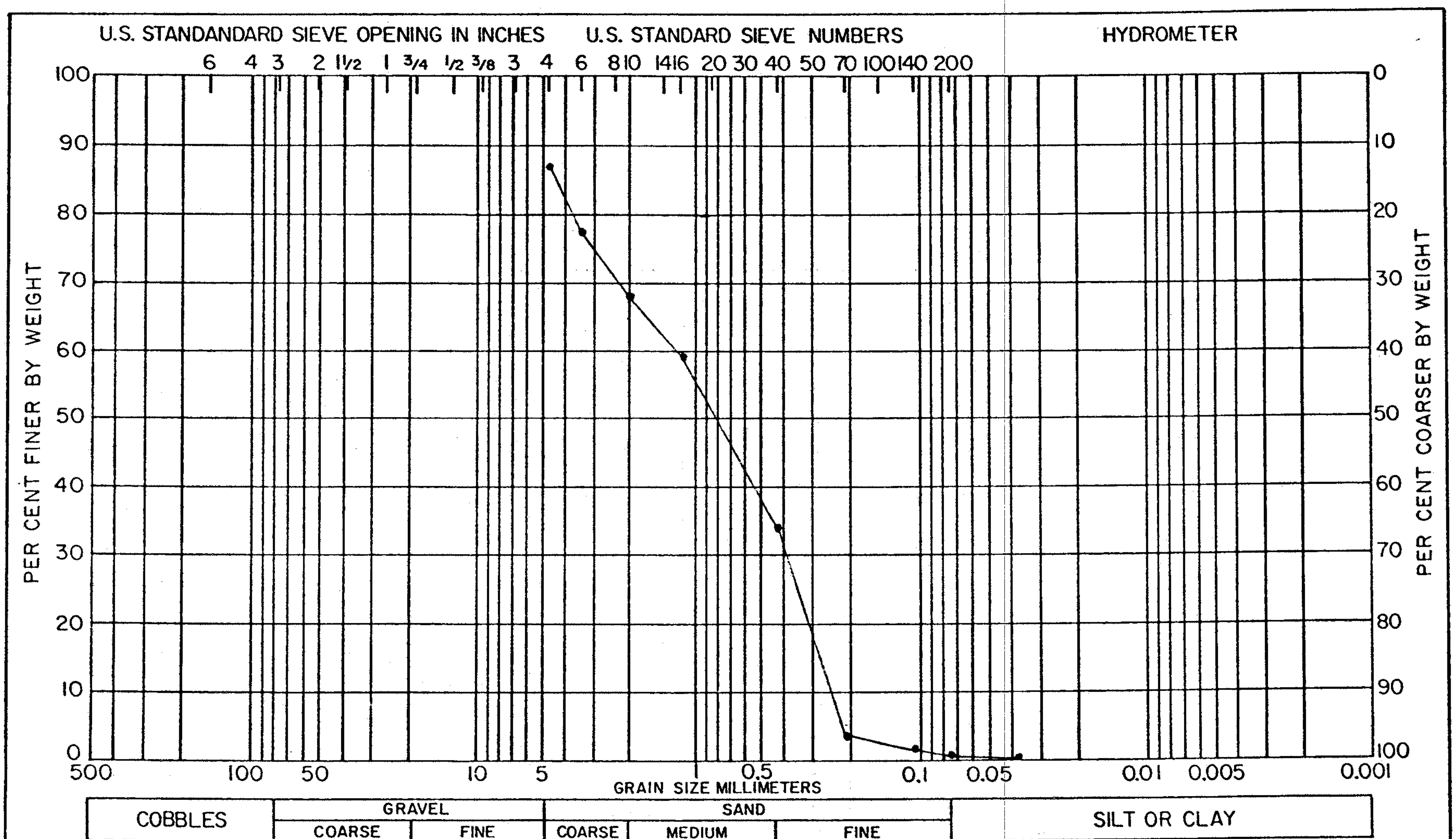

SAMPLE NO.	DEPTH	CLASSIFICATION (USDA TEXTURE TRIANGLE)	θ_i	d_{10}	d_{50}	d_{60}	C_u	C_c
M1-RC			1.80	0.25	0.81	1.30	5.20	0.47

d30	d16	d84
0.39	0.28	4.30

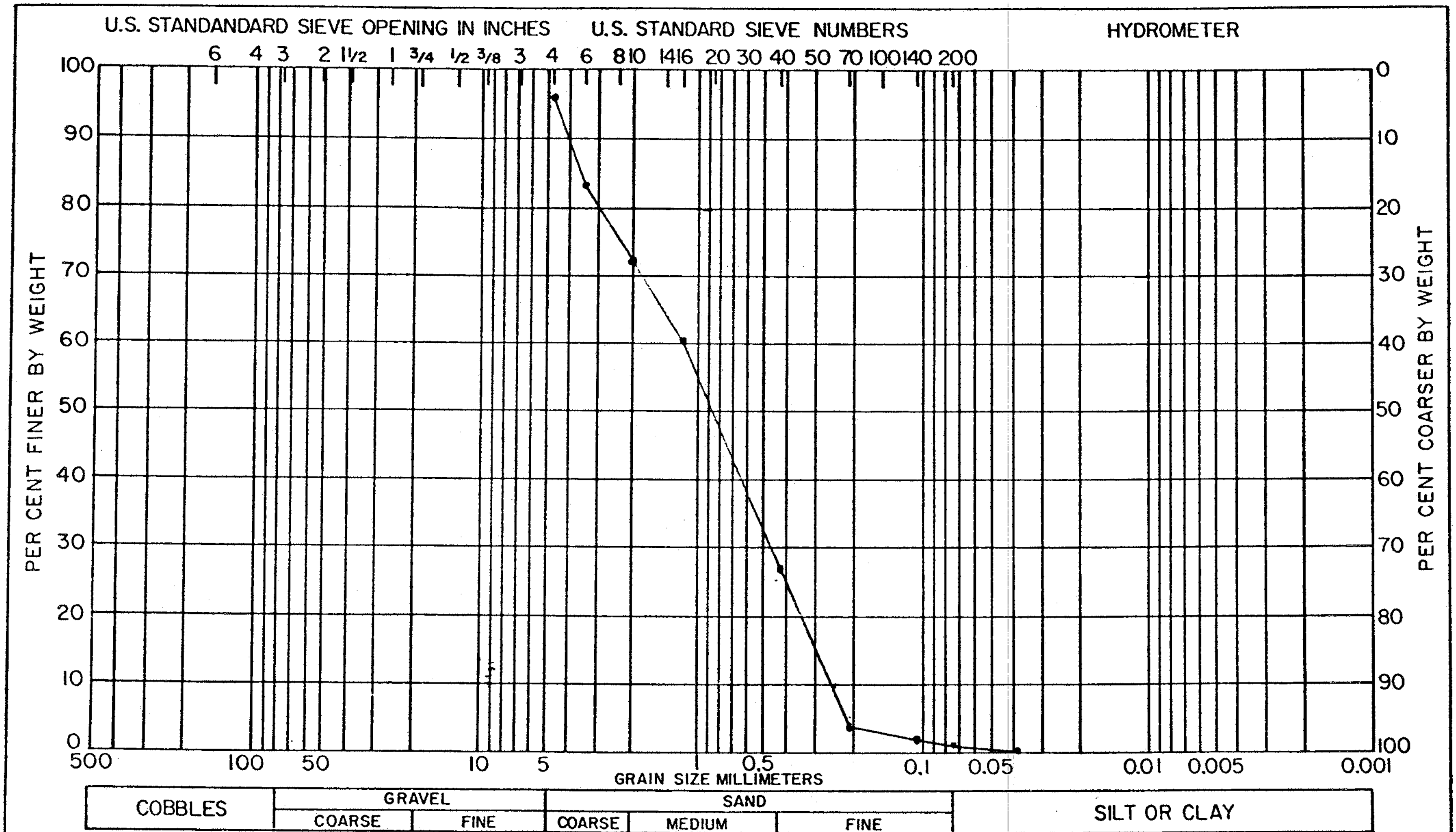

SAMPLE NO.	DEPTH	CLASSIFICATION (USDA TEXTURE TRIANGLE)	θ_i	d_{10}	d_{50}	d_{60}	C_u	C_c
M1-Th			1.55	0.26	0.86	1.20	4.62	0.71

d30	d16	d84
0.47	0.30	3.50

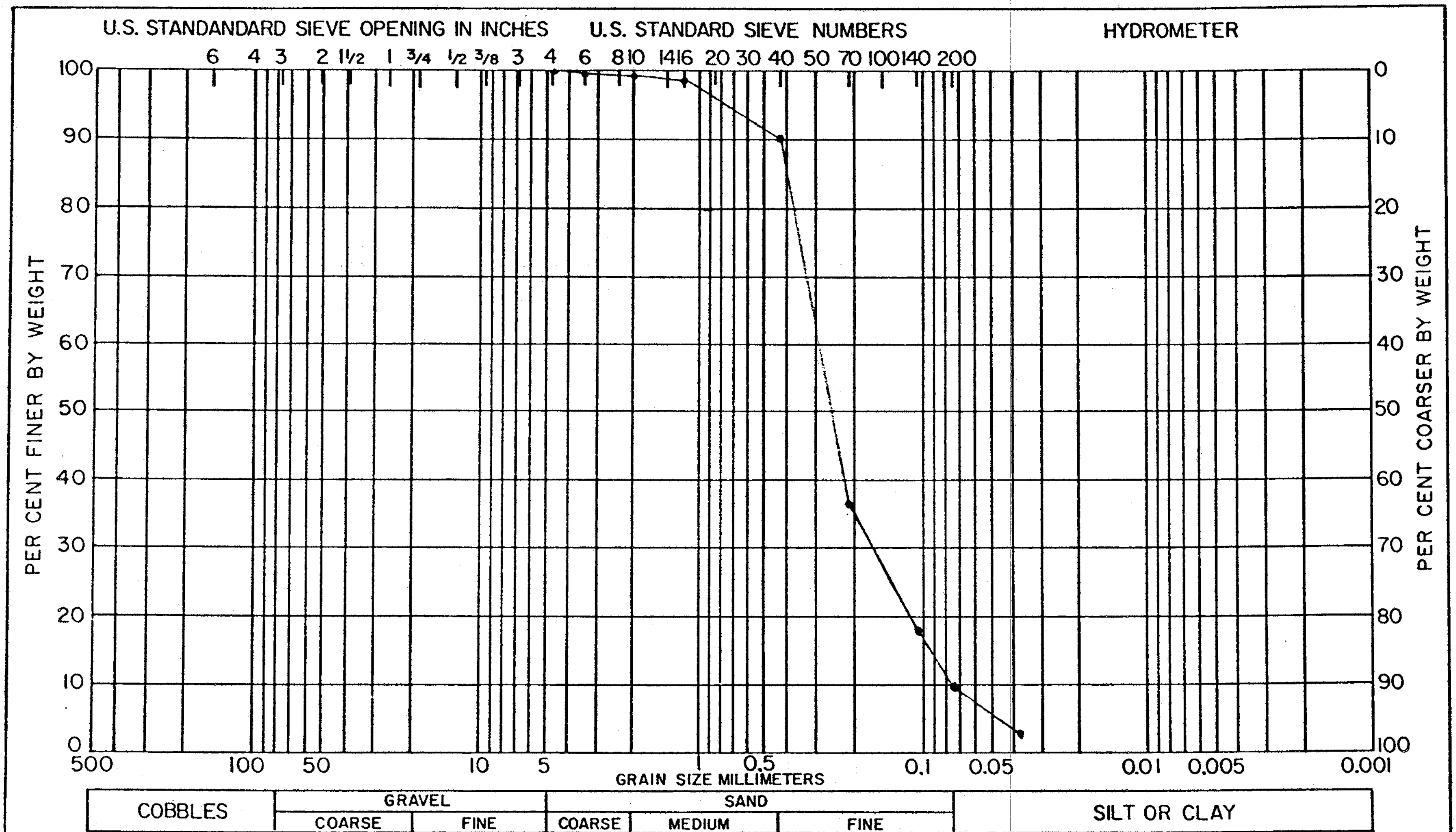

SAMPLE NO.	DEPTH	CLASSIFICATION (USDA TEXTURE TRIANGLE)	θ_i	d_{10}	d_{50}	d_{60}	C_u	C_c
M1-SB			0.25	0.075	0.25	0.29	3.87	1.33

d30	d16	d84
0.17	0.094	0.40

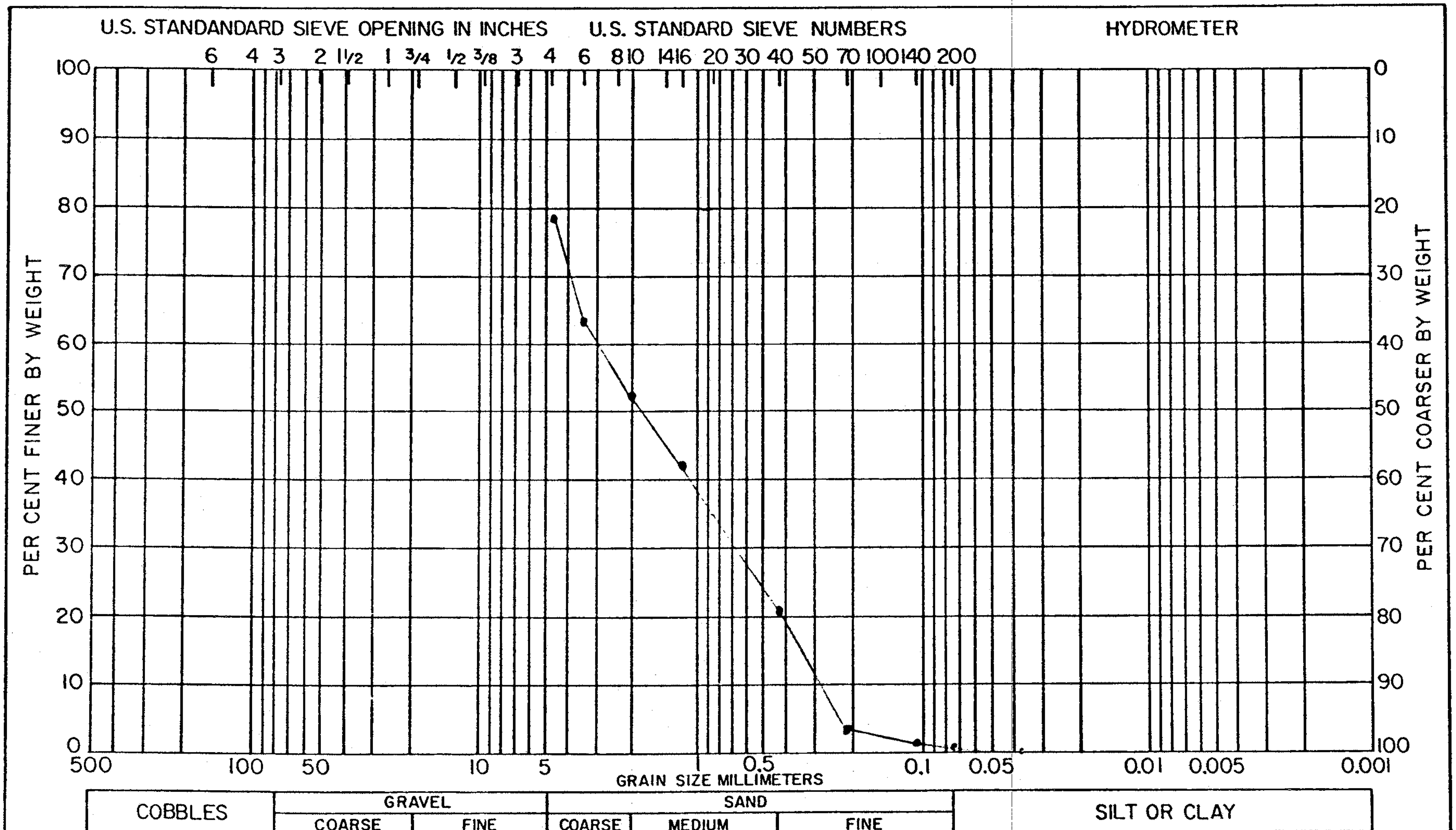

SAMPLE NO.	DEPTH	CLASSIFICATION (USDA TEXTURE TRIANGLE)	θ_i	d_{10}	d_{50}	d_{60}	C_u	C_c
M2-Th			2.4(est)	0.28	1.80	3.00	10.71	0.55

d30	d16	d84
0.68	0.36	5.0(est)

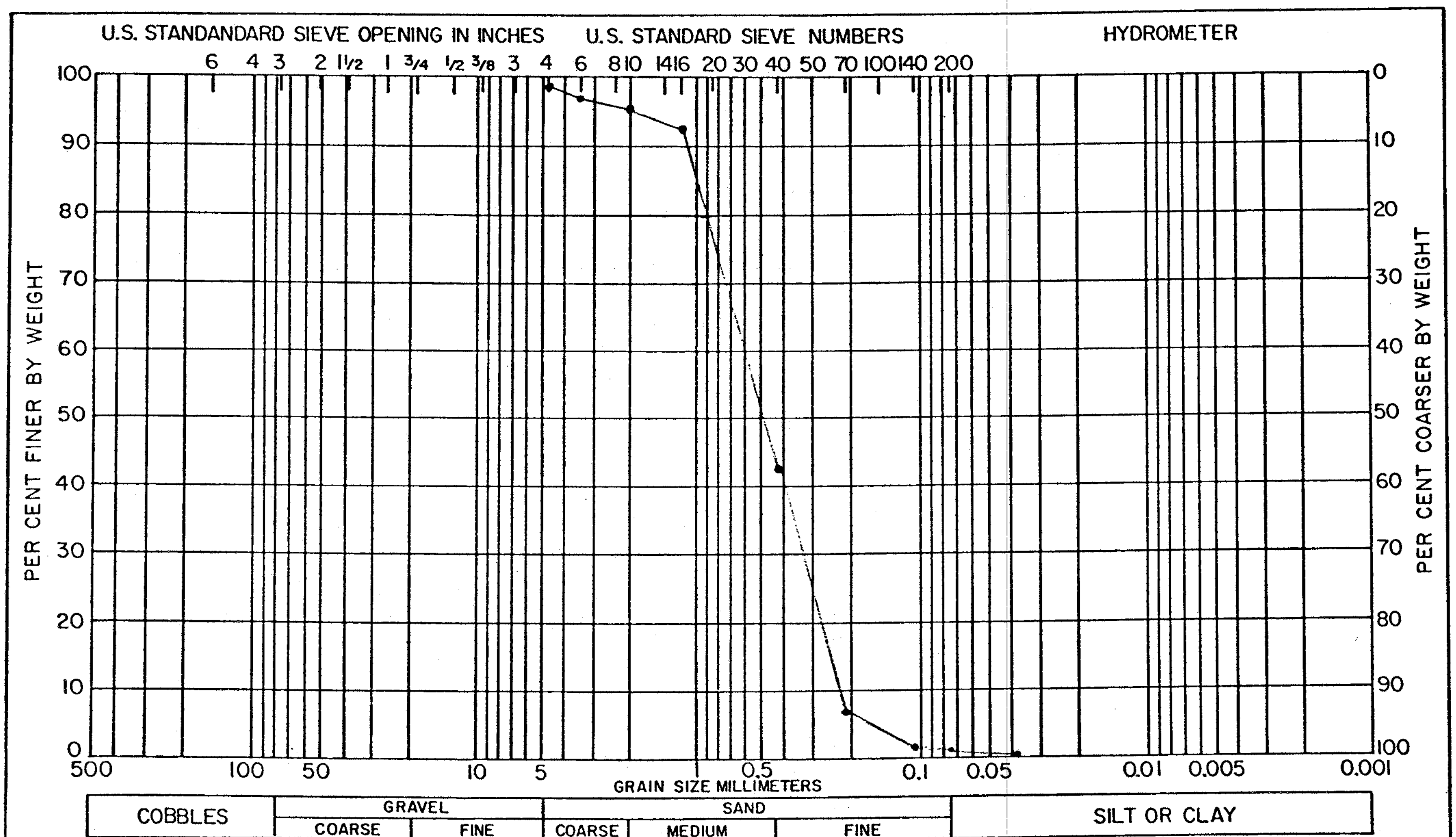

SAMPLE NO.	DEPTH	CLASSIFICATION (USDA TEXTURE TRIANGLE)	θ_i	d_{10}	d_{50}	d_{60}	C_u	C_c
D1-Th			0.58	0.23	0.49	0.60	2.61	0.79
				d_{30}	d_{16}	d_{84}		
				0.33	0.26	0.98		

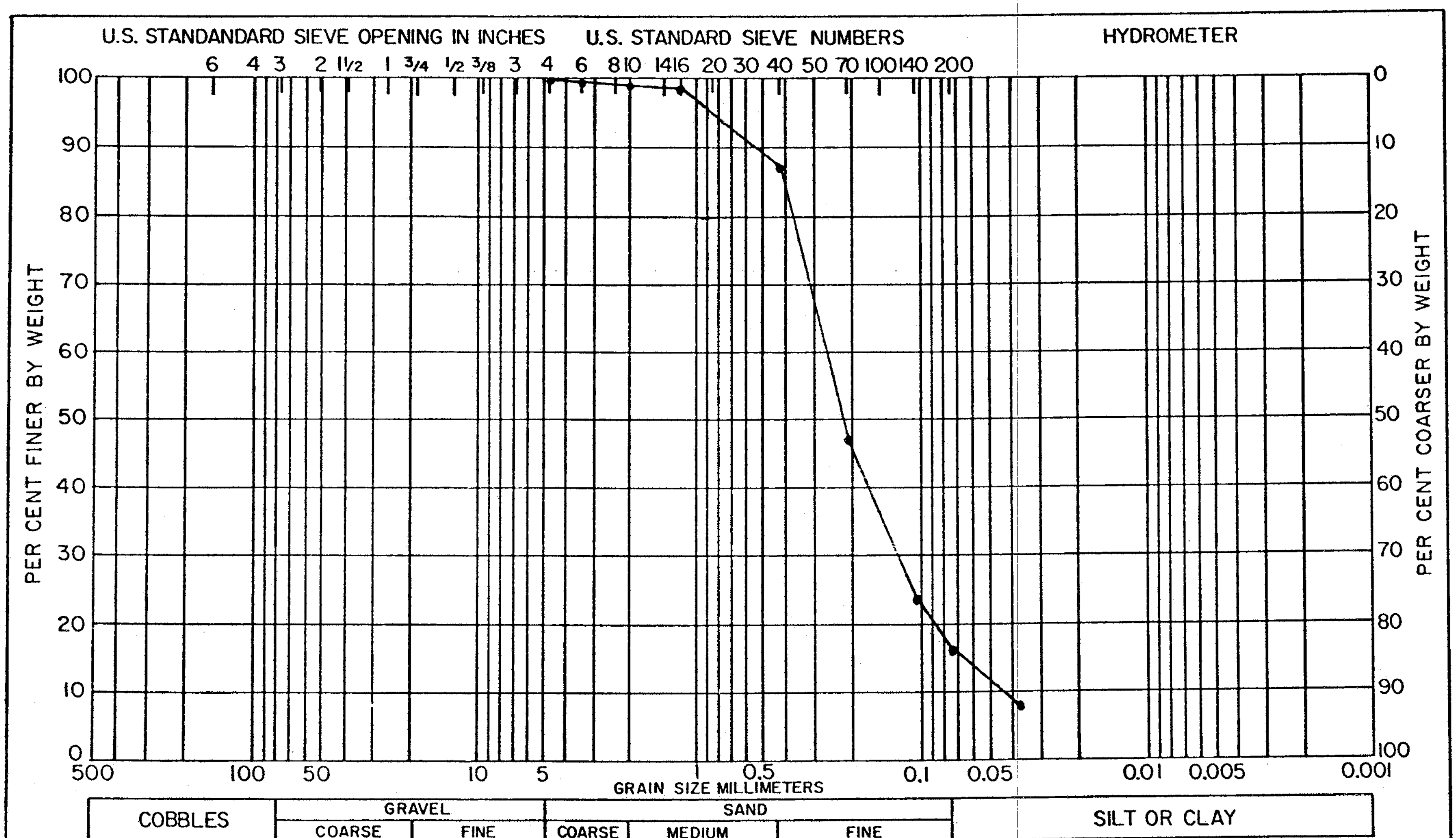

SAMPLE NO.	DEPTH	CLASSIFICATION (USDA TEXTURE TRIANGLE)	θ_i	d_{10}	d_{50}	d_{60}	C_u	C_c
D1-EB			0.23	0.044	0.22	0.27	6.14	1.42

d30	d16	d84
0.13	0.070	0.40

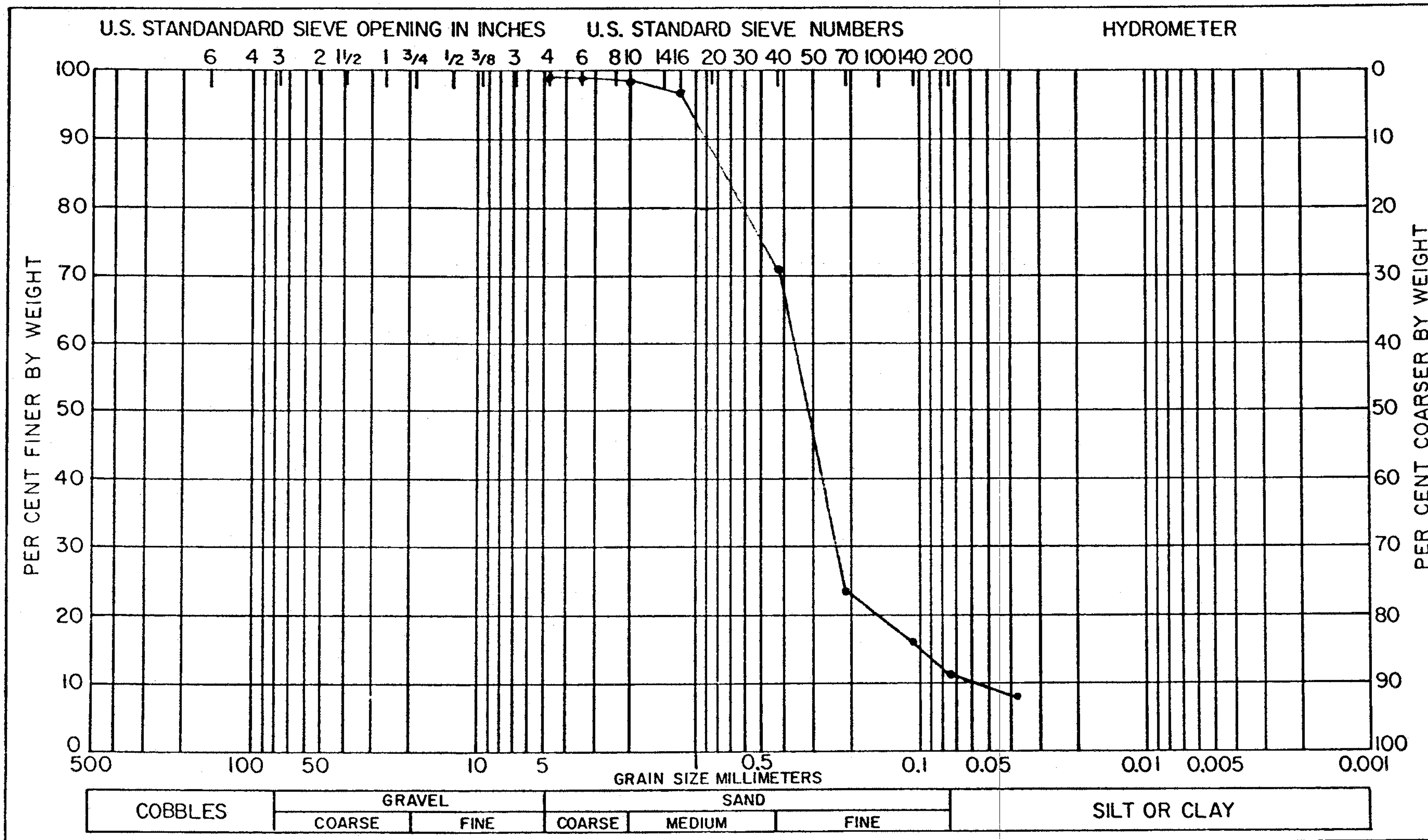

SAMPLE NO.	DEPTH	CLASSIFICATION (USDA TEXTURE TRIANGLE)	θ_i	d_{10}	d_{50}	d_{60}	C_u	C_c
D1-WB			0.38	0.059	0.32	0.37	6.27	2.64

d30	d16	d84
0.24	0.11	0.72

APPENDIX E: Field Station Maps

EXPLANATION

Field maps redrawn from originals. All distances and locations are approximate.

Hachures indicate slope. Down towards hachured side of line

 vegetation, predominantly low grasses and tamarisk.

 Trees, predominantly cottonwoods and juniper.

Geologic descriptions placed where appropriate.

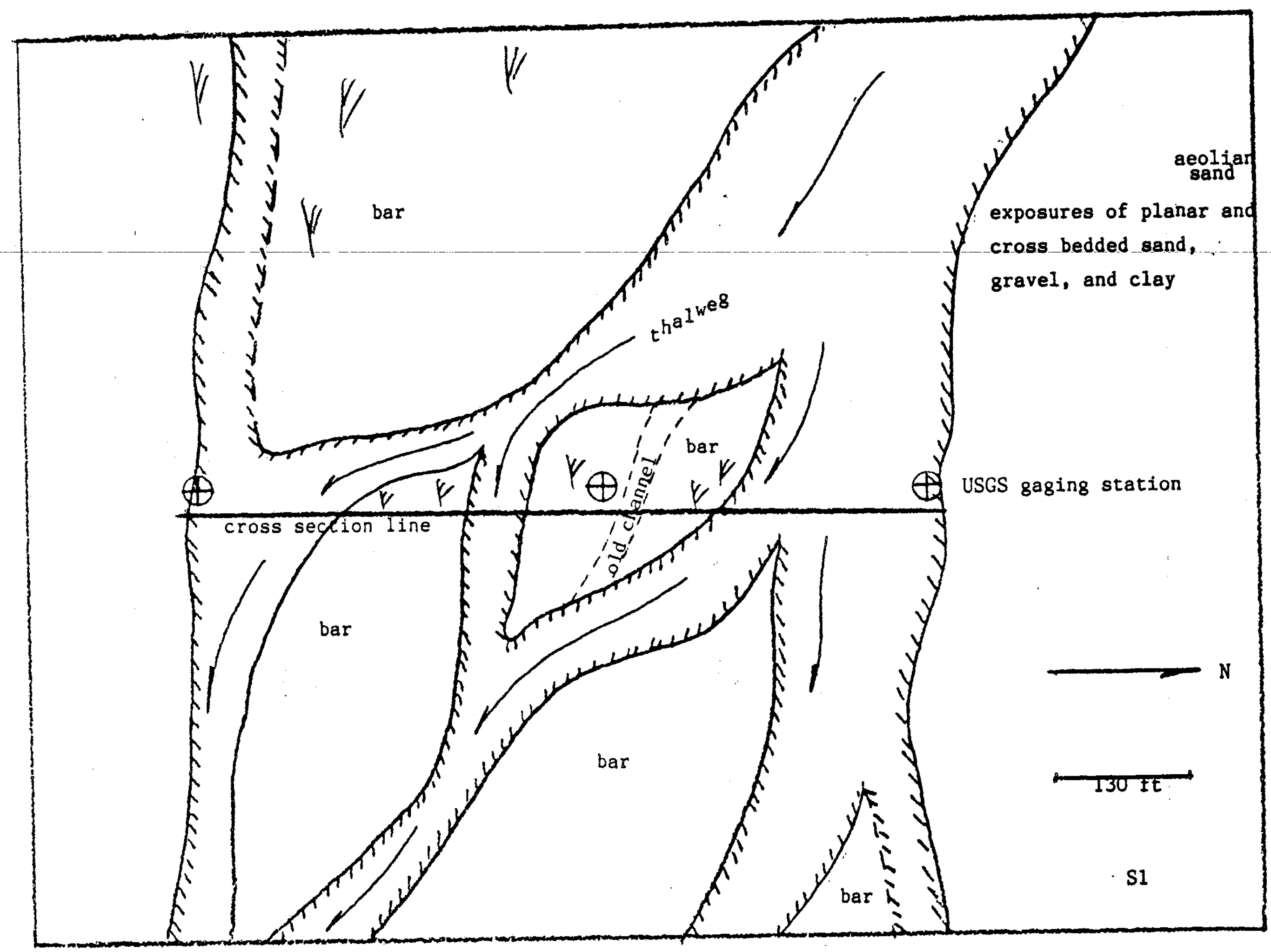

aeolian sand
bar
exposures of planar and cross bedded sand, gravel, and clay
thalweg
bar
old channel
USGS gaging station
cross section line
bar
N
bar
130 ft
S1
bar

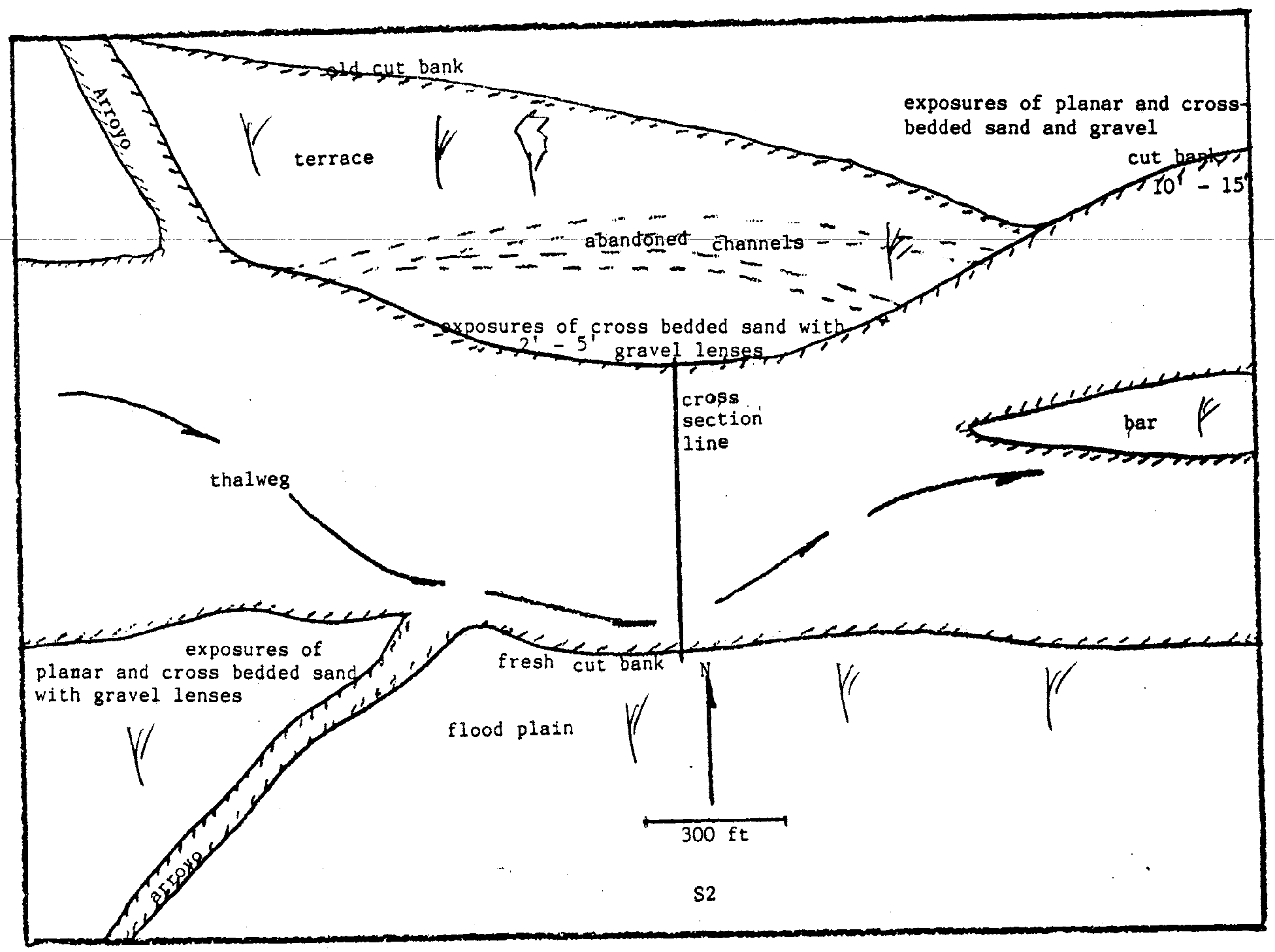
old cut bank
Arroyo
terrace
exposures of planar and cross-bedded sand and gravel
cut bank 10' - 15'
abandoned channels
exposures of cross bedded sand with 2' - 5' gravel lenses
cross section line
bar
thalweg
exposures of planar and cross bedded sand with gravel lenses
fresh cut bank
flood plain
N
300 ft
arroyo
S2

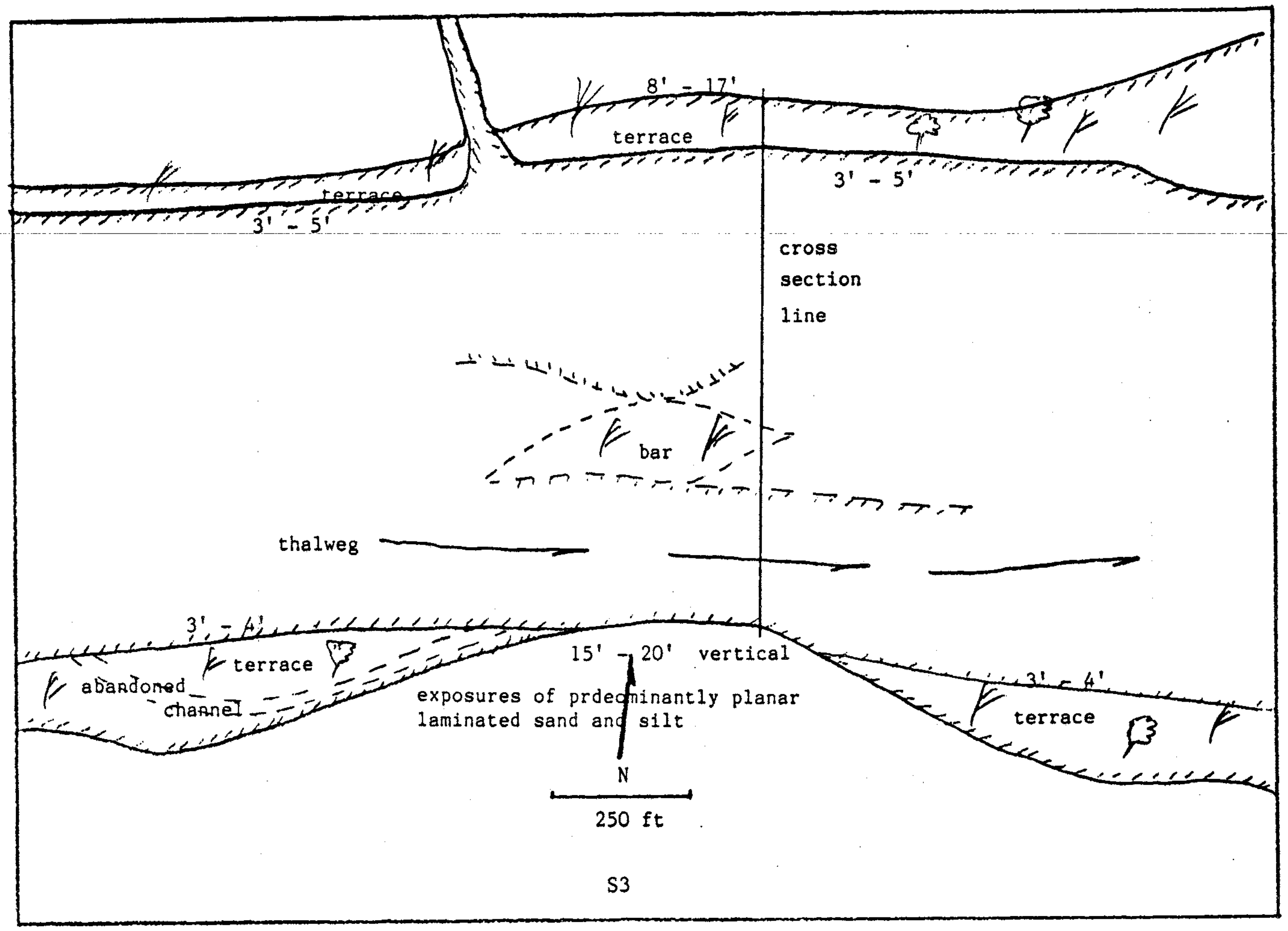
8' - 17'
terrace
terrace
3' - 5'
3' - 5'
cross
section
line
bar
thalweg
3' - 4'
terrace
abandoned
channel
15' - 20' vertical
exposures of prdeominantly planar
laminated sand and silt
3' - 4'
terrace
N
250 ft
S3

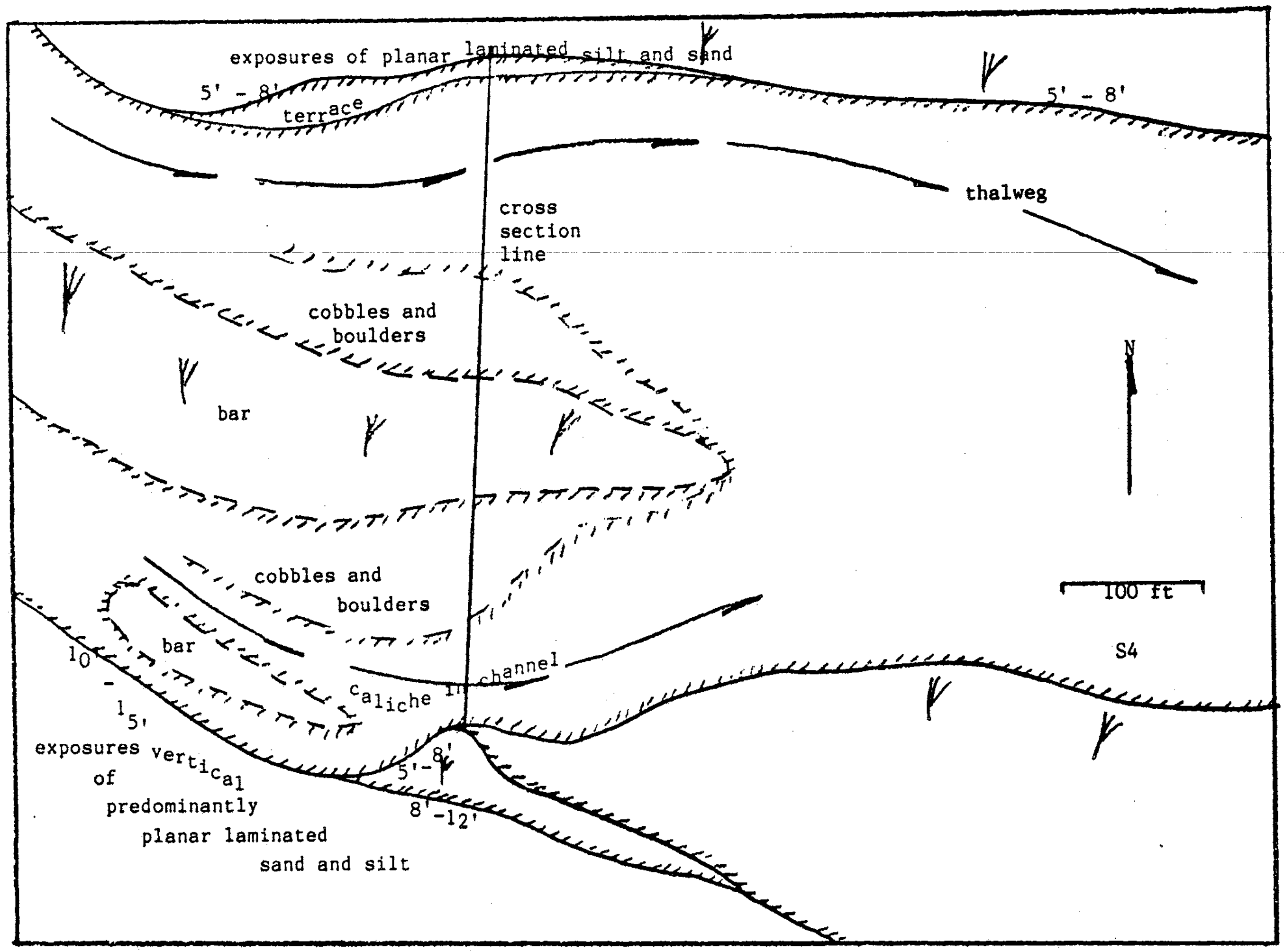
exposures of planar laminated silt and sand
5' - 8'
terrace
5' - 8'
thalweg
cross
section
line
cobbles and
boulders
bar
N
cobbles and
boulders
100 ft
bar
S4
channel
caliche in
10
-
15'
exposures vertical
of
predominantly
planar laminated
sand and silt
5'-8'
8'-12'

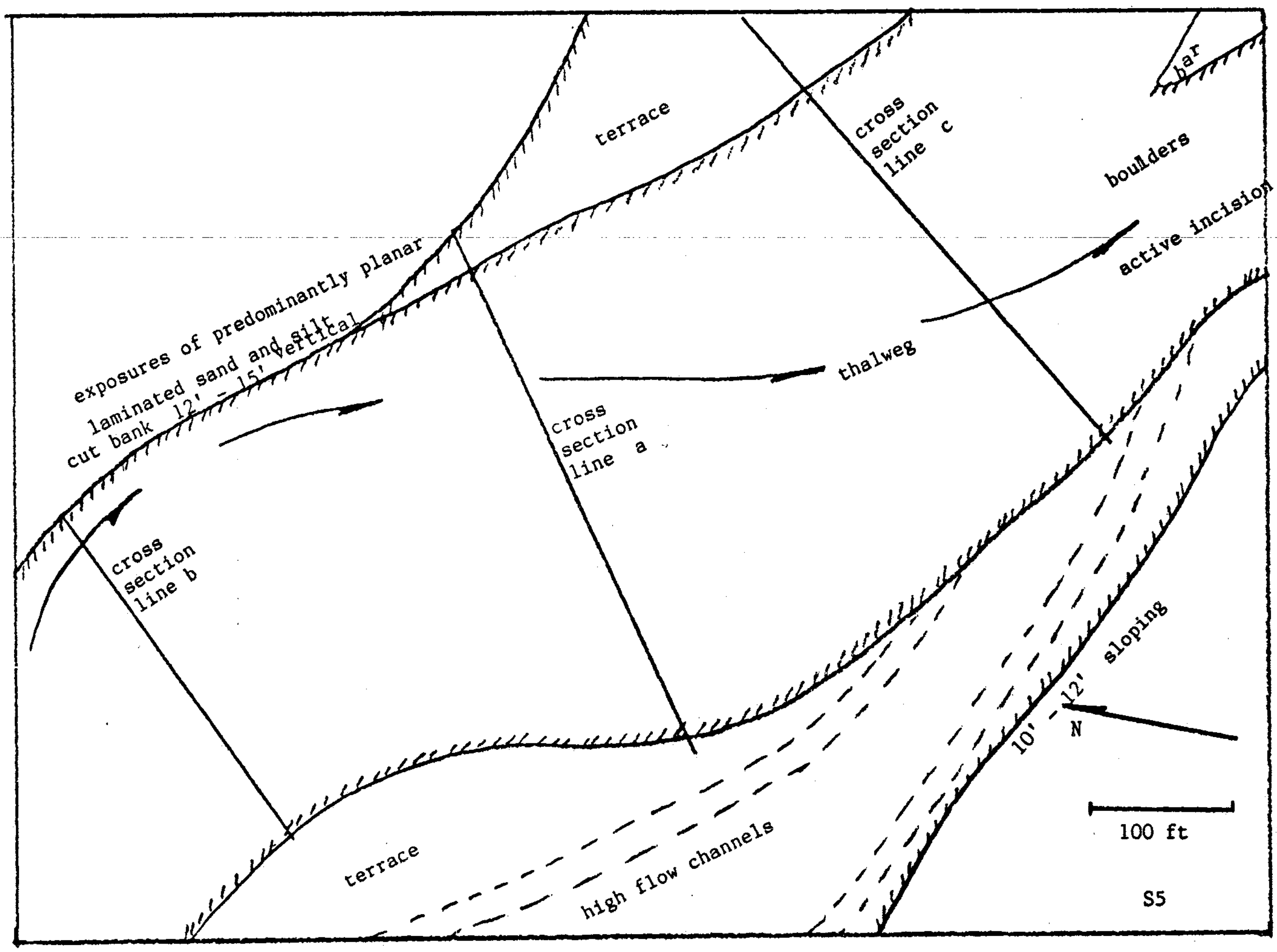
terrace
cross section line c
bar
boulders
active incision
exposures of predominantly planar laminated sand and silt
cut bank 12' - 15' vertical
thalweg
cross section line a
cross section line b
sloping
10' - 12'
N
100 ft
terrace
high flow channels
S5

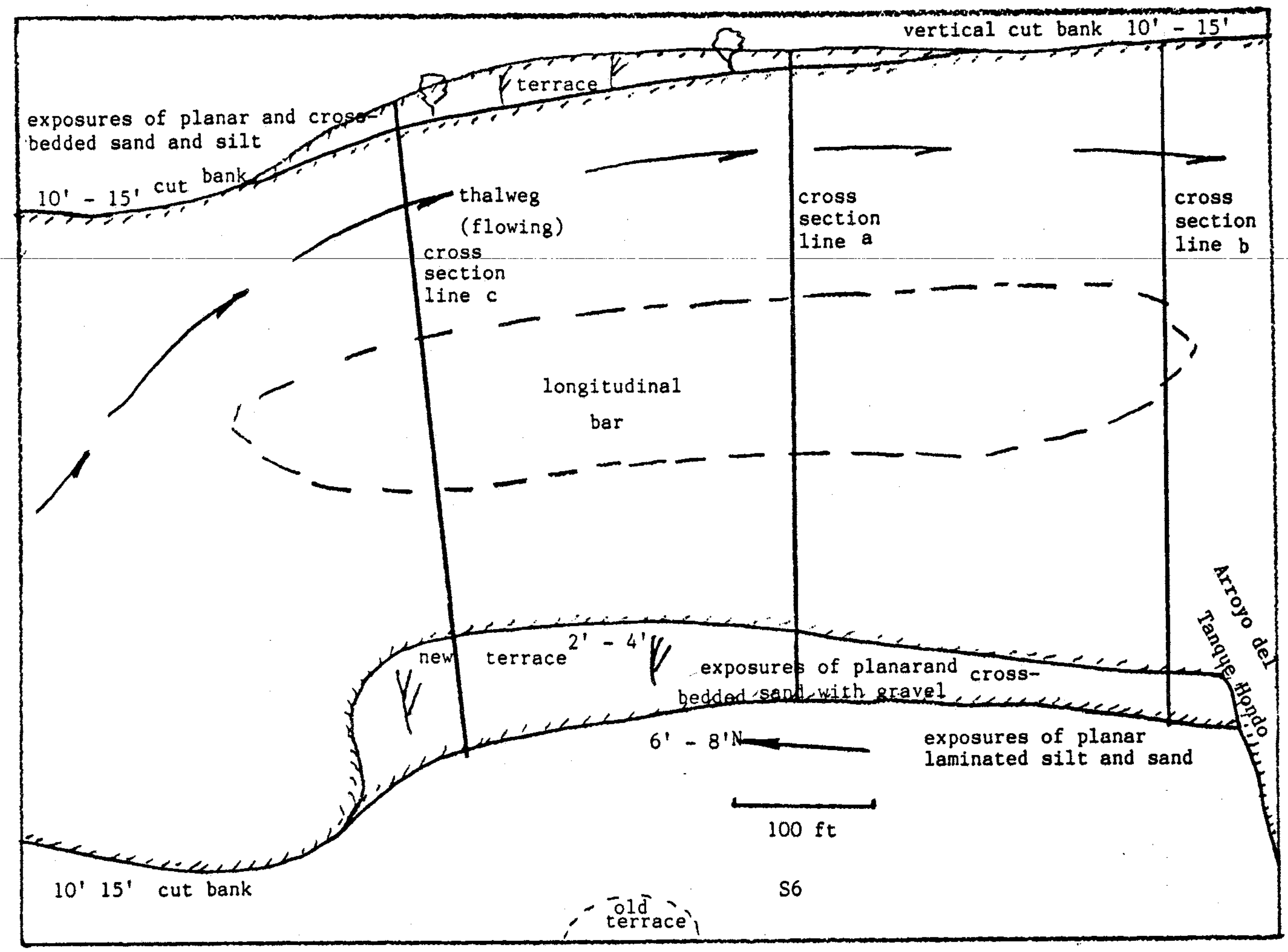
vertical cut bank 10' - 15'
terrace
exposures of planar and cross-bedded sand and silt
10' - 15' cut bank
thalweg (flowing)
cross section line c
cross section line a
cross section line b
longitudinal bar
Arroyo del Tanque Hondo
new terrace 2' - 4'
exposures of planar and cross-bedded sand with gravel
6' - 8' N
exposures of planar laminated silt and sand
100 ft
10' 15' cut bank
S6
old terrace

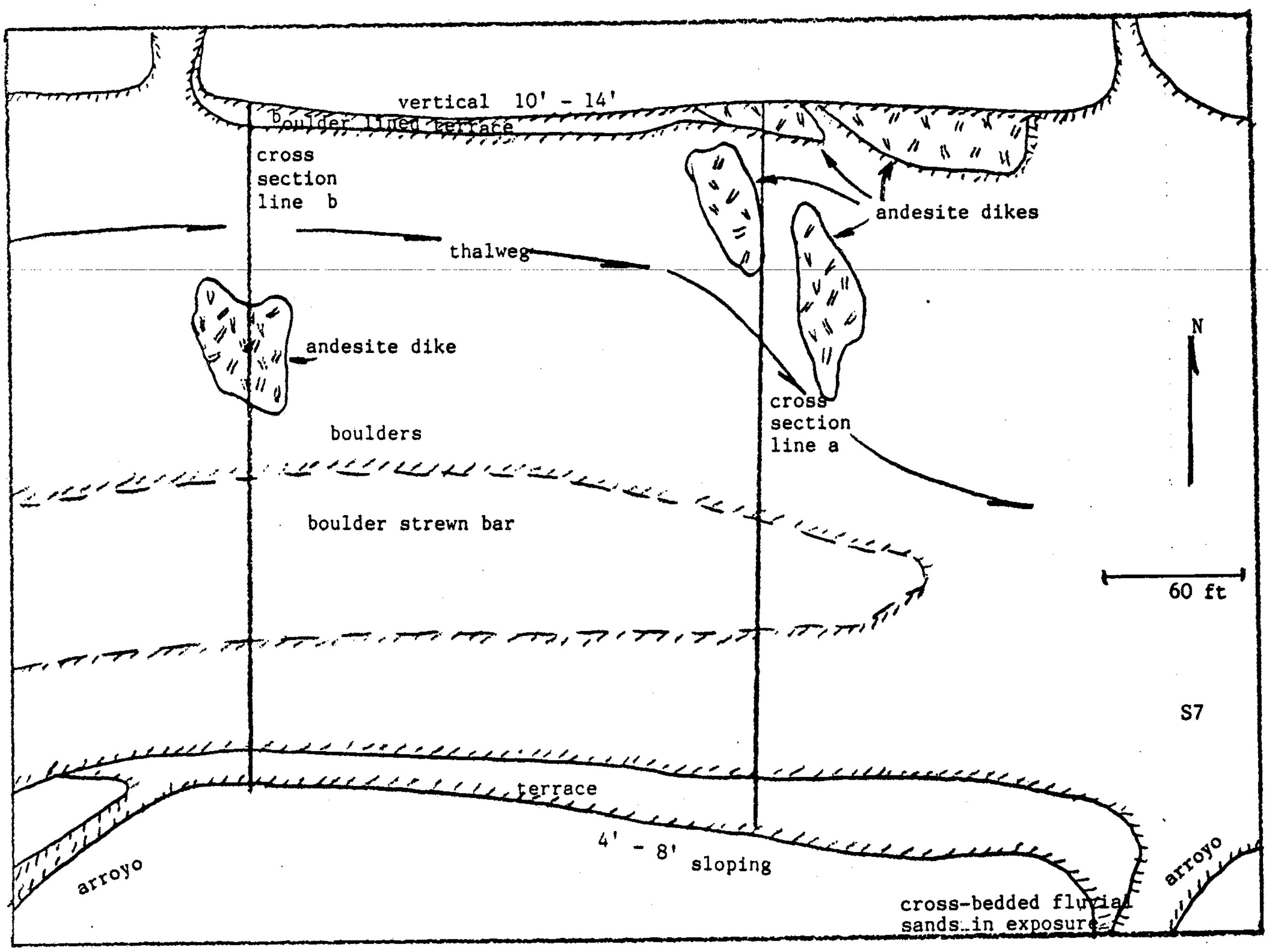
vertical 10' - 14'
boulder lined terrace
cross
section
line b
thalweg
andesite dikes
andesite dike
N
cross
section
line a
boulders
boulder strewn bar
60 ft
S7
terrace
4' - 8' sloping
arroyo
arroyo
cross-bedded fluvial
sands in exposure

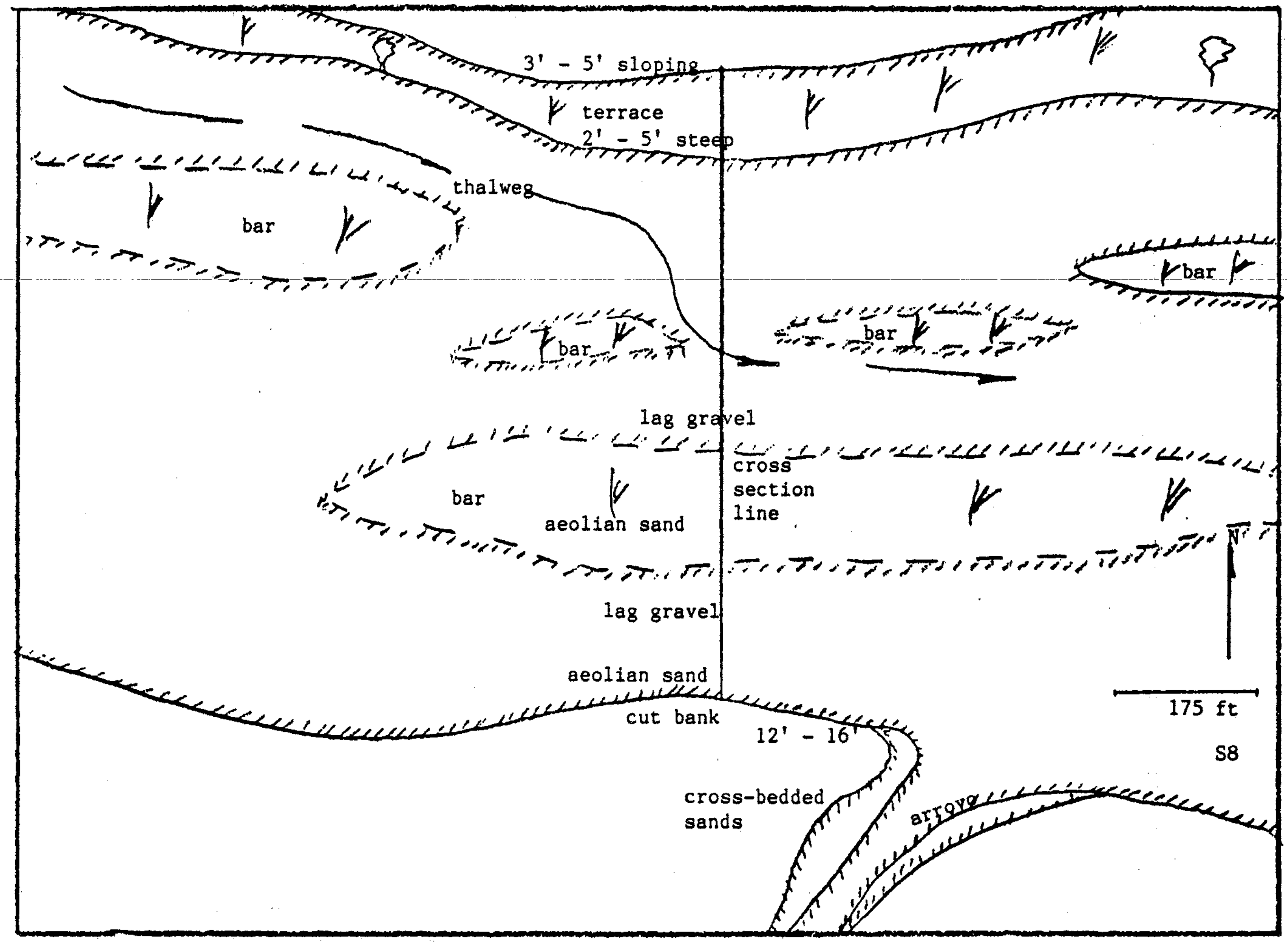
3' - 5' sloping
terrace
2' - 5' steep
thalweg
bar
bar
bar
bar
lag gravel
cross
section
line
bar
aeolian sand
lag gravel
aeolian sand
cut bank
12' - 16'
cross-bedded
sands
arroyo
N
175 ft
S8

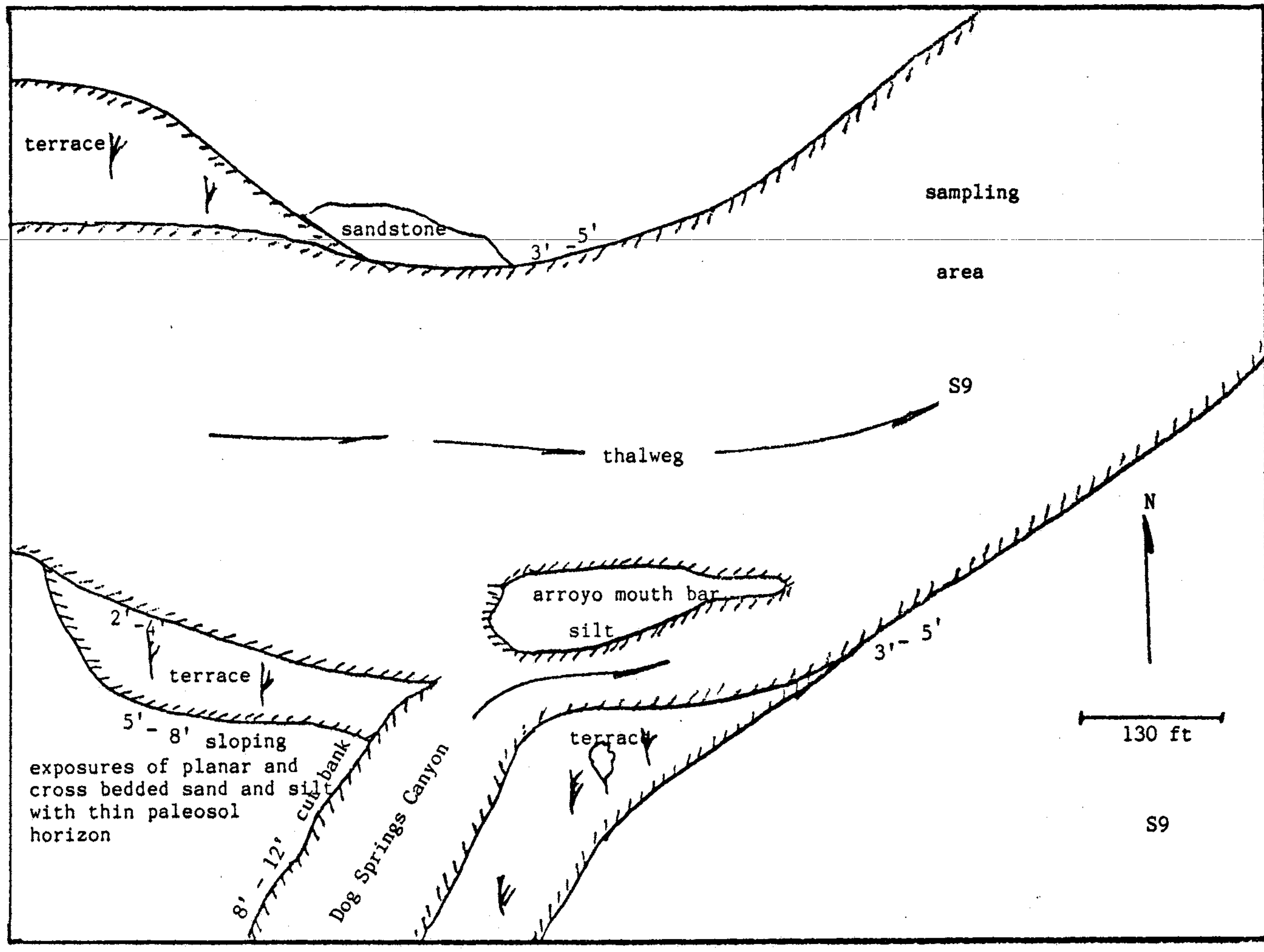
terrace
sandstone
3' - 5'
sampling
area
S9
thalweg
N
arroyo mouth bar
silt
2' - 4'
terrace
3' - 5'
5' - 8' sloping
exposures of planar and
cross bedded sand and silt
with thin paleosol
horizon
cutbank
8' - 12'
Dog Springs Canyon
terrace
130 ft
S9

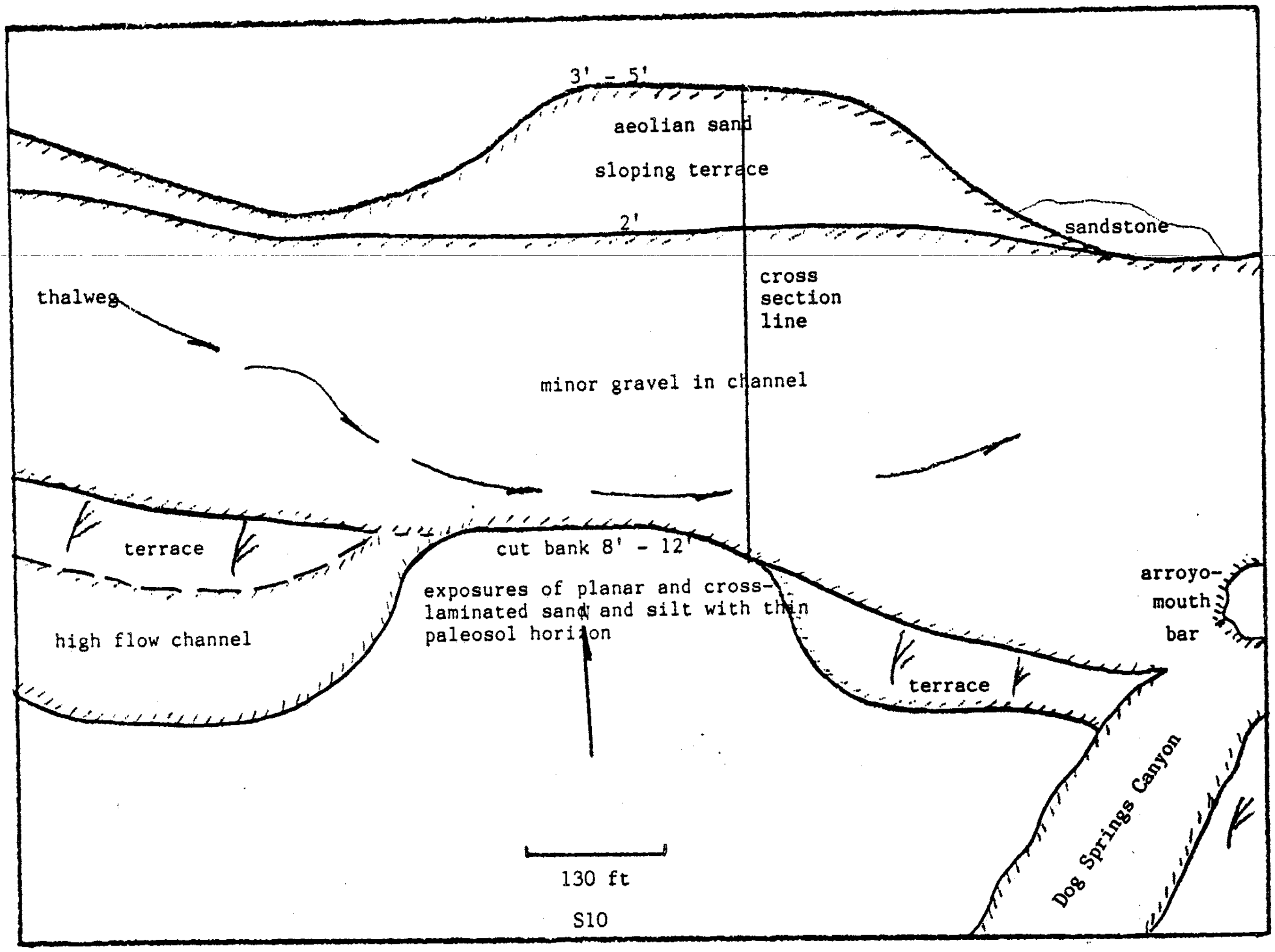
3' - 5'
aeolian sand
sloping terrace
2'
sandstone
thalweg
cross
section
line
minor gravel in channel
terrace
cut bank 8' - 12'
exposures of planar and cross-laminated sand and silt with thin paleosol horizon
high flow channel
arroyo-
mouth
bar
terrace
Dog Springs Canyon
130 ft
S10

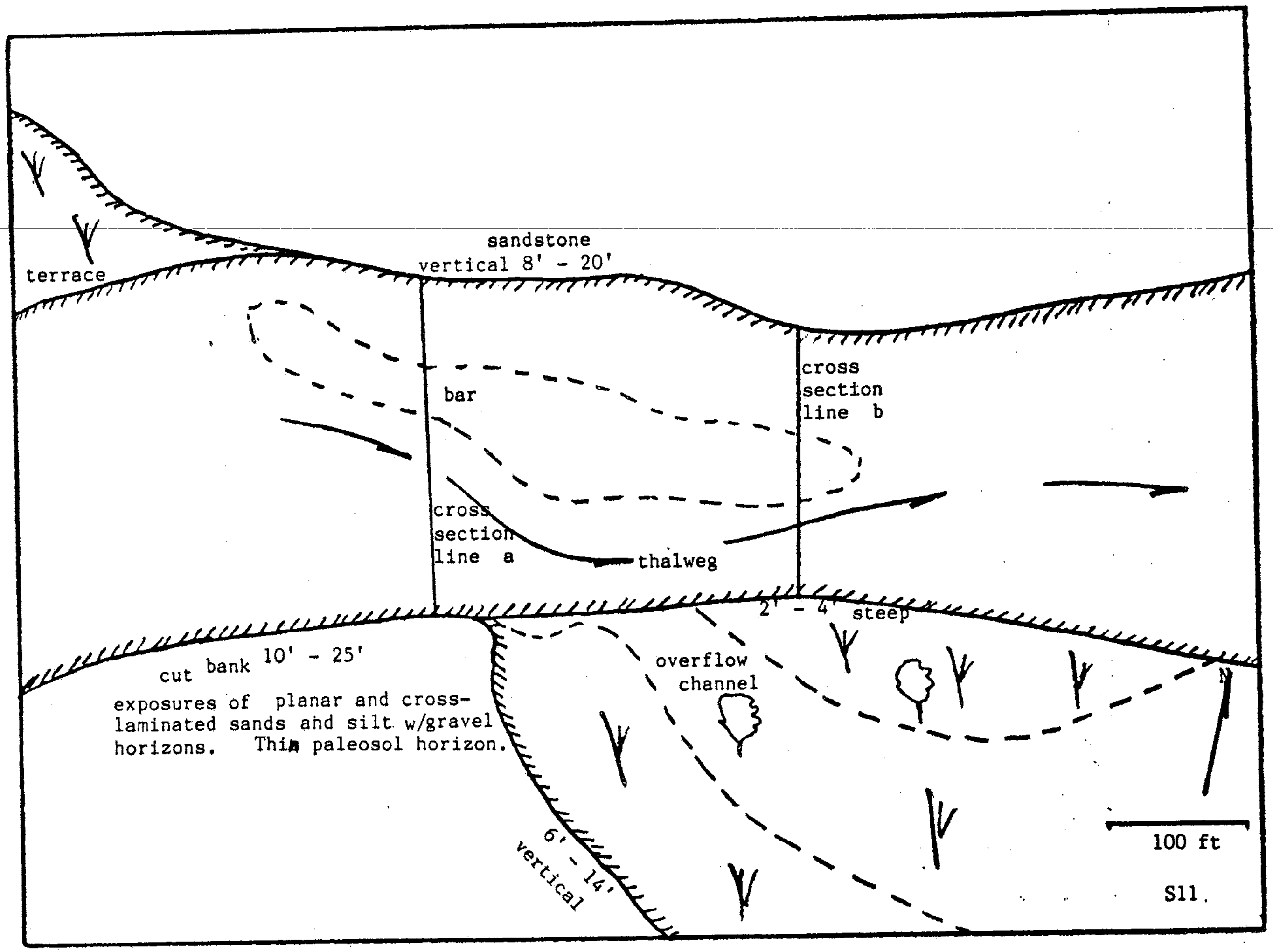
sandstone
vertical 8' - 20'
terrace
bar
cross
section
line b
cross
section
line a
thalweg
2' - 4' steep
cut bank 10' - 25'
exposures of planar and cross-
laminated sands and silt w/gravel
horizons. Thin paleosol horizon.
overflow
channel
6' - 14'
vertical
N
100 ft
S11.

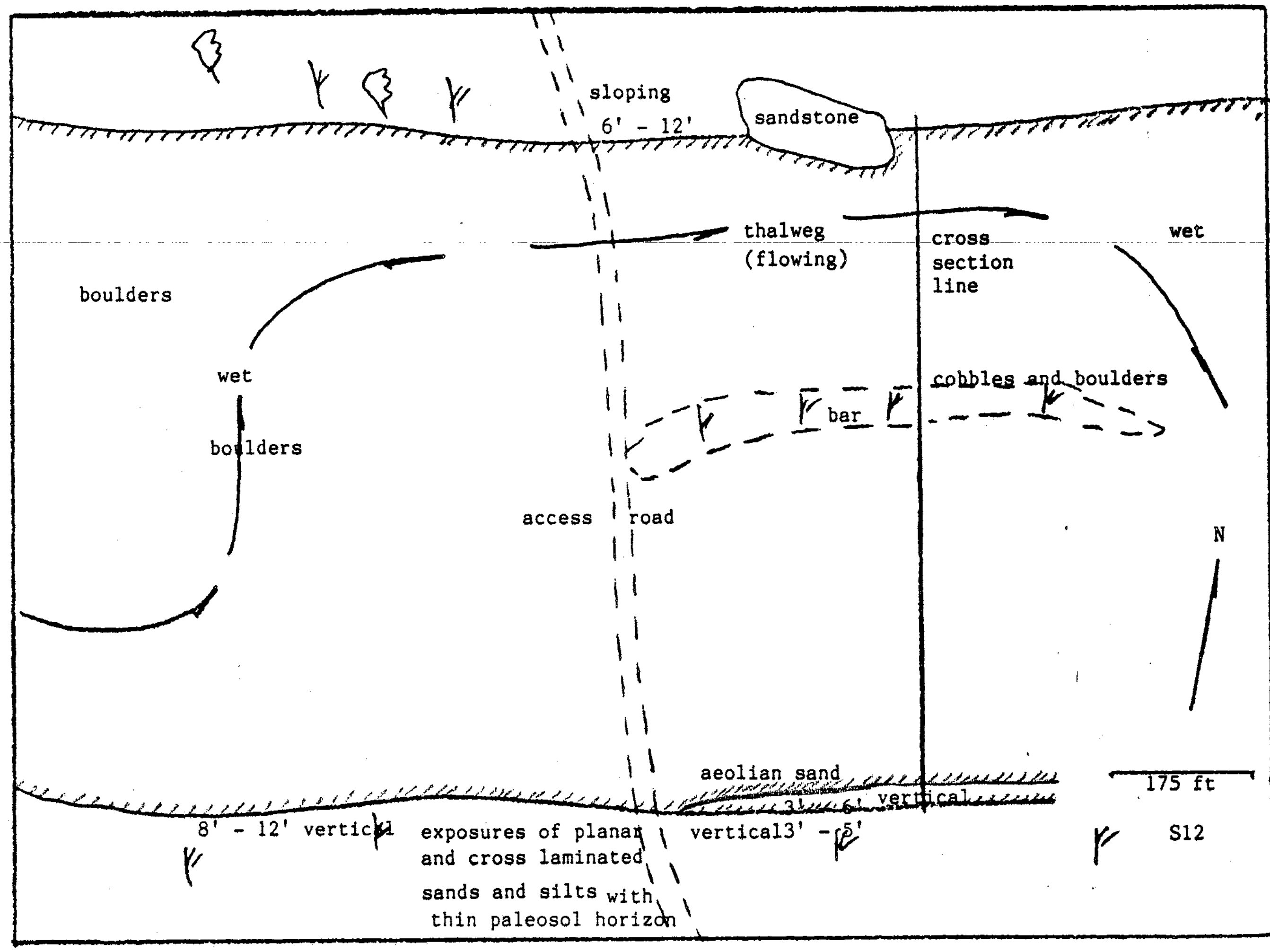
sloping
6' - 12'
sandstone
thalweg
(flowing)
cross
section
line
wet
boulders
wet
boulders
cobbles and boulders
bar
access road
N
aeolian sand
3' - 6' vertical
175 ft
8' - 12' vertical
exposures of planar
and cross laminated
sands and silts with
thin paleosol horizon
vertical 3' - 5'
S12

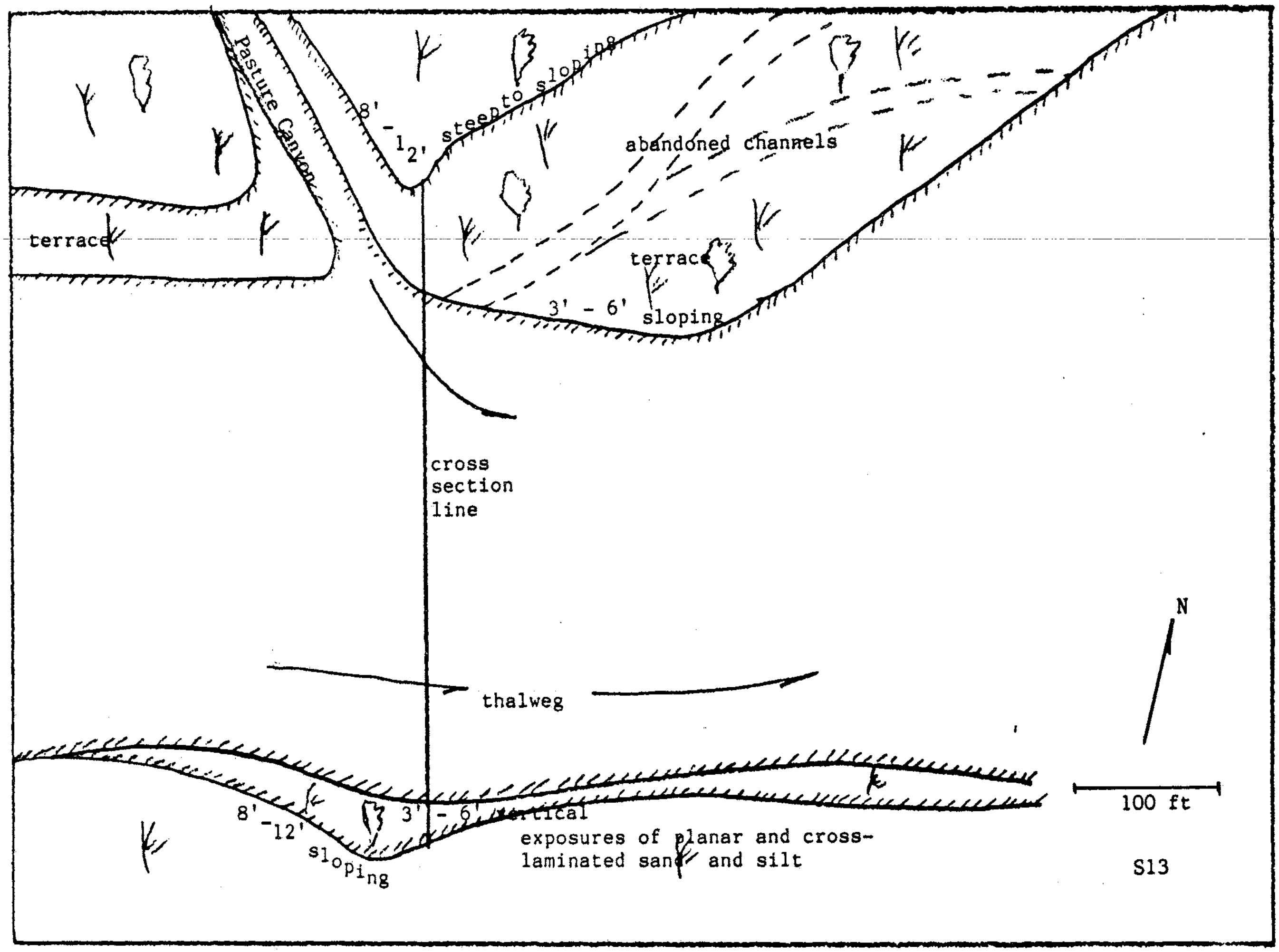
Pasture Canyon
8' - 12' steep to sloping
abandoned channels
terrace
terrace
3' - 6' sloping
cross section line
thalweg
N
100 ft
8' - 12' sloping
3' - 6' vertical
exposures of planar and cross-laminated sand and silt
S13

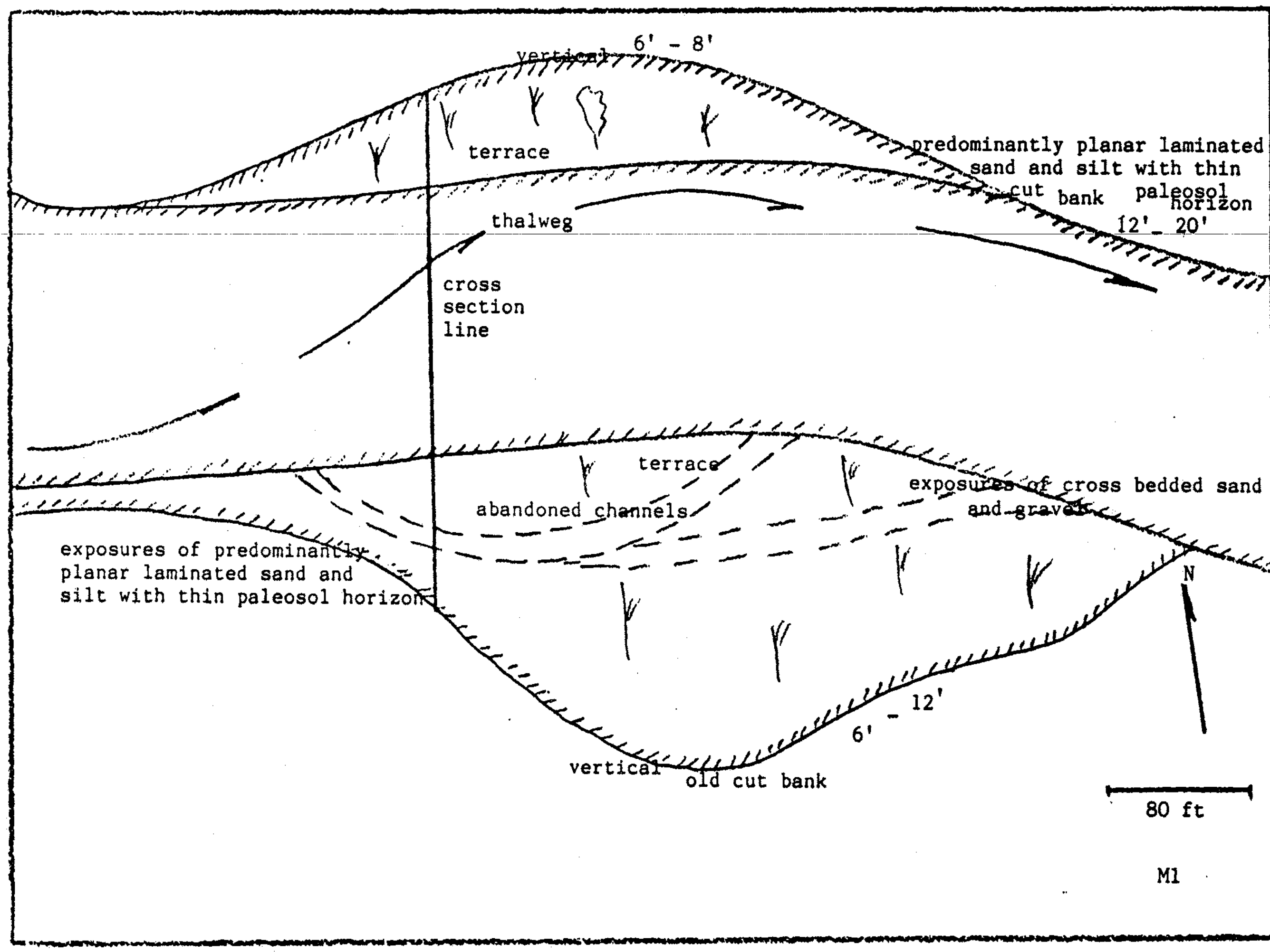

vertical 6' - 8'
terrace
predominantly planar laminated sand and silt with thin paleosol horizon
cut bank
12' - 20'
thalweg
cross section line
terrace
abandoned channels
exposures of cross bedded sand and gravel
exposures of predominantly planar laminated sand and silt with thin paleosol horizon
N
6' - 12'
vertical
old cut bank
80 ft
M1

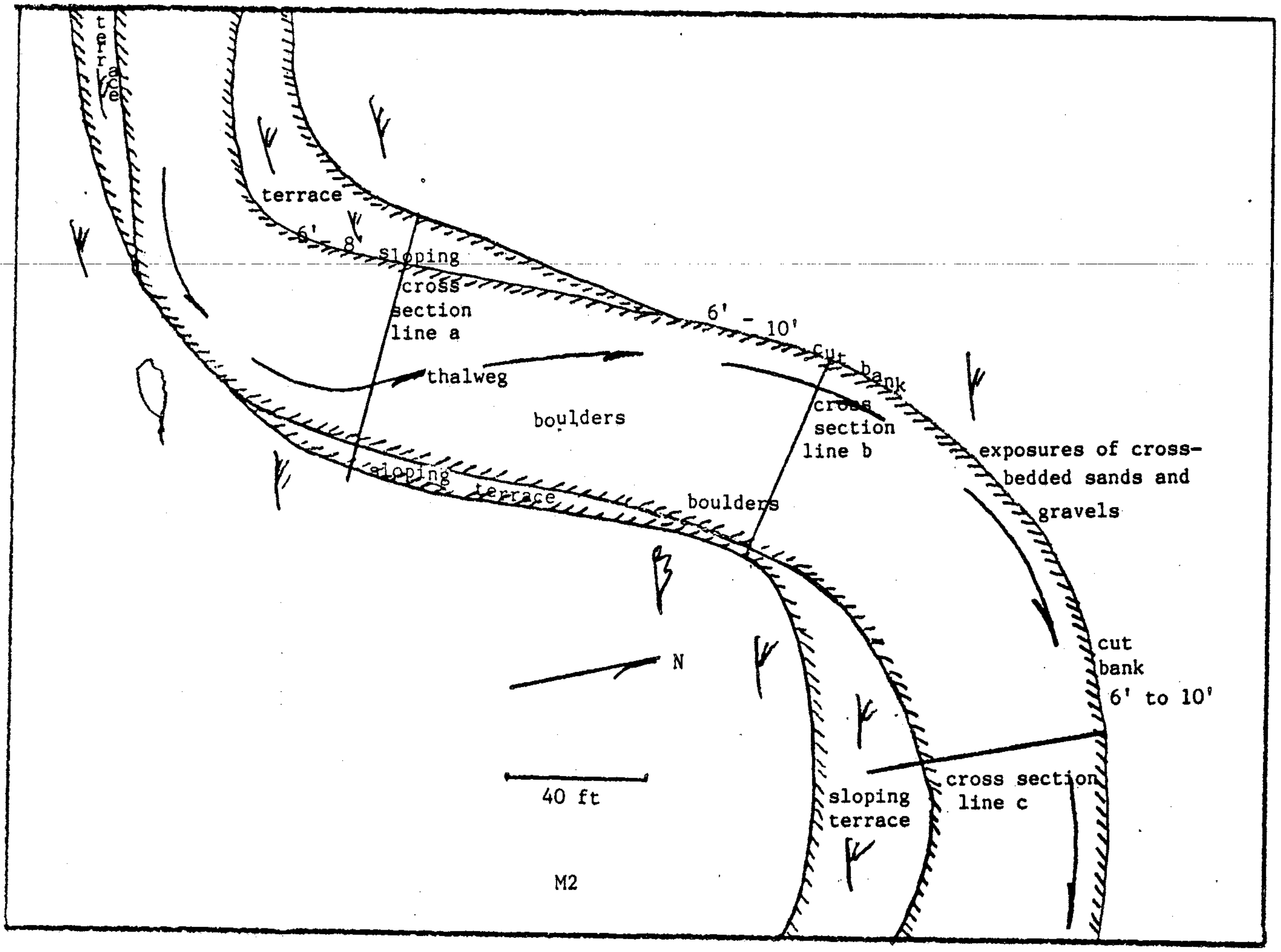
terrace
terrace
6' - 8'
sloping
cross
section
line a
thalweg
boulders
6' - 10'
cut bank
cross
section
line b
exposures of cross-
bedded sands and
gravels
sloping terrace
boulders
N
cut
bank
6' to 10'
40 ft
sloping
terrace
cross section
line c
M2

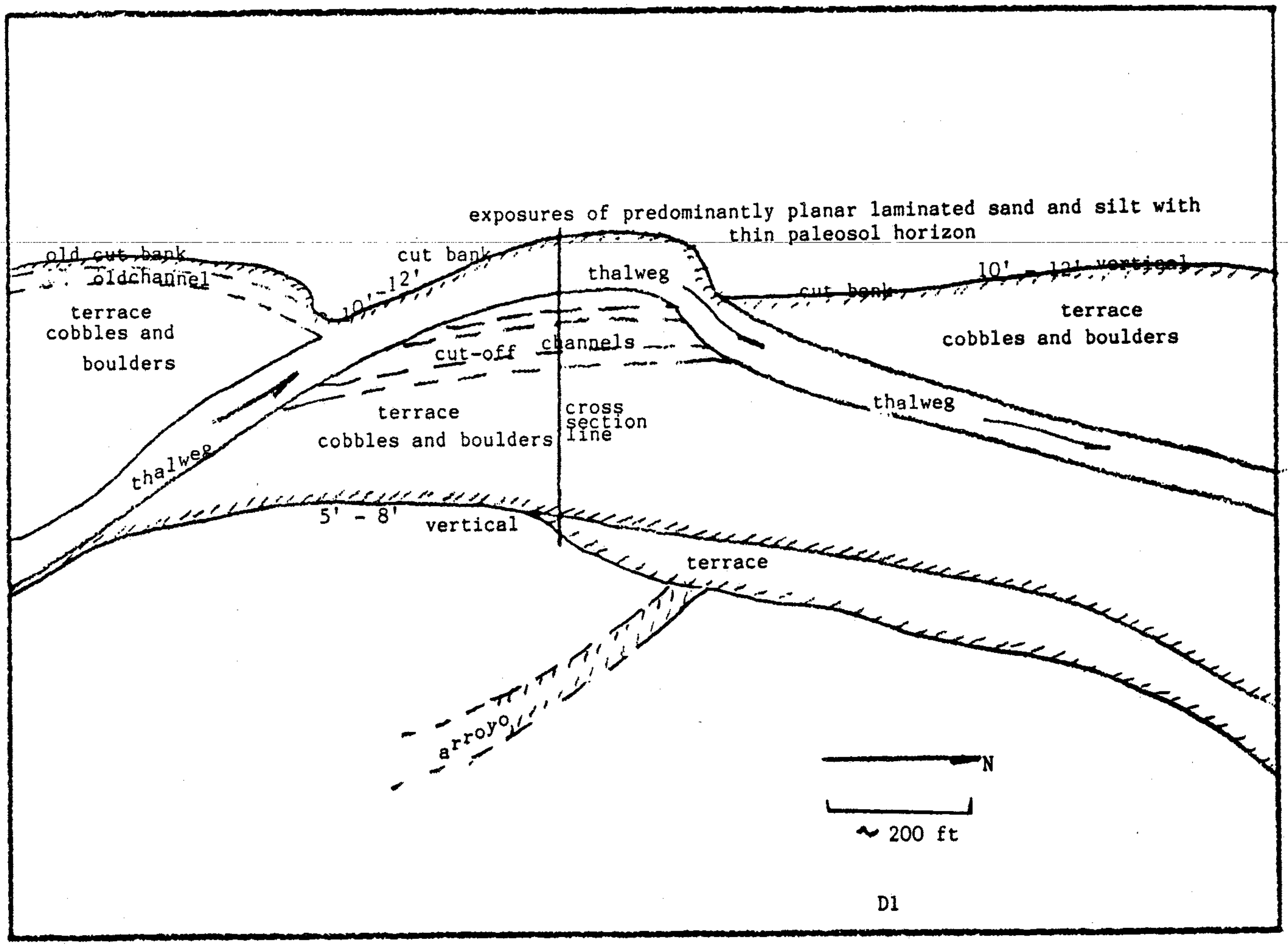

exposures of predominantly planar laminated sand and silt with thin paleosol horizon
old cut bank
oldchannel
cut bank
12'
10'
thalweg
cut bank
10' - 12' vertical
terrace cobbles and boulders
cut-off channels
terrace cobbles and boulders
terrace cobbles and boulders
thalweg
cross section line
thalweg
5' - 8'
vertical
terrace
arroyo
N
~ 200 ft
D1

APPENDIX F: Computer Programs

PROGRAM NORM-MAG: Generates files for normalized magnitude plots

```
10 DIM DIST(500),MAG(500),ELEV(500)
20 INPUT "in file ";INFILE$
30 INPUT "out file ";OTFILE$
40 INPUT "elev at mouth ";EL
50 OPEN "i",1,INFILE$
60 I=2:TOTDIST=0:TOTELEV=0:TOTMAG=1
70 IF EOF(1) GOTO 150
80 INPUT# 1,DIST(I),MAG(I),ELEV(I)
90 PRINT DIST(I),MAG(I),ELEV(I)
100 TOTMAG=TOTMAG+MAG(I)
110 IF DIST(I)>TOTDIST THEN LET TOTDIST=DIST(I)
120 IF ELEV(I)>TOTELEV THEN LET TOTELEV=ELEV(I)
130 I=I+1
140 GOTO 70
150 CLOSE #1
160 '
170 DIST(1)=0:MAG(1)=0:ELEV(1)=EL
180 MAG(I-2)=MAG(I-2)+1
190 I=I-1
200 FOR K=1 TO I
210 FOR J=1 TO I-K
220 IF DIST(K)<DIST(J+K) GOTO 260
230 XTEMP=DIST(J+K):YTEMP=MAG(J+K):ZTEMP=ELEV(J+K)
240 DIST(J+K)=DIST(K):MAG(J+K)=MAG(K):ELEV(J+K)=ELEV(K)
250 DIST(K)=XTEMP:MAG(K)=YTEMP:ELEV(K)=ZTEMP
260 NEXT J
270 NEXT K
280 '
290 PRINT " ":PRINT " "
300 OPEN "o",1,OTFILE$
310 NORMDIST=0:MAGGIE=0:NORMMAG=0:SORCDIST=0:INCMAG=0
320 FOR M=I-1 TO 1 STEP -1
330 SORCDIST=TOTDIST-DIST(M)
340 NORMDIST=SORCDIST/TOTDIST
350 INCMAG=MAG(M)+INCMAG
360 NORMMAG=INCMAG/TOTMAG
370 NORMELEV=(ELEV(M)-EL)/(TOTELEV-EL)
380 MAGGIE=1-NORMMAG
390 PRINT DIST(M),MAGGIE,NORMELEV
400 WRITE# 1,NORMDIST,MAGGIE,NORMELEV
410 NEXT M
420 CLOSE #1
430 GOTO 20
```

PROGRAM HIPSAREA: Calculates basin area, hypsometric integrals and generates hypsometric curves.

```
10 DIM X(3000),Y(3000),Z(3000),COUNTY(100),KK(100)
20 INPUT "infile ";INFILE$
30 INPUT "out file ";OTFILE$
40 ZHIGH=0:ZLOW=10000:I=0
50 OPEN "i",1,INFILE$
60 IF EOF(1) GOTO 120
70 INPUT# 1,X(I+1),Y(I+1),Z(I+1)
80 IF Z(I+1)>ZHIGH THEN LET ZHIGH=Z(I+1)
90 IF Z(I+1)<ZLOW THEN LET ZLOW=Z(I+1)
100 I=I+1
110 GOTO 60
120 CLOSE #1
150 OPEN "o",1,OTFILE$
160 L=1
170 FOR K=1 TO -.001 STEP-.05
180 COUNT=0
190 FOR J=1 TO I
200 ZED=(Z(J)-ZLOW)/(ZHIGH-ZLOW)
210 IF ZED>K THEN LET COUNT=COUNT+1
220 NEXT J
230 IF K<.001 THEN LET K=0
240 COUNTY=COUNT/I
250 COUNTY(L)=COUNTY
260 KK(L)=K
270 WRITE# 1,COUNTY,K:PRINT COUNTY,K
280 L=L+1
290 NEXT K
300 CLOSE #1
310 '
320 SLICE=0
330 FOR H=1 TO L
340 IF KK(H-1)=KK(H) GOTO 360
350 SLICE=SLICE+((KK(H-1)+KK(H))*((COUNTY(H)-COUNTY(H-1))))/2
360 NEXT H
370 HIPSO=SLICE*100
379 PRINT " "
380 LPRINT INFILE$," area= ";I;" km sq ","Hypsometric integral=";HIPSO
390 GOTO 20
```

PROGRAM SUBBASIN: Selects x,y,z data for sub-basin from main elevation file, using sub-basin boundary file

```
10 DIM X(500),Y(500),Z(500)
20 OPEN "i",1,"nodeelev.dat"
30 INPUT "in-file"; INFILE$
40 INPUT "out file"; OTFILE$
50 OPEN "i",2,INFILE$
60 OPEN "o",3,OTFILE$
70 INPUT# 2,MAXY,MAXX,ZED
80 INPUT# 2,MINY,MINX,ZED
90 PRINT MINY,MAXY,MINX,MAXX
100 I=1
110 IF EOF(1) GOTO 150
120 INPUT# 1,A,B,C
130 IF A>MINX AND A<MAXX AND B>MINY AND B<MAXY THEN LET X(I)=A:Y(I)=B:Z(I)=C:I=I
+1
140 GOTO 110
150 K=0:PRINT I
160 IF EOF(2) GOTO 220
170 INPUT# 2,XX,YMIN,YMAX
180 FOR J=1 TO I-1
190 IF XX=X(J) AND Y(J)>YMIN AND Y(J)<YMAX THEN PRINT X(J),Y(J),Z(J):WRITE# 3,X(
J),Y(J),Z(J): LET K=K+1
200 NEXT J
210 GOTO 160
220 CLOSE #1,#2,#3
230 PRINT K;" km sq"
240 END
```

PROGRAM SUBDIVID: Extracts rectangular sub-areas from main basin Useful for looking at cross-sections across the width or height of the basin

```
10 OPEN "i",1,"nodeelev.dat"
20 INPUT "outfile";OUTFILE$
30 INPUT "x low ";XLOW
40 INPUT "x high ";XHIGH
50 INPUT "y low ";YLOW
60 INPUT "y high ";YHIGH
70 OPEN "o",2, OUTFILE$
80 INPUT# 1,X,Y,Z
90 IF EOF(1) GOTO 120
100 IF X <=XHIGH AND X >=XLOW AND Y <=YHIGH AND Y >=YLOW THEN WRITE# 2,X,Y,Z:PRI
NT X,Y,Z
110 GOTO 80
120 CLOSE #1:CLOSE #2
130 END
```

PROGRAM INCREMENT: Calculates cross sectional areas and corresponding hydraulic radii for given flow depth at a given cross section. Developed during, but not used for, the present study.

```
10 DIM X(200),Y(200)
20 J=1
30 INPUT "infile";INFILE$
40 INPUT "depth of streamflow"; H
50 INPUT "depth increment"; STEPP
60 OPEN"i",1,INFILE$
70 IF EOF(1) GOTO 120
80 INPUT# 1, X,Y
90 X(J)=X:Y(J)=Y
100 J=J+1
110 GOTO 70
120 FOR I=0 TO H STEP STEPP
130 FOR K=1 TO J+1
140 IF Y(K)<I (I-Y(K))>STEPP THEN NEXT K
150 Z=X(K-1):ZZ=X(K+1)
160 IF Y(K-1)<I AND Y(K+1)>I THEN GOSUB 250
170 IF Y(K-1)<I AND Y(K+1)<I THEN GOSUB 300
180 IF Y(K-1)>I AND Y(K+1)>I THEN GOSUB 360
190 IF Y(K-1)>I AND Y(K+1)<I THEN GOSUB 400
200 NEXT K
210 NEXT I
220 LPRINT "flow depth: ";I,"cross-sectional area: ";S,"hydraulic radius: ";PERI
M
230 CLOSE 1
240 END
250 Z=X(K)-(Y(K)-I)*(X(K)-X(K-1))/(Y(K)-Y(K-1))
260 S=S+(((ZZ-Z)/2)*(Y(K)-I))+(Y(K+1)-Y(K))*(ZZ-X(K))/8
270 PER=SQR((X(K)-Z)^2+Y(K)-I)^2)+SQR(((ZZ-X(K))/2)^2+((Y(K+1)-Y(K))/2)^2)
280 PERIM=PER+PERIM
290 RETURN
300 Z=X(K)-(Y(K)-I)*(X(K)-X(K-1))/(Y(K)-Y(K-1))
310 ZZ=X(K)+(Y(K)-I)*(X(K+1)-X(K))/(Y(K)-Y(K+1))
320 S=S+3*(Y(K)-I)*(ZZ-Z)/8
330 PER=SQR(((ZZ-X(K)))^2+((Y(K)-I))^2)+SQR(((X(K)-Z))^2+((Y(K)-I))^2)
340 PERIM=PERIM+PER
350 RETURN
360 S=S+(Y(K)-I)*(ZZ-Z)/2+((Y(K+1)-Y(K))*(ZZ-X(K))-(Y(K)-Y(K-1))*(X(K)-Z))/8
370 PER=SQR(((X(K)-Z)/2)^2+((Y(K)-Y(K-1))/2)^2)+SQR(((ZZ-X(K))/2)^2+((Y(K+1)-Y(K
))/2)^2)
380 PERIM=PERIM+PER
390 RETURN
400 ZZ=X(K)+(Y(K)-I)*(X(K+1)-X(K))/(Y(K)-Y(K+1))
410 S=S+(Y(K)-I)*(ZZ-Z)/2+((Y(K-1)-Y(K))*(X(K)-Z))/8
420 PER=SQR((ZZ-X(K))^2+(Y(K)-I^2)+SQR(((X(K)-Z)/2)^2+((Y(K-1)-Y(K))/2)^2)
430 PERIM=PERIM+PER
440 RETURN
450 END
```

APPENDIX G: Data Diskettes

EXPLANATION

All Data files are in DOS ASCII format. Diskettes are 256K format, double-sided, double density.

Each diskette contains a directory, which is included as a file named "READ.ME".

All data generated and used during the study is included in this appendix.

NOT INCLUDED IN THIS DISTRIBUTION COPY